Innovative materials for packaging

Nour Halawani

N°d'ordre NNT : 2017LYSEI010

THESE de DOCTORAT DE L'UNIVERSITE DE LYON
opérée au sein de
INSA de Lyon

Ecole Doctorale EDA160
Electronique, Electrotechnique, Automatique

Spécialité/ discipline de doctorat :

Génie Electrique

Soutenue publiquement le 14/02/2017, par :

Nour HALAWANI

Innovative Materials for Packaging

Devant le jury présidé par le P. Stéphane HOLE et composé de :

Nom, prénom	grade/qualité	établissement/entreprise
NASSIET, Valérie	Professeur des Universités	ENI de Tarbes — Rapporteuse
HOLE, Stéphane	Professeur des Universités	UPMC-Sorbonne Universités — Rapporteur
MIJANGOS-UGARTE, Carmen	Professeur	ICTP-Madrid — Examinatrice
GRISERI, Virginie	Maître de Conférences	LAPLACE-Toulouse — Examinatrice
MOREL, Hervé	Directeur de Recherche	INSA-LYON — Directeur de thèse
PRUVOST, Sébastien	Maître de Conférences HDR	INSA-LYON — Co-directeur de thèse
AUGE, Jean-Louis	Maître de Conférences	UCBL-Lyon1 — Encadrant
GAIN, Olivier	Ingénieur de Recherche	UCBL-Lyon1 — Co-encadrant

Département FEDORA – INSA Lyon - Ecoles Doctorales – Quinquennal 2016-2020

SIGLE	ECOLE DOCTORALE	NOM ET COORDONNEES DU RESPONSABLE
CHIMIE	**CHIMIE DE LYON** **http://www.edchimie-lyon.fr** Sec : Renée EL MELHEM Bat Blaise Pascal 3e etage secretariat@edchimie-lyon.fr Insa : R. GOURDON	M. Stéphane DANIELE Institut de Recherches sur la Catalyse et l'Environnement de Lyon IRCELYON-UMR 5256 Équipe CDFA 2 avenue Albert Einstein 69626 Villeurbanne cedex directeur@edchimie-lyon.fr
E.E.A.	**ELECTRONIQUE, ELECTROTECHNIQUE, AUTOMATIQUE** **http://edeea.ec-lyon.fr** Sec : M.C. HAVGOUDOUKIAN Ecole-Doctorale.eea@ec-lyon.fr	M. Gérard SCORLETTI Ecole Centrale de Lyon 36 avenue Guy de Collongue 69134 ECULLY Tél : 04.72.18 60.97 Fax : 04 78 43 37 17 Gerard.scorletti@ec-lyon.fr
E2M2	**EVOLUTION, ECOSYSTEME, MICROBIOLOGIE, MODELISATION** **http://e2m2.universite-lyon.fr** Sec : Sylvie ROBERJOT Bât Atrium - UCB Lyon 1 04.72.44.83.62 Insa : H. CHARLES secretariat.e2m2@univ-lyon1.fr	M. Fabrice CORDEY CNRS UMR 5276 Lab. de géologie de Lyon Université Claude Bernard Lyon 1 Bât Géode 2 rue Raphaël Dubois 69622 VILLEURBANNE Cédex Tél : 06.07.53.89.13 cordey@univ-lyon1.fr
EDISS	**INTERDISCIPLINAIRE SCIENCES-SANTE** **http://www.ediss-lyon.fr** Sec : Sylvie ROBERJOT Bât Atrium - UCB Lyon 1 04.72.44.83.62 Insa : M. LAGARDE secretariat.ediss@univ-lyon1.fr	Mme Emmanuelle CANET-SOULAS INSERM U1060, CarMeN lab, Univ. Lyon 1 Bâtiment IMBL 11 avenue Jean Capelle INSA de Lyon 696621 Villeurbanne Tél : 04.72.68.49.09 Fax :04 72 68 49 16 Emmanuelle.canet@univ-lyon1.fr
INFOMATHS	**INFORMATIQUEET MATHEMATIQUES** **http://infomaths.univ-lyon1.fr** Sec :Renée EL MELHEM Bat Blaise Pascal 3e etage infomaths@univ-lyon1.fr	Mme Sylvie CALABRETTO LIRIS – INSA de Lyon Bat Blaise Pascal 7 avenue Jean Capelle 69622 VILLEURBANNE Cedex Tél : 04.72. 43. 80. 46 Fax 04 72 43 16 87 Sylvie.calabretto@insa-lyon.fr
Matériaux	**MATERIAUX DELYON** **http://ed34.universite-lyon.fr** Sec : M. LABOUNE PM : 71.70 –Fax : 87.12 Bat. Direction Ed.materiaux@insa-lyon.fr	M. Jean-Yves BUFFIERE INSA de Lyon-MATEIS Bâtiment Saint Exupéry 7 avenue Jean Capelle 69621 VILLEURBANNE Cedex Tél : 04.72.43 71.70 Fax 04 72 43 85 28 jean-yves.buffiere@insa-lyon.fr
MEGA	**MECANIQUE, ENERGETIQUE, GENIE CIVIL, ACOUSTIQUE** **http://mega.universite-lyon.fr** Sec : M. LABOUNE PM : 71.70 –Fax : 87.12 Bat. Direction mega@insa-lyon.fr	M. Philippe BOISSE INSA de L yon Laboratoire LAMCOS Bâtiment Jacquard 25 bis avenue Jean Capelle 69621 VILLEURBANNE Cedex Tél : 04.72 .43.71.70 Fax : 04 72 43 72 37 Philippe.boisse@insa-lyon.fr
ScSo	**ScSo*** **http://recherche.univ-lyon2.fr/scso/** Sec : Viviane POLSINELLI Brigitte DUBOIS Insa : J.Y. TOUSSAINT Tél : 04 78 69 72 76 viviane.polsinelli@univ-lyon2.fr	M. Christian MONTES Université Lyon 2 86 rue Pasteur 69365 LYON Cedex 07 Christian.montes@univ-lyon2.fr

*ScSo : Histoire, Géographie, Aménagement, Urbanisme, Archéologie, Science politique, Sociologie, Anthropologie

ACKNOWLEDGMENTS

First, I would like to thank the members of the jury who accepted to examine this PhD work. I would like to thank Stéphane HOLE and Valérie NASSIET for reporting this manuscript and Carmen MIJANGOS-UGARTE and Virginie GRISERI for examining it.

I would like to thank my supervisors Hervé MOREL, Sébastien PRUVOST, Jean-Louis AUGE and Olivier GAIN for their guidance, advices and encouragement during the three years of this PhD. I would like to thank them for always finding time for their PhD student and for always being there to overpass together all the challenges we had to face during this PhD. I have learnt a lot from them, from their patience and wisdom. It has been a pleasure to work with them.

I express my gratitude for the director of the IMP@INSA Etienne FLEURY for his support.

I would like to thank Gilbert TEYSSEDRE and Virginie GRISERI for providing their time and giving me the chance to perform current measurements in their laboratory (LAPLACE Toulouse).

I would like to thank Pierre Alcouffe for realizing the TEM image at the Centre Technologique des Microstructures CTμ of the University of Lyon. I would like to thank him as well for training me on the ESEM at the CLYM (Centre LYonnais des Microscopies).

These acknowledgements would not be complete without appreciating persons I worked with in IMP laboratory like Jocelyne GALY for participating in meetings and Guilhem QUINTARD, Raphaël BRUNEL, Julien CHATARD and Marion COLELLA for performing the trainings for the needed machines.

I would like to thank persons I am glad that I have met in IMP and AMPERE and encouraged me all over the three years like Nicolas LAFOREST, Ly NGUYEN Thi Khanh, Jing YANG, Yann ROSETTI, Florence Russo, Justine BILLORE, Amelie GASTON, Sophie

IGLESIAS, Suzanne LAIK, Noëllie YLLA, Afef HOUACHTIA and Atef LEKDIM. I will never forget the PhD students and friends with whom I have shared offices like Constance ROBEYNS, Loraine DESMARS and Thomas THEODOROU.

My deepest appreciation belongs to my family, my mother Fatima, my father Mohammad, my brother Ahmad and my sisters Houda and Safaà and my best friend Inas, as well as my Grandmothers Hafiza and Samia and my Grandfathers Abdallah and Hassan. I would like to thank them all, for their motivation, patience and support in everything in my life and especially during these three years of Phd. Their support means a lot and makes always the difference. I would like to thank as well all my friends, especially Jamal, Gilles and Ali whose support and encouragements always contribute to the good motivation.

Résumé

Ce travail porte sur l'étude du mélange thermodurcissable - thermoplastique (époxy-amine / polyetherimide avec séparation de phase) pour évaluer les performances électriques et thermiques. Ces matériaux seraient des nouveaux candidats pour remplacer la couche d'encapsulation dans les semi-conducteurs, par exemple ceux utilisés comme interrupteur dans les applications électroniques de puissance. Les mélanges de polymères seraient un nouveau candidat en tant qu'isolant pour le système. La matrice époxy-amine seule et les mélanges époxy / Polyetherimide ont été caractérisés par microscopie électronique à transmission, microscopie électronique à balayage, Calorimétrie différentielle à balayage, analyse thermogravimétrique, analyse mécanique dynamique, analyse diélectrique avec modélisation analytique et des mesures de conductivité électrique et de tension de claquage ont également été réalisées.

Ces techniques complémentaires ont d'abord été utilisées pour étudier la séparation de phases et ensuite pour quantifier la taille des nodules de thermoplastiques dans la matrice thermodurcissable. Cette séparation de phase a été examiné et à montrer une diminution des valeurs diélectriques de 15% et une augmentation de la tension de claquage par rapport au système époxy-amine pur.

Abstract

This work deals with the study of thermoset-thermoplastic blend (epoxy-amine/poly-etherimide phase separated) to assess the electrical and thermal performances. These materials would be new candidates to replace the encapsulation layer in semiconductors, for example ones used as switches in power electronic applications. Polymers blends would be a novel candidate as an insulator for the system. Pure epoxy system as well as Epoxy/Polyetherimide blends where characterized by transmission electron microscopy, scanning electron microscopy, differential scanning calorimetry, thermogravimetric analysis, dynamic mechanical analysis, dielectric analysis with analytical modelling, electrical conductivity and breakdown voltage measurements.

These complementary techniques were used first to investigate the presence of the phase separation phenomenon and secondly to quantify the separated nodules size. The effect of this phase separation was examined and showed a decrease in the dielectric values of 15 % and an increase in the breakdown voltage compared to the pure epoxy system. It was finally modulated to show a close assumption of what is found experimentally.

General Introduction

Power electronics are gaining more and more importance in the industry. The demands are to improve its reliability and its performance under severe conditions. One of the main limitations in terms of high voltage and high temperature is the use of silicone gel as encapsulating layer. The maximum temperature that can be used with this silicone gel is 200 °C. IGBT, one of the power electronics devices, is limited at 6.5 kV nowadays. It is used in different industrial domains such as the high-voltage, direct current (HVDC) electric power transmission system, aircraft motor nacelle, railway device and many others. The environment in which the module is subjected to recommends high resistance to variation of temperature. The future of the modules demands higher electrical insulation that can go up to 30 kV. For these reasons the module components have to be evolved. One of the components of the module to try to replace is the silicone gel acting as an encapsulating layer. The material replacing it must withstand higher temperatures and have higher electrical resistivity.

In this context, this PhD work consists of presenting a novel material subjected to replace the present encapsulating layer made up of a polymer blend having a phase separation phenomenon and characterizing it. The first part will introduce the material and why it is interesting to study its properties. The second part will give the main thermal, mechanical and electrical characteristics of it.

This dissertation is composed of four chapters:

Chapter 1 presents a bibliographic work on the evolution of the power module domain and describes the main characteristics of the components of an IGBT module. Silicone gel advantages and drawbacks are discussed concerning its role as an encapsulating layer in the module. The parameters that should be considered to replace this material are listed. In a second part, bibliography of polymer blends and polymer composites is presented and discussed.

Chapter two gives an introduction about epoxy/polyetherimide blend, its preparation method and its main characteristics. A full description of the characterization methods used in this work is presented.

Chapter three presents the main results obtained upon studying the epoxy/PEI blend. The phase separated morphology is studied using SEM (Scanning electron microscopy) and TEM (transmission electron microscopy). Glass transition temperature for the pure epoxy material

and the blends is characterized using DSC (Differential scanning calorimetry). The phase separation phenomenon is verified by means of DMA (Dynamic mechanical analysis).

In addition to that, dielectric spectroscopy is used to measure the relative permittivity of the blends and compare it with the pure epoxy and other studies present in literature. Modeling work on the permittivity of the blends is performed using the experimental results of the pure epoxy and PEI materials.

Chapter four discusses the conductivity and the breakdown values of the materials. Conductivity results are presented from measurements done using high voltages at room temperature as well as from measurements done using low voltage but at high temperatures. The essential breakdown voltage measurement presented is carried out at room temperature.

Finally general conclusion and perspectives are developed.

Chapter 1

Power Modules & Polymer Blends

1.1. Perspectives on Power Electronics

Many of our daily used products have advanced in a glance for us and are available to be used easily, but behind these products there are huge scientific studies during decades made to present for us facilities in life with less consummation of energy. Take every automotive product, where through years it was enhanced in a way it became friendly to the environment and is getting more intelligent and less power consuming. This is one example from many electronic devices, starting from **LED** going through everyday simple electronics to the space rockets, containing an uncountable number of electronic products that have changed the twenty first century. Behind these advances there are several decades of material properties studies to develop the power electronic technology.

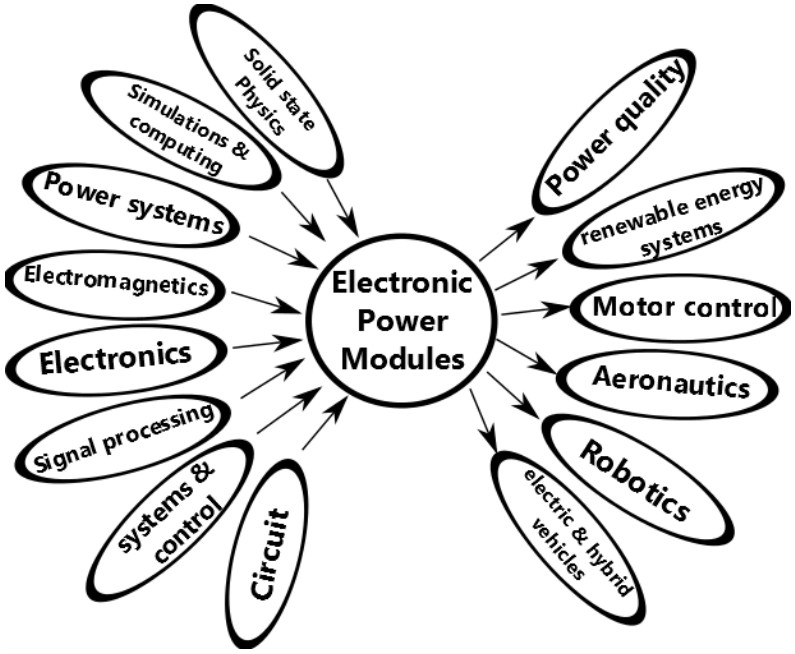

Figure 1: Interdisciplinary nature of power electronics and Products getting benefit from it.

Power electronics involve several scientific disciplines to form a complex system that is then involved in the resulting technologies and applications as illustrated in Figure 1. There are many potential studies and advances that are improving the power electronic technology.

Power electronics is a multidisciplinary field; it will continue in advancing as well as opening the opportunities to apply it on new applications.

1.1.1. History and applications

Power electronics have existed as rectifiers in the beginning of 1900s, when mercury arc rectifiers where introduced, before the development of semiconductors that were then integrated into the power devices by Hall in the beginning of 1950s [*Hall'52*]. It was the first significant power device, based on semiconductor technology, fabricated from germanium mesa alloy junctions and showed impressive electrical characteristics in that time; with a continuous forward current capability of 35 A and a reverse blocking voltage of 200 V. The discovery work was fabricated using germanium but then improved and commercialized in 1954 using silicon, which have higher energy gap of 1.1 eV compared to 0.67 eV for germanium, under the name of thyristors or **SCR** (Silicon-Controlled-Rectifier) by General Electrics [*Krein'11*]. Silicon was the main base of the electronic revolution of the 20th century, which can be regarded as the first-generation of semiconductors. In the late 1950s large systems were anticipated to be replaced by built-in semiconductor power devices. Jack Kilby presented, in 1958, an integrated circuit (**IC**) interconnected by means of deposition of aluminum on a layer of SiO_2 covering the semiconductor material to form a functional circuit, which was later achieved by Robert Noyce in 1959 to be the first **IC** [*Ross'98*]. In 1960 the first metal oxide semiconductor field effect transistor (**MOSFET**) was presented [*Kahng'60*] and later in 1963 Steven Hofstein and Fredric Heiman published a paper on silicon **MOSFET** [*Hofstein'63*]. The power electronics domain continued in advancing rapidly due to the multidisciplinary studies and in the late 1970s the power transistors **MCT**s (MOS-controlled thyristor) and **IGBT**s (insulated-gate-bipolar transistors) were introduced commercially [*DOS Santos'2015*]. The conventional diodes along with **MOSFET**, **MCT** or **IGBT** were used together to form the **IC** of a power electronic module.

In the end of the 20th century (**GaAs**) gallium arsenide and (**InP**) indium phosphide made the second-generation of semiconductors, constituting the base for the wireless and information revolution. The demand on the development of semiconductor devices for reliable operation for an extended period at high temperatures was high even though it is a complex process in which a number of physical effects have to be considered with increasing temperature [*Neudeck'02*] [*Dreike'94*]. The dividing point for high temperature electronic materials was considered as 300 °C, due to several point of views, e.g. packaging, wiring,

connecting, etc. [*Willander'06*]. This temperature is approximately the maximum temperature at which low-power silicon or conventional gallium arsenide devices can operate reliably. The intrinsic carrier concentration for several semiconductors as a function of temperature is shown in Figure 2. It is clear that the silicon have the highest number of intrinsic carrier concentration at the lowest temperature compared to the other presented materials.

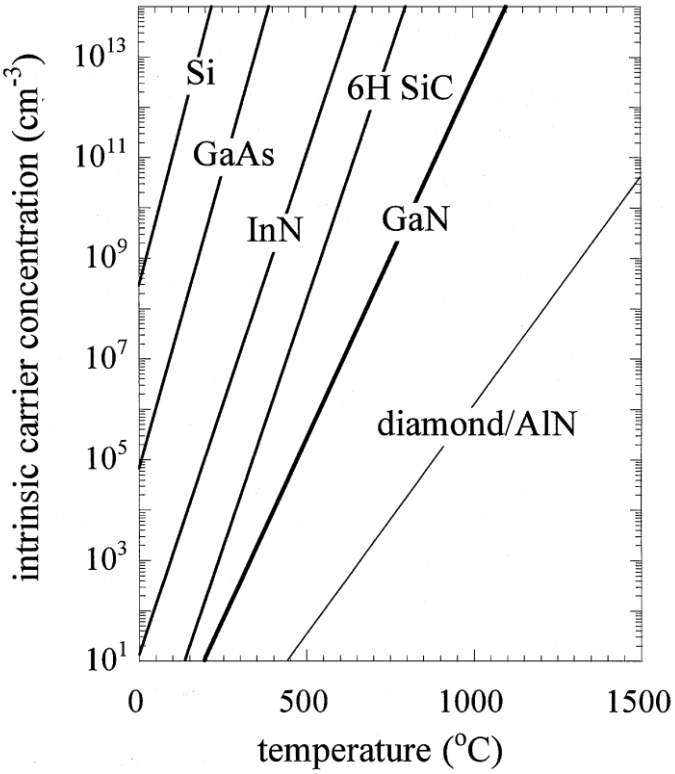

Figure 2: Intrinsic carrier concentration as a function of temperature of several semiconductors [Zolper'98]

In the beginning of the 21st century the third generation of semiconductors was introduced with silicon carbide (**SiC**) and gallium nitride (**GaN**) being the semiconductors with wide-band-gap, of 3.25 eV for 4H-SiC [*Ng'03*] and 3.65 eV for 2H-GaN [*Ke'96*], making a revolution in the electronic and optoelectronic industries. **SiC** consists up of a large substrate made of the same material with the presence of SiO_2, both n- and p-type conductivity may be created in **SiC** where any type of semiconductor power device may be created. With each year, their quality improves, and their diameter increases. Today, diameters of about 100 mm are possible [*Silva'15*]. Many attempts are done to obtain a fully functional **MOSFET** [*Baliga'98*] [*Rebello'96*] and **IGBT** [*Zhang'05*] [*Zhang'08*] based on SiC technology. As researches are still studying their advantages and their drawbacks some **IC**s are assembled where the primary **IGBT** modules were replaced by hybrid Si **IGBT**/SiC Schottky modules, due to the overall gain in the efficiency [*Sugawara'01*] [*Elasser'02*]. The

fourth expected generation of semiconductors is the diamond with its superior properties; many researches are done nowadays to advance the use of diamond in the semiconductor electronic field [*Willander'06*].

As discussed previously the power electronic modules are used in a diversity of electronic products. Let's consider the example of **IGBT**, its symbol is represented in Figure 3, it is a unique type of power electronics and has good characteristics for applications such as invertors.

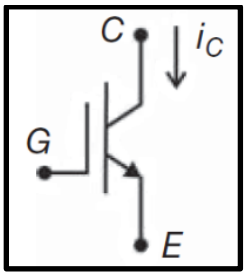

Figure 3: The symbol of IGBT

IGBTs offer low switching losses and a simplified gate circuit [*Yilmaz'90*] [*Muni'91*] [*Petterteig'91*]. The switching frequency operation decreases quickly with the blocking voltage. For 6.5 kV, the maximum frequency is typically of 1 kHz compared to some 10 kHz for lower blocking voltage. It is one of the most significant developments in device technology during the last decades, which blocks high voltages but at the same time has a high conduction current. The device operates between 600 V and 6.5kV where the current varies over 1–2200 A [*Fabian'05*] [*Willander'06*]. The isolation has to be reliable during the operational time of the module under severe mechanical, thermal and chemical stress, which makes it necessary to carefully select the materials involved in the module design. An **IGBT** module can be used in several electronic applications. Nowadays, a lot of researches are performed to improve the reliability of the converters for applications intended to the HVDC links and high integration converters. In all the cases the reliability of the insulation is a key point.

Figure 4 illustrates an example of the use of an **IGBT** in an **HVDC** system. The **IGBT** in this case works as an inverter of DC to AC. The voltage-source-converter **VSC HVDC** is a relatively new development that came after the development of the insulated gate bipolar transistor (**IGBT**) for high power applications [*Hertem'10*]. The converter delivers a constant DC voltage and the current is controlled to alter the power flow.

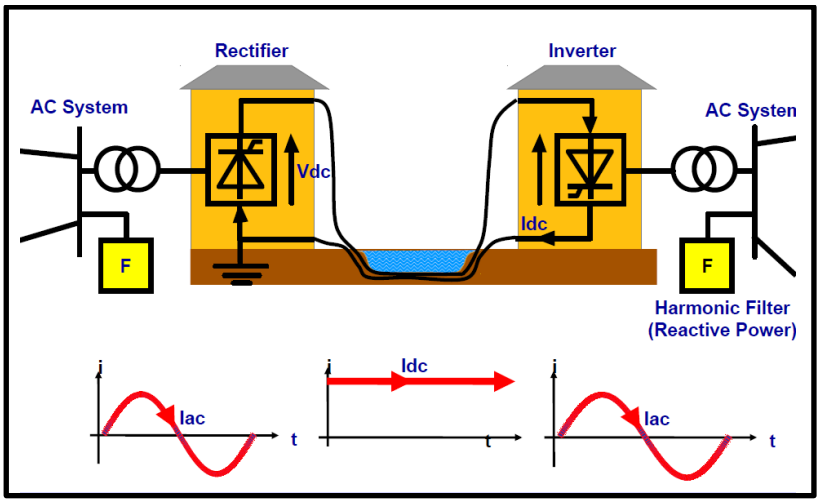

Figure 4: Scheme representing a system that converts alternating current to direct current and back in an HVDC system [Hertem'15]

Another important example of the use of an **IGBT** module is within the airplane's motor nacelle which is a non-pressurized zone of an airplane. A complete invertor box containing the **IGBT** module is therefore subjected to strong combined constraints: thermal, mechanical (vibrations and shock) and pressure/depression/damping [*Lhommeau'05*]. Future aims are to replace the mechanical or hydraulic systems by electronic devices which would result in increased performance and reduced weight of the system. However, this novel designs would imply placing power electronics devices near the actuators or close to the engine. This location will incur the device in harsh environmental constraints, involving extreme thermal excursions. Another application field for the IGBT is the railway device where components have to be efficient in spite of the harsh environment where voltage and temperature can be high. Power modules, specifically an IGBT, are subjected to be used in different electrical, thermal or mechanical environment and thus need to be able to work properly under all different circumstances.

1.1.2. Structure of power module (IGBT)

The assembly structure of an **IGBT** module, presented in Figure 5, has to be perfectly assembled to meet the operating requirements of the component. The design of an IGBT must take into consideration the properties of each component as well as the environmental constraints. A typical IGBT module consists of three layers soldered on according to the following sequence: Active chips (**IGBT** and Diode), metalized ceramic (AlN, Al_2O_3 …) substrate and a base plate. A primary thin passivation layer of polyimide covers the active elements, a relatively thick encapsulation layer often composed of silicone gel covers the

whole module and finally the total assembly is covered with a plastic box. The choice of the components depends on the electrical, thermal and mechanical aspects.

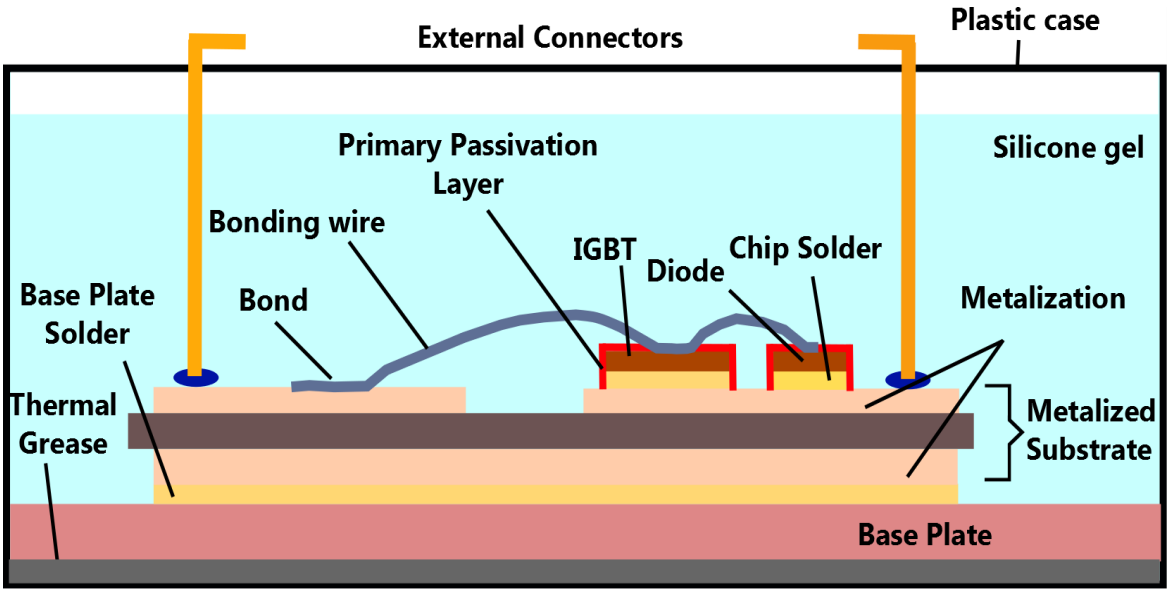

Figure 5: Cross section of an IGBT module

1.1.2.1. Semi-conductor Chips

The semiconductor is metallized with a layer of few hundreds of micrometers from both sides. **Si**, **SiC** and **GaN** are the three common used materials for power modules. **Si** can operate up to 250 °C with low voltage applications of the order of 100 V, while it can operate only up to 150 °C for higher voltage values of the order of 1000 V. On the contrary **SiC** can function normally up to a temperature of 650 °C under high voltage applications higher than10 kV [*Wondrak'99*]. Table 1 presents the Physical properties of the susceptible used semiconductor materials in a chip.

Table 1: Physical properties of semiconductor materials at 25 °C [*Dupont'06*] [*Diaham'07*] [*Watanbe'04*[1]] [*Li'87*[2]] [*Yam'11*[3]] [*kidalov'09*[4]]

Physical properties	Material					
	Si	**4H-SiC**	**6H-Sic**	**3C-GaN**	**2H-GaN**	**Diamond**
CTE (ppm/°C)	2.63[1]	3.09[2]	3.18[2]	3.17[3]	3.7[3]	1.1[4]
Thermal conductivity ($W.m^{-1}.K^{-1}$)	150	450	450	130	130	2000
Breakdown Voltage (kV/mm)	20	200	240	100	330	560
Energy Band Gap (eV)	1.1	3.26	3	3.27	3.29	5.45

1.1.2.2. Substrates

The substrates insure the electrical insulation between the semiconductor chip and the base plate (generally grounded). It should have a coefficient of thermal expansion (**CTE**) of the same order of magnitude as with all the other components of the module to avoid differential expansion. The chemical stability with increasing temperature must also be ensured. High resistivity to reduce the leakage current and a high dielectric strength to withstand the voltage are required. In addition to that the mechanical strength must be as high as possible to resist the constraints of handling. There are four common ceramic substrates, used in an **IGBT** module: Aluminum oxide or alumina (**Al_2O_3**), aluminum nitride (**AlN**), beryllium oxide or beryllia (**BeO**) and silicon nitride **(Si_3N_4)** [*Chasserio' 08*] [*Ménager'10*]. A metallization layer is deposited on both sides of the substrate which is classically made up of a copper layer using **DCB** (Direct Copper Bonding); nevertheless some researches are done to replace this layer with Aluminum (Al) using **DAB** (Direct Aluminum Bonding) [*Lhommeau'05*] [*Boettge'13*]. Table 2 presents the physical properties of common used insulating ceramics. **AlN** is the ceramic substrate mostly used by the industry with either copper or aluminum metallization.

Table 2: Physical properties at 25 °C of insulating ceramics used as substrates [*Dupont'06*] [*Occhionero'99*]

Physical properties	Material			
	Al_2O_3	**AlN**	**BeO**	**Si_3N_4**
CTE (ppm/°C)	7.5 – 8.1	4.2 – 5.2	6.8 – 7.5	2.7 – 3.4
Thermal conductivity ($W.m^{-1}.K^{-1}$)	20 – 30	170 – 260	250	60
Breakdown Voltage (kV/mm)	11 – 16	14 – 17	10 – 14	15
Young's modulus (GPa)	300 – 400	300 – 310	300 – 350	300
Bending strength (MPa)	250 – 300	300 – 500	170 – 250	> 700

1.1.2.3. Base plate

The base plate is soldered to the inferior layer of metallization of the substrate from one side and from the other side it is connected to the cooling system. Its role is to insure the mechanical stability of the module. However; it should also have compatible physical properties with the other components of the module (thermal and mechanical properties) insuring a low thermal resistance. Some of the used base plates in the industry are aluminum silicon carbide (**AlSiC**), copper – tungsten (**CuW**), copper-molybdenum (**CuMo**) or Kovar

which is a nickel–cobalt ferrous alloy [*Hopkins'06*] [*Ménager'10*]. Table 3 presents the physical properties of used base plates. The good choice of base plates increases the lifetime of the device.

Table 3: Physical properties of base plates at 25 °C[*Occhionero'99*]

Physical properties	Material			
	AlSiC (60% SiC)	CuW (10 – 20 % Cu)	CuMo (15 -20 % Mo)	Kovar
CTE (ppm/°C)	6.9 – 9.9	6.5 – 8.3	7 – 8	5.2
Thermal conductivity ($W.m^{-1}.K^{-1}$)	150 – 180	180 – 200	160 – 170	11 - 17
Young's modulus (GPa)	175 – 207	367	313	131

1.1.2.4. Solders

Soldering is one of the delicate processes in the buildup of a module, as the choice of solders as well as the technology used in this process is crucial to the reliability of the assembly [*Herr'97*] [*Hamidi'99*]. The semiconductor material of the active chip must be soldered to the substrate with a material electrically conductive, having a high physical resistance to temperature, and imparting little stress on them. Many materials and technologies could be candidates of this process [*Hopkins'06*] [*Coppola'07*]. A common used solder for high temperature applications, up to 250 °C, is an alloy of lead, silver and tin (95,5Pb/2,5Ag/2Sn) [*Ménager'10*], its physical properties are presented in Table 4.

Table 4: Physical properties of 95,5Pb/2,5Ag/2Sn at 25 °C[*Coppola'07*][*Ménager'10*]

Properties	CTE (ppm/°C)	Thermal conductivity ($W.m^{-1}.K^{-1}$)	Electrical resistivity (µΩ.cm)	Young's modulus (GPa)
95,5Pb/2,5Ag/2Sn	30	23	29	16

1.1.2.5. Internal Connections

The most common power interconnection method is wire bonding using either **Au** or **Al** [*Mustain'05*]; their physical properties are presented in Table 5. Electrical interconnections associated by aluminum wire bonding have a diameter between 100 µm to 500 µm, shown in Figure 6 soldered on the semiconductor chips. Concerning modules with high currents; wire bonding can be replaced with stripes of 1 mm width [Amro'05].

Table 5: Physical properties of selected wire bonding materials [*Coppola'07*]

Properties	CTE (ppm/°C)	Thermal conductivity ($W.m^{-1}.K^{-1}$)	Electrical resistivity (µΩ.cm)	Young's modulus (GPa)
Al	24	240	2.6 – 4.3	68
Au	14.5	310	2.2	77

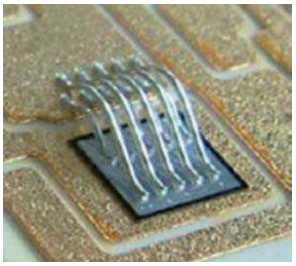

Figure 6: Aluminum wire bonding [*Amro'05*]

The maximum continuous temperature in which the module components can work normally is represented in the graph of Figure 7. After preparing the whole assembly with considering all the physical, mechanical and thermal properties of each component, the active elements will be covered with a first passivation layer. After all, the whole system embedded in a plastic box will be encapsulated by an insulating material to insure the isolation protection against potential differences. The plastic cover protects the system from moisture and contamination. A module covered with an insulating material (silicone gel) is shown in Figure 8.

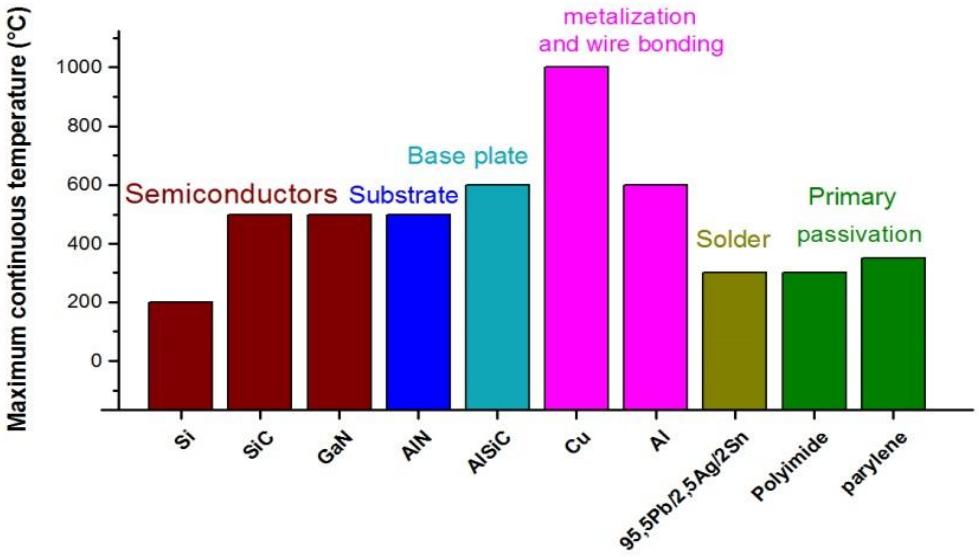

Figure 7: Maximum functioning temperature of power module components [*Dupont'06*] [*Ménager'10*] [*Diaham'12*] [*Diaham'14*]

Figure 8: Power module covered with insulating silicone gel [Ménager'10]

A commonly IGBT module, discussed in the following paragraph, consists of an AlN substrate metalized with Cu, a base plate made from AlSiC, soldered with 95,5Pb/2,5Ag/2Sn and interconnected with aluminum wire bonding.

1.1.3. Encapsulation

The encapsulation material replaces the presence of air and thus is used to enhance the electrical insulation between various conducting elements with high potential differences in the power module. A primary passivation layer deposited on the superior surface of the electric chips is used as a complementary insulating layer to decrease the possibility of electrical breakdown and to limit current leakage on the surface. As the high current running in a power module creates a heat load that requires dissipation, the encapsulation layer plays a leading role in thermal management. Final plastic box is used for external environmental protection.

1.1.3.1. Primary passivation layer

Polyimide, **PI**, is one of the most used materials as primary passivation layer; a lot of studies are done to adapt its properties with the high temperature – high voltage demands. Parylene is another material that is under study to be used for the passivation purposes and many researches studies are done to adapt it with the modules.

Polyimide:

Many studies have been made to evaluate the electrical properties of **PI** starting from 1970s [*Hanscomb'73*] [*Sawa'80*], due to its compatibility with semiconductor manufacturing process and the reliability of the resulting devices. There are several types of **PI** that have different **CTE**, glass transition temperature (**Tg**) and other characteristics depending on the precursor and the hardener used. The **CTE** of **PIs** is between 3 and 6 ppm/°C [*Numata'86*]. These values are small and in the same range of the **CTE** of the chips and the substrates used in a power module which makes it a compatible material. The deposition of polyimide can be realized using spin coating technique to obtain, after several depositions, few to tens of µm. One example is in the work of Diaham et al. where after three depositions a 4 µm layer of **PI**, **BPDA-PDA** (*BPDA: 3,4,3',4'-biphenyltetracarboxylic dianhydride – PDA: p-phenylenediamine*), is deposited on a diode **SIC** [*Diaham'12*]. **PI** is known for its low dielectric constant ≈ 2.3 at room temperature [*Diaham'13*] [*Chen'15*]. Breakdown voltage of **PI** depends strongly on the thickness as well as the surrounding temperature. For a **PMDA-ODA PI** (*poly (pyromellitic dianhydride-co-4,4'-oxydianiline)*) with a thickness of 25 µm, the breakdown voltage at room temperature is 2.7 kV/mm [*Chen'15*]. Various measurements were made at elevated temperatures on different thicknesses varying from 1 to 10 µm. As observed for different materials, the breakdown voltage of BPDA-**PDA** at 300 °C, below its **Tg** > 330 °C, decreases with the increase of the thickness as illustrated in Figure 9 [*Diaham'12*].

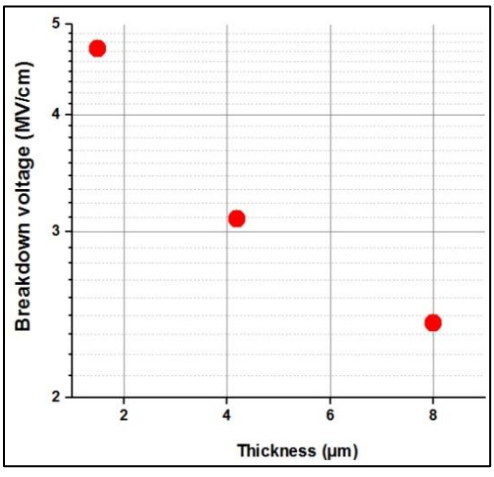

Figure 9: Breakdown field in air for three different thicknesses of BPDA-PDA measured at 300 °C, knowing its Tg is 330°C [*Diaham'12*].

Due to its high glass transition temperature ≈ 330°C, **PI** has physical and chemical stability under a wide range of temperature. This is one of its advantages for using it for high temperature power electronic device insulation. An aging experiment for polyimide,

BPDA/PPD (*biphenyldianhydride/1,4 phenylenediamine*), was tested and showed that when aged at 350 °C in an air chamber, it decomposed and completely volatilized after 100 h, showing that it was not suitable for applications at 350 °C and higher [*Johnson'07*]. Its low dielectric permittivity, its flexibility and good resistance to stretching make it a good candidate to support thermomechanical deformation below its T_g. Nevertheless; the thickness of the deposited film cannot be thick enough to cover the whole assembly including the electronic connectors. PI cannot be used alone to protect the module where another encapsulation layer, such as silicone gels, is usually deposited above the **PI** layer.

Parylene:

Over the last four decades, researches and development resulted in many types of Parylene but only three of them were widely commercialized (parylene N, C and D) [*Kumar'04*]. New studies developed and commercialized new kinds of fluorinated parylene such as parylene HT and parylene-VT4. Parylene-VT4 can be deposited using **CVD** chemical vapor deposition process to form a thin film of 2.74 µm thickness [*Kahouli'14*]. Parylene HT can be deposited using **VDP**, vapor deposition polymerization, and a maximum of 50 µm can be obtained with a speed of 1µm/h as demonstrated in the work of Kumar et al. [*Kumar'09*]. The **VDP** technique gives the deposited film good planarization [*Yang'98*]. Both deposition methods are time consuming and cannot provide thick enough layers. Parylene material is known for its high breakdown voltage due to the high purity of the material. Parylene PA-HT points out a breakdown field, varying from 480 kV/mm to 1000 kV/mm at room temperature depending on the thickness used as shown in Figure 10 [*Diaham'14*].

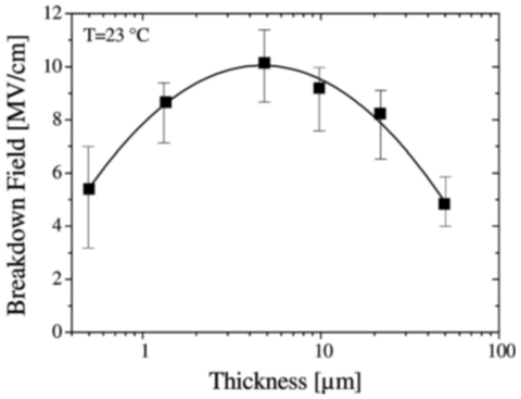

Figure 10: Thickness-dependence of the DC dielectric strength for PA-HT films. Error bars represent the minimum and maximum values obtained for each thickness [*Diaham'14*]

It has high electrical resistivity of 2.10^{17} Ω.cm and a low dielectric constant of 2 -2.4, **PA-HT**, [*Kumar'09*]. These compatible characteristics with the need in a power module are accompanied with a relatively high **CTE** value of 36 ppm/°C at room temperature that is only consistent with the wire bonds used [*Kumar'10*].

1.1.3.2. Encapsulation Layer: Criteria

The main goal of the encapsulating process is to protect the system, precisely the active chip and the wires, from increased potential difference between conductors. It also provides a safe protector from the harsh environment, like moisture, chemicals and gases. Different families of materials are studied and are susceptible to be used for this purpose such as silicone gels, silicone elastomers, polyurethane and acrylic [*sheng'04*]. Nevertheless, many criteria have to be considered before choosing the material, such as the deposition technique and temperature, electrical, thermal and mechanical properties. The chosen material must also possess low moisture absorption, low gas permeability and high chemical resistance.

A. Deposition

The first criterion of the deposition process is to be able to obtain a thick layer of the encapsulation layer of couple of millimeters to insure covering the whole assembly including the connecting wires. For this reason polyimide and parylene, as discussed previously, are not good candidates. Furthermore, the temperature of elaboration must not exceed the maximum temperature that the weakest power module components can endure. Thus, if the module includes the presence of **Si** chip then 200 °C must be the maximum temperature applied during the deposition process. In all the other cases 300 °C is the maximum temperature allowed because it's the maximum supported by the solders as seen in **Figure 7**. Careful cleaning before encapsulation, to avoid the presence of impurities, is vital to ensure long-term reliability. The easier the way of deposition is, the better for the fabrication process is.

B. Electrical properties

The encapsulation material replacing the presence of air must insulate different potentials present between different conducting zones such as the surface of the chips and the connecting wires. To insure low capacity of the encapsulation material the dielectric constant must be low. It must have high breakdown voltage, few hundreds of kV/mm, to confirm high insulation; in addition to possessing high electrical resistivity greater than 10^{12} Ω.cm under all

accepted temperature variations. To avoid electrical losses, the material should have low imaginary dielectric constant associated with low **DC** (Direct Current) conductivity values.

C. Mechanical and thermal standards

The **CTE** of the material must be compatible with the other components of the module, and if it is not the case, the material must have high flexibility, such as silicone gel which will be discussed in the following paragraph. During temperature-cycling, each material tends to expand and contract according to its own thermal expansion coefficient and exert thermo-mechanical stress onto other components, thus any excess stress might present cracks in the system which will lower the electrical reliability. The power modules are subjected to a wide range of temperatures, - 50 °C to 300 °C, depending on its environment such as in aeronautics; accordingly the encapsulation material must exhibit good thermal stability within these limits.

1.1.3.3. Nowadays used encapsulant: the silicone gel

Dielectric silicone gel is one of the most reputable and effective materials used as encapsulation material in a power module, chosen for its flexibility that does not induce thermomechanical stresses [*Ning'10*] [*Xu'13*] [*Li'15*]. It is a fluid polymer partially crosslinked made up of polydimethylsiloxane (**PDMS**), its chemical structure is presented in Figure 11. It is known with its easy way of preparation: filling the liquid in a controlled environment, degassing it at room temperature and finally crosslinking at room temperature or at 65 °C to obtain a stiffer material, which is a convenient feature to the thermal criterion needed [*Wang'04*].

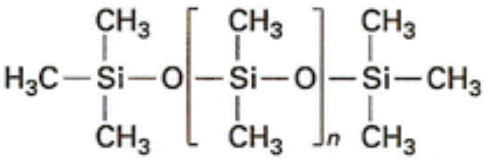

Figure 11: Chemical structure of PDMS

Silicone gels are known to be self-healing material. When the electrical breakdown in silicone gel causes decomposition of the material that gives rise to the formation of gas that result in the presence of voids. These voids vanish with time and the silicone gel can regain its insulating properties as shown by Ebke et al. [*Ebke'00*]. It has a low dielectric constant 2 – 4 under a frequency range of 1 Hz to 60 MHz [*Locatelli'14*]. Few studies dealing with high temperature electrical characterization on silicone gels are present, showing that the

maximum temperature for continuous use is 200 °C [*Vanlathem'12*] [*Yao'12*] [*Li'15*]. Their volume electrical resistivity is favorable for the application with a value of 10^{15} Ω.cm at room temperature [*Chu'13*]. Along with all these conveniences, it also has some drawbacks for the reliability of the module. The first major drawback is the low breakdown voltage of 15-20kV/mm at room temperature. The second drawback corresponds to the DC conductivity value which is higher than 10^{-12} S/cm above 60 °C and increases with the temperature as shown in Figure 12. The third one is that typical silicone gel has high value of CTE of more than 200 ppm/°C, which is higher than all the components present in a power module.

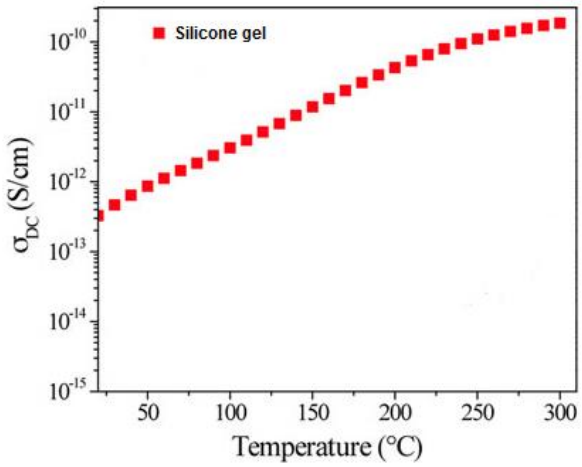

Figure 12: Temperature dependence of the dc conductivity for silicone gel (derived from σ_{AC} (f) at 0.1 Hz during cooling) [*Locatelli'14*].

1.1.3.4. New proposed materials for encapsulation material at high temperatures

In the recent years, high-temperature operation of power module is needed to enhance performance of the module. SiC for example enables the development of smaller chips that are capable to withstand much higher electrical field compared to the silicon chips currently available. High voltage SiC modules are making major revolution [*Kimoto'14*] [*Mad'12*]. For example, Ryu et al. presented a 1 cm x 1 cm 4H-SiC N-IGBT exhibiting a blocking voltage of 20.7 kV [*Ryu'13*]. To meet their high voltage and high temperature requirements many researches are operated to adapt the characteristics of the power module substituents.

We must notify that, some studies are taking place and going to develop the use of silicone gel and replace it with silicon elastomers that can stand up to 300 °C [*Keyrouz'11*]. Another example is demonstrated by Wang et al. attempting to replace silicone gel (encapsulation) by

silicone gel filled with 15 vol% of barium titanate to reduce the electric field enhancement at the edge of the substrate metallization. They showed an increase in breakdown voltages introducing barium titanate. Viscosity of the gel has increased but the gel is still applicable and is considered as a promising route for the future [*Wang'10*]. Other studies have proposed novel architecture for the metalized ceramic substrate that is in direct contact with encapsulating gel and the metallization [*Hourdequin'16*]. A newly **IGBT** module combined with liquid epoxy resin encapsulation replacing silicon gels was performed , where they have developed an insulating metal baseplate (**IMB**) that replaces the conventional base plate – soldering – substrate combination [*Kaji'16*]. The new proposed module is presented in Figure 13. They showed that the **IMB IGBT** module has large mounting area, and epoxy resin encapsulation can reduce the solder crack under the semiconductor chip at heat cycle testing. The kind of epoxy tested was not demonstrated in their work, while they have mentioned the use of acid anhydride hardener.

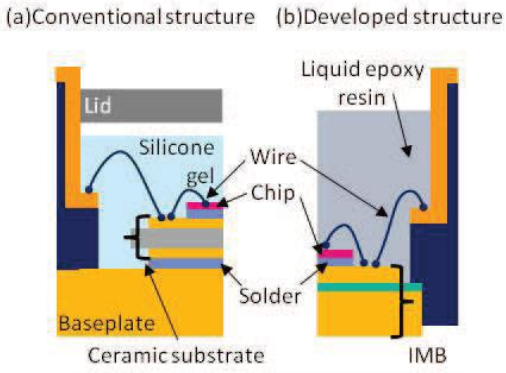

Conventional	Developed
chip(2~3ppm)	
solder	
ceramic substrate (≈7ppm)	IMB (≈17ppm)
solder	–
Baseplate(17ppm)	

Figure 13: Cross-sectional views of IGBT modules proposed by Kaji et al. [*Kaji'16*]

In this work, we focus on a novel material that can be a candidate to replace the primary passivation layer and/or the encapsulating gel. The material is an organic-organic polymer blend with phase separation phenomenon. The second part of this chapter will explain more the general properties and uses of this kind of proposed material.

1.2. Polymer Composites and Polymer Blends

Composites, in general, are made up of materials combinations differing in their properties, where the individual constituents retain their separate identities. There are several families of composites. Metal matrix composites (MMC) that are attractive materials for automotive, aerospace, and many other applications due to their superior mechanical and physical properties [Ibrahim'91] [Lindroos'95]. Ceramic matrix composites (CMC) are used in many high temperature applications due to their very high thermal shock and creep resistance, which enable designs with large mechanical and thermal loads. Another material combination is the polymer composites or polymer blends. They are two types of material combination being one an organic – inorganic mixture and the latter an organic – organic blend. They differ in their compositions and thus in their applications and characteristics.

Epoxy composites and blends, are interesting materials that are going to be developed in the following paragraphs. There are several advantages using them as composites with inorganic fillers or blending them with an organic material. Epoxy/filler composites studies can be divided into three major different groups depending on the size of the filler used, being micro-sized, nano-sized or a combination of both micro and nano-sized fillers. They are extensively studied to show the influence of the fillers on different properties of the epoxy network and precisely the thermal and electrical ones. Knowing that, epoxy resin is a common electrical insulating polymer, which is used in high voltage cast resin transformers, cable joints, terminations and other accessories. On the other side polymer blends and especially epoxy/thermoplastic blends are also extensively studied to show the influence of incorporating a thermoplastic on the mechanical, thermal and solvent resistance properties of the epoxy network.

In the following part of this chapter some examples of the influence of incorporating inorganic fillers into the epoxy network is going to be presented. The influence of the size, shape, modified or non-modified fillers and the percentage used on the mechanical and electrical properties of the epoxy matrix will be discussed. Due to the criteria needed for an encapsulating material, the following characteristics values will be investigated: the real and imaginary parts of permittivity, DC conductivity and resistivity, breakdown voltage, mechanical and thermal properties. Few studies analyze the electrical properties of an epoxy/thermoplastic polymer blend network and thus we will be interested in the influence of such blends on the morphology, thermal and mechanical properties of the epoxy network

[*Mac'92*] [*Lestriez'98*]. In the following chapters, the electrical properties of an epoxy/thermoplastic blend are going to be illustrated.

1.2.1. Polymer composites based on a mixture of polymer/fillers.

Polymer composites employed in several technological applications are used as electrical insulators in the power industry incorporating inorganic fillers to achieve specific electrical, mechanical, thermal properties and sometimes to reduce the cost. Their properties thus depend on the nature of the inorganic filler, starting from its chemical composition, to its size, shape, kind of dispersion in the matrix, interaction with the polymer and their physical properties.

Epoxy/inorganic composite, with nano and micro sized fillers, have shown mechanical and thermal improvement in comparison to conventional composites and have gained more attention in many applications. Addition of these kinds of fillers in the formulation reduces cost and improves for example fire resistance. Khan et al. showed how the mechanical properties of an epoxy matrix have been improved with the incorporation of ceramic nanoparticles [khan'15]. They filled the epoxy with four different kinds of ceramics, zirconium dioxide ZrO_2, zinc oxide ZnO, ferric oxide Fe_2O_3, and silica SiO_2, having the same size of 50 ± 5nm. Good dispersion was proven using 2 wt% of the nanoparticles with an increase in the elastic modulus and hardness of the material. The addition of silica in the epoxy matrix showed higher values than neat epoxy and the rest of epoxy composites as shown in Figure 14. In addition to that better thermal stability was achieved with the addition of silica in comparison with the other nanoparticles. During the last decade, some extensive researches were performed to improve the fracture toughness of epoxies with the addition of inorganic fillers, showing increase in the modulus and the glass transition temperatures [Lee'01] [Kinloch'03] [Bala'05].

The field of dielectrics and electrical insulation took advantage from the evolution of the epoxy – inorganic nano/micro composites domain. Many investigations were and are still performed to show and compare the effects of micro, nano and/or micro and nano fillers together on the final electrical characteristics of the epoxy network.

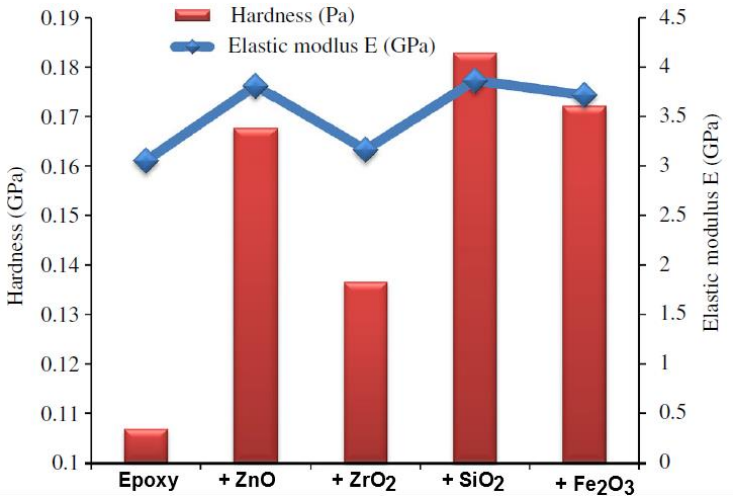

Figure 14: Comparison of hardness and elastic modulus for neat and reinforced epoxy samples [*khan'15*]

1.2.1.1. Epoxy Micro-composites

An investigation on the influence of the addition of different percentages of 20 µm sized silica, SiO_2, particles on the epoxy network is one example of epoxy micro-composites shown by Kochetov et al. [Kochetov'10]. As demonstrated in Figure 15(a), the relative permittivity values increased under the influence of 20 and 40 wt % of silica fillers. At 60 wt % of silica the relative permittivity value was reduced by 6% compared to the neat epoxy. The probable purpose of this decrease is that at higher amount of filler material the mobility of the chains would be limited, lowering the effective relative permittivity. Knowing that the relative permittivity value of the used silica at 1 kHz is 3.9, which is slightly higher than that of the epoxy at 1 kHz for example which is 3.4. The fillers showed the same influence on the epoxy matrix along with the variation of temperature up to 120 °C as shown in Figure 15(b). At high percentage of silica into the epoxy network, the system can be considered as silica with epoxy and not as epoxy modified with silica. The epoxy network presents only 40 wt% of the whole system and thus the final permittivity value cannot be compared to pure epoxy network since the majority of the network is not of epoxy.

With the addition of micro-fillers to the epoxy network, the relative permittivity of the epoxy micro-composite is always higher than that of the pure epoxy network as seen in several researches. An example of that is demonstrated by Singha et al. dealing with 0.5 µm Zinc-Oxide micro-particles [Singha'09], and 0.5 µm titania micro-particles [Singha'08]. Iyer et al. and Castellon et al. studied the influence of 16 µm micro-sized epoxy-silane modified silica particles on the epoxy matrix [Iyer'11] [Castellon'11]. They showed that even with

modified surfaces of micro-fillers, the introduction of micro-particles does not decrease the permittivity value of the composite; in the contrary they are increasing it.

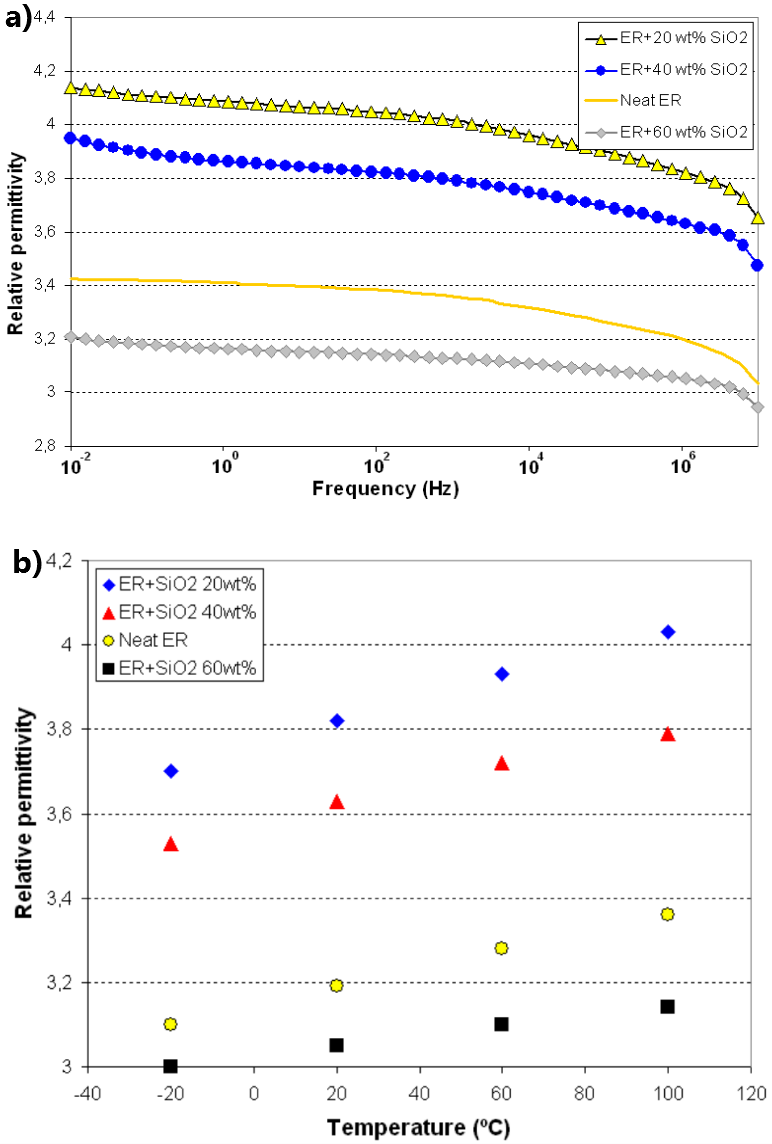

Figure 15: Relative permittivity of Epoxy/silica (ER-SiO_2) at 20 °C as a function of frequency (a) and at 1.15 MHz as a function of temperature [*Kochetov'10*].

Table 6 summarizes the values of permittivity obtained by different researches. A higher permittivity means higher capacity which leads to higher reactive currents and moving from insulating material to a semi-insulating one which is the case in the majority of the cited references.

Table 6: Comparison of different kinds of epoxy and kind of micro-fillers on the dielectric values

Ref	epoxy+ hardener	kind of filler	size	wt %	ε' @ 20 °C	ε''
Kochetov'10	Cycloaliphatic + anhydride	pure		0	3.2 @ 1MHz	-
		Alumina	4 µm	10-60	↗ 2.5 - 36 % with the same influence up to 120 °C	-
		Silica	20 µm	20 -40	↗ 19 % - 13 %	-
				60	↘ 4.7%	
Singha'09	Cycloaliphatic + tetramine	pure		0	4.4 @ 1kHz	-
		ZnO	0.5 µm	5	↗ 4.5 %	-
Iyer'11	Cycloaliphatic + anhydride	pure		0	3.3 @ 1kHz	↗ (10^{-3} - 10^{3} Hz) ↘ (10^{3} - 10^{4} Hz)
		epoxy-silane modified Silica	16 µm	65	↗15 %	
Singha'08	Cycloaliphatic + tetramine	pure			4.5 @ 1kHz	tan δ 0.02 @ 1kHz
		Titania	0.5 µm	5	↗ 33 %	↗ 250 %
				10	↗ 100 %	↗ 900 %

Breakdown tests were also performed to present similar decrease in the values with the increase of the percentage of micro-particles as shown in the work of Singha et al. on epoxy incorporated with 0.5 µm titania particles and 50 to 60 µm alumina particles [Singha'08]. They demonstrated that the addition of micro particles, that are considered naturally insulators, to the epoxy system with 10 wt % TiO_2 decreased the breakdown voltage of the epoxy network from 52 kV/mm to 38 kV/mm in an AC breakdown voltage test. This 26 % drop due to the incorporation of TiO_2 particles is lower than the effect of adding 5 wt % of Al_2O_3 that reduced the value by 37 %. Li et al. performed similar ac dielectric breakdown test but with the incorporation of 60 wt % of 10 µm sized alumina particles [Li'10]. They pointed out a 54% decrease in the breakdown value. Similar effect in the breakdown voltage was demonstrated in the work of Hu et al. with the incorporation of 10 wt% of 1.5 µm TiO_2 particles [Hu'06]. The presented decrease can be due to the introduction of defects by addition of micro-filler playing an important role in reducing the breakdown strength of composite. Table 7 presents a brief comparison of the influence of different kind of fillers used on the resistivity and breakdown voltage of the epoxy network.

The majority of micro-fillers incorporated to an epoxy network decreased the breakdown voltage value with respect to pure epoxy and increased the permittivity values. This kind of micro-composite is shown to be good for the mechanical achievements and not

to enhance the electrical properties, of an epoxy network, needed for an insulator used in the high voltage industry.

Table 7: Comparison of the effect of micro-fillers on the resistivity and breakdown values of different epoxy systems and micro-fillers

Ref	epoxy	kind of filler	size	wt %	resistivity	E(kV/mm)
Singha'09	Cycloaliphatic + tetramine	pure		0	7 x 10^17	AC 56 kV/mm
		ZnO	0.5 µm	5	↘ 75 %	↘ 45 %
Iyer'11	Cycloaliphatic + anhydride	pure		0	-	AC 37 kV/mm
		Epoxy-silane modified Silica	16 µm	65	-	↘8 %
Singha'08	Cycloaliphatic + tetramine	pure			7.5 x 10 ^17	AC 52 kV/mm
		Titania	0.5 µm	10	↘ 20 %	↘ 27 %
		Alumina	50-60 µm	5	↘ 27 %	↘ 38 %
Li'10	Cycloaliphatic + amine	pure			-	AC 203 kV/mm
		Spherical Alumina	10 µm	60	-	↘ 56 %
Hu'06	Cycloaliphatic + amine	pure			-	DC 330 kV/mm AC 230 kV/mm
		Titania	1.5 µm	10%	-	DC ↘ 10 % AC ↘ 15 %

1.2.1.2. Epoxy Nano-composites

Over the last decade, the interest in the use of nano-sized fillers as additives to polymer materials (nanocomposites) and specifically in an epoxy based material has increaed. An essential criterion in the preparation of this type of material is the uniformity in dispersion of the nanofillers in the epoxy network. Many families of nanofillers were studied, such as silica, alumina, titania, zinc-oxide, barium titanate and many more used in different nano sizes with or without surface modification. Some of the researches showed an enhancement in the electrical properties below critical percentages. However it has been reported that nanofillers have showed deterioration in the electrical characteristics of the epoxy network as well. One example is demonstrated by Katayama et al. where they studied the influence of three different surface treated nanoparticles on the electrical properties of the epoxy network [*Katayama'13*]. The fillers are surface treated in order to make their surfaces hydrophobic and compatible with the epoxy matrix. They have incorporated 5 wt % of nanoparticles to the

epoxy network. The three demonstrated nanoparticles are titania, silica and boehmite alumina {aluminum oxide hydroxide (γ-AlO(OH))}. Both titania and silica have spherical shape with a size of 50 nm and 14 nm respectively, while boehmite alumina had a plate like shape of 10x45x45 nm size. It is clear from Figure 16 that the relative permittivity (ε'_r) and the loss (ε''_r) are significantly higher with the incorporation of boehmite alumina and titania than in neat epoxy and epoxy with silica nanoparticles. The addition of silica nanoparticles did not decrease the values of the dielectric constant but relatively reduced the loss value at this concentration value of 5 wt %. Silica fillers have the smallest size of nanofillers used in the present research. It has the largest specific surface area with respect to titania and boehmite alumina and seems to have the strongest interaction with the epoxy matrix that would restrict the molecular motion of epoxy. This decrease in the loss factor at low frequencies with respect to the pure epoxy network is rarely found in literature for other similar kind of material at this concentration value. The compatibility between the fillers and the epoxy network is a key factor of the influence on the electrical properties. If the interaction between nanofillers and epoxy matrix is weak the opposite effect would occur. Weak interaction can lead to the presence of voids that have negative influence on the electrical properties of the epoxy network and can enhance higher breakdown voltages.

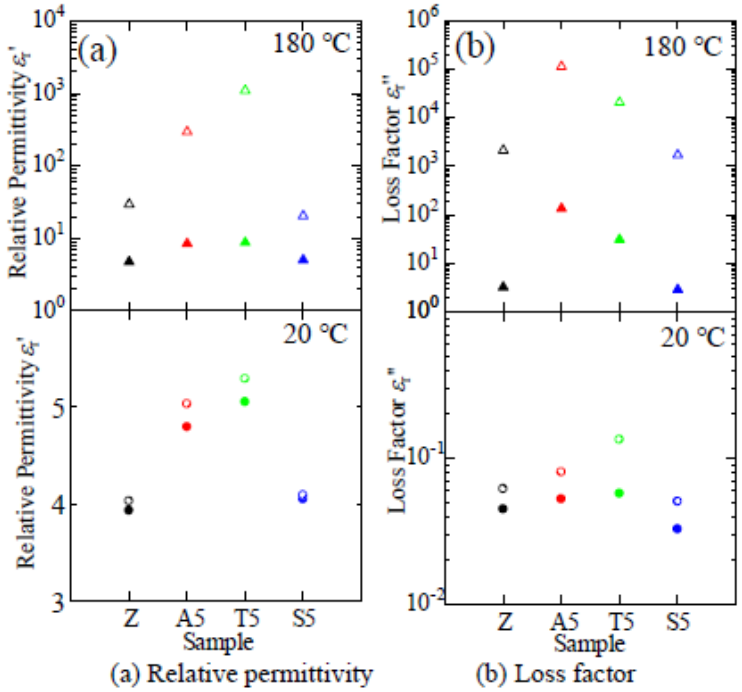

Figure 16: ε'_r (a) and ε''_r (b) measured at 0.1 Hz (open) and 63 Hz (solid). (Z) neat epoxy, (A5) boehmite alumina, (T5) Titania, and (S5) silica [*Katayama'13*].

More researches are to be done to explain this unique phenomenon, decrease of permittivity, as the way in which the particles interact with the polymer is not well defined.

The majority of studies dealing with the incorporation of nanoparticles to the epoxy network show that the decrease of the permittivity value takes place below a low critical percentage of nano-filler. Nevertheless, the value of the loss factor stays higher than that of neat epoxy network. Only a few studies indicated that it stays in the same range or relatively below as rare cases. Tsekmes et al. study the effect of boron nitride (**BN**) nanoparticles as fillers in an epoxy network [Tsekmes'14]. BN particles, with 70 nm diameter, were modified with EPPS ((3-Glycidyloxypropyl) trimethoxysilane) to improve the adhesion between epoxy matrix and the fillers.

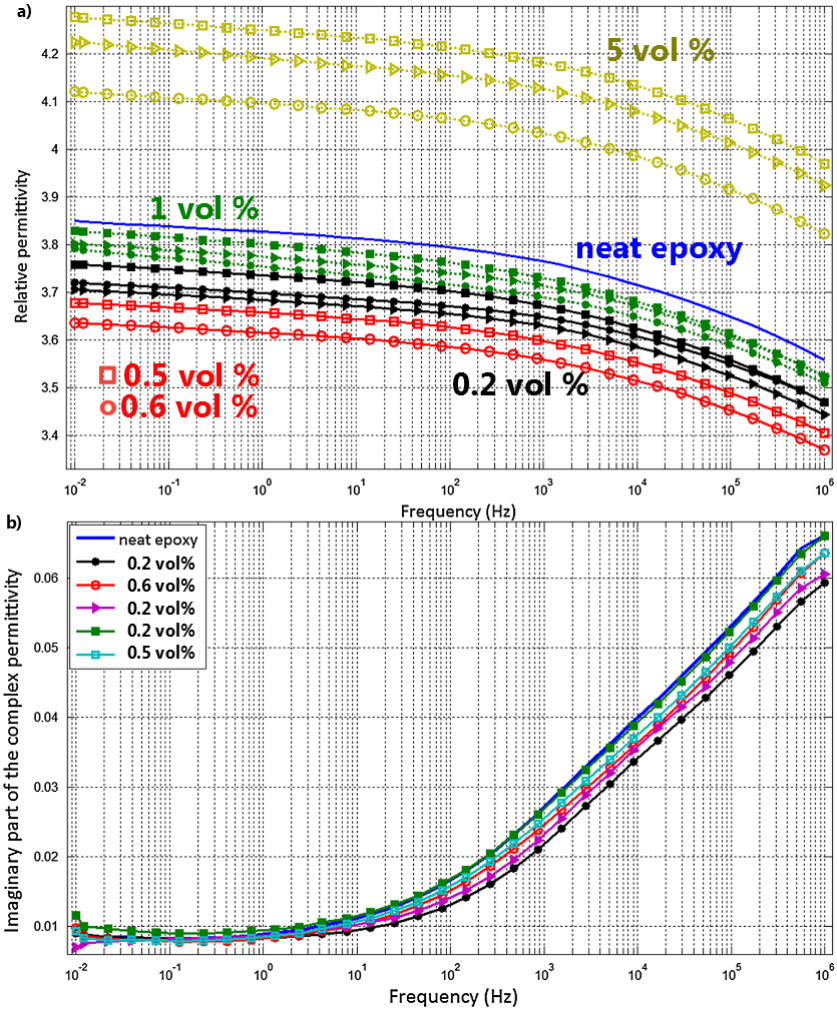

Figure 17: a) ε'_r of neat epoxy and all produced nanocomposites and b) ε''_r of neat epoxy and nanocomposites with <1 vol% (mixed in different techniques) filler at 20 °C [*Tsekmes'14*]

The used concentrations were 0.2, 0.5, 0.6, 1 and 5 vol % of nanofillers in the epoxy network. Mixing nanoparticles in the epoxy matrix using different techniques, speedmixer, solvent and nanomizer, did not lead to a significant effect of the dispersion process to the morphology of the composite. Slight differences can be observed on their dielectric response were explained by the amount of water uptake in the composite, rather than the particle distribution. Complex

permittivity values are presented in Figure 17. The nanocomposites with low filler concentrations (≤ 1 vol %) exhibit a lower relative permittivity (ε'_r) compared to the neat epoxy. Relative permittivity of epoxy composites decreased with the increase of filler percentage while the filler concentration is lower or egal to 0.6 % vol%. However, after this critical filler concentration, the relative permittivity starts to increase reaching values higher than the pure epoxy. The decrease in ε'_r values is attributed to the surface modification of the particles. Chemical bonding between the fillers and the epoxy chains results in the immobilization of the epoxy chains and thus decrease the relative permittivity. The specific surface area of the nanoparticles increases between 0.2 and 0.6 vol % and thus gives the capability to immobilize larger quantity of epoxy chains and decreases the value of the relative permittivity. Above this critical percentage (0.6 vol %) nanoparticles start to approach from each other and can form agglomerates decreasing the specific surface area and thus increasing relative permittivity values. Furthermore, the imaginary part was studied and divided into two different parts above the critical concentration and below it. Above, the imaginary part had higher values than the neat epoxy and below this critical value the nanocomposites exhibiting lower ε'_r values showed lower losses only at high frequencies. This decrease of the imaginary values at high frequencies is also due to the immobilization of the epoxy side chains in the proximity of particles. This result in the suppression of β-relaxation process and as consequence decreases the loss value.

This example was to show that the incorporation of nanoparticles with an epoxy network might decrease the permittivity values below critical concentration. Nevertheless, their effect on the imaginary permittivity is unstable and depends on the surface interaction between the fillers and the epoxy network, filler sizes and the frequency and temperature used. Other researches evaluated the influence of nano-fillers on the permittivity of the epoxy composites where several results explanations were demonstrated, like the work of Kochetov et al. on surface modified nanoparticles alumina, aluminum nitride and magnesium oxide [Kochetov'12]. Table 8 presents a comparison of the influence of different kinds of modified nanofillers on the relative permittivity values of the epoxy composite.

Table 8: Comparison of different kinds of epoxy and kind of modified nano-fillers on the dielectric values

Ref	epoxy	kind of filler	size	wt %	ε' @ 20 °C	ε'' @ 20 °C
Katatayama'13	Cycloaliphatic + amine	pure			3.9 @ 63 Hz	4.5 x 10^{-2} @ 63 Hz
		plate like shape **Bohemite alumina**	10 x 45 x 45 nm	3 - 5 %	↗ 23 %	↗ 11 %
		spherical titania	50 nm	3 - 5 %	↗ 31 %	↗ 50 %
		spherical fumed **silica**	14 nm	3 - 5 %	↗ 2.5 %	↘ 22 %
Tsekmes'14	Cycloaliphatic + anhydride	pure		vol%	3,75 @ 1kHz	0,026 @ 1kHz
		hBN	av. 70 nm 30 - 300 nm	0.2	↘ 1 %	↘1 4 %
				0.5	↘ 4 %	↘ 7 %
				0.6	↘ 5.5 %	↘ 11 %
				1	=	↘ 3 %
				5	↗ 11 %	↗ 4 %
kochetov'12	Cycloaliphatic + anhydride	pure		wt%	3,55 @ 1kHz	
		spherical **Alumina**	30 nm	0.5	↘ 2 %	the dielectric loss of the composites containing up to 5 wt% do not differ much compared to neat epoxy
				2	↘ 7 %	
				5	↘ 1.5 %	
				10	↘ 1.5 %	
		spherical, cubic, hexagonal **AlN**	60 nm	0.5	↘ 2 %	
				2	↘ 3 %	
				5	↗ 3 %	
				10	↗ 9 %	
		spherical and cubic **MgO**	22 nm	0.5	↘ 13 %	
				2	↘10 %	
				5	↘ 9 %	
				10	↘ 7 %	
		spherical **Silica**	20 nm	0.5	↗ 3 %	
				2	↗ 4 %	
				5	↗ 6 %	
		spherical **BN**	70 nm	10	↘ 1.5 %	

Breakdown voltage is also an important factor to study in epoxy/nano-composites because the filler concentrations as well play a huge role in effecting the breakdown voltage response. Nascimento et al. studied the effect of incorporating nano-particles having different diameters, 100nm Zinc-Oxide and 10 nm alumina nano-particles [*Nasciment'16*]. The concentrations used were 0.4, 1.2, 2.4 and 6 vol % for alumina composites and 0.2, 0.6, 1.2 and 3 vol % for ZnO composites. The breakdown voltage of the neat epoxy, made up of DGEBA as the epoxy resin and o-tolyl biguanidine, OTGB ($C_9H_{13}N_5$), as the hardener, was in the value of 47 kV/mm. The use of 0.4 vol% of alumina has increased this value with 45 %. Above 0.4 vol%, this value decreased and they obtained a similar value at 6 vol% in comparison with the pure neat epoxy. The incorporation of ZnO showed an increase of 25 % using only 0.2 vol %. In the same way, above this concentration the breakdown value with 3 vol % became lower than that of pure epoxy network. The results clearly show that the incorporation of nanoparticles must not exceed critical very low concentrations to increase the level of breakdown voltage. Moreover, the critical percentage below which electrical enhancement take place strictly depends on the size of the nanoparticle. The absolute number of particles would rise rapidly by a factor of 1000 by changing the particle size by a factor of only 10, such as 100 nm to 10 nm. The use of ≈ 3 vol % of 10 nm alumina increased the breakdown voltage with 20% while the use of the same percentage of 100 nm ZnO decreased the value by 20%. Due to its small size, 10 nm alumina didn't reach its percolation percentage at 3 vol% and influenced the breakdown voltage by decreasing it. When the diameter of the particles is small, e.g.less than 50 nm, they cause better influence due to the large interfacial regions at small particle loadings depending on their size, whereas larger size of nanoparticles (>50 nm) need very small critical percentages to increase the breakdown of the epoxy network [*Tsekmes'15-1*]. The smaller the particles are, the larger the relative interfacial layer and the larger the total interface volume are. Along with good compatibility between the epoxy and the filler, below critical percolation threshold values, fillers immobilize the movement of polymer chains and thus help in increasing the breakdown values. But above the percolation threshold the interfaces can act as a bridge and thus paths of conductivity are created leading to the decrease of the dielectric breakdown.

Dispersion phenomenon of the fillers is another critical character to consider for studying the influence of the fillers on the electrical properties of the epoxy network. Hu et al. show that incorporating 10 wt % of 23 nm TiO_2 in an epoxy network increased the breakdown voltage by 18% values [Hu'06]. Whereas Nelson et al., showed that using the same nanoparticle at the same amount, a decrease in the breakdown voltage of 12 % [*Nelson'04*] was pointed out. The

only difference between these two studies is the mixing method. Hu et al. obtained a better homogenous dispersion and thus increased the value of the breakdown voltage. Other researches highlighted an increase in the dielectric breakdown of nanocomposites compared to the neat epoxy matrix. Imai et al. demonstrated the influence of several kinds of fillers (ZnO, TiO_2 and layered silicate) of less than 20 nm size and showed an increase of breakdown voltage by 12 to 57 % using 5 and 7.5 wt% of nanoparticles respectively [*Imai'08*]. Even though, the size of nanoparticles was small with 20 nm, this increase in the breakdown values can be explained by keeping below the critical percentage above which aggregates were created. Other studies have also reported an increase of the breakdown values [*Ding'04*] [*Singha'09*] [*Iyer'11*] [*Tsekmes'15-1*]. Different studies using different percentages and different nanoparticles sizes showed a decrease in the dielectric breakdown of nano-composites in comparison with the neat epoxy network even at low weight percentages. In such case the explanation proposed is the presence of incompatibility at the interface between the epoxy network and the fillers, such as [Singha'08] [*Preetha'10*] [*Tuncer'07*] [*Tsekmes'15-1*].

Conflicting results on the performance of nanocomposite fillers have been reported and the underlying mechanisms are not adequately understood. As discussed, several factors can interfere with the influence of incorporating nanoparticles on the electrical properties of the epoxy network. In order to increase the breakdown voltage value or decrease the permittivity values, the nanoparticles should be relatively small (< 50 nm) and should have surface compatibility otherwise they will act as defects. Moreover adequate surface modification to the fillers can be added as well as adequate dispersion method to avoid aggregates or voids. Last but not least they should respect the critical small percentages above which aggregates can be formed.

1.2.1.3. Epoxy Nano/Micro-composites

From the previous discussions on micro and nano epoxy composites, it was noticed that micro filled epoxy suffers from low breakdown voltage along with an increase in the permittivity values. In the other hand some incorporation of nanofillers has showed some enhancement following critical conditions. For that reason in the last years some researchers suggested that the addition of nanofillers to a micro-composite epoxy mixture can be useful to raise the breakdown strength and decrease the permittivity. It was figured out that this nanofiller modification in a micro-composite epoxy increased the values of dielectric

breakdown but in general it has values lower than the neat epoxy network. The advantage of this kind of mixture was the increase in the thermal conductivity values and not the enhancement of the electrical properties of the epoxy composite. Guo et al. demonstrated the influence of adding 5 and 2 wt % of 30 nm alumina and 10 nm titania nanoparticles within an epoxy modified with 63 and 65 wt % of micro-alumina ranging from 12 to 21 µm [*Guo'14*]. The breakdown strength of the neat epoxy (69 kV/mm) has decreased by 17 % when loaded with alumina micro-fillers. With the addition of nano-alumina this value has increased 8% and decreased 4% with the addition of nano-titania, in comparison with epoxy-micro composite. In comparison with the presence of nanofillers only, nano-alumina has decreased the breakdown strength of the neat epoxy by 25% and nano-titania by 12% as shown in Figure 18. The higher the permittivity of the inorganic nanofiller is the better the breakdown strength is, knowing that the permittivity of alumina is 10 [*Thorp'90*] and the permittivity of titania is 100 [*Wypych'14*].

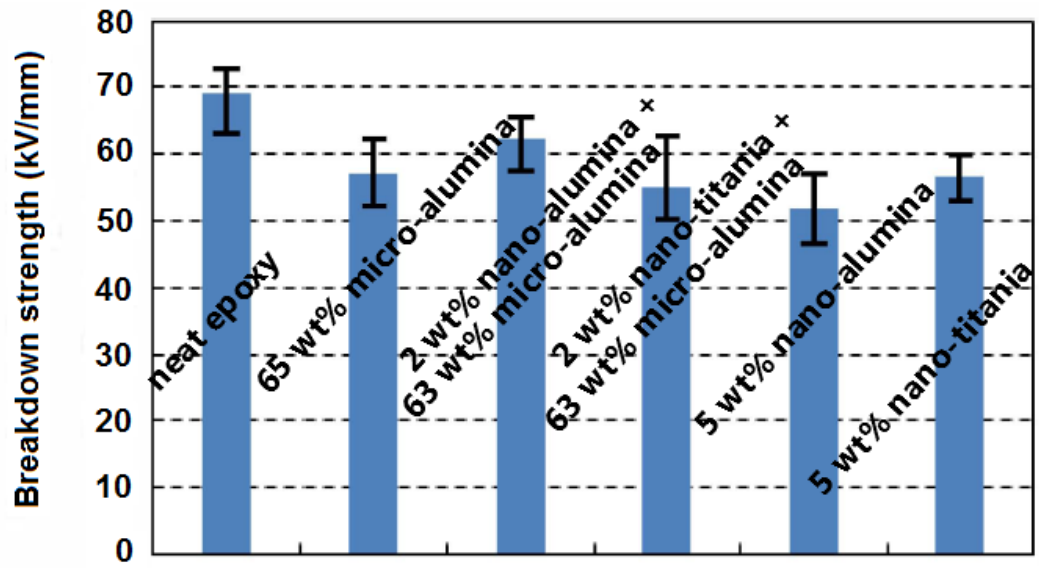

Figure 18: Breakdown strength of epoxy composites [*Guo'14*]

Similar effect was observed on the dielectric breakdown with the incorporation of nanofillers to a micro-composite epoxy, as described by Li et al. on nano-micro alumina/epoxy composite [*Li'10*] and by Tsekmes et al. [*Tsekmes'15-2*]. These later authors showed the influence upon adding nanosized hexagonal boron nitride (hBN) particles and mesosized cubic boron nitride (cBN) fillers on micro-alumina and micro-silica epoxy composites. Both hBN and cBN particles were modified with EPPS ((3-glycidyloxypropyl)trimethoxysilane) to improve the adhesion between the epoxy network and fillers. They have observed that the addition of small amounts of nanosized fillers (less than 1 vol %) improves both the thermal

and electrical behavior of micro-composites based on epoxy. Nevertheless, the breakdown values stayed lower than that of pure epoxy network. The dielectric values of nano-micro composites showed similar behavior, where the incorporation of nanofillers to a micro-composite epoxy decreased the value of permittivity in comparison to the micro-composite but stayed higher than that of the neat epoxy matrix, as shown in by Castellon et al. [*Castellon'11*]. They studied the influence of adding 5 wt% of nano-metric spherical silica fillers of 20 nm to an epoxy micro-composite containing 60, 62.5 and 65 wt% of silica having 16 µm sized treated with epoxy-silane for surface modifications. As shown in Figure 19, the addition of 5 wt% of nanoparticles has increased the permittivity values by 2% for the 65 wt% micro-composite and decreased it by 2% in the condition of decreasing the value of micro-particles to 60 wt%. The values were still higher than the relative permittivity values by 17% in average. This decrease in the permittivity values can be related to the decrease of the micro-particles in the epoxy network and it appears difficult to understand the real cause of this decrease in the value of the relative permittivity of the micro-composite.

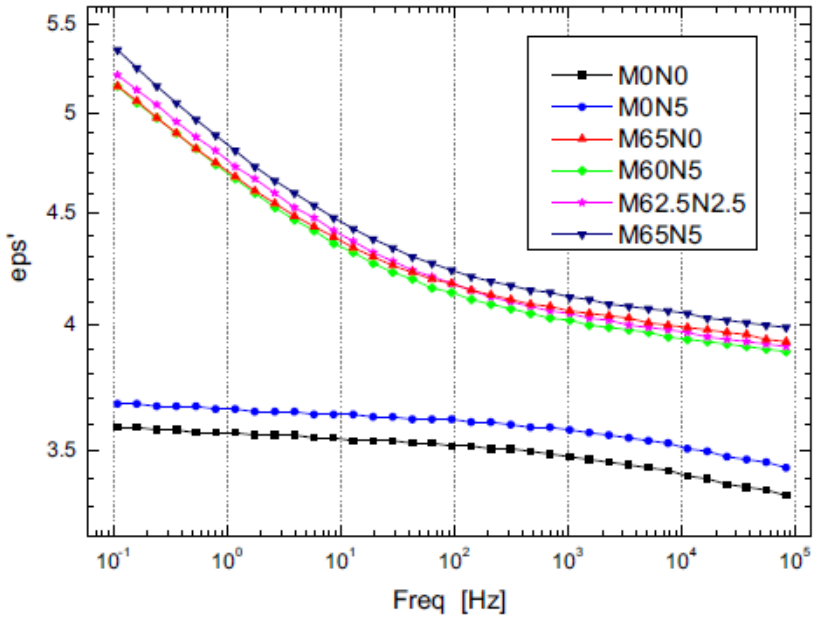

Figure 19: Real permittivity with respect to frequency at 40 °C. M0NO neat epoxy, M0N5 epoxy + 5 wt% nano-particles, M65N0 epoxy + 65 wt% micro-particles, M60N5 epoxy + 60 wt% micro + 5 wt% nano, M62.5N2.5 epoxy + 62.5 wt% micro + 2.5 wt% nano, M65N5 epoxy + 65 wt% micro + 5 wt% nano [Castellon'11].

1.2.1.4. Polymer composite conclusion

The choice of an epoxy network is due to its insulating characteristics and its capability in having new properties upon the addition of micro or nano fillers. The previous discussion showed that in general, the addition of micro-particles to an epoxy network didn't

have any significant enhancement on the electrical properties of the epoxy network such as the relative permittivity and the breakdown voltage. The incorporation of nanoparticles with critical size, mixing, surface modification and critical percentage, allowed some electrical improvements in the relative permittivity values and the breakdown voltage. And finally the incorporation of nano-particles to an epoxy micro-composite did neither decrease the permittivity nor increase the breakdown voltage in comparison to the neat epoxy network. In the following paragraph, a novel material made up of a mixture of organic polymers (epoxy thermoset and a thermoplastic) will be described. The thermal, mechanical and electrical properties of the proposed epoxy/thermoplastic blend are going to be discussed.

1.2.2. Polymer Blends

Polymer blends are obtained by mixing two or more polymers together in order to fuse the characteristics of each of the individual polymers. Polymer blending from existing polymers is a convenient and effective approach to create new materials. They are designed and manufactured to modify some properties in order to meet the requirements of the targeted applications. Some works were performed for mechanical applications where one of the properties, most often, to be improved is fracture toughness. Basically, when mixing two polymers together three different types of blends can be distinguished; completely miscible, immiscible, and compatible blends. Miscible polymer blends have single-phase structure behaving as if it is a single polymer. Only one glass transition temperature can be observed. Immiscible blends are made up of two polymers with two observed glass transitions. And finally compatible polymer blends that are called semi-immiscible blends, since they are considered immiscible blends that exhibit macroscopically uniform physical properties. The main interactions in a polymer blend are hydrogen bonding, Van der Waals interaction, and dipole-dipole interactions. The 2nd law of thermodynamics can establish the miscibility in a polymer blend by the free energy of mixing ΔG_m shown in **Eq. 1**:

$$\Delta G_m = \Delta H_m - T\,\Delta S_m \qquad \textbf{Eq. 1}$$

where ΔH_m and ΔS_m are the enthalpy and the entropy of mixing at a temperature T. Miscibility is satisfied when $\Delta G_m < 0$, but major factors can influence the polymer miscibility such as entropy, interaction energy, free volume and specific interactions such as hydrogen bonding [*Chen'99*]. The miscibility of non-polar polymers can be estimated by the Flory-Huggins equation (**Eq. 2**) [*Flory'53*]:

$$\frac{\Delta G_m}{RT} = \left(\frac{\varphi_1}{N_1} ln\ \varphi_1 + \frac{\varphi_2}{N_2} ln\ \varphi_2 + \varphi_1 \varphi_2 . \chi_{12}\right) \quad \text{Eq. 2}$$

where ΔG_m is the free energy change due to non-polar interaction, R is the gas constant, T is the absolute temperature, φ represents the volume fraction, N is the number of segments in the chain, χ the Flory-Huggins interaction parameter and subscripts 1 and 2 refer to the blending polymers. The first two terms on the right side of **Eq. 2** are related to the entropy of mixing while the third term is related to the enthalpy of mixing. From this equation and knowing the values of the molecular masses of the polymers with their fraction volume, the experimental results can be estimated as well as, knowing χ, the interaction parameter. A phase diagram can be created, which is presented in Figure 20.

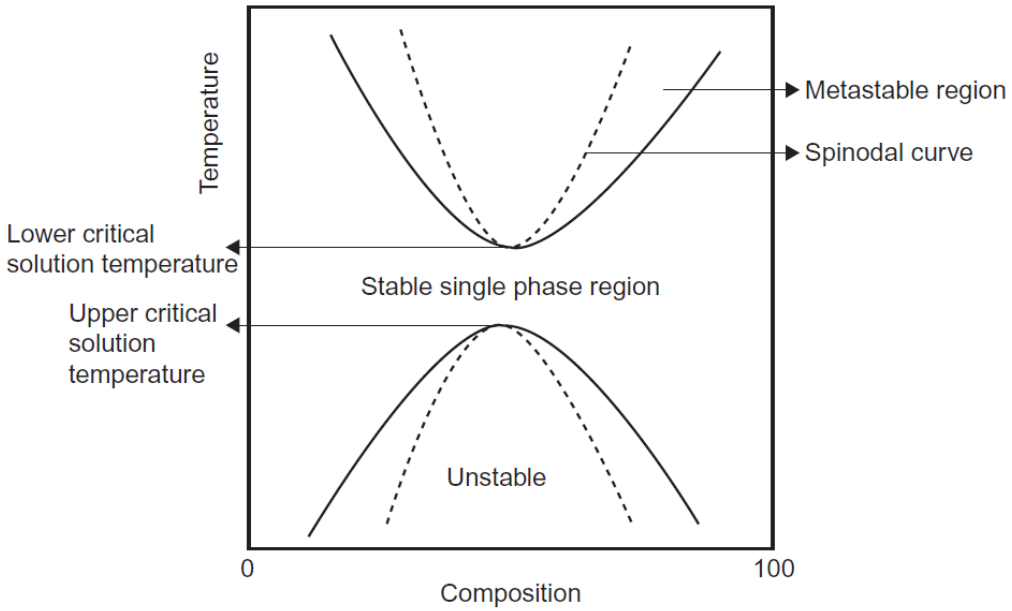

Figure 20: Temperature - composition phase diagram for a binary polymer blend

After finding the right miscibility temperature using a specified concentration, the miscible mixture can undergo two different phenomena; first the mixture can stay miscible during the polymerization reaction forming one unified structure having singular characteristics. Otherwise, the mixture can undergo phase separation phenomenon between the two polymers giving two distinct characteristics representing each of the presented polymers. When two polymers mix at low temperatures and phases separate on heating they are said to exhibit lower critical solution temperature (**LCST**). Whereas if two polymers remain phase separated at ordinary temperatures and form a single phase at high temperatures, they show upper critical solution temperature (**UCST**) behavior. In any mixture the boundary between stable and metastable compositions is called the binodal and the boundary between metastable and

unstable compositions is called the spinodal. In the metastable region, phase separation takes place by a nucleation-growth (**NG**). This process can lead to the formation of small polymer-rich domains (droplets) in a polymer-poor matrix. If the blend reaches the unstable region the phase separation occurs by spinodal demixing (**SD**). This process leads to the formation of a bicontinuous structure, in which the polymer-rich and polymer-poor phases are both continuous phases; this phase is transformed to homogenous separated nodules of polymer-poor domain in a polymer rich domain when the composition's time of equilibrium is reached [*Gir'96*]. Thus, the miscibility in polymer blends is a function of temperature and each binary blend of polymers can be characterized by an interaction parameter [*Chen'99*].

The majority of polymers are incompatible with each other (but this is not a general rule), and mixing them by several kinds of methods usually results in both phases. However, and as discussed, with calculations and knowing their characteristics even the most incompatible binary blends must exhibit some degree of molecular mixing. By choosing the adequate temperature of mixing conditions, polymers miscibility could be obtained. By mixing polymers different kind of structures can be obtained such as: phase separated polymer blend, graft copolymer and block copolymers. The scheme demonstrated in Figure 21 presents the possible structures where solid and dotted lines indicate polymer 1 and polymer 2, respectively and the dots indicate cross-links or covalent bonds. The phase separation phenomenon in a polymer blend is going to be discussed in the epoxy blend part. Graft copolymer (b) is represented with a polymer bonded to the side of the other, where block copolymer (c) is demonstrated by chains bonded end-on-end.

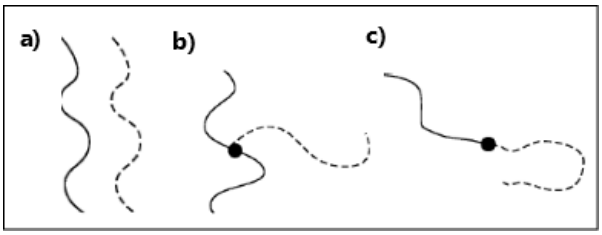

Figure 21: Combinations of two polymers. (a) Polymer blends; (b) graft copolymer; (c) a block copolymer [*Jacq'03*].

1.2.3. Epoxy Blends

Epoxy is a thermosetting polymer, obtained by the cross-linking of epoxy prepolymer with a chosen kind of hardener. A typical epoxy prepolymer used to generate a polymer network has two or more epoxy groups per molecule. Knowing that, the functionality of an

epoxy prepolymer is defined by the number of epoxy groups that play a major role in the formation of the polymer network. For example, diglycidylether of bisphenol A (DGEBA) has two epoxy groups in its structure while tetraglycidyl methylenedianiline (TGMDA) has four epoxy groups per molecule as shown in Figure 22.

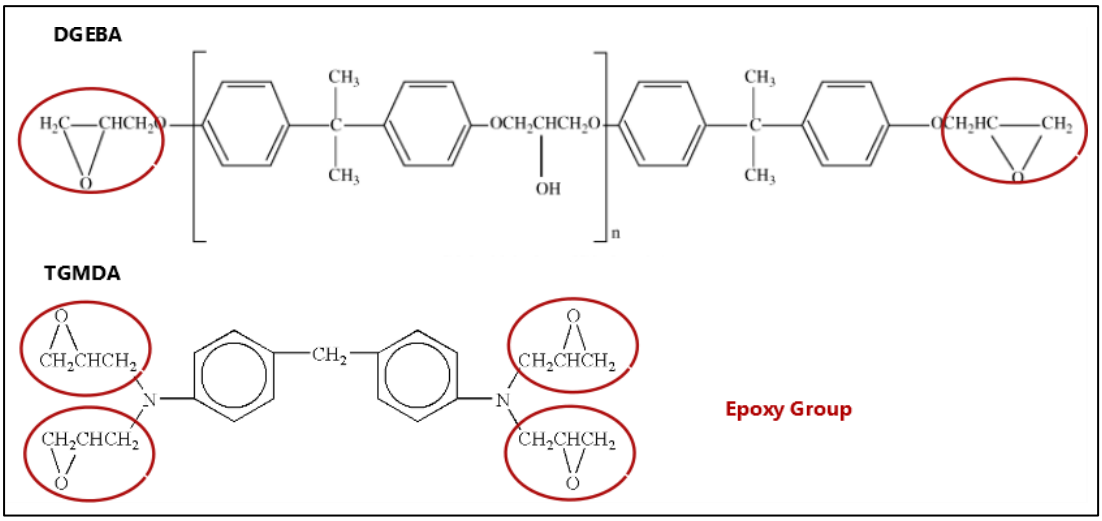

Figure 22: Different epoxy structures

Some examples of used hardeners are amine, anhydrides, phenols and thiols. The amines and the anhydrides are the most used and tested hardeners. Typically, aliphatic, cycloaliphatic or aromatic diamines are employed to generate a crosslinked polymer by reaction with DGEBA. The most common combination is the cycloaliphatic epoxy accompanied with anhydride hardener as seen in majority of the electrical studies done on micro and nano epoxy composites discussed previously. Epoxy crosslinked network is well known in several industrial domains such as in the electronic industry, as discussed in the polymer composite section, the aeronautics and automotive industry for adhesives and coatings applications. Some of the reasons of choosing it are:

- High insulating properties having high breakdown voltages 100 - 200 kV/mm [*Li'10*] [*Hu'06*] [*tuncer'07*].
- No emitted volatile products during polymerization reaction, which is interesting for the production process.
- Wide number of epoxy monomers and hardeners, which allow modulating the characteristics (glass transition temperature, mechanical properties, thermal properties etc.). High adhesion to a variety of surfaces due to the polar groups present in the structure.

- Initiators can interfere in the polymerization step and give new properties.

To obtain an epoxy network the reaction goes through two main structural transformation, gelation and vitrification. Passing from the liquid region to the rubbery region, with a tridimensional molecule occupying all the reactional volume is called the gelation transformation. The vitrification takes place when passing from the rubbery region to the solid glass region. When the solid glass region is attained, the reaction evolution stops and the glass transition temperature (**Tg**) is defined to be in the same order of the reaction temperature. This phenomenon is explained by Enns et al. where they summarized this phenomenon by a time-temperature-transformation T-T-T Diagram as shown in Figure 23 [*Enns'83*]. The time needed to reach the gelation or the vitrification transformation depends on temperatures.

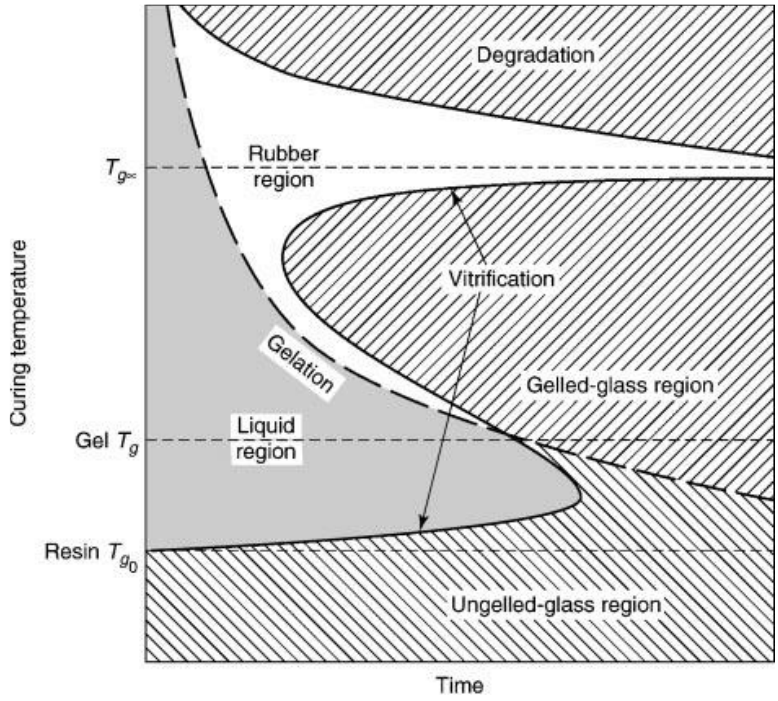

Figure 23: Time–temperature-transformation diagram [*Enns'83*].

In this work we are interested in the epoxy blends and more precisely the epoxy/thermoplastic blends having phase separation phenomenon. The reaction of thermoset (epoxy) in the presence of thermoplastics can produce most of the time a phase separated system with different morphologies. Epoxies, depending on the resin and the hardener chosen, can have different glass transition temperatures. A list of different glass transitions temperature (T_g) is presented in Table 9. In the electronic industry, as discussed in the criteria needed for replacing the encapsulating layer, the chosen materials must have good thermal stability in a wide range of temperatures between -50 °C and 300 °C. For this reason the thermoplastics that are going to be discussed are categorized having high glass transition temperature.

Table 9: list of T_g corresponding to different kinds of epoxy

Epoxy	Hardener	Tg (°C)	ref
Bisphenol A	Tetramine	89	***Nelson'04***
Bisphenol-A	Amine	110	***Katayama'13***
DGEBA	DDS aromatic diaminodiphenyl sulfone	99	***Lee'01***
DGEBA	anhydride MA	175	***Qipeng'92***
DGEBA	anhydride PA	133	***Qipeng'92***
DGEBA	anhydride HHPA	144	***Qipeng'92***

Many examples of blending using high T_g thermoplastics have been studied and elaborated in literature such as polysulphone (**PSF**) {T_g = 187 °C}[*Hedrick'91*] [*Hedrick'85*], Poly-ethersulfone (**PES**) {T_g = 190 °C}[*Blanco'03*] and poly-etherimides (**PEI**) {T_g = 217 °C}[*Gir'97*] [*Bucknall'89*] [*Bonnet'99*]. For example, Blanco et al. demonstrated a phase separated epoxy and a copolymer, 40: 60 polyethersulfone: polyetherethersulfone (40PES:60PEES) blend. They used a DGEBA type epoxy cured by a diamine. The **SEM** image of 15 wt% of thermoplastic PES:PEES in the epoxy network is shown **Figure 24** where particulate morphology was observed associated with phase separation following a spinodal mechanism.

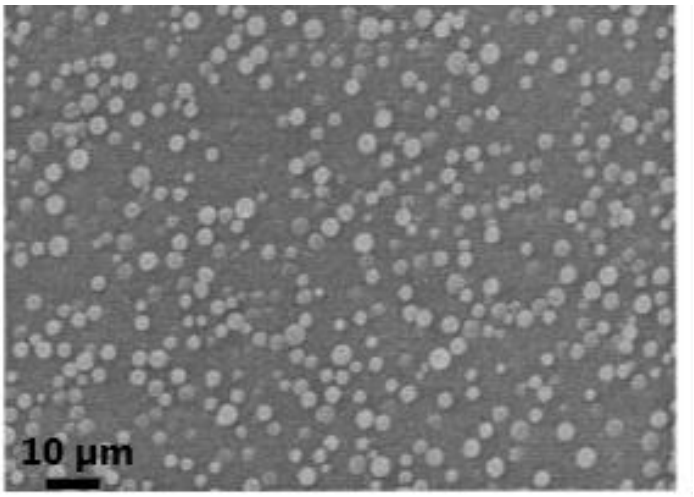

Figure 24: SEM micrographs of epoxy/15 wt% PES [*Blanco'03*]

The polymerization reaction in a thermoset/thermoplastic blend is called reaction-induced phase separation, by which most thermoset/thermoplastic blends are prepared [*Williams'97*] [*Pascault'00*]. The initial thermoset/thermoplastic mixture is miscible under temperature and homogenous; the phase separation phenomenon takes place in the cure of the thermoset

leading to several types of morphology. Final morphology of a thermoset (**TS**)/thermoplastic (**TP**) phase separated blend can be estimated using a conversion – composition diagram at constant temperature as shown in Figure 25.

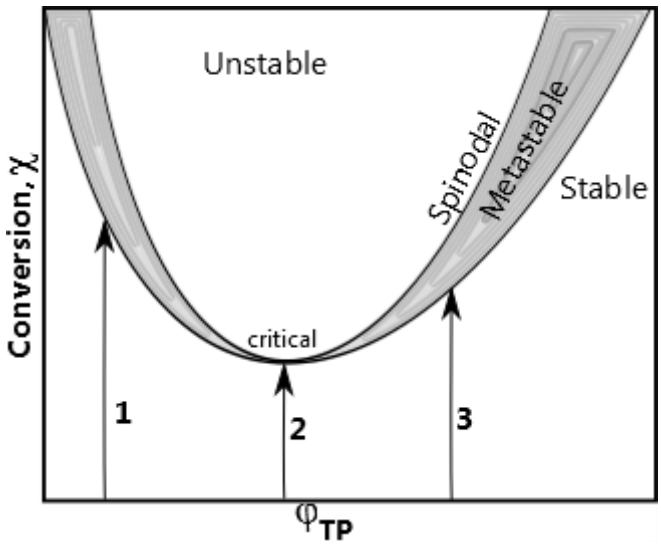

Figure 25: Conversion – Composition transformation diagram at constant temperature; 1,2 and 3 are different trajectories, starting from different initial TP/TS concentrations and leading to different morphologies [*Pascault'00*]

The final obtained morphology at a chosen temperature depends on the volume fraction chosen as seen in the diagram. If φ_{TP} (volume fraction of thermoplastic) is located in the left side of the critical percentage, the final morphology will consist of a dispersion of thermoplastic-rich particles in a thermoset-rich matrix, named particulate morphology, as demonstrated in Figure 26 scheme 1. On the other hand, when the volume fraction is located on the right side of the critical percentage, the final morphology will be demonstrated as scheme 3. It represents a dispersion of thermoset-rich particles in thermoplastic-rich matrix that is often called phase inverted morphology. Finally, and close to the critical percentage, variety of morphologies can be developed, such as bicontinuous structures, double phase morphologies and ribbon like structures [*Pascault'00*].

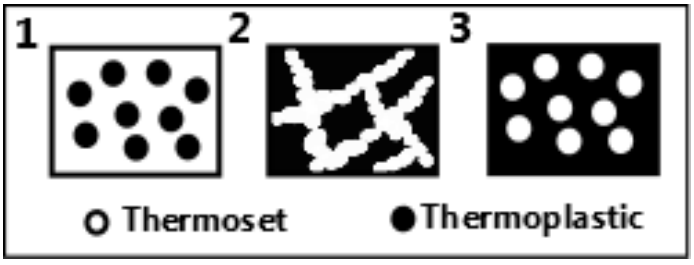

Figure 26: (1) Particulate morphology, (2) Bicontinuous structure and (3) Phase inverted morphology

Thermoset/thermoplastic blend is used to improve properties of the initial thermoset, such as the mechanical, thermal and solvent resistance properties. A new material is always generated with new distinct properties different than those of the pure thermoset. A typical example of toughness increase in thermoset-thermoplastic blends prepared by reaction-induced phase separation is shown in Figure 27. DGEBA-MDEA was the epoxy-amine system blended with **PPE**, Polyphenyl ether [*Pascault'00*].

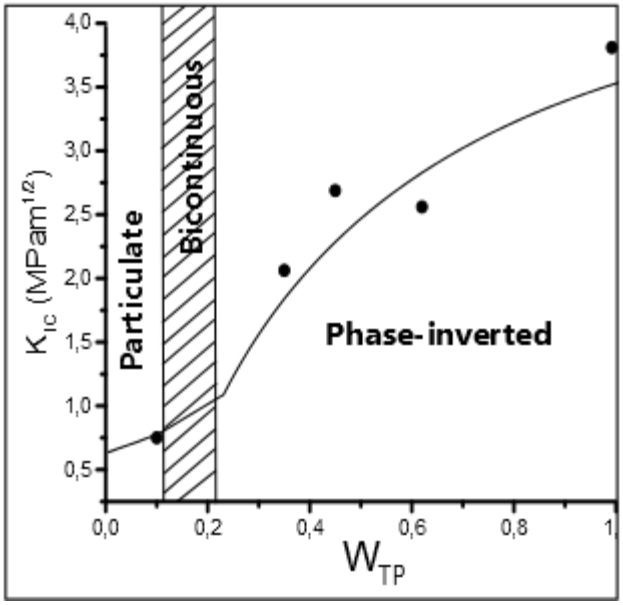

Figure 27: Critical stress-intensity as a function of the thermoplastic mass fraction for PPE/ DGEBA-MCDEA blend, prepared by reaction-induced phase separation [*Pascault'00*].

Fracture toughness of thermoset-thermoplastic blends is usually expressed in terms of the critical stress-intensity K_{IC} (MPa.m$^{1/2}$). In the particulate morphology phase at 10 wt% of thermoplastic K_{IC} exhibited an increase of 20 % in comparison with the neat epoxy network. This feature describes the ability of a material to resist cracks and stop the fracture. The presence of the soft thermoplastic particles in a rigid epoxy network acted as an obstacle against the propagation of the crack and thus allowed to increase the K_{IC} value. The propagation of crack is attenuated by homogenously distributed thermoplastic particles. The K_{IC} value experiences greater increase in the region when the thermoplastic becomes the continuous phase which is described as the phase inverted structure. The pure thermoplastic has a K_{IC} value higher than that of pure epoxy which plays a role in increasing the value of the blend when attaining the phase inverted morphology.

Few studies analyze the electrical properties of a thermoset/thermoplastic polymer blend network. Jilani et al. presented the dielectric properties of an epoxy network [*Jilani'15*]. The hardeners used in the polymerization of the epoxy have a significant effect on the epoxy

structure which in turn influences the dielectric properties. They suggested that epoxy polymer made with an aromatic hardener, **DDS** (diaminodiphenyl sulfone), is more suitable for applications as insulators, than the polymer based on aliphatic hardener, i.e. ethylenediamine. Indeed the conductivity of aliphatic hardener is higher than aromatic ones. There are no presented studies on the electrical properties of epoxy blends with phase separation, so our comparison is going to be made with the previously presented epoxy composites.

When the thermoset-thermoplastic blend have the particulate morphology, as we said the thermoplastic particles are acting as an obstacle against any crack propagation passing through the material. This interesting characteristic gives rise to the idea of having the same influence in the creation of cracks during a breakdown voltage test. Our assumption is that the particulate morphology of the blend would stop the treeing that takes place upon applying high voltages to the epoxy network, increasing the capability of the resin in resisting voltage and giving it higher breakdown value voltage. This assumption is going to be discussed with a new proposed material in the last chapter.

1.3. General conclusion

In this chapter, power module and specifically an IGBT module was presented defining all its internal products and their characteristics. The draw backs of the nowadays used encapsulation layer (silicone gel) was demonstrated showing that with the demand of increasing the voltage and temperature in a power module the existing silicone gel must be replaced.

Some proposed materials for replacing the present materials were listed. In this chapter we are suggesting the use of polymer blends to investigate the substitution of the encapsulating and/or the passivation layer. Polymer blends can be divided into two main groups: organic/inorganic composites and organic/organic blends.

The literature study of organic/inorganic composites such as epoxy/nano and/or micro-composites was demonstrated; showing that the use of micro fillers incorporated with an epoxy network decrease the dielectric breakdown value and increase the relative permittivity values. In some particular cases like with alumina micro-particles the thermal conductivity of the composite is improved. This effect is considered as a drawback considering the insulating properties needed in a power module, as the use of power modules demands an improvement in the electrical properties of the proposed materials. The incorporation of nano-fillers needs to follow several critical conditions in order to enhance the dielectric breakdown values or decrease the relative permittivity values. Thus the size of the nanoparticle must be small and must have surface compatibility with the epoxy network. They must be homogenously dispersed otherwise the nanoparticles will form aggregates acting as defects in the matrix. Furthermore, the appropriate dispersion method must be used to avoid the insertion of voids and to distribute the nano-particles homogeneously. Critical very low percentages depending on the size of the nanoparticle must not be exceeded to increase the specific surface area without reaching the percolation level. The incorporation of nano-particles to the micro-composite did not show any interesting influence with respect to the pure epoxy network.

Organic/organic blend is our suggested material composed of a thermoset/thermoplastic blend namely the epoxy blend. The preparation and transformation processes were explained giving us the procedure of preparing a phase separated epoxy/thermoplastic blend. In the following chapters the characteristics of the phase separated epoxy/thermoplastic blend are going to be discussed.

1.4. In this PhD work

In this PhD work, the chosen studied material is a thermoset/thermoplastic blend having a phase separation phenomenon. This kind of material is usually established to enhance the mechanical properties of the thermoset network in literature. The thermoset is **DGEBA** epoxy resin with an aromatic amine hardener chosen due to its high glass transition temperature ($\mathbf{T_{g\ epoxy+amine}}$ = 164°C). This high glass transition temperature will confirm the stability of the system to a wide range of applied temperatures. The thermoplastic blended with the epoxy is polyetherimide (**PEI**) having glass transition temperatures higher than that of the epoxy network respectively. The mechanism of phase separation of this blend has been studied in the thesis work of Anthony Bonnet and Emmanuel Girard-Reydet. They described how to find the critical point of conversion and obtain a homogeneous phase separated material. The critical stress intensity is also studied showing an increase in its values with the addition of 10 wt% of **PEI**. The way of how the improvement of this candidate takes place gives us the idea of having similar effect on the enhancement of the electrical properties of the blend.

We are going to present different percentages of PEI with a chosen curing temperature allowing the phase separation process, which is going to be characterized by means of electronic microscopy (**TEM** and **SEM**).

The influence of the thermoplastic used in this blend is going to be analyzed thermally and mechanically by differential scanning calorimetry (**DSC**), thermogravimetric analysis (**TGA**) and dynamic mechanical analysis (**DMA**).

The effect of the used thermoplastic will be studied electrically using dielectric analysis (**DEA**), DC conductivity measurements extrapolated from the dielectric analysis as well as from a conduction current measurement. DC breakdown voltage measurements at room temperature of the selected networks are going to be evaluated in the following chapters.

References

- **Amro'05:** Amro, R., Lutz, J., Rudzki, J., Thoben, M. & Lindemann, A. Double-sided low-temperature joining technique for power cycling capability at high temperature. in 2005 European Conference on Power Electronics and Applications 10 pp.-pp.P.10 (2005).
- **Bala'05:** Balakrishnan, S., Start, P. R., Raghavan, D. & Hudson, S. D. The influence of clay and elastomer concentration on the morphology and fracture energy of preformed acrylic rubber dispersed clay filled epoxy nanocomposites. Polymer 46, 11255–11262 (2005).
- **Baliga'98:** Baliga, B. J. High Voltage Silicon Carbide Devices. in Symposium F – Wide Bandgap Semiconductors for High Power, High Frequency 512, 77 (12 pages) (1998).
- **Blanco'03:** Blanco, I., Cicala, G., Faro, C. L. & Recca, A. Development of a toughened DGEBS/DDS system toward improved thermal and mechanical properties by the addition of a tetrafunctional epoxy resin and a novel thermoplastic. J. Appl. Polym. Sci. 89, 268–273 (2003).
- **Boettge'13:** Boettge, B., Naumann, F., Klengel, R., Klengel, S. & Petzold, M. Packaging material issues in high temperature power electronics. in Microelectronics Packaging Conference (EMPC) , 2013 European 1–6 (2013).
- **Bonnet'99:** Bonnet, A., Pascault, J. P., Sautereau, H., Taha, M. & Camberlin, Y. Epoxy−Diamine Thermoset/Thermoplastic Blends. 1. Rates of Reactions before and after Phase Separation. Macromolecules 32, 8517–8523 (1999).
- **Bucknall'89:** Bucknall, C. B. & Gilbert, A. H. Toughening tetrafunctional epoxy resins using polyetherimide. Polymer 30, 213–217 (1989).
- **Butterfield'16:** Butterfield, L. et al. Morphology and Thermomechanical Properties in Epoxy Acrylate Interpenetrated Networks. Macromol. Symp. 365, 59–66 (2016).
- **Castellon'11:** Castellon, J. et al. Electrical properties analysis of micro and nano composite epoxy resin materials. IEEE Transactions on Dielectrics and Electrical Insulation 18, 651–658 (2011).
- **Chasserio' 08:** Chasserio, N., Guillemet-Fritsch, S., Lebey, T. & Dagdag, S. Ceramic Substrates for High-temperature Electronic Integration. Journal of Elec Materi 38, 164–174 (2008).
- **Chen'15:** Chen, M. et al. Dielectric and mechanical properties and thermal stability of polyimide–graphene oxide composite films. Thin Solid Films 584, 232–237 (2015).
- **Chen'99:** Chen, J.-L. & Chang, F.-C. Phase Separation Process in Poly(ε-caprolactone)−Epoxy Blends. Macromolecules 32, 5348–5356 (1999).
- **Chu'13:** Chu, K. et al. Electrical and Thermal Properties of Carbon-Nanotube Composite for Flexible Electric Heating-Unit Applications. IEEE Electron Device Letters 34, 668–670 (2013).
- **Coppola'07:** Coppola, L., Huff, D., Wang, F., Burgos, R. & Boroyevich, D. Survey on High-Temperature Packaging Materials for SiC-Based Power Electronics Modules. in 2007 IEEE Power Electronics Specialists Conference 2234–2240 (2007).
- **Diaham'07:** Diaham, S. Etude du comportement sous haute température de matériaux polyimides en vue de la passivation de composants de puissance à semi-conducteurs grand gap. Thesis (Toulouse 3, 2007).
- **Diaham'12:** Diaham, S., Locatelli, M.-L. & Khazak, R. in *High Performance Polymers - Polyimides Based - From Chemistry to Applications* , Chapter 2, (ed. Abadie, M.) (InTech, 2012).

- **Diaham'13:** Diaham, S. & Locatelli, M.-L. Dielectric properties of polyamide-imide. *J. Phys. D: Appl. Phys.* **46,** 185302 (2013).
- **Diaham'14:** Diaham, S. et al. Dielectric strength of parylene HT. Journal of Applied Physics 115, 54102 (2014).
- **Ding'04:** Ding, H. Z. & Varlow, B. R. Effect of nano-fillers on electrical treeing in epoxy resin subjected to AC voltage. in *2004 Annual Report Conference on Electrical Insulation and Dielectric Phenomena, 2004. CEIDP '04* 332–335 (2004).
- **Do'08:** Do, M. T., Auge, J.-L. & Lesaint, O. Breakdown field in silicone gel under needle-plane geometry. in 222–225 IEEE, (2008).
- **DOS Santos'15:** Dos Santos, E. & Da Salvia, E. R. Advanced Power Electronics Converters: PWM Converters Processing AC Voltages. January (2015), Wiley-IEEE Press 3-5.
- **Dreike'94:** Dreike, P. L., Fleetwood, D. M., King, D. B., Sprauer, D. C. & Zipperian, T. E. An overview of high-temperature electronic device technologies and potential applications. IEEE Transactions on Components, Packaging, and Manufacturing Technology: Part A 17, 594–609 (1994).
- **Dupont'06:** Dupont, L. Contribution à l'étude de la durée de vie des assemblages de puissance dans des environnements haute température et avec des cycles thermiques de grande amplitude (Cachan, Ecole normale supérieure, 2006).
- **Dupont'06:** Dupont, L. Contribution à l'étude de la durée de vie des assemblages de puissance dans des environnements haute température et avec des cycles thermiques de grande amplitude. (École normale supérieure de Cachan - ENS Cachan, 2006).
- **Ebke'00:** Ebke, T., Khaddour, A. & Peier, D. Degradation of silicone gel by partial discharges due to different defects. in Dielectric Materials, Measurements and Applications, 2000. Eighth International Conference on (IEE Conf. Publ. No. 473) 202–207 (2000).
- **Elasser'02:** Elasser, A. & Chow, T. P. Silicon carbide benefits and advantages for power electronics circuits and systems. Proceedings of the IEEE 90, 969–986 (2002).
- **Enns'83:** Enns, J. B. & Gillham, J. K. Time–temperature–transformation (TTT) cure diagram: Modeling the cure behavior of thermosets. J. Appl. Polym. Sci. 28, 2567–2591 (1983).
- **Fabian'05:** Fabian, J. H., Hartmann, S. & Hamidi, A. Analysis of insulation failure modes in high power IGBT modules. in Fourtieth IAS Annual Meeting. Conference Record of the 2005 Industry Applications Conference, 2, 799–805 Vol. 2 (2005).
- **Flory'53:** Flory, P. J. Principles of Polymer Chemistry. P.509 (Cornell University Press, 1953).
- **Gir'96:** Girard-Reydet, E. Phénomène de séparation de phase induit par une réaction chimique dans des mélanges thermoplastique/polyépoxy : contrôle des morphologies et propriétés. (Lyon, INSA, 1996).
- **Gir'97:** Girard-Reydet, E., Vicard, V., Pascault, J. P. & Sautereau, H. Polyetherimide-modified epoxy networks: Influence of cure conditions on morphology and mechanical properties. J. Appl. Polym. Sci. 65, 2433–2445 (1997).
- **Guo'14:** Guo, J. et al. Study on electrical properties of micro-nano structured epoxy composites. in Proceedings of 2014 International Symposium on Electrical Insulating Materials (ISEIM) 441–444 (2014).
- **Hall'52:** Hall, R. N. Power Rectifiers and Transistors. *Proceedings of the IRE* **40,** 1512–1518 (1952).
- **Hamidi'99:** Hamidi, A., Beck, N., Thomas, K. & Herr, E. Reliability and lifetime evaluation of different wire bonding technologies for high power IGBT modules. Microelectronics Reliability 39, 1153–1158 (1999).

- **Hanscomb'73:** Hanscomb, J. R. & Calderwood, J. H. Thermally assisted tunnelling in polyimide film under steady-state and transient conditions. J. Phys. D: Appl. Phys. 6, 1093 (1973).
- **Hedrick'85:** Hedrick, J. L., Yilgör, I., Wilkes, G. L. & McGrath, J. E. Chemical modification of matrix Resin networks with engineering thermoplastics. Polymer Bulletin 13, 201–208 (1985)
- **Hedrick'91:** Hedrick, J. L. et al. Chemical modification of matrix resin networks with engineering thermoplastics: 1. Synthesis, morphology, physical behaviour and toughening mechanisms of poly(arylene ether sulphone) modified epoxy networks. Polymer 32, 2020–2032 (1991).
- **Herr'97:** Herr, E., Frey, T., Schlegel, R., Stuck, A. & Zehringer, R. Reliability of Electron Devices, Failure Physics and AnalysisSubstrate-to-base solder joint reliability in high power IGBT modules. Microelectronics Reliability 37, 1719–1722 (1997).
- **Hertem'10:** Hertem, D. V., Ghandhari, M. & Delimar, M. Technical limitations towards a SuperGrid - A European prospective. In Energy Conference and Exhibition (EnergyCon), IEEE International 302–309 (2010).
- **Hertem'15:** Dirk Van Hertem, A supergrid for Europe KuLeuven (2015)
- **Hofstein'63:** Hofstein, S. R. & Heiman, F. P. The silicon insulated-gate field-effect transistor. Proceedings of the IEEE 51, 1190–1202 (1963).
- **Hopkins'06:** Hopkins, D. C., Kellerman, D. W., Wunderlich, R. A., Basaran, C. & Gomez, J. High-temperature, high-density packaging of a 60kW converter for> 200 C embedded operation. in Applied Power Electronics Conference (APEC) 871–877 (2006).
- **Hourdequin'16:** Hourdequin, H., Laudebat, L., Locatelli, M. L. & Bidan, P. Design of packaging structures for high voltage power electronics devices: Electric field stress on insulation. in 2016 IEEE International Conference on Dielectrics (ICD) 2, 999–1002 (2016).
- **Hu'06:** Hu, Y., Smith, R. C., Nelson, J. K. & Schadler, L. S. Some mechanistic understanding of the impulse strength of nanocomposites. in 2006 IEEE Conference on Electrical Insulation and Dielectric Phenomena 31–34 (2006).
- **Ibrahim'91:** Ibrahim, I. A., Mohamed, F. A. & Lavernia, E. J. Particulate reinforced metal matrix composites — a review. J Mater Sci 26, 1137–1156
- **Imai'08:** Imai, T. et al. Improving Epoxy-based Insulating Materials with Nano-fillers toward Practical Application. in Conference Record of the 2008 IEEE International Symposium on Electrical Insulation, 2008. ISEI 2008 201–204 (2008).
- **Iyer'11:** Iyer, G., Gorur, R. S., Richert, R., Krivda, A. & Schmidt, L. E. Dielectric properties of epoxy based nanocomposites for high voltage insulation. IEEE Transactions on Dielectrics and Electrical Insulation 18, 659–666 (2011).
- **Jacq'03:** Jacqueline I. K., Mark H. F. Encyclopedia of polymer science and technology-Wiley-Interscience Vol. 10 p. 273 (2003-2004).
- **Jilani'15:** Jilani, W. et al. Effects of curing agent on conductivity, structural and dielectric properties of an epoxy polymer. Polymer 79, 73–81 (2015).
- **Johnson'07:** Johnson, R. W., Wang, C., Liu, Y. & Scofield, J. D. Power Device Packaging Technologies for Extreme Environments. IEEE Transactions on Electronics Packaging Manufacturing 30, 182–193 (2007).
- **Kahng'60:** D. Kahng and M. M. Atalla, "Silicon-silicon dioxide field induced surface devices", in Solid State Res. Conf., Pittsburgh, USA, (1960).
- **Kahouli'14:** Kahouli, A. et al. Structural and dielectric properties of parylene-VT4 thin films. Materials Chemistry and Physics 143, 908–914 (2014).

- **Kaji'16:** Kaji, Y. et al. Novel IGBT modules with epoxy resin encapsulation and insulating metal baseplate. in 2016 28th International Symposium on Power Semiconductor Devices and ICs (ISPSD) 475–478 (2016).
- **Katayama'13:** Katayama, J., Ohki, Y., Fuse, N., Kozako, M. & Tanaka, T. Effects of nanofiller materials on the dielectric properties of epoxy nanocomposites. IEEE Transactions on Dielectrics and Electrical Insulation 20, 157–165 (2013).
- **Ke'96:** Ke, S., Zhang, K. & Xie, X. Band line-ups and band-gap behaviour of new-type superlattices (3C-BN)/(2H-BN), (3C-GaN)/(2H-GaN) and (3C-SiC)/(2H-SiC). J. Phys.: Condens. Matter 8, 10209 (1996).
- **Keyrouz'11:** Keyrouz, M. B. Etude des matériaux isolants d'encapsulation pour la montée en température des modules de puissance haute tension. (Université Paul Sabatier - Toulouse III, 2011).
- **Khan'15:** Khan, R. et al. Facile synthesis of epoxy nanocomposite coatings using inorganic nanoparticles for enhanced thermo-mechanical properties: a comparative study. J Coat Technol Res 13, 159–169 (2015).
- **Kidalov'09:** Kidalov, S. V. & Shakhov, F. M. Thermal Conductivity of Diamond Composites. Materials 2, 2467–2495 (2009).7
- **Kimoto'14:** Kimoto, T., Kawahara, K., Niwa, H., Kaji, N. & Suda, J. Ion implantation technology in SiC for power device applications. in 1–6 (IEEE, 2014). doi:10.1109/IWJT.2014.6842018
- **Kinloch'03:** Kinloch, A. J. *et al.* Toughening structural adhesives via nano- and micro-phase inclusions. *The Journal of Adhesion* **79,** 867–873 (2003).
- **Kirschman'99:** Kirschman, R. in High-Temperature Electronics 752–769 (Wiley-IEEE Press, 1999).
- **Kochetov'10:** Kochetov, R., Andritsch, T., Morshuis, P. H. F. & Smit, J. J. Thermal and electrical behaviour of epoxy-based microcomposites filled with Al2O3 and SiO2 particles. in Conference Record of the 2010 IEEE International Symposium on Electrical Insulation (ISEI) 1–5 (2010).
- **Kochetov'12:** Kochetov, R., Andritsch, T., Morshuis, P. H. F. & Smit, J. J. Anomalous behaviour of the dielectric spectroscopy response of nanocomposites. IEEE Transactions on Dielectrics and Electrical Insulation 19, 107–117 (2012).
- **Kong'05:** Kong, C., Bang, J. & Sugiyama, Y. Structural investigation of composite wind turbine blade considering various load cases and fatigue life. Energy 30, 2101–2114 (2005).
- **Krein'11**: Krein, P. T. in Power Electronics Handbook: Devices, Circuits, and Applications. (Third Edition) by Rashid MH. San Diego, CA: Elsevier; p 1–2 (2011)
- **Kumar'04:** Kumar, R., Molin, D., Young, L. & Ke, F. New high temperature polymer thin coating for power electronics. in Nineteenth Annual IEEE Applied Power Electronics Conference and Exposition, 2004. APEC '04 2, 1247–1249 vol.2 (2004).
- **Kumar'09:** Kumar, R. Parylene HT®: A High Temperature Vapor Phase Polymer for Electronics Applications. Additional Conferences (Device Packaging, HiTEC, HiTEN, & CICMT) 2010, 000108–000113 (2009).
- **Kumar'10:** Kumar, R. Parylene HT®: A High Temperature Vapor Phase Polymer for Electronics Applications. Additional Conferences (Device Packaging, HiTEC, HiTEN, & CICMT) 2010, 108–113 (2010).
- **Lee'01:** Lee, J. & Yee, A. F. Inorganic particle toughening I: micro-mechanical deformations in the fracture of glass bead filled epoxies. Polymer 42, 577–588 (2001).
- **Lestriez'98:** Lestriez, B. et al. Is the Maxwell–Sillars–Wagner model reliable for describing the dielectric properties of a core–shell particle–epoxy system? Polymer 39, 6733–6742 (1998).

- **Lhommeau'05:** Lhommeau, T., Meuret, R. & Karama, M. Technological study of an IGBT module for an aeronautical application in zone engine. in 2005 European Conference on Power Electronics and Applications 6 pp.-pp.P.6 (2005).
- **Li'10:** Li, Z., Okamoto, K., Ohki, Y. & Tanaka, T. Effects of nano-filler addition on partial discharge resistance and dielectric breakdown strength of Micro-Al2O3Epoxy composite. IEEE Transactions on Dielectrics and Electrical Insulation 17, 653–661 (2010).
- **Li'15:** Li, Z. et al. Silicone Protection Solution for IGBT Modules: from Dielectric Encapsulation to Thermal Management. in Renewable Energy and Energy Management; Proceedings of PCIM Asia 2015; International Exhibition and Conference for Power Electronics, Intelligent Motion 1–5 (2015).
- **Li'87:** Li, Z. & Bradt, R. C. Thermal Expansion and Thermal Expansion Anisotropy of SiC Polytypes. Journal of the American Ceramic Society 70, 445–448 (1987).
- **Lindroos'95:** Lindroos, V. K. & Talvitie, M. J. Recent advances in metal matrix composites. Journal of Materials Processing Technology 53, 273–284 (1995).
- **Locatelli'14:** Locatelli, M. L. et al. Evaluation of Encapsulation Materials for High-Temperature Power Device Packaging. IEEE Transactions on Power Electronics 29, 2281–2288 (2014).
- **Ma'94:** Ma, S. & Tang, X. in Interpenetrating Polymer Networks 239, 405–426 (American Chemical Society, 1994).
- **Mac'92:** MacKinnon, A. J., Jenkins, S. D., McGrail, P. T. & Pethrick, R. A. A dielectric, mechanical, rheological and electron microscopy study of cure and properties of a thermoplastic-modified epoxy resin. Macromolecules 25, 3492–3499 (1992).
- **Mad'12:** Madhusoodhanan, S. et al. Comparison study of 12kV n-type SiC IGBT with 10kV SiC MOSFET and 6.5kV Si IGBT based on 3L-NPC VSC applications. in 310–317 (IEEE, 2012).
- **Ménager'10:** Ménager L., Allard B., Bley V. Conditionnement des Modules de Puissance. Ed. Techniques Ingénieur. Ref :e3385 (2010)
- **Muni'91:** Muni, B. P., Gokuli, A. V. & Saxena, S. N. Gating and protection of IGBT in an inverter. In 1991 International Conference on Industrial Electronics, Control and Instrumentation, 1991. Proceedings. IECON '91 662–667 vol.1 (1991).
- **Mustain'05:** Mustain, H. A., Lostetter, A. B. & Brown, W. D. Evaluation of gold and aluminum wire bond performance for high temperature (500 deg;C) silicon carbide (SiC) power modules. in Proceedings Electronic Components and Technology, 2005. ECTC '05. 1623–1628 Vol. 2 (2005).
- **Nasciment'16:** Nascimento, E. do et al. Breakdown, free-volume and dielectric behavior of the nanodielectric coatings based on epoxy/metal oxides. J Mater Sci: Mater Electron 27, 9240–9254 (2016).
- **Nelson'04:** Nelson, J. K. & Fothergill, J. C. Internal charge behaviour of nanocomposites. Nanotechnology 15, 586–595 (2004).
- **Neudeck'02:** Neudeck, P. G., Okojie, R. S. & Chen, L.-Y. High-temperature electronics - a role for wide bandgap semiconductors? Proceedings of the IEEE 90, 1065–1076 (2002).
- **Ng'03:** Ng, B. K. et al. Performance of thin 4H-SiC UV avalanche photodiodes. IEE Proceedings - Optoelectronics 150, 187–190 (2003).
- **Ning'10:** Ning, P. et al. A Novel High-Temperature Planar Package for SiC Multichip Phase-Leg Power Module. IEEE Transactions on Power Electronics 25, 2059–2067 (2010).
- **Numata'86:** Numata, S. 'ichi, Oohara, S., Fujisaki, K., Imaizumi, J. & Kinjo, N. Thermal expansion behavior of various aromatic polyimides. J. Appl. Polym. Sci. 31, 101–110 (1986).

- **Occhionero'99:** Occhionero, M. A., Hay, R. A., Adams, R. W. & Fennessy, K. P. Cost-effective manufacturing of aluminium silicon carbide (AlSiC) electronic packages. in International Symposium on Advanced Packaging Materials: Processes, Properties and Interfaces. Proceedings 118–124 (1999).
- **Pascault'00:** Pascualt, J.P., Williams R.J.J. Polymer Blends: Formulation and Performance, In: Donald R. Paul, Clive B. Bucknall. p. 379-415. Chapter 13. wiley (2000).
- **Petterteig'91:** Petterteig, A., Lode, J. & Undeland, T. M. IGBT turn-off losses for hard switching and with capacitive snubbers. in , Conference Record of the 1991 IEEE Industry Applications Society Annual Meeting, 1991 1501–1507 vol.2 (1991). doi:10.1109/IAS.1991.178059
- **Preetha'10:** Preetha, P. & Thomas, M. J. AC breakdown characteristics of epoxy alumina nanocomposites. in 2010 Annual Report Conference on Electrical Insulation and Dielectric Phenomena (CEIDP) 1–4 (2010).
- **Qipeng'92:** Qipeng G., Jinyu H., Liaohai G. and Zhuiliu F. phase separation in anhydride-cured epoxy resin containing phenolphthalein poly(ether ether keton). Eur. Polym. J. Vol. 28, No. 4, pp. 405-409, (1992).
- **Rebello'96:** Rebello, N. S., Shoucair, F. S. & Palmour, J. W. 6H silicon carbide MOSFET modelling for high temperature analogue integrated circuits (25-500 deg;C). IEE Proceedings - Circuits, Devices and Systems 143, 115–122 (1996).
- **Reichwein'10:** Reichwein, H. G., Langemeier, P., Hasson, T., & Schendzielorz, M. Light, strong and economical epoxy fiber reinforced structures for automotive mass production. In SPE Automotive Composites Conference. Troy, United States (2010).
- **Ross'98**: Ross, I. M. The invention of the transistor. Proceedings of the IEEE 86, 7–28 (1998).
- **Ryu'13:** Ryu, S. et al. Ultra-high voltage IGBTs in 4H-SiC. in 2013 IEEE Workshop on Wide Bandgap Power Devices and Applications (WiPDA) 36–39 (2013).
- **Sanchez'01:** Sánchez, M. S. et al. Forced compatibility in poly(methyl acrylate)/poly(methyl methacrylate) sequential interpenetrating polymer networks. Polymer 42, 10071–10075 (2001).
- **Sawa'80:** Sawa, G., Nakamura, S., Iida, K. & Ieda, M. Electrical Conduction of Polypyromellitimide Films at Temperatures of 120-180°C. *Jpn. J. Appl. Phys.* **19,** 453 (1980).
- **Sheng'04:** Sheng, W. W. & Colino, R. P. Power Electronic Modules: Design and Manufacture. Chapter 3. CRC press (2004).
- **Silva'15:** Silva, F. A. Chapter two: Semiconductor power switches and passive components. In Power Electronics Basics: Operating Principles, Design, Formulas, and Applications. IEEE, 80-82 (2015).
- **Singha'08:** Singha, S. & Thomas, M. J. Dielectric properties of epoxy nanocomposites. IEEE Transactions on Dielectrics and Electrical Insulation 15, 12–23 (2008).
- **Singha'09:** Singha, S. & Thomas, M. J. Influence of filler loading on dielectric properties of epoxy-ZnO nanocomposites. IEEE Transactions on Dielectrics and Electrical Insulation 16, 531–542 (2009).
- **Sperling'81:** Sperling, L. H. in Interpenetrating Polymer Networks and Related Materials 1–10 (Springer US, 1981).
- **Sugawara'01:** Sugawara, Y. et al. 12-19 kV 4H-SiC pin diodes with low power loss. in Proceedings of the 13th International Symposium on Power Semiconductor Devices and ICs, 2001. ISPSD '01 27–30 (2001).
- **Thorp'90:** Thorp, J. S., Akhtaruzzaman, M. & Evans, D. The dielectric properties of alumina substrates for microelectronic packaging. J Mater Sci 25, 4143–4149 (1990).

- **Tsekmes'14:** Tsekmes, I. A., Kochetov, R., Morshuis, P. H. F. & Smit, J. J. The role of particle distribution in the dielectric response of epoxy–boron nitride nanocomposites. J Mater Sci 50, 1175–1186 (2014).
- **Tsekmes'15-1:** Tsekmes, I. A., Kochetov, R., Morshuis, P. H. F. & Smit, J. J. AC breakdown strength of epoxy-boron nitride nanocomposites: Trend & reproducibility. in 446–449 (IEEE, 2015).
- **Tsekmes'15-2:** Tsekmes, I. A., Morshuis, P. H. F., Smit, J. J. & Kochetov, R. Enhancing the thermal and electrical performance of epoxy microcomposites with the addition of nanofillers. IEEE Electrical Insulation Magazine 31, 32–42 (2015).
- **Tuncer'07:** Tuncer, E. et al. Electrical properties of epoxy resin based nano-composites. Nanotechnology 18, 25703 (2007).
- **Vanlathem'12:** vanlathem, E., Enami, H. & Hyun, D. S. Linknovate : New generation of silicone gels for power devices encapsulation. PCIM Europe Conference Proceedings (2012)
- **Wang'04:** Wang, Z., Volinsky, A. A. & Gallant, N. D. Crosslinking effect on polydimethylsiloxane elastic modulus measured by custom-built compression instrument. J. Appl. Polym. Sci. 131, 41050 (2014).
- **Wang'10:** Wang, N. et al. Partial discharge control in a power electronic module using high permittivity non-linear dielectrics. IEEE Transactions on Dielectrics and Electrical Insulation 17, 1319–1326 (2010).
- **Wang'16:** Wang, F., Drzal, L. T., Qin, Y. & Huang, Z. Enhancement of fracture toughness, mechanical and thermal properties of rubber/epoxy composites by incorporation of graphene nanoplatelets. Composites Part A: Applied Science and Manufacturing 87, 10–22 (2016).
- **Watanbe'04:** Watanabe, H., Yamada, N. & Okaji, M. Linear Thermal Expansion Coefficient of Silicon from 293 to 1000 K. International Journal of Thermophysics 25, 221–236
- **Willander'06:** Willander, M., Friesel, M., Wahab, Q. & Straumal, B. in Springer Handbook of Electronic and Photonic Materials (eds. Prof, S. K. & Dr, P. C.) 537–563 Springer (2006).
- **Williams'97:** Williams, R. J. J., Rozenberg, B. A. & Pascault, J.-P. Reaction-induced phase separation in modified thermosetting polymers. In Polymer Analysis Polymer Physics 95–156 (Springer Berlin Heidelberg, 1997).
- **Wondrak'99:** Wondrak, W. Physical limits and lifetime limitations of semiconductor devices at high temperatures. Microelectronics Reliability 39, 1113–1120 (1999).
- **Wypych'14:** Wypych, A. et al. Dielectric Properties and Characterisation of Titanium Dioxide Obtained by Different Chemistry Methods. Journal of Nanomaterials 2014, e124814 (2014).
- **Xu'13:** Xu, F. et al. Development of a SiC JFET-Based Six-Pack Power Module for a Fully Integrated Inverter. IEEE Transactions on Power Electronics 28, 1464–1478 (2013).
- **Yam'11:** Yam, F. K., Li, L., Ann, S. & Hass, Z. in Optoelectronics - Materials and Techniques (ed. Predeep, P.) (InTech, 2011).
- **Yang'98:** Yang, G.-R., Ganguli, S., Karcz, J., Gill, W. N. & Lu, T.-M. High deposition rate parylene films. Journal of Crystal Growth 183, 385–390 (1998).
- **Yao'12:** Yao, Y., Chen, Z., Lu, G. Q., Boroyevich, D. & Ngo, K. D. T. Characterization of Encapsulants for High-Voltage High-Temperature Power Electronic Packaging. IEEE Transactions on Components, Packaging and Manufacturing Technology 2, 539–547 (2012).

- **Yao'16:** Yao, Y., Zhou, T., Yang, C., Liu, Y. & Leng, J. Preparation and characterization of shape memory composite foams with interpenetrating polymer networks. Smart Mater. Struct. 25, 35002 (2016).
- **Yilmaz'90:** Yilmaz, H., Owyang, K., Chang, M. F., Benjamin, J. L. & Dell, W. R. V. Recent advances in insulated gate bipolar transistor technology. IEEE Transactions on Industry Applications 26, 831–834 (1990).
- **Zhang'05:** Zhang, Q. et al. 10kV Trench Gate IGBTs on 4H-SiC. in Proceedings. ISPSD '05. The 17th International Symposium on Power Semiconductor Devices and ICs, 2005. 303–306 (2005).
- **Zhang'08:** Zhang, Q., Das, M., Sumakeris, J., Callanan, R. & Agarwal, A. 12-kV p-Channel IGBTs With Low On-Resistance in 4H-SiC. IEEE Electron Device Letters 29, 1027–1029 (2008).
- **Zolper'98:** Zolper, J. C. A review of junction field effect transistors for high-temperature and high-power electronics. Solid-State Electronics 42, 2153–2156 (1998).

Chapter 2

Epoxy/Polyetherimide Blend: Preparation and Characterization techniques

The first part of this chapter will present the preparation procedure of pure epoxy network, epoxy/thermoplastic blends with different percentages and the pure thermoplastic film. The epoxy network and blend are going to be tested in the form of 1 mm thick films with different dimensions depending on the needs of the characterizations; the thermoplastic film is of 200 µm thickness.

We will present in the second part of this chapter different experimental techniques used in this study to characterize the morphology as well as thermal, mechanical and electrical properties of the samples.

2.1. Choice of the material

The objective of this research is to study the characteristics of a novel material of epoxy/thermoplastic with phase separation phenomenon susceptible to replace the encapsulation layer in a power module. The chosen material must respect different criteria needed to be able to replace the used silicone gel. It should be able to cover the power module respecting the maximum temperature of 200 °C that the module can resist. It should resist the wide variation of temperature solicited depending on the environment such as -50 to 300 °C in the aeronautics domain. Its coefficient of thermal expansion must be in the same range of other components used in the module. Finally, it should protect the module electrically, having low permittivity, low DC conductivity and high breakdown voltage.

The choice of this kind of epoxy to be blended with PEI is due to several aspects:

- First this material has been studied extensively in terms of kinetics and of cure conditions by Riccardi et al. [Riccardi'96], in the thesis work of Emmanuel Gerard-Reydet [*Gir'96*] and in the thesis work of Anthony Bonnet [*Bonnet'99-2*]. The cure conditions were defined to obtain a fully cured system with homogenous phase separation phenomenon.
- The thermoset/thermoplastic system showed better fracture toughness than the pure epoxy system particularly in the epoxy/PEI blend. This was shown in a critical stress

intensity test on pure epoxy DM and DM10PEI where an enhancement of 10 % is obtained in comparison with the neat epoxy [Gir'97]. This enhancement is due to the present of the phase separated PEI in the epoxy network as they absorbed the wave of propagation and eliminate the propagation of the fracture contributing in strengthening of the material as represented in Figure 28.

From this point our idea was to prove similar effects in the electrical properties, where it is suggested that the PEI nodules can limit treeing effect during the dielectric electrical breakdown.

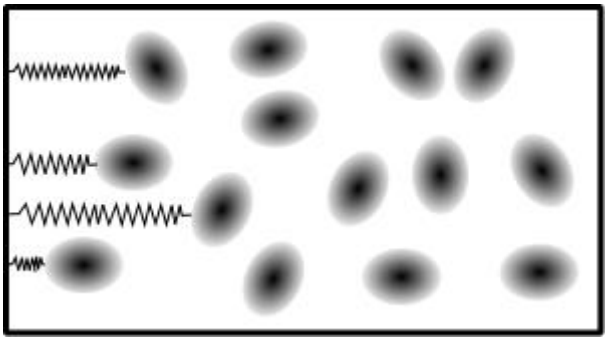

Figure 28: Schematic representation of the absorption of the treeing fracture phenomenon

- High glass transition of the epoxy matrix (160 °C), gives the epoxy an advantage of using it under a wide range of temperature without having any transition in comparison to other epoxies found in literature.
- The chosen PEI have a T_g of higher values than the epoxy system, this is due to the same reason of having the widest range of temperature without transition. In addition to that, one can distinguish it from that of epoxy in the characterization techniques.

2.2. Material Preparation

The epoxy prepolymer used in this work is liquid at room temperature, diglycidylether of bisphenol A **DGEBA** $\bar{n}$ = 0.15**,** commercialized by Huntsman under the name of Araldite® LY556, where, $\bar{n}$ denotes the degree of polymerization and its epoxide equivalent weight (EEW) equal to 183-189 $g.eq^{-1}$. The curing agent is an aromatic diamine with low reactivity in the form of powder, 4,4'-methylenebis-[2,6-diethylaniline], M-DEA supplied by Lonzacure™. The curing agent had an amine equivalent weight of 78 $g.eq^{-1}$. The thermoplastic used is a polyetherimide in the form of powder, PEI Ultem 1010, supplied by General Electric. Their chemical structures and principal characteristics are presented in Table 10.

2.2.1. DGEBA/MDEA (DM)

The neat epoxy network is prepared by adding the diamine in the stoichiometric ratio. It means that the ratio of epoxy to amine hydrogen groups equal to 1 (**Eq. 1**).

$$\frac{amine\ hydrogen\ function}{epoxy\ function} = 1 \qquad \textbf{Eq. 3}$$

The mixture was heated up to 90 °C and stirred under vacuum for 30 minutes to remove present bubbles. The mixture is then poured into preheated silicon molds, pre-cured for 4 h at 135 °C and post cured for 2 h at 200 °C following the method given by [*Bonnet'99-2*]. Silicon molds must be at the same temperature as the mixture (90 °C) to insure its fluidity when poured and to avoid the presence of bubbles into the cured sample. The mixture becomes viscous when cooled down below this temperature. Several sample sizes are established depending on the characterization technique, which will be indicated in the description of each technique. All samples have a thickness between 0.5 and 1 mm depending on the depth of the mold used. The term **DM** denotes the pure epoxy network.

Table 10: Characteristics of the used materials

Reactants	Formula	$\overline{M_n}$ (g.mol^{-1})	Density (g.cm^{-3})	Viscosity (mPa s)
DGEBA	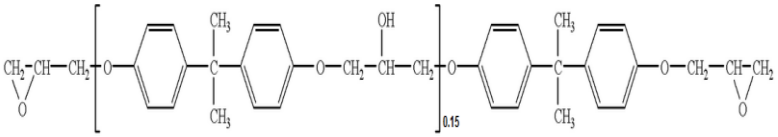	382	1,17	10000 – 12000 @25°C
MDEA	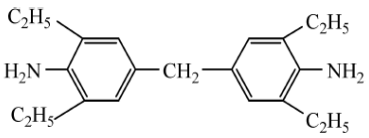	310	1,35	25 @ 90 °C
PEI	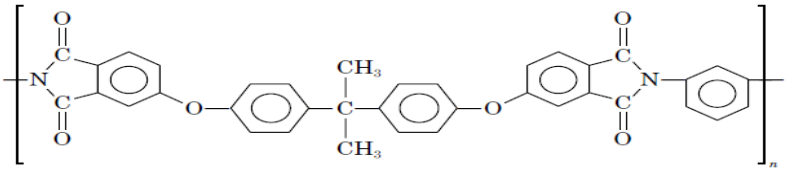	26,000	1,27	

The reaction mechanism of epoxy-amine takes place within three widely studied steps which are presented in Figure 29 [*Horie'70*], where k_1, k_2 and k_3 represent the kinetic catalytic and non-catalytic constants:

(1) The reaction of a primary amine on an epoxy group. This reaction opens the epoxy ring and creates a secondary amine and a hydroxyl function.
(2) The secondary amine reacts with an epoxy group producing tertiary amine and a hydroxyl function.
(3) Finally the hydroxyl group reacts with the epoxy group, which is a rare case without the presence of catalyzer. It can take place if the mixture of epoxy and the amine is non-stoichiometric and thus there exist an excess of epoxy group [Dusek'77]. Noting that the studied samples do not have this step as we are using a stoichiometric ratio.

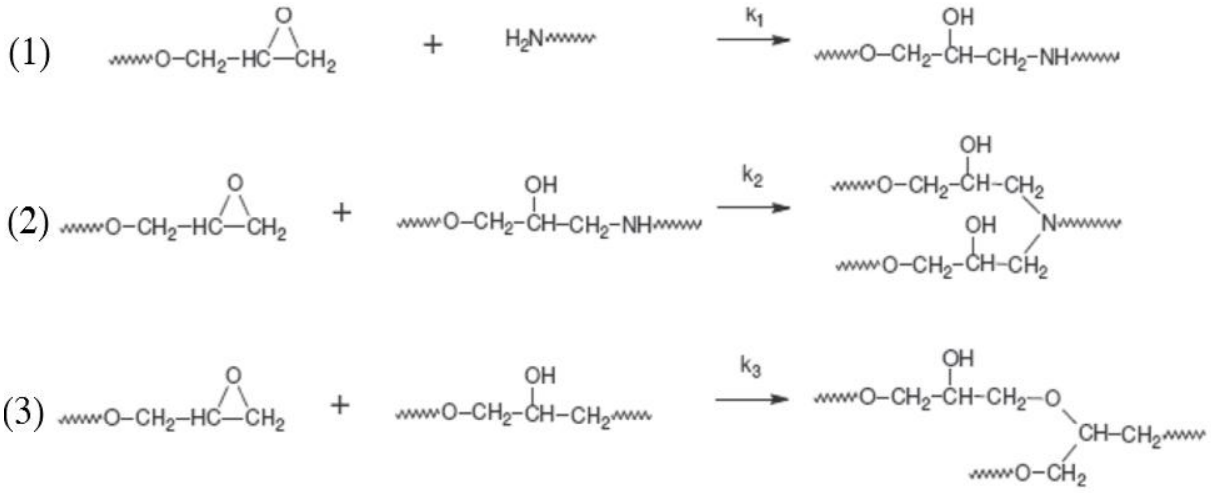

Figure 29: Reaction mechanisms of epoxy-amine [*Horie'70*]

2.2.2. Epoxy/polyetherimide blend (DM#PEI)

The process to obtain the phase separated epoxy/polyetherimide samples is as follows. First the powder of polyetherimide (thermoplastic component **TP**) is heated at 150 °C for 4 hours to remove all the possible humidity. It is then dissolved into the epoxy resin at 140 °C for 24 hours to insure full solubility. When the mixture is homogenous, the temperature is decreased till 90 °C and the curing agent is added. This mixture is mixed again at 90 °C for an hour and poured into the silicon molds. All the mixing steps are done under vacuum.

The phase diagram, Figure 30, of the DGEBA-MDEA/PEI let to the determination of the reaction kinetics and the thermodynamic calculations done by Girard-Reydet et al. [Gir'95] [Gir'95-2] [Gir'98]. They present a typical system exhibiting upper critical solution

temperature (UCST). Above this temperature (which depends on the fraction of the PEI), the system exhibits a single phase. The theoretical composition of the thermodynamic critical point is φ_{Mcrit} = 10.7 wt%. Using PEI with concentrations φ_{PEI} close to φ_{Mcrit}, such as 10 wt%, the system is considered in the unstable region where the phase separation phenomenon takes place by spinodal demixing (SD). When the weight percentage is much higher than φ_{Mcrit}, the homogeneous solution of epoxy and the thermoplastic enters into the metastable region and thus the phase separation proceeds via nucleation growth (NG).

The samples were then pre-cured at 160 °C for 4 h and post cured for 2 h at 185 °C. Precuring durations where chosen larger than the vitrification time to insure that most of the microstructures are developed isothermally. This precuring temperature determines the final morphology of the PEI thermoplastic into the epoxy network that will be discussed furtherly. Two different percentages were examined in this thesis work: 5 wt% and 10 wt% of PEI.

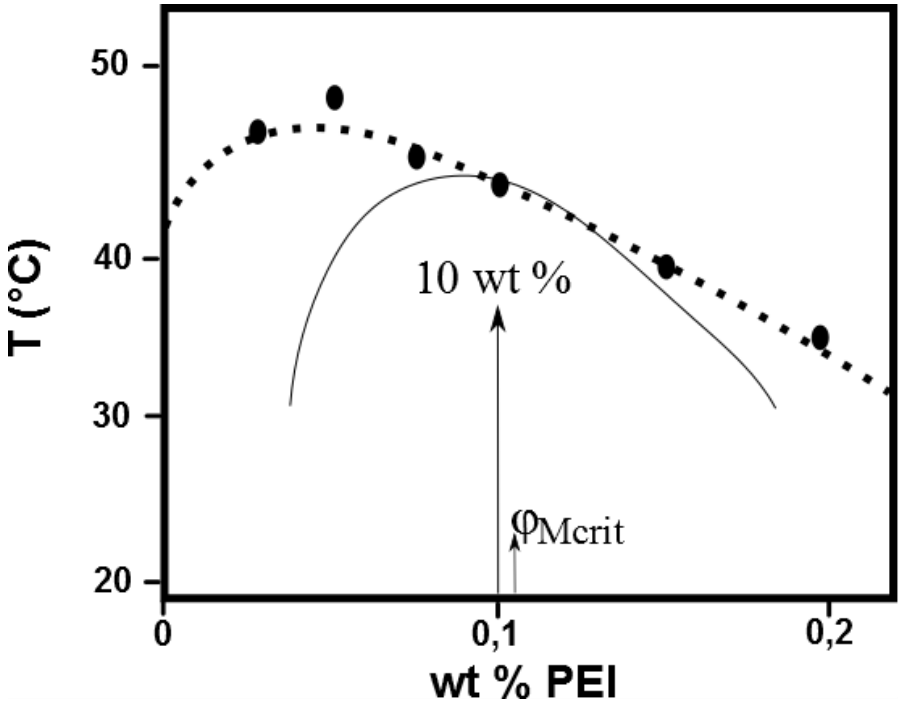

Figure 30: Initial cloud point curve for the DGEBA– MCDEA/PEI system. (—) (…) CPC calculated from thermodynamic models [*Gir'96*].

2.2.3. PEI films

PEI powder is pressed between two metallic plates covered with Teflon sheets. The plates are pressed 15 min at 270 °C that is bigger than the known softening temperature (218 °C). Then the films are pressed 5 min at 270 °C and 30 bars. The obtained films have a homogeneous average thickness of 200 µm.

2.3. Characterization techniques

Many characterization techniques have to be carried out after the preparation of each kind of sample. First step is to observe the phase separation morphology by Scanning electron microscopy (SEM) and transmission electron microscopy (TEM). The phase separation then must be confirmed by means of differential scanning calorimetry (DSC) and dynamic mechanical analysis (DMA). Thermogravimetric analysis (TGA) is used to verify the maximum temperature that each sample can withstand before the decomposition process. The electrical properties are measured by means of dielectric analysis (DEA), DC conductivity and breakdown voltage measurements.

2.3.1. Electron Microscopy

After preparing the samples and prior to any characterization, the morphological structure was verified by means of **SEM**. The DM#PEI samples were etched to remove a layer of the epoxy network and generate the necessary topographical contrast between the two constituents [*Mac'92*]. To prepare the samples first we fractured them at room temperature which is below the glass transition temperature of the epoxy $T_{g\ epoxy}$ = 164 °C. Then they were etched with a 1 wt. % solution of potassium permanganate in a 5:2:2 volume mixture of concentrated sulfuric acid, phosphoric acid and distilled water respectively. After etching, the samples were sequentially washed in aqueous sulfuric acid, hydrogen peroxide (100 volumes), water, and finally acetone for two minutes in each bath. All samples were then sputter coated with a 30 nm layer of gold using BAL-TEC SCD 005 Cool Sputter Coater. The images were taken by the secondary electron (**SE**) mode with 15 kV. The SEM used was ESEM-FEG FEI XL30 present at CLYM (Centre LYonnais des Microscopies). After obtaining the images, particle sizes and distribution were investigated using ImageJ software.

In order to investigate the interface between the PEI nodules and the epoxy network **TEM** images were recorded. Samples were sliced using an ultra-microtome to obtain slices of 60 to 70 nm in thickness. The prepared samples were placed onto 300 mesh copper grids for observation with an accelerating voltage of 80 kV. The analysis was performed on Philips CM120 transmission electron microscope (at the Centre Technologique des Microstructures CTμ of the University of Lyon).

2.3.2. Thermal analysis

2.3.2.1. Differential scanning calorimetry

DSC measures heat flow rate difference between the sample and an inert reference as a function of time and temperature. Heat flow (W) rate is the description of energy transfer in a time unit (W = J/sec). TA Q20 is the DSC instrument used for the measurements. It can provide a signal that converts the heat flow signal into a heat capacity signal using the following equation, **Eq. 4**:

$$\frac{dH}{dt} = C_p \frac{dT}{dt} + f(T,t) \qquad \textbf{Eq. 4}$$

C_p = sample specific heat x sample weight **Eq. 5**

dH/dt is the DSC heat flow signal, Cp is the sample heat capacity, dT/dt is the heating rate and finally f (T, t) is the heat flow in function of time at an absolute temperature. The measurement of the heat flow equation shows how the total heat flow reacts with heating rate due to the heat capacity of the sample. With the comparison with the empty pan it can evaluate the values of the measured sample. The sample of around 5 mg is sealed into an aluminum hermetic pan. The aluminum hermetic pans are placed onto two sample sensors in the same chamber as seen in Figure 31.

Figure 31: DSC chamber

The unique chamber for both pans insures the equilibrium in temperature flow on both sample holders. The temperature of the DSC apparatus is controlled with a liquid nitrogen cooling system (LNCS) that provides high performance temperature control system. Measurements are done under controlled atmosphere of helium in a temperature range from -100 to 300 °C at

a heating rate of 10 °C/min. Temperature and heat flow were calibrated using indium. Purged helium gas is used during the test to insure an inert atmosphere. The glass transition temperature can be characterized in amorphous polymers, knowing that both epoxy and PEI are amorphous materials. The glass transition is determined as the temperature at the half of the height of the heat capacity known as midpoint temperature T_g as shown in Figure 32. T_b and T_e are the beginning and the end of the transition from which the T_g is determined.

In crosslinked polymers, such as our epoxy samples, the glass transition takes place from glass to rubber phase and is represented as an endothermic step. The presence of an exothermic peak during the measurements reveals that the system is not fully cured. Knowing the glass transition temperatures will give us the knowledge on the phase separation phenomenon taking place in the DM#PEI samples.

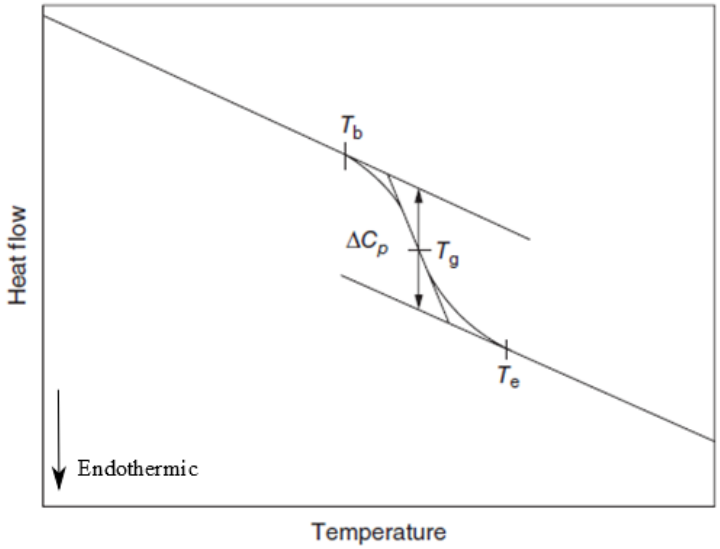

Figure 32: Glass transition temperature in a heating cycle

2.3.2.2. Thermo-gravimetric analysis

TGA characterizes the thermal stability of the samples. This technique measures the variation taking place in the sample's weight while increasing temperature and up till the sample is totally decomposed. Heating the sample will be the source of energy put into the system, and results in breaking down of the covalent bonds. The analysis was performed using TA Q500 analyzer equipped with a thermobalance that provides the accurate weight change detection from ambient to 1000 °C. The characterized samples have similar shape and are analyzed from 25 °C to 800 °C at a heating rate of 10 °C/min in both nitrogen and air

atmospheres. A schematic presentation of the TGA quartz furnace chamber is shown in Figure 33.

The degradation mechanisms of polymers are initiated by the dissociation of the weakest bonds at the temperature of pyrolysis and it is free from radicals [*Wampler'06*]. So it is related to the bond strengths and the structure of each polymer. There are three kinds of degradation mechanisms, random scission, monomers reversion and side group scission. The degradation mechanism does not only depend on the nature of the material but also on the atmosphere surrounding it. Different degradation mechanisms can be obtained using inert gas or in the presence of air. The analysis under inert gas avoids the presence of degradation caused by an oxidation process.

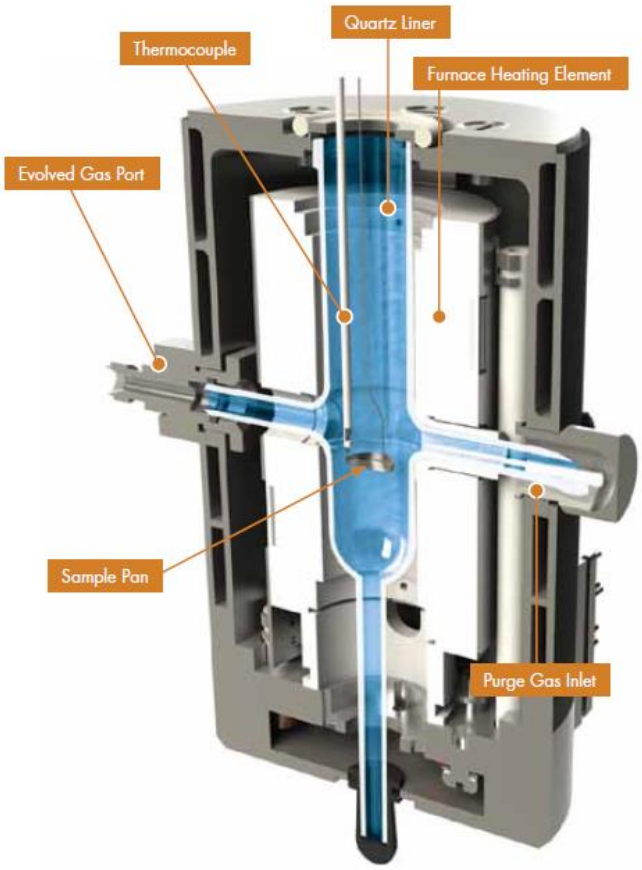

Figure 33: TGA Q500 schematic description [*TA_TGA*]

2.3.3. Dynamic Mechanical Analysis

DMA involves imposing a cyclic strain on a sample and measuring the resulting stress response and the phase shift that is represented in Figure 34. The phase angle δ measured is between 0° and 90°. The DMA measures the damping and the stiffness of the material

expressed by the storage modulus and tan δ. Storage modulus is represented by E' and the loss factor by E" modulus. The ratio of the loss modulus to the storage one is tan δ.

Damping is the dissipation of energy reported in a material under cyclic load and it expresses the ability of the material to absorb mechanical energy depending on the nature of the material as well as temperature and frequency. The stress applied at any point of the figure is described in **Eq. 6**

$$\sigma(t) = \sigma_0 \sin \omega t \qquad \textbf{Eq. 6}$$

where σ is the stress at time t, σ_0 is the maximum stress that can be applied and ω is the frequency of oscillation.

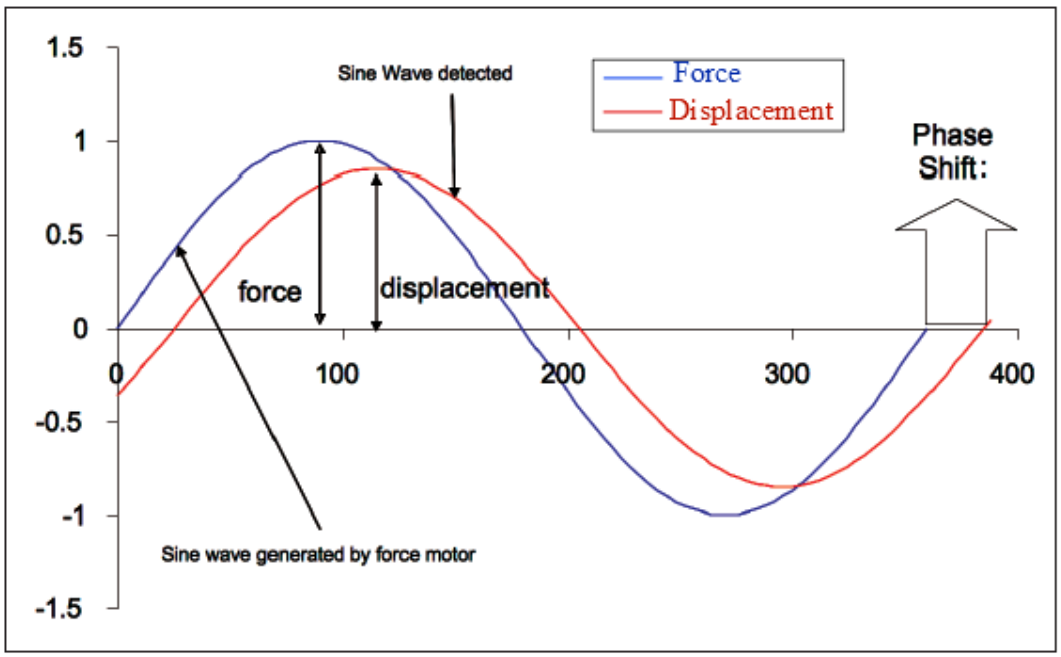

Figure 34: Applied sinusoidal strain (displacement) and the measured phase shifted sinusoidal stress (force)

The strain will result depending on the viscous and the elastic behavior of the examined sample. In a pure elastic material, strain will be in phase with the applied stress and can be expressed by **Eq. 7**:

$$\varepsilon(t) = \varepsilon_0 \sin \omega t \qquad \textbf{Eq. 7}$$

where ε (t) is the strain at any time, ε_0 is the strain at the maximum stress. δ will be at 0° and E is the modulus of the material that is the ratio between the strain and the stress in the linear region $E = \varepsilon_0/\sigma_0$. When the material is purely viscous and the stress is proportional to the strain rate, δ will be at 90° and the strain will behave as expressed in **Eq. 8**.

$$\varepsilon(t) = \omega\sigma_0 \sin(\omega t + \pi/2) \quad \textbf{Eq. 8}$$

Considering a material that have a behavior that lies between the pure elasticity and pure viscosity, named the viscoelastic behavior, where δ has a value between 0° and 90 °. The strain can be expressed at any time as represented in **Eq. 9**:

$$\varepsilon(t) = \varepsilon_0 [\sin(\omega t)cos\ \delta + \cos(\omega t) \sin \delta] \quad \textbf{Eq. 9}$$

This equation is divided into two parts; in-phase and out-of-phase strain and they are expressed as following:

$$\varepsilon' = \varepsilon_0 \sin(\delta) \quad \textbf{Eq. 10}$$

$$\varepsilon'' = \varepsilon_0 \cos(\delta) \quad \textbf{Eq. 11}$$

The modulus is divided into two parts as well, the storage modulus (E') measuring the stored energy in the sample that represents the elastic behavior, and the loss modulus (E ") measuring the energy dissipated representing the viscous behavior.

$$E^* = E' + iE'' \quad \textbf{Eq. 12}$$

$$\frac{E''}{E'} = \frac{\sin \delta}{\cos \delta} = \tan \delta \quad \textbf{Eq. 13}$$

Polymers have different physical characteristics depending on the temperature, frequency and the applied stress and considered as a viscoelastic material. One of the mechanical tests using DMA is the tension test demonstrated in **Figure 35** (a). The sample is subjected to a tensile force F and will deform in the same direction. The stress applied is expressed as following:

$$\sigma = \frac{F}{A_0} \quad \textbf{Eq. 14}$$

where, A_0 is the constant cross section of the material. The engineering strain is defines as:

$$\varepsilon = \frac{l - l_0}{l_0} \quad \textbf{Eq. 15}$$

here, l is the length of the sample that changes with the applied stress. The tensile stress-strain behavior is demonstrated in Figure 35 (b); the initial part corresponding to the elastic region is a straight line passing through the origin and has a slope of Y the Young's modulus of the material. The elastic region will help us to find the values of stress and strain that must not be exceeded in a DMA scan.

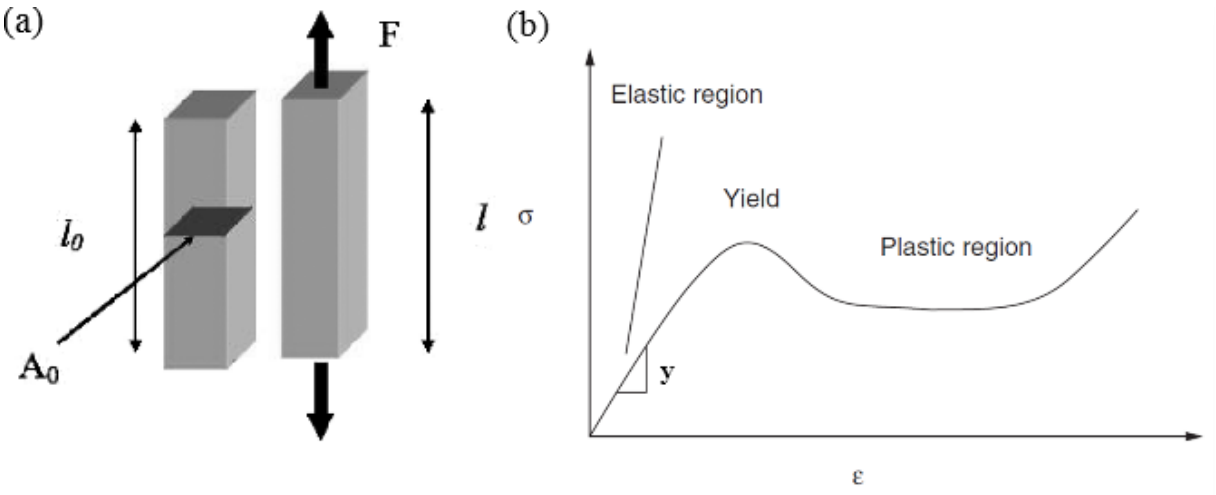

Figure 35: (a) Sample under tensile load with deformation in the direction of the applied force, (b) typical stress-strain behavior [*Chartoff'09*]

After choosing the maximum value of a sinusoidal applied stress or strain, a DMA scan under chosen frequencies can be applied with an increasing temperature. The ideal storage modulus response is demonstrated in Figure 36. Different numbers describe different molecular motion for each recorded transition. Thermal transitions in polymers can be described in terms of free volume changes. Free volume is considered to be between the parts of a molecule. With the variation of temperature, the molecules will interact by changing its form and thus changing the total occupied volume fraction. In the glassy plateau which is below the glass transition, sub-glass transitions take place due to bending or stretching of molecular bonds. β relaxation can be obtained from the movement of a specific chain and not the whole molecules in a polymeric material. Around the glass transition temperature, the sample becomes softer as the storage modulus decreases and tan δ peak increases. Tan δ peak height is typically between 0.1 and 1.2 depending on the material.

In our case, DMA was carried out using a TA Q800 instrument. Tensile testing clamp for rectangular samples was used. Samples have a thickness between 0.5 and 1 mm, a length of 20 mm and a width of 10 mm. The tensile strain is applied at a frequency of 1, 3, 5 and 10 Hz and its value is equal to 0.01 %. Storage modulus E', Loss Modulus E'' and the loss factor tan δ were recorded during temperature ramps from -100 °C up to 300 °C with a rate of 3 °C/min.

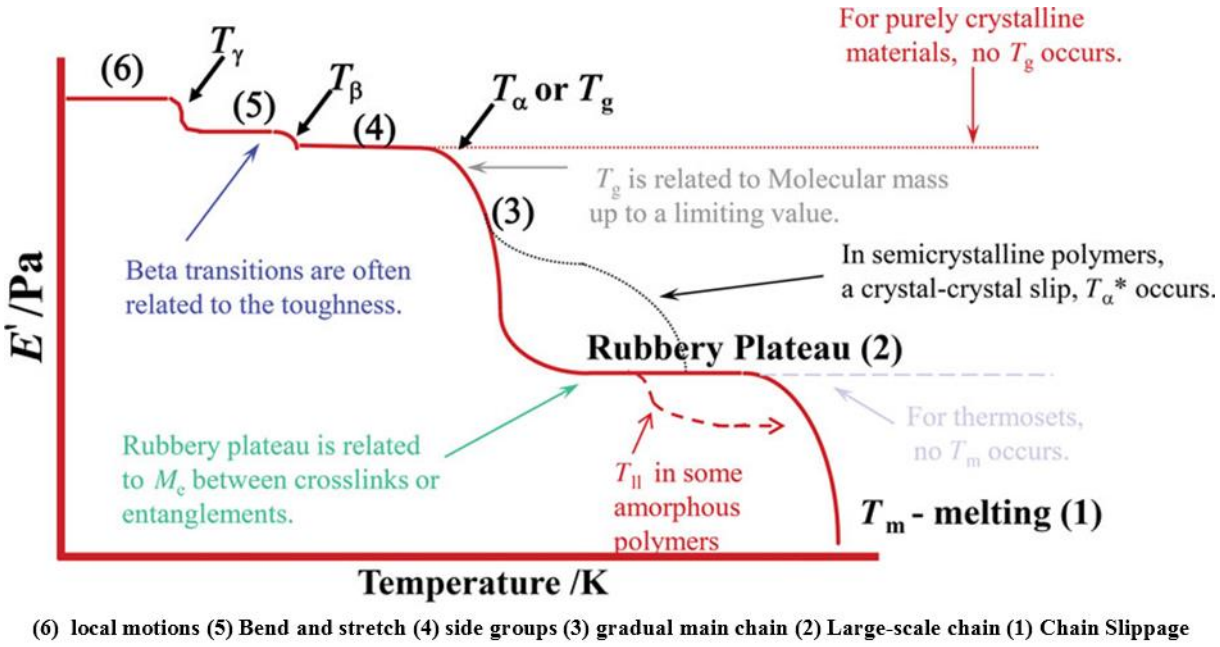

Figure 36: Idealized DMA scan [Menard'02]

2.3.4. Electrical characterizations

2.3.4.1. Dielectric Analysis

Dielectric analysis of materials plays a fundamental role in the description of the electrical properties of the studied material and the determination of the transitions taking place. It provides a link between transitions corresponding to the dynamics of molecular motion relaxations and the characterization of its bulk properties. Few studies only have demonstrated the dielectric response of epoxy/thermoplastic phase separated blend [*Mac'92*] [*Lestriez'98*]. Moreover, several studies were carried out in monitoring in real time the phase separation process using the dielectric spectroscopy during the crosslinking process[*Delides'92*] [*Brown'96*] [*Poncet'99*] [*Bonnet'00*] [*Pethrick'02*] [*Kran'03*] [*Montserrat'03*] [*Montserrat'06*].

DEA is a measurement technique that characterizes the behavior of the complex permittivity in function of frequency and temperature. Complex permittivity is expressed by the interaction of the applied electric field with the dipole moments present in the dielectric sample. Sinusoidal Voltage U (t) is applied on the sample and the resulting sinusoidal current I (t) is measured with the phase shift φ occurring between them. Phase angle and the relative amplitudes of both voltage and current are the basis to calculate the complex impedance with its real and imaginary parts:

$$Z^*(\omega) = Z'(\omega) + i\,Z''(\omega) = \frac{U_0}{I_0}\{\cos(\theta\omega) + isin(\theta\omega)\} \qquad \textbf{Eq. 16}$$

Where Z' and Z" are the real and imaginary components of the complex impedance and ω is the angular frequency with ω = 2πf. Impedance leads to defining the complex relative permittivity of the material (ε_r^*) which represents the effect of polarization on the response to the applied electric field. The dielectric material can be represented as a capacitor and a resistor in parallel and the current must have both real and imaginary component [*Menguy'97*], and thus the complex permittivity can be defined as:

$$\varepsilon_r^* = \varepsilon_r' + i\,\varepsilon_r'' = \frac{1}{i\omega Z^*(\omega) C_0} \qquad \textbf{Eq. 17}$$

Where ε_r' is real part of the complex permittivity and defines the ability of a material in storing potential energy under the influence of an external electric field. ε_r'' is the imaginary part representing the losses involved in the polarization process and the energy dissipation in the material, C_0 is the vacuum capacitance and its expressed as:

$$C_0 = \frac{\varepsilon_0 S}{d} \qquad \textbf{Eq. 18}$$

Where ε_0 is dielectric constant of vacuum. The ratio between the imaginary part and the real part can be defined as the tan δ as shown below:

$$\text{Tan } \delta = \frac{\varepsilon_r''}{\varepsilon_r'} = -\frac{Z'(\omega)}{Z''(\omega)} \qquad \textbf{Eq. 19}$$

It defines the ratio between the dissipated energy to the stored one. With every variation taking place in the real part of permittivity the loss factor ε_r'' peak defines the presence of a molecular relaxation in the material as explained by Debye's model and presented in Figure 37. Relaxation time τ is defined by the time where the relaxation have a maximum value where τ = 1/ω (sec). Pure Debye behavior is hardly found in material relaxations responses according to several experimental results [*Jonscher'99*]. The time of dipolar relaxations is in function of temperature. Relaxations in polymers can vary following either Arrhenius law or Vogel-Fulcher-Tamman law (**VFT**). Arrhenius law is generally observed when the temperature is lower than the glass transition temperature, where the evolution of the mean relaxation with respect to temperature is expressed as following:

$$\tau\,(T) = \tau_0 \exp\left(\frac{E_a}{K_B T}\right) \qquad \textbf{Eq. 20}$$

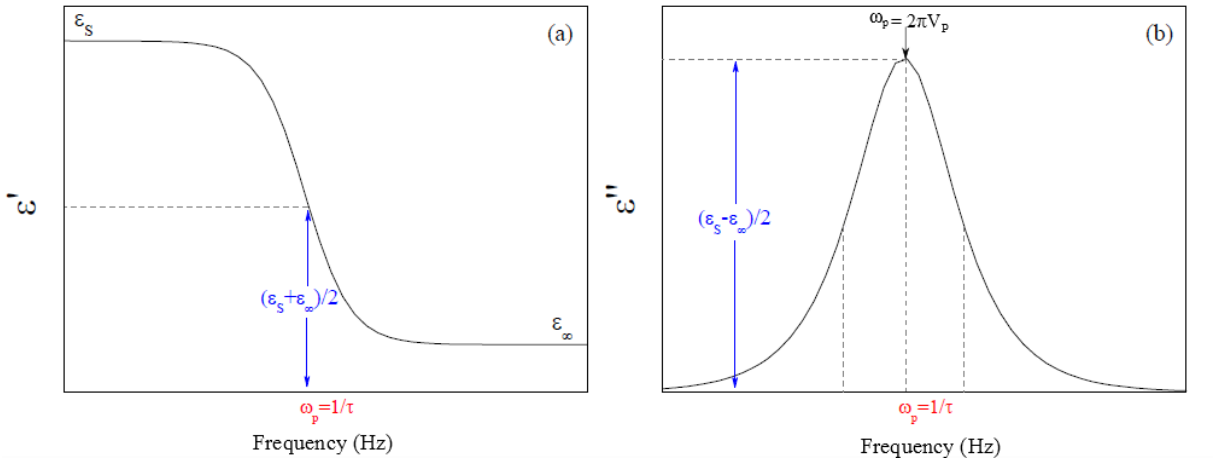

Figure 37: (a) Real and (b) imaginary part of the complex permittivity in function of frequency according to Debye relaxation process [*Schonhals'03*]

Where E_a is the activation energy, τ_0 relaxation time at an infinite, k_B Boltzmann's constant (k_B=8.617 × 10^{-5} eV. K^{-1}) and T the temperature. VFT relaxation is mainly observed when the temperature is higher than the glass transition temperature and is described as following [*Garca'89*]:

$$\tau\,(T) = \tau_0 \exp\left(\frac{E_a}{K_B(T-T_V)}\right) \qquad \textbf{Eq. 21}$$

Where T_V is the Vogel's temperature that is usually 50 °C lower than the glass transition temperature.

Relaxations can be also extracted from the peaks of M'' the imaginary part of the complex electric modulus M*, which is the reciprocal of the relative permittivity ε_r*, and is expressed as follows:

$$M^*(\omega) = M'(\omega) + iM''(\omega) \qquad \textbf{Eq. 22}$$

Consider a capacitor filled with a dielectric material with an applied sinusoidal voltage on it the dielectric function is defined as:

$$\varepsilon_r^* = \frac{C^*(\omega)}{C_0} \qquad \textbf{Eq. 23}$$

The measurement can be done under a wide range of frequency between 10^{-6} Hz to 10^{12} Hz, but in order to cover this entire frequency domain several measurement techniques are needed to avoid parasitic impedances caused by cables and connectors [*Kremer'89*]. We are interested in the frequency domain of 10^{-1} to 10^{6} Hz where impedance analysis is involved. The dielectric derived response is obtained from the microscopic fluctuation of molecular dipoles, propagation of mobile free charge carriers and the separation of charges at the interface

increasing the polarization in the characterized sample [*Bottcher'78*]. The increase in polarization can be explained by two different mechanisms, Maxwell/Wagner/Sillars (MWS) polarization that exist in heterogeneous dielectrics, and is due to a delay in charge transfer at the interface between components with different dielectric permittivity [*Tsangris'96*], and/or electrode polarization that takes place at the external electrodes contacting the sample. The polarization contributes in increasing the loss factor much higher than the order of magnitude of the dielectric response.

Several types of relaxations can be characterized from the complex permittivity in an epoxy network. The common relaxations at a constant frequency with the variation of temperature are represented in Figure 38. α relaxation is associated to the glass transition temperature T_g, it is distinguished by a high narrow peak with respect to β relaxation. β relaxation, originating from the fluctuation of hydroxyether units, is characterized by a broad relaxation peak at low temperatures [Heux'97]. Conductivity, as shown in **Figure 38** is very close to α relaxation and may hide it and in certain conditions it becomes complicated and hard to determine accurately α relaxation [*Forthergill'10*].

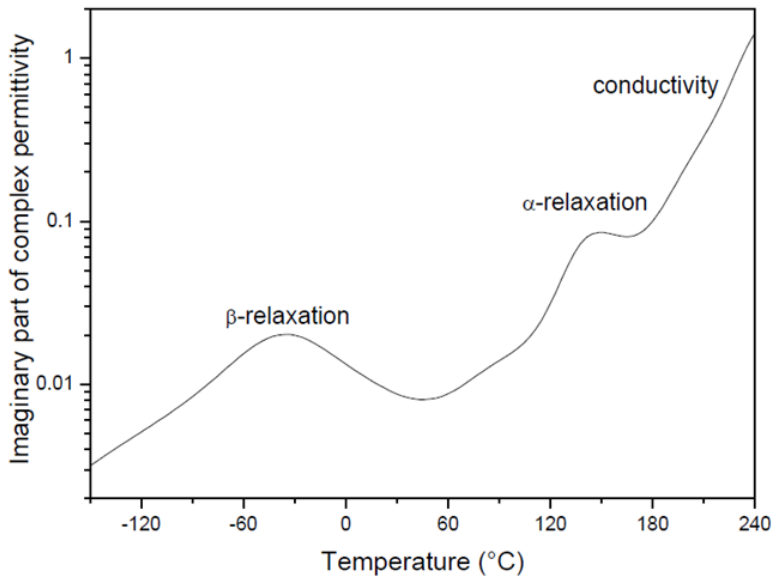

Figure 38: Schematic representation of loss factor of relative permittivity in an epoxy network as function of temperature [*Forthergill'10*]

The relationship between the applied electric field (E) on the sample and the obtained current density (J) arises the conductivity according to Ohm's law [Schonhals'03] :

$$J = \sigma^* E \qquad \textbf{Eq. 24}$$

Where, E is the electric field and the complex conductivity is σ*:

$$\sigma^*(\omega) = \sigma'(\omega) + i\sigma''(\omega) \quad \textbf{Eq. 25}$$

σ' and σ" are the corresponding real and imaginary parts. The derivative of dielectric displacement (D) is represented as following:

$$\frac{dD}{dt} = i\omega\varepsilon^* \varepsilon_0 E \quad \textbf{Eq. 26}$$

According to Maxwell's equation the current density eq. 18 and the derivative of the time displacement eq. 20 are equivalent, which gives us for a sinusoidal electric field E (ω):

$$\sigma^*(\omega) = i\omega\varepsilon_0 \varepsilon^*(\omega) \quad \textbf{Eq. 27}$$

and the real and imaginary parts are defined as following:

$$\sigma'(\omega) = \omega\varepsilon_0 \varepsilon''(\omega) \quad \textbf{Eq. 28}$$

$$\sigma''(\omega) = \omega\varepsilon_0 \varepsilon'(\omega) \quad \textbf{Eq. 29}$$

The σ*(ω) represents the ac conductivity of the material where at low frequencies in pure electronic conduction conditions no contribution arises to the ε' and thus the imaginary part σ'' increases linearly with the frequency. In the contrary σ' becomes constant equal to σ_0 and $\varepsilon''(\omega)$is defined as:

$$\varepsilon''(\omega) = \frac{\sigma_0}{\varepsilon_0 \omega} \quad \textbf{Eq. 30}$$

σ_0 is considered as the dc conductivity of the tested sample and can be extrapolated from the σ' (ω) at different temperatures for lower frequencies. The activation energy can be deduced by Arrhenius law:

$$\sigma_{DC}(T) = \sigma_0 \exp\left(-\frac{E_a}{K_B T}\right) \quad \textbf{Eq. 31}$$

or by Vogel-Fulcher-Tammann VFT law:

$$\sigma_{DC}(T) = \sigma_0 \exp\left(-\frac{E_a}{K_B(T-T_V)}\right) \quad \textbf{Eq. 32}$$

In this work Solatron analytical (Modulab MTS) dielectric spectrometer, equipped with the LakeShore 335 Temperature controller, is used to characterize the dielectric properties of samples under a temperature range of -100 to 250 °C in a Helium atmosphere as shown in Figure 39. Temperature control is guided by the use of liquid nitrogen circulating around the chamber that contains the sample. Dielectric measurements are carried out applying Vrms=5V from 10^6 to 10^{-1} Hz (10 points per decade) under isothermal conditions. Measurements are acquired increasing the temperature with a step of 3 °C. Samples used are of circular shape

with a 3 cm diameter and thicknesses of 0.5 up to 1 mm. Two gold electrodes, of 25 mm in diameter, were sputtered on both sides using BAL-TEC SCD 005 Cool Sputter Coater. The model used for measurement is metal-insulator-metal (MIM) capacitor.

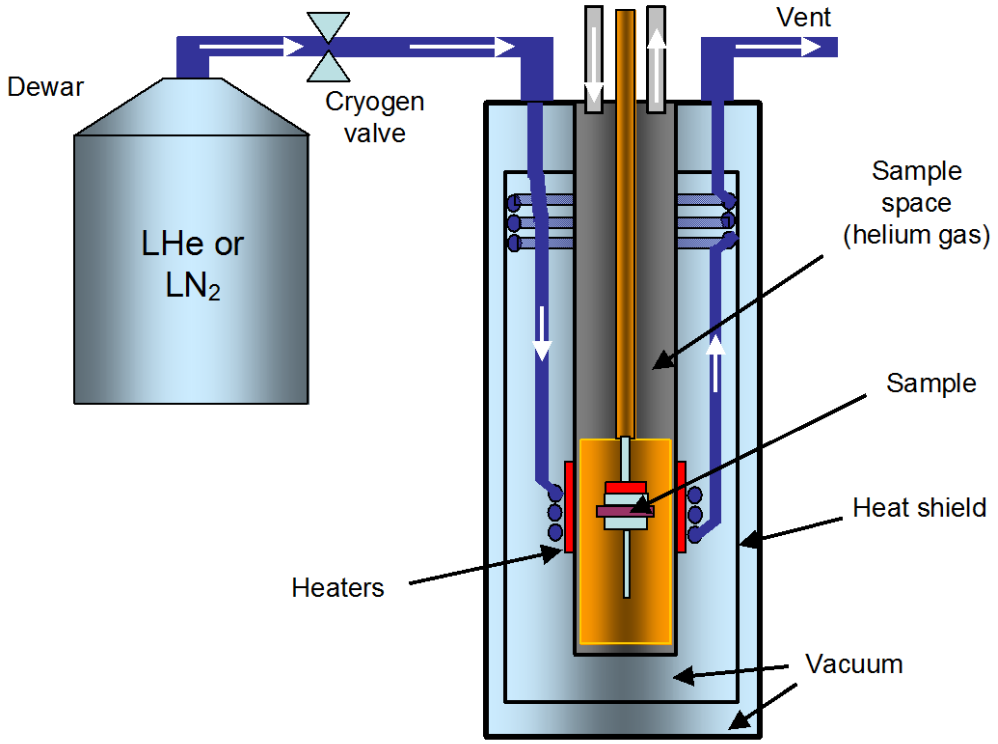

Figure 39: Internal assembly of the cryostat where the sample is measured [*Modulab'14*]

2.3.4.2. Electrical Conductivity

Electrical conductivity or resistivity measurement is performed when an electrical field is applied on an insulating material. The resulting current can be measured and thus the resistance of the material R= U/I can be calculated. The electrical resistivity ρ of the material can be deduced:

$$\rho = \frac{R.S}{l} \qquad \textbf{Eq. 33}$$

Where S is the surface area of the material and l represents its thickness. The SI unit of electrical resistivity is the ohm-meter (Ω.m) but for insulating material ohm-cm (Ω.cm) is used. Conductivity σ is the reciprocal of the resistivity:

$$\sigma = \frac{1}{\rho} \qquad \textbf{Eq. 34}$$

Its SI unit is Siemens per meter $S.m^{-1}$. It can be directly calculated from the recorded measurements of the current by calculating the current density J (A/m^2):

$$J = \sigma E \qquad \textbf{Eq. 35}$$

Where, E is the applied electric field.

When a constant voltage is applied between the two electrodes of the sample, a current will pass through it having decreasing values with time corresponding to the polarization current, I_P, as shown in Figure 40. I_P is divided into two parts, I_A the absorption current and I_C the conduction current. The absorption current is presented as:

$$I_A = I_P + I_C \qquad \textbf{Eq. 36}$$

When the applied field is stopped the depolarization current I_D, with its negative value, tends to return to zero. I_D in its ideal case is presented as following:

$$I_D = - I_A \qquad \textbf{Eq. 37}$$

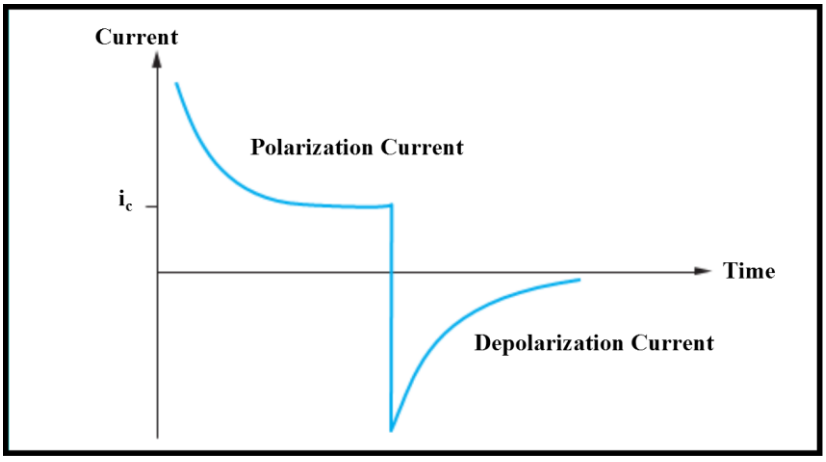

Figure 40: Classical evolution of polarization and depolarization current due to an applied electric field [*Segui'00*]

When the two currents are reversible, having two superposed graphs, the polarization phenomenon is related to purely to dipolar movements. The uniform distribution of the applied electric field in a uniform material gives this reversible response; this is usually convenient for non-highly resistive polymers [*Guill'06*]. When the two currents are not superposed, the presence of space charge in the material is susceptible. This case is in general present in solids with charged impurities that are able to accumulate on the electrodes [*Segui'00*].

Charge injection:

Conduction phenomenon in insulating materials needs charge injection phenomenon. It can be defined as Schottky effect which is also named field enhanced thermionic emission or by Fowler-Nordheim effect. Current density according to the Schottky law is presented as following:

$$J_s = A_s T^2 \exp\left(-\frac{\emptyset_0 - \beta_s\sqrt{E}}{K_B T}\right) \quad \textbf{Eq. 38}$$

Where A_s is the Richardson-Dushman constant for thermionic emission, $\emptyset_0$ is the barrier height and E the field at the cathode. β_s is the Schottky constant:

$$\beta_s = \sqrt{\frac{q^3}{4\pi\varepsilon_0\varepsilon_r}} \quad \textbf{Eq. 39}$$

where q is the elementary charge. Such a mechanism is represented by the graph ln J = f($\sqrt{E}$) where a linear relation exists. The slope is equal to $\frac{\beta_s}{K_B T}$ that only depends on the relative permittivity of the material.

Fowler-Nordheim effect describes the pathway of charges through the potential barrier depending on the tunneling effect. Current density in this case is represented as following:

$$J = AE^2 \exp\left(-\frac{B}{E}\right) \quad \textbf{Eq. 40}$$

where,

$$A = \frac{q^3}{8\pi h \emptyset_0} \quad \textbf{Eq. 41}$$

and

$$B = 4\left[(2m)^{\frac{1}{2}}\emptyset_0^{\frac{3}{2}}\right] \quad \textbf{Eq. 42}$$

where h is the zero-field height of the barrier and m is the mass of an electron. If the conduction phenomenon is controlled by this mechanism, then the representation of ln(J/E^2) versus 1/E will give a straight line. This mechanism is usually present at low temperatures and/or very high electric fields.

Conduction mechanisms:

Number of conduction mechanisms can contribute to the conduction current through the dielectric film at the same time [*Chiu'14*]. The mechanisms can be ohmic conduction, Poole-Frenkel mechanism, hopping conduction, space-charge-limited conduction (**SCLC**), ionic conduction and grain-boundary-limited conduction. From measurements using different electric field and temperature, conduction mechanisms can be determined.

The ohmic conduction mechanism, for example, is stablished due to the movement of mobile electrons in the conduction band and the holes in the valence band. Under low voltages the materials obey Ohm's law [*Segui'00*]. A linear relationship with a slope of 1 exists between the current density and the electric field applied that defines this mechanism as shown in the first part of the graph represented in Figure 41.

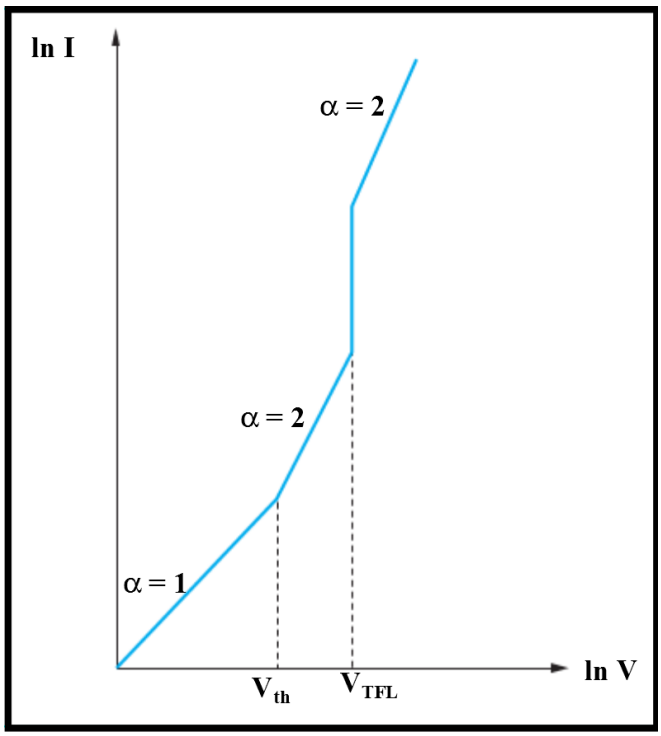

Figure 41: Current-voltage characteristic for a conduction mechanism limited by space charge [*Segui'00*]

Above the transition voltage (V_{th}) the slope changes and it can have slopes different than 1 corresponding to different regimes. If the slope has a value of 2, this defines the limitation of the current by space charge phenomenon. Above trap filled limit voltage (V_{TFL}), no more free traps exist and are they are all filled with charges. When higher voltage is applied the system has more energy which enables the conduction of free charges and a slope of 2 reappears [*Lampert'70*]. In the Poole-Frenkel mechanism, electrons are trapped in localized state where

upon applying either sufficient temperature or high voltage they move to the conduction band and freely in the material. The conductivity in such case obeys the following equation:

$$\sigma = \sigma_0 \ exp\left(\frac{\beta_{PF}\sqrt{E}}{k_B T}\right) \qquad \textbf{Eq. 43}$$

where k_B Boltzmann's constant , T the temperature and β_{PF} Poole-Frenkel constant [*O'Dwyer'73*] depends on the relative permittivity of the material and is represented as following:

$$\beta_{PF} = \left(\frac{q^3}{\pi\varepsilon_0\varepsilon_r}\right)^{1/2} \qquad \textbf{Eq. 44}$$

Poole-Frenkel mechanism usually takes place when a limited value of traps is found in the material. As the density of traps increases, the voltage barriers increases and the hopping mechanism interacts.

For this study the volume resistivity of the sample is considered. Two electrodes are placed on both sides of the sample. The electric field is applied continuously between the two electrodes. The current, in an ideal pathway, must traverse the volume of the sample, but due to insulating properties of the materials it preferably goes along the surface of the sample to join the electrode placed on the other side. The recorded current in such a case cannot implicate the volume resistivity of the sample. In order to avoid this phenomenon, guard electrode has to be used as shown in Figure 42. The role of the guard electrode connected to ground is to avoid the current from going along the surface.

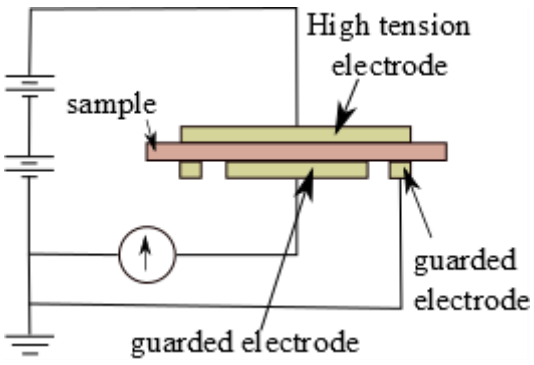

Figure 42: Guard electrode for the measurement of volume electrical resistivity [*Menguy'97*]

Another way to avoid the current to go along the surface is by depositing a thick insulating material that can block all the current from following the surface as shown in Figure 43.

The conductivity has a dependence on temperature obeying Arrhenius or VFT law. When the temperature increases, the amplitude of the current passing through the sample increases as the conductivity increases, that is to say the resistivity decreases. Under the effect of the electric field as well as the increase in the temperature, charge carriers can move in an easier way increasing the conductivity as well.

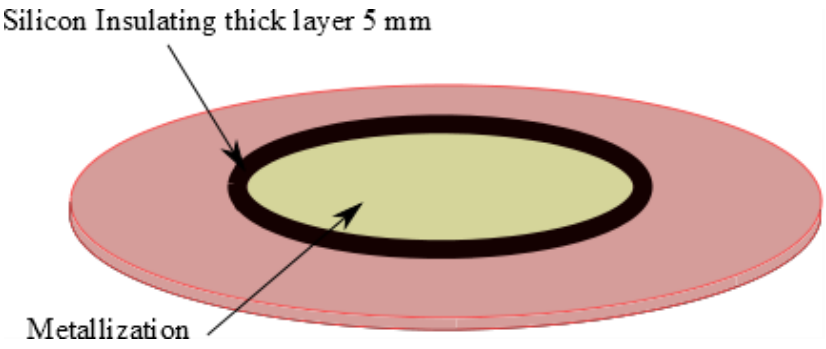

Figure 43: Measured sample with an insulating material surrounding the electrode.

In our work, measurements at room temperature were done using Keithley 6512 electrometer. Samples have 6 cm diameter and of a thickness between 0.5 and 1 mm. Electrodes were deposited using BAL-TEC SCD 005 with gold 4 cm diameter. The electrodes were surrounded by a thick layer of silicon (LOCTITE SI 5130). The samples were polarized at room temperature for 1000 seconds and then short-circuited for the same duration. During these measurements the current was recorded and saved electronically. The ambient measurements were done at LAPLACE laboratory, Université Paul Sabatier (Toulouse).

2.3.4.3. Breakdown voltage

The term breakdown is the destruction of the sample by the conducting pathway. This kind of measurement gives the maximum electric field that a material can handle. Electrical breakdown is always electrically power driven but there is a process that leads to the final breakdown. This process can be from electronic, thermal or electromechanical origin.

Breakdown fields in the material can be lowered due to the presence of any imperfection in an insulating system. The breakdown is usually initiated at an inhomogeneity present either in the bulk of the material or at the electrode/insulator interface. The inhomogeneity or defects can be due to irregularities in the electrode, presence of free volume with sizes less than 10 nm or the presence of impurities in the material such as moisture or an imperfection mixture [*Dissado'92*].

In electronic breakdown, the general cause is the increase in the number of electrons reaching high magnitudes that causes the destruction of the lattice of the material. This mechanism is very fast. It is divided into two different kinds intrinsic or avalanche [*Dissado'92*]. The intrinsic breakdown takes place when, at a high critical electric field, the electrons acquire indefinite and instable energy faster than they can lose by electron-phonon scattering and thus they cause the breakdown. The electrons can lose energy as well by collision with material defects or with other electrons. Lattice destruction takes place directly as it is considered weak to the amount of energy given to it. The avalanche breakdown is also due to high electric filed resulting in high energy gain to the electrons. The electrons with their sufficient energy can cause a second generation of collision doubling their number. This rapid chain reaction continues until causing local lattice destruction and thus the breakdown of the sample. Electronic breakdown can also be due to partial discharge phenomenon. Its main cause is the presence of free volumes which are difficult to completely eliminate in polymeric materials [*Stevens'88*]. Air filled cavities have low permittivity and low breakdown strength, in comparison to any insulating material, which leads to an enhanced electric field in the void. The walls of the voids are likely to be more conducting making a new source of energy and causing a faster breakdown in the material. This may not cause the whole polymer to breakdown and that is why it is called partial discharging phenomenon.

In thermal breakdown, heating of the sample by Joule effect occurs due to the dissipation of electrical power above critical temperatures. As the electric field increases the temperature increases and the electrons gain more mobility resulting directly or indirectly in the breakdown phenomenon. It is difficult to monitor the spatial and temporal evolution of the temperature of a polymer film after the application of the electric field. Some researches demonstrated the presence of randomly distributed hot spots in tested samples. Nevertheless, it was not said to be a pure thermal breakdown mechanism [*Dissado'92*].

Electromechanical breakdown takes place when a mechanical compressive stress is applied due to the electrostatic force attracting both electrodes to each other and increasing the pressure on the sample. In this case the thickness of the sample is decreased as it could not balance the electrostatic force by its elasticity. With the same voltage, the thickness is decreased and thus the electric field increases that increases the probability to breakdown. The dielectric elasticity and the electrostatic attraction of the electrodes before the breakdown can be considered in equilibrium and are equated in the following equation [*Stark'55*]:

$$\frac{\varepsilon_0 \varepsilon_r}{2}\left(\frac{V}{l}\right)^2 = Y\, log_e\left(\frac{l_0}{l}\right) \qquad \textbf{Eq. 45}$$

where Y is the Young's modulus of the dielectric polymer, l_0 is the initial dielectric thickness, and l, voltage dependent, is the thickness of the sample under electrical field. The voltage, permittivity of the material and air and the Young's modulus are known values of the studied epoxy. From this equation the probability of having a decrease in the thickness of the sample can be evaluated.

In this work, the dielectric breakdown strength of the samples was measured by applying a linearly increasing DC voltage up till the breakdown takes place. The sample of 6 cm diameter and a thickness between 300 µm and 1 mm is placed between two spherical electrodes, where the whole assembly is covered with silicon insulating oil. The sample and electrodes are shown in Figure 44.

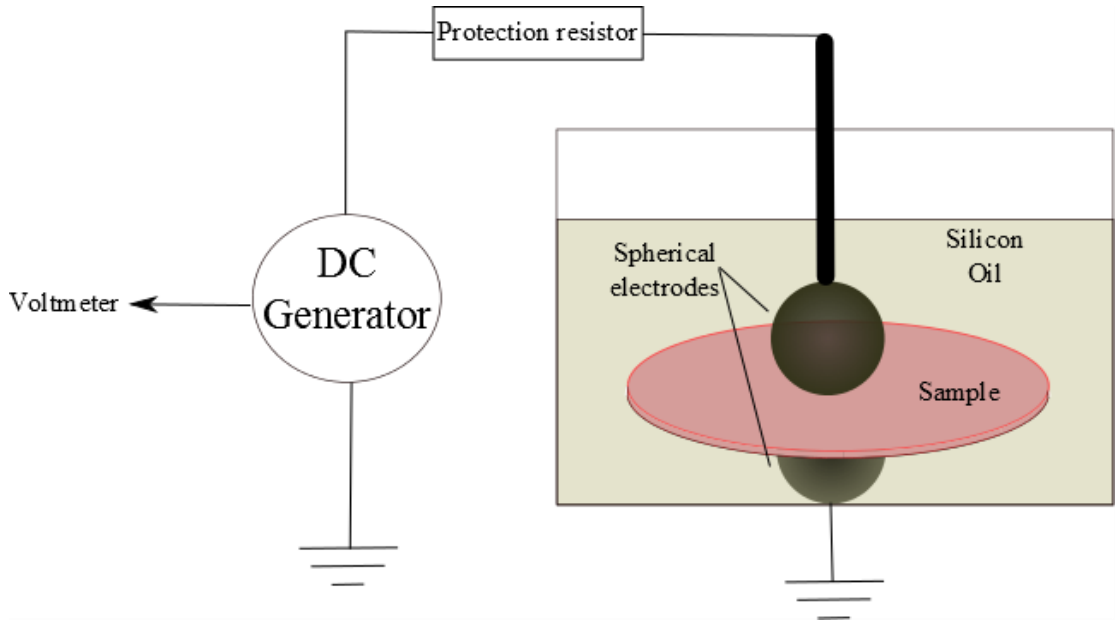

Figure 44: Scheme of the elctrical breakdown test under dc voltage

The breakdown values were analyzed using two-parameter Weibull statistical function, commonly used to analyze the insulation breakdown. Measurements were done on a minimum of 10 samples for each kind of material. Two parameters α and β can be extracted from the Weibull distribution formula:

$$F(x) = 1 - \exp\left[-(x/\alpha)^{\beta}\right],\ x > 0 \qquad \textbf{Eq. 46}$$

Where, α, β and x are the scale parameter, shape parameter and the voltage studied in our case. In the representing graphs, the obtained values are distributed into the graph with

different percentages using Weibull formula, where all the points are situated in an interval of 95 % of confidence. α and β (Breakdown voltage E_c) can be deduced from the slope of the probability of breakdown line, where E_c is the breakdown voltage value at 63 % of the probability interval. The relationship between the scale parameter and the value field E_m (most probable breakdown field) for which the samples have the highest probability of breakdown is defined by:

$$E_m = \left(\frac{\alpha-1}{\alpha}\right)^{\frac{1}{\alpha}} E_c \qquad \textbf{Eq. 47}$$

2.4. Conclusion

The aim of this chapter was to present the chosen material to be studied in this thesis work, and to present the characterization techniques performed to evaluate the properties of the material.

DM, DM5PEI, DM10PEI and PEI will be studied and the influence of PEI in the Epoxy network will be evaluated.

Electron Microscopy images are going to show the morphological behavior of DM and DM#PEI, defining the phase separation phenomenon taking place.

DSC is going to investigate the influence of PEI on the T_g of the blend, and to differentiate between the T_g of epoxy and that of PEI. TGA analysis will give us an idea of the thermal range in which the materials can be used without having degradation.

DMA is going to present for us the mechanical properties of the material, giving us an idea about the separation phenomenon that took place in the blend.

The effect of this phase separation phenomenon is going to be studied on the electrical properties. The influence will be studied on the permittivity values, conductivity, and breakdown voltage values.

References

- **Altshuller'54:** Altshuller, A. P. The Shapes of Particles from Dielectric Constant Studies of Suspensions. J. Phys. Chem. 58, 544–547 (1954).
- **Asami'02:** Asami, K. Characterization of heterogeneous systems by dielectric spectroscopy. Progress in Polymer Science 27, 1617–1659 (2002).
- **Bonnet'00:** Bonnet, A., Pascault, J. P., Sautereau, H., Rogozinski, J. & Kranbuehl, D. Epoxy-Diamine Thermoset/Thermoplastic Blends: Dielectric Properties before, during, and after Phase Separation. Macromolecules 33, 3833–3843 (2000).
- **Bonnet'99-2:** Bonnet, A. Etude de la mise en œuvre par extrusion bi-vis de thermoplastiques amorphes à l'aide d'un solvant réactif: propriétés après réaction. Thesis, École Doctorale des Matériaux, (1999).
- **Bottcher'78:** Bottcher, C. J. F. & Bordewijk, P. in Dielectrics in Time-dependent Fields Chapter X. in Theory of electric polarization Vol II. (Second Edition) 2, 139–167 (Elsevier, 1978).
- **Brown'96:** Brown, J. M. et al. Production of controlled networks and morphologies in toughened thermosetting resins using real-time, in situ cure monitoring. Polymer 37, 1691–1696 (1996).
- **Chartoff'09:** Chartoff, R. P., Menczel, J. D. & Dillman, S. H. Dynamic mechanical analysis (DMA) in Thermal Analysis of Polymers (eds. Menczel, J. D. & Prime, R. B.) 387–495 (John Wiley & Sons, Inc., 2009).
- **Chiu'14:** Chiu, F.-C. A Review on Conduction Mechanisms in Dielectric Films. Advances in Materials Science and Engineering 2014, e578168 (2014).
- **Delides'92:** Delides, C. G., Hayward, D., Pethrick, R. A. & Vatalis, A. S. Real time dielectric investigations of phase separation and cure in rubber modified epoxy resin systems. European Polymer Journal 28, 505–512 (1992).
- **Dissado'92:** Dissado, L. A. & Fothergill, J. C. Electrical Degradation and Breakdown in Polymers. (IET, 1992).
- **Dusek'77:** Dušek, K., Bleha, M. & Luňák, S. Curing of epoxide resins: Model reactions of curing with amines. J. Polym. Sci. Polym. Chem. Ed. 15, 2393–2400 (1977).
- **Fothergill'10:** Forthergill, J. C. Electrical properties in Dielectric Polymer Nanocomposites. (Springer US, 2010).
- **Fricke'53:** Fricke, H. The Maxwell-Wagner Dispersion in a Suspension of Ellipsoids. J. Phys. Chem. 57, 934–937 (1953).
- **Garca'89:** Garca-Coln, L. S., del Castillo, L. F. & Goldstein, P. Theoretical basis for the Vogel-Fulcher-Tammann equation. Phys. Rev. B 40, 7040–7044 (1989).
- **Gir'95:** Girard-Reydet, E., Riccardi, C. C., Sautereau, H. & Pascault, J. P. Epoxy-Aromatic Diamine Kinetics. Part 1. Modeling and Influence of the Diamine Structure. Macromolecules 28, 7599–7607 (1995).
- **Gir'95-2:** Girard-Reydet, E., Riccardi, C. C., Sautereau, H. & Pascault, J. P. Epoxy-Aromatic Diamine Kinetics. 2. Influence on Epoxy-Amine Network Formation. Macromolecules 28, 7608–7611 (1995).
- **Gir'96:** Girard-Reydet, E. Phénomène de séparation de phase induit par une réaction chimique dans des mélanges thermoplastique/polyépoxy : contrôle des morphologies et propriétés. Thesis, Lyon, INSA, (1996).
- **Gir'97:** Girard-Reydet, E., Vicard, V., Pascault, J. P. & Sautereau, H. Polyetherimide-modified epoxy networks: Influence of cure conditions on morphology and mechanical properties. J. Appl. Polym. Sci. 65, 2433–2445 (1997).

- **Gir'98:** Girard-Reydet, E., Sautereau, H., Pascault, J.P., Keates, P., Navard, P., Thollet, G., and Vigier G. Reaction-induced phase separation mechanisms in modified thermosets. Polymer 39, 2269–2279 (1998).
- **Guill'06:** Guillermin, C., Rain, P. & Rowe, S. W. Transient and steady-state currents in epoxy resin. J. Phys. D: Appl. Phys. 39, 515 (2006).
- **Heux'97:** Heux, L., Halary, J. L., Lauprêtre, F. & Monnerie, L. Dynamic mechanical and 13C n.m.r. investigations of molecular motions involved in the β relaxation of epoxy networks based on DGEBA and aliphatic amines. Polymer 38, 1767–1778 (1997).
- **Horie'70:** Horie, K., Hiura, H., Sawada, M., Mita, I. & Kambe, H. Calorimetric investigation of polymerization reactions. III. Curing reaction of epoxides with amines. J. Polym. Sci. A-1 Polym. Chem. 8, 1357–1372 (1970).
- **Jonscher'99:** Jonscher, A. K. Dielectric relaxation in solids. J. Phys. D: Appl. Phys. 32, R57 (1999).
- **Kran'03:** Kranbuehl, D. et al. Dielectric in situ sensor monitoring of phase separation and changes in the state of each phase. Macromol. Symp. 198, 377–388 (2003).
- **Kremer'89:** Kremer, F., Boese, D., Meier, G. & Fischer, E. W. in Relaxation in Polymers (eds. Pietralla, M. & Pechhold, W.) 129–139 (Steinkopff, 1989).
- **Lampert'70:** Lampert, M. A. & Schilling, R. B. in Semiconductors and Semimetals (ed. R.K. Willardson, A. C. B.) 6, 1–96 (Elsevier, 1970).
- **Lestriez'98:** Lestriez, B. et al. Is the Maxwell–Sillars–Wagner model reliable for describing the dielectric properties of a core–shell particle–epoxy system? Polymer 39, 6733–6742 (1998).
- **Mac'92:** MacKinnon, A. J., Jenkins, S. D., McGrail, P. T. & Pethrick, R. A. A dielectric, mechanical, rheological and electron microscopy study of cure and properties of a thermoplastic-modified epoxy resin. Macromolecules 25, 3492–3499 (1992).
- **Matsuoka'61:** Matsuoka, S. Hypothesis of Voids in Semicrystalline Polymers. Journal of Applied Physics 32, 2334–2336 (1961).
- **Menard'02:** Menard, K. P. & Menard, N. R. Dynamic mechanical analysis in the analysis of polymers and rubbers, in Encyclopedia of Polymer Science and Technology (John Wiley & Sons, Inc., 2002).
- **Menguy'97:**Menguy, C. Mesure des caractéristiques des matériaux isolants solides | Techniques de l'Ingénieur. Ref: D2310 (1997)
- **Modulab'14:** ModuLab XM MTS Materials Test System: User Guide (2014)
- **Montserrat'03:** Montserrat, S., Roman, F., Basany, M. & Colomer, P. Phase separation in a poly(ether sulfone) modified epoxy-amine system studied by temperature modulated differential scanning calorimetry and dielectric relaxation spectroscopy. Macromol. Symp. 198, 399–410 (2003).
- **Montserrat'06:**Montserrat, S., Roman, F. & Colomer, P. Vitrification, devitrification, and dielectric relaxations during the non-isothermal curing of diepoxy-cycloaliphatic diamine. J. Appl. Polym. Sci. 102, 558–563 (2006).
- **O'Dwyer'73:** O'Dwyer, J. J. The theory of electrical conduction and breakdown in solid dielectrics. (Clarendon Press, 1973).
- **Pethrick'02:** Pethrick, R. A. & Hayward, D. Real time dielectric relaxation studies of dynamic polymeric systems. Progress in Polymer Science 27, 1983–2017 (2002).
- **Polder'46:** Polder, D. & van Santeen, J. H. The effective permeability of mixtures of solids. Physica 12, 257–271 (1946).
- **Poncet'99:** Poncet, S. et al. Monitoring phase separation and reaction advancement in situ in thermoplastic/epoxy blends. Polymer 40, 6811–6820 (1999).
- **Riccardi'96:** Riccardi, C. C. et al. Thermodynamic analysis of the phase separation in polyetherimide-modified epoxies. J. Polym. Sci. B Polym. Phys. 34, 349–356 (1996).

- **Schonhals'03:** Schönhals, A. & Kremer, F. in Broadband Dielectric Spectroscopy (eds. Kremer, P. D. F. & Schönhals, P.-D. D. A.) 59–98 (Springer Berlin Heidelberg, (2003).
- **Segui'00:** Segui, Y. Diélectriques - Courants de conduction. Techniques de l'Ingénieur. Ref: D2301(2000).
- **Stark'55:** Stark, K. H. & Garton, C. G. Electric Strength of Irradiated Polythene. Nature 176, 1225–1226 (1955).
- **Stevens'88:** Stevens, G. C., Perkins, E. & Champion, J. V. Microvoid formation and growth in epoxy resins under mechanical and electrical stress by laser light scattering. in , Fifth International Conference on Dielectric Materials, Measurements and Applications, 1988 234–237 (1988).
- **TA_TGA:** Q50 & Q500 TGA – TA Instruments.
- **Tsangris'96:** Tsangaris, G. M., Kouloumbi, N. & Kyvelidis, S. Interfacial relaxation phenomena in particulate composites of epoxy resin with copper or iron particles. Materials Chemistry and Physics 44, 245–250 (1996).
- **Wampler'06:** P. Wampler, T. Applied Pyrolysis Handbook. Chapter 1, 2nd edition CRC Press (2006).

Chapter 3

Epoxy/Polyetherimide Blend Characterization

This chapter presents results of the study on the influence of the PEI on the epoxy system first by showing the morphological phase separation that will be discussed in terms of glass transition temperature. Secondly, the influence of the PEI nodules will be presented on the mechanical and electrical properties of the blend

3.1. Morphology

Electronic microscopy is used to characterize the morphological structure of the epoxy/PEI blend. Scanning electron microscopy and transmission electron microscopy were used to determine the phase separation phenomenon.

3.1.1. Scanning Electron Microscopy (SEM)

SEM imaging was performed on the neat matrix DM and the blends DM5PEI and DM10PEI. The Images were taken by the secondary electron (**SE**) mode with 15 kV. Figure 45 presents SEM image of the pure epoxy network DM, which was not etched, acting as a reference matrix that can be compared with the epoxy/PEI blend.

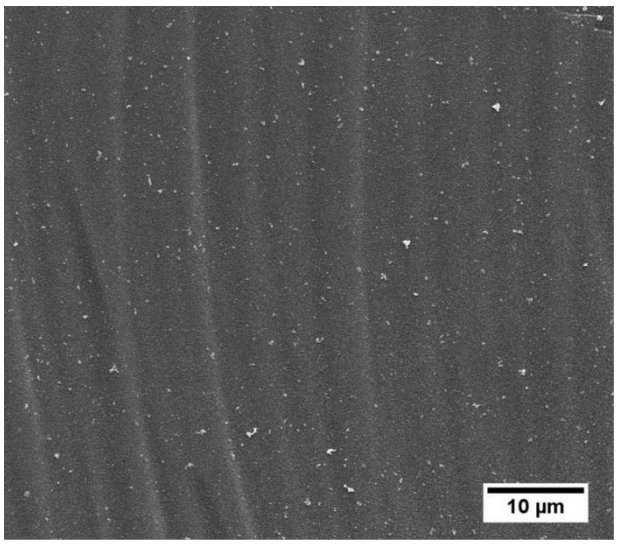

Figure 45: SEM image of DM, pure epoxy network.

Figure 46 (a) and **Figure 47** (a) highlight the SEM images of DM5PEI and DM10PEI. Both samples were etched to remove an epoxy layer and to obtain better topographic contrast between the PEI nodules and the epoxy network [*Mac'92*]. Phase separation phenomenon is

observed in the two studied blends and due to the low reactivity of DGEBA-MDEA the phase separation was proceeded via spinodal demixing (SD) mechanism, explained in chapter 1 [Gir'98]. The dark part corresponds to the epoxy rich phase and the bright parts correspond to the PEI rich phase. The size distribution graph is represented in Figure 46 (b) and 47 (b) for DM5PEI and DM10PEI respectively. Both kinds of blends show a homogenous well distributed PEI nodules in continuous epoxy network while having smaller size of nodules for DM5PEI. The separated nodules have a spherical or ellipsoidal form with an average diameter of 1.5 to 2 µm in DM5PEI samples and 2 to 3 µm in DM10PEI samples. The size distribution is obtained using ImageJ software.

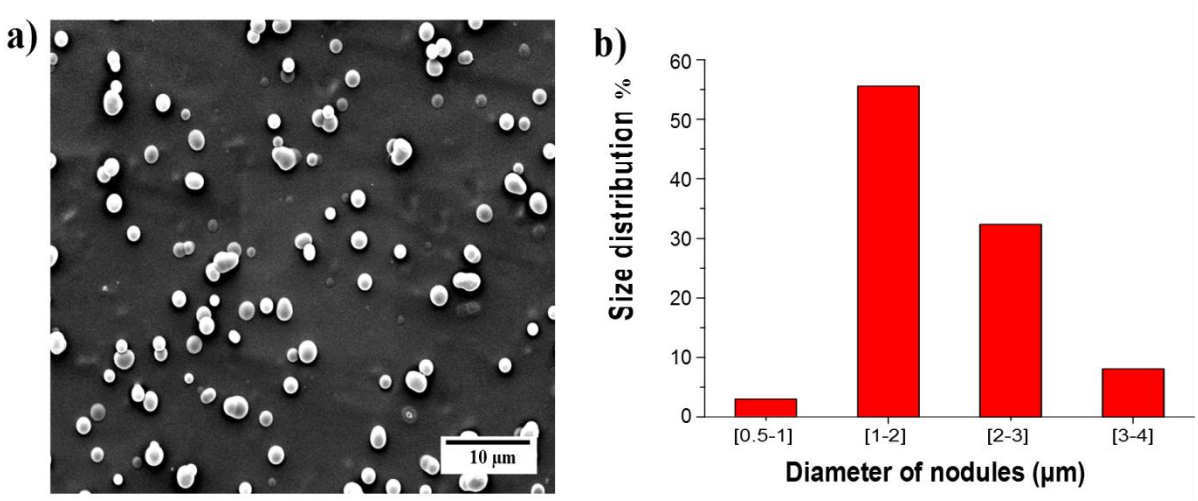

Figure 46: (a) SEM image of DM5PEI, etched and (b) size distribution of PEI nodules in the epoxy network

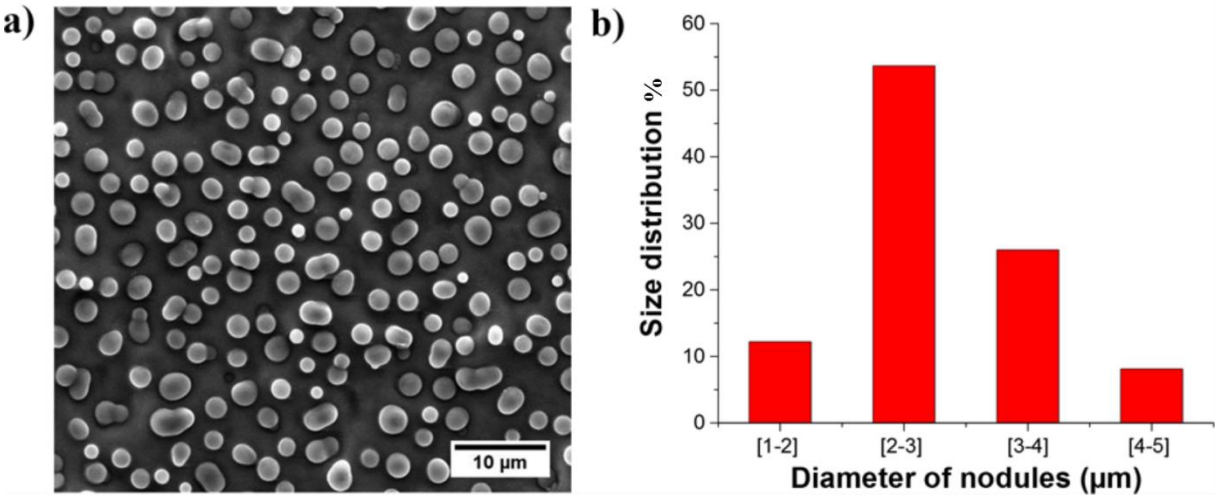

Figure 47: (a) SEM image of DM10PEI, etched and (b) size distribution of PEI nodules in the epoxy network

According to similar studies in literature, similar morphology was observed for the same range of weight percentage of PEI but within a tetrafunctional amine hardener [Bucknall'89]

[Hourston'92] [Cho'93]. The shape of the nodules was spherical due the choice of the pre-curing temperature (160 °C). Lower temperature and slower curing rates, where long gel times obtained, result in non-spherical thermoplastic domains [Gir'97].

3.1.2. Transmission Electron Microscopy

Figure 48 and Figure 49 show the images of DM5PEI and DM10PEI respectively at different magnifications. In these TEM images, the dark part corresponds to the PEI nodules and the bright continuous phase corresponds to the epoxy network. These images confirm the relative homogeneous distribution of the PEI nodules in the epoxy network in both used percentages of PEI. The nodules have an ellipse form in both blends, with the major diameter between 0.5 - 2 µm for DM5PEI and 1 - 2 µm for DM10PEI. A size distribution analysis is represented in the graphs of Figure 50.

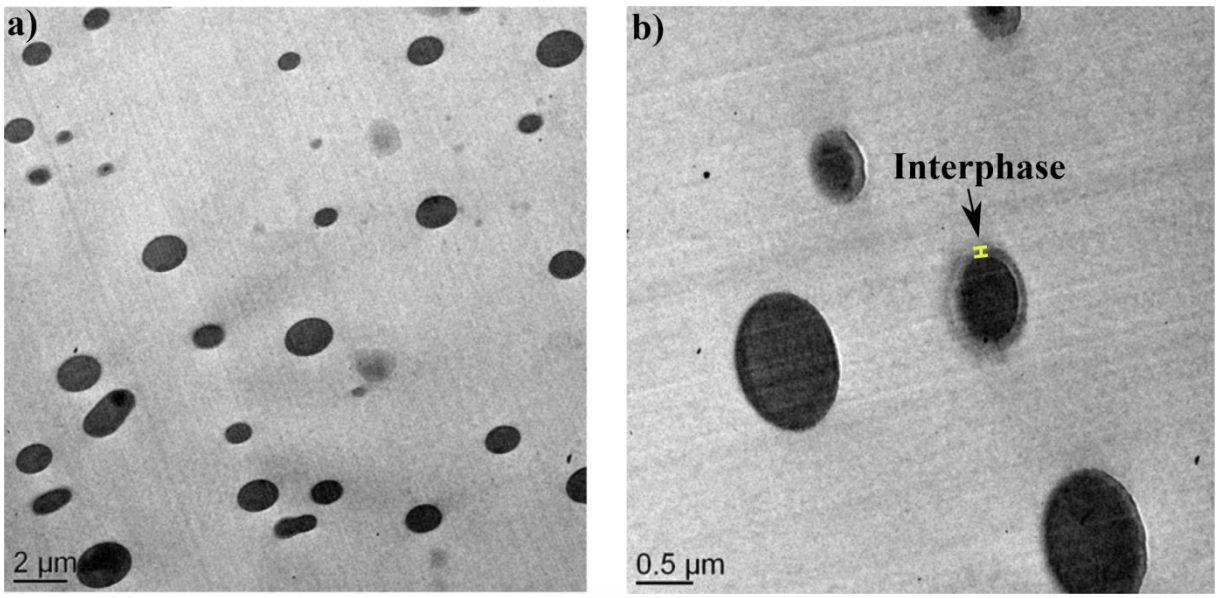

Figure 48: TEM images of DM5PEI at different magnification

It can be noticed that the average diameter is a little smaller for TEM images than for SEM images due to the difference in sample preparation and imaging. In the SEM image the topographical view is seen where a layer of epoxy is removed that can show the PEI nodules standing freely on the epoxy network as demonstrated in Figure 51 (a). The orientation of the sample with respect to the incident electrons beam and the detected one decide the plan of the image that we are receiving. Difference in the orientation can show different zones of the spheres of the PEI nodules. In the TEM imaging the samples are cut into slices of 60 to 70 nm thickness as shown in **Figure 51** (b). This thickness is 3 to 6% from the average diameter of a nodule that can be placed anywhere in the nodule as demonstrated in Figure 51 (c). Therefore,

the image taken by means of TEM gives an idea about the distribution as well as the interphase between the two materials, whereas the diameter size measured cannot be considered as the average diameter of the nodules. The considered diameter in further studies will be taken from the measurements done on SEM images.

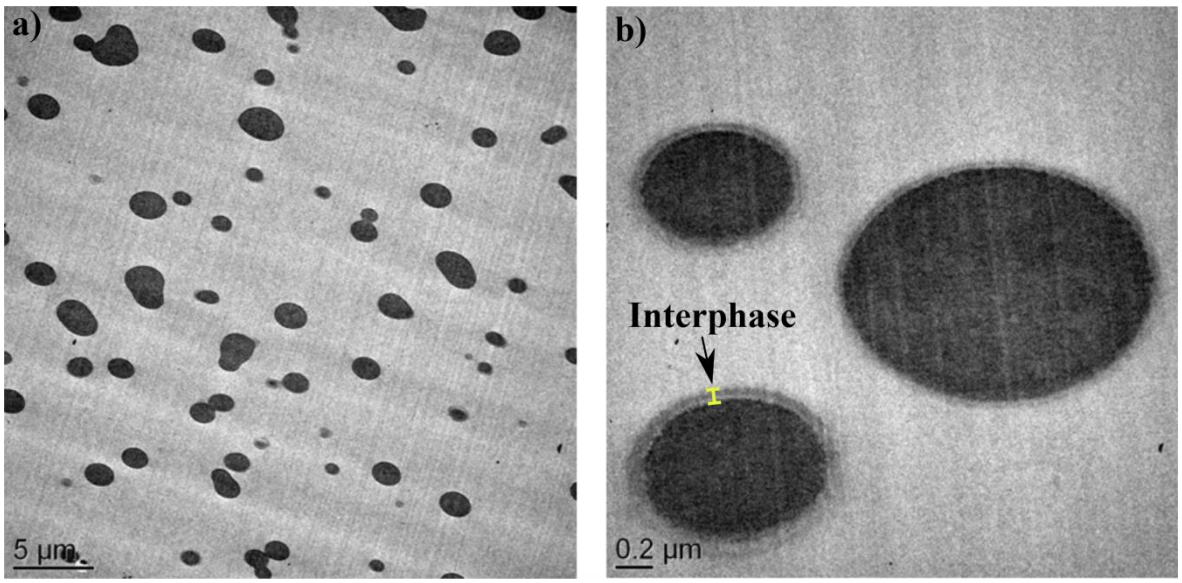

Figure 49: TEM images of DM10PEI at different magnification

An interphase is seen in some of the nodules present in the epoxy network in both blends as seen in Figure 48 (b) and 5 (b). This interphase has an average thickness of 20 to 50 nm which is considered as an average of 5% from the total volume of the PEI nodule. In both blends, nodules with an interphase are considered to be around 20 % of the present nodules in the network. The percentage of the interphase is calculated from all the present TEM images. This interphase can be explained by low molar masses of epoxy-amine dissolved in the PEI phase.

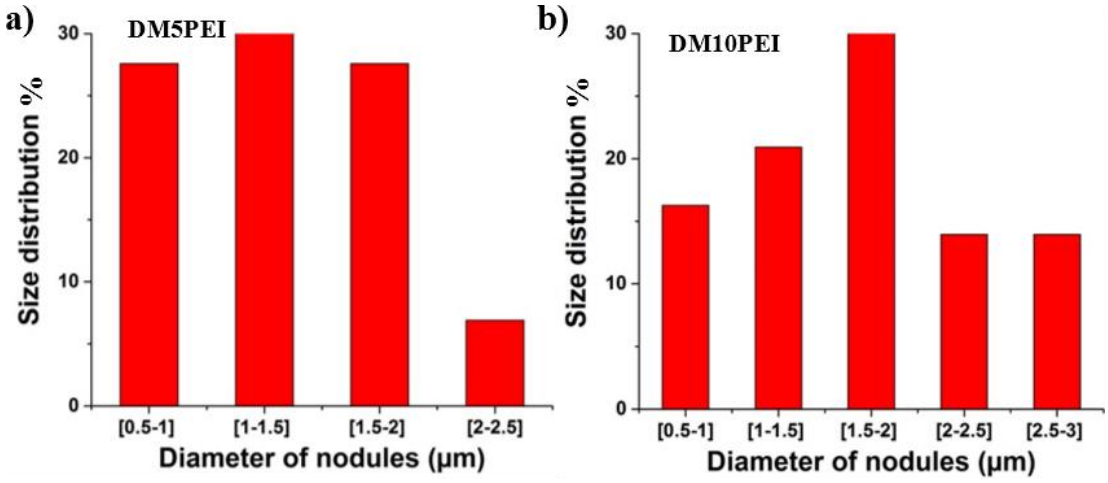

Figure 50: Size distribution of PEI nodules in the epoxy blends of a) DM5PEI and b) DM10PEI.

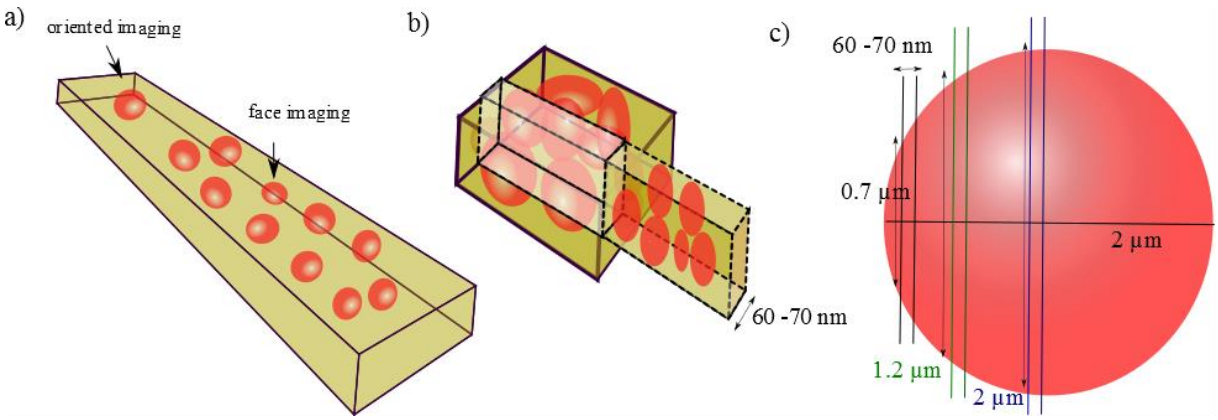

Figure 51: Scheme of a) SEM sample, b) TEM sample and c) sliced nodule

3.2. Thermal resistance under the influence of PEI

The degradation process is not the same under air and nitrogen atmosphere as seen in the thermo-gravimetric diagrams displayed in Figure 52 and Figure 53 respectively. The system is considered stable until 5 % of its mass is lost where the initial degradation process takes place. The neat epoxy system showed good thermal stability up to 350 °C under nitrogen atmosphere and up to 350 °C under air atmosphere with a Tmax peak of the derivative weight change at 400 °C and 380 °C respectively. Under the influence of inert atmosphere, nitrogen gas, pure thermal one-step degradation process takes place leading to char material which is around 10 % of the initial mass that is stable at least up till 800 °C. In the contrary, a two-step degradation process was observed under air atmosphere. The first one corresponds to the thermal degradation and the second, at higher temperature around 500 °C, corresponds to the oxidation process [*Bishop'67*]. The degradation process results in chain scission of the epoxy network yielding combustible gases, water, amines, and small volatile molecules, etc. [*Levchik'04*]. At the end of the degradation and above 650 °C no residual product was remained indicating the oxidation of all the present material.

The pure PEI system showed similar stability under both atmospheres up to 525 °C with a difference in the residual mass due to the oxidation process. The addition of PEI in the epoxy network did not significantly affect its thermal stability upon modifying it with 5 or 10 wt. % of PEI due to the low percentage used. This thermal stability is interesting giving the blend material a wide range of stability under the influence of temperature which is an important characteristic for the insulating material in modules working at high temperatures. As discussed in the first chapter silicone can resist temperature up to 200 °C which is one of its

main drawbacks in using it in the future for power modules. In the following section of the chapter dielectric characterization under a variation of temperature is going to be studied.

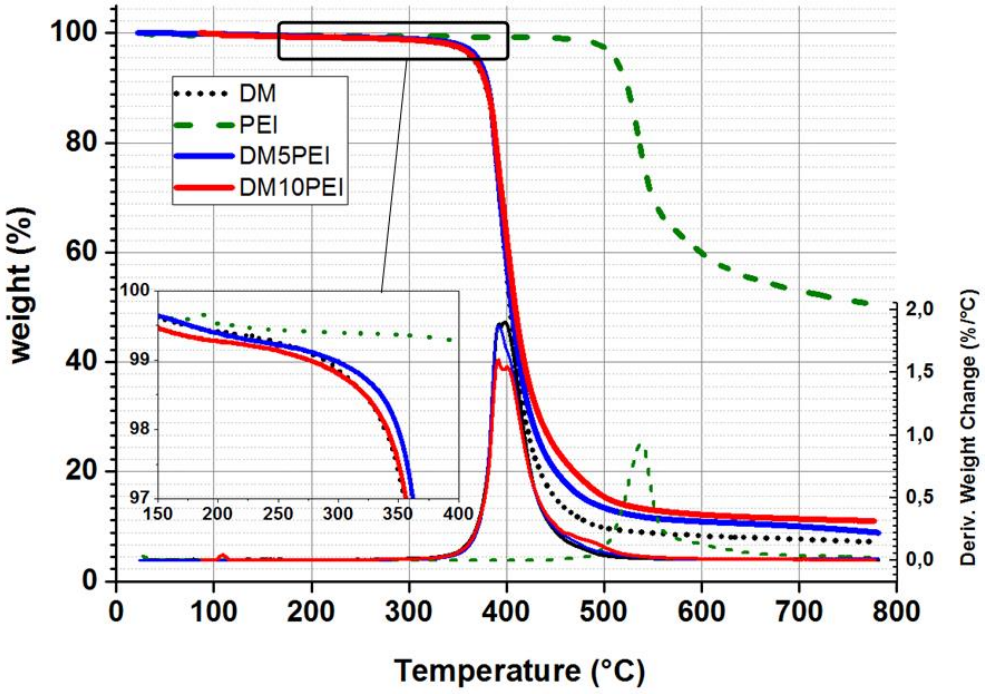

Figure 52: Weight loss and derivative of weight change of DM, PEI, DM5PEI and DM10PEI under nitrogen atmosphere. The inset is a zoom on the beginning of the degradation.

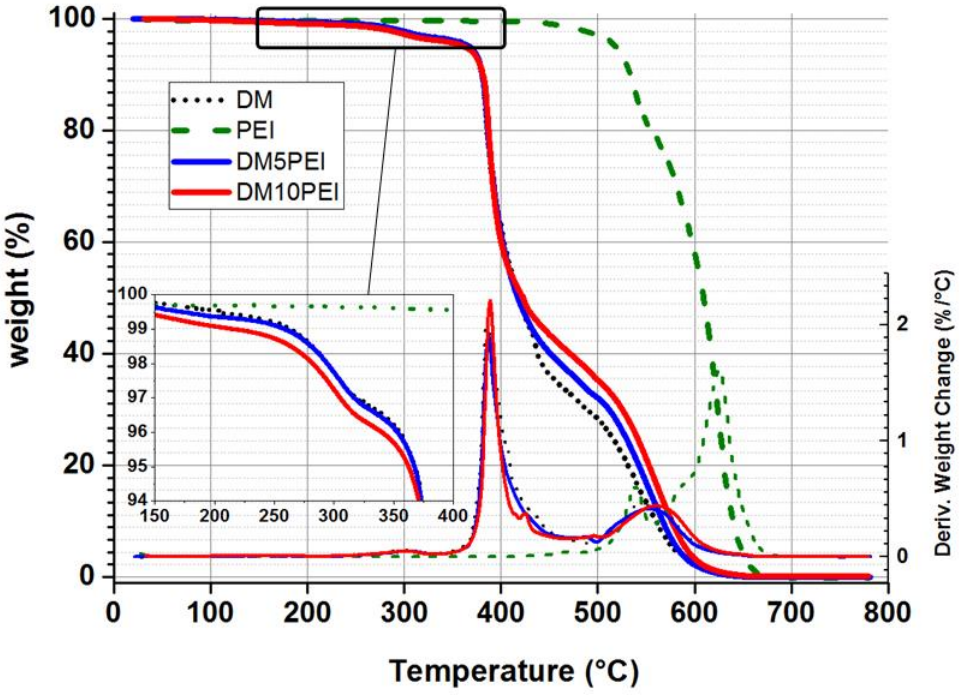

Figure 53: Weight loss and derivative of weight change of DM, PEI, DM5PEI and DM10PEI under air atmosphere. The inset is a zoom on the beginning of the degradation.

3.3. Glass transition temperature

3.3.1. Differential Scanning Calorimetry

Glass transition temperature of pure materials and the blends was measured by means of DSC (Figure 54). DM sample showed a single transition corresponding to the glass transition temperature of epoxy-amine network at 164 °C and for PEI film this transition takes place at 216 °C.

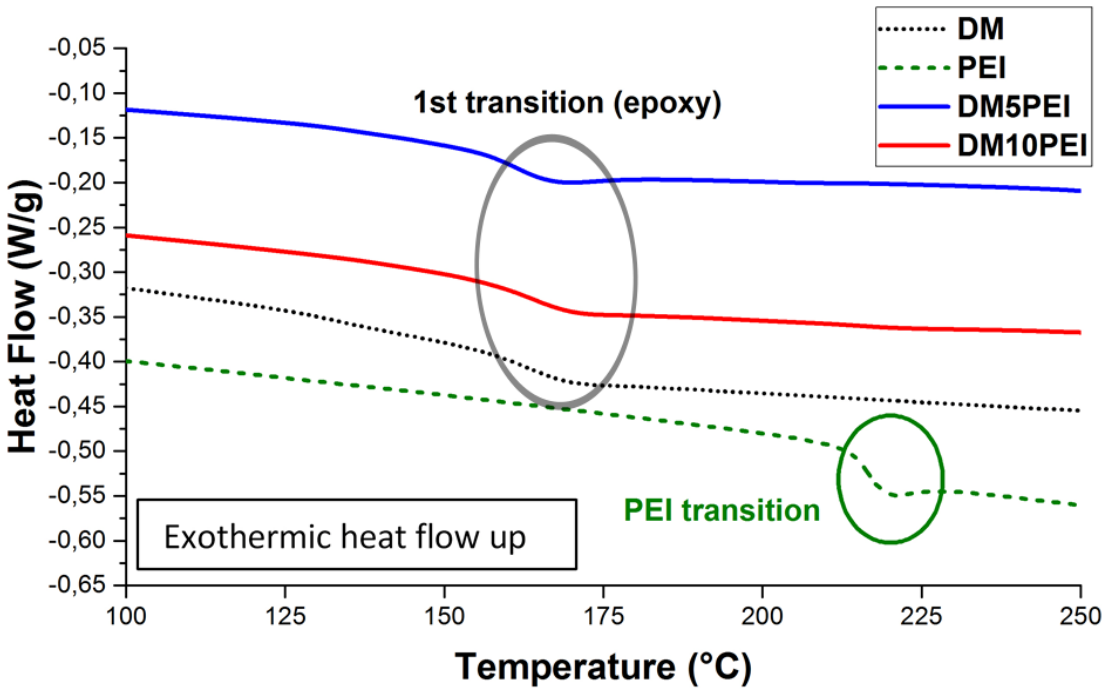

Figure 54: DSC thermograms of DM, PEI, DM5PEI and DM10PEI

Table 11 summarizes the glass transition for all the compositions (T_g). The blends with 5 and 10 wt% present the glass transition temperature corresponding to the epoxy network. The second glass transition corresponding to the thermoplastic phase in the blend is not visible in the heat flow curve due to low instrumental signal. Thus, derivatives of the heat flow of the blends with respect to temperature are demonstrated in Figure 55. Thus we can point out the first measured transition corresponding to the epoxy network (164 °C) and the second one corresponding to the PEI rich phase (216 °C). The phase separation phenomenon is confirmed by the presence of two distinct glass transitions temperatures. For DM10PEI blend, relevant values without shifting to the pure epoxy and PEI network prove a total separation of the system.

Table 11: Glass transition temperatures obtained by means of DSC

	$T_{g\ epoxy}$ (°C)	$T_{g\ PEI}$ (°C)
DM	164	-
PEI	-	216
DM5PEI	161	205
DM10PEI	164	216

In the case of DM5PEI, the two transitions are observed with a slight shift toward lower values. This shift can be due to the interference of PEI into the epoxy network without being separated from it and the presence of epoxy in the PEI nodules as well. The blend is phase separated with a small percentage of interphase residues of the materials in each other.

The three systems DM, DM5PEI and DM10PEI did not present an exothermic peak on the first run, which insures full cross-linking of the epoxy amine network. The same temperature of the glass transition was obtained on the first and second run (increasing temperature) confirming this conclusion.

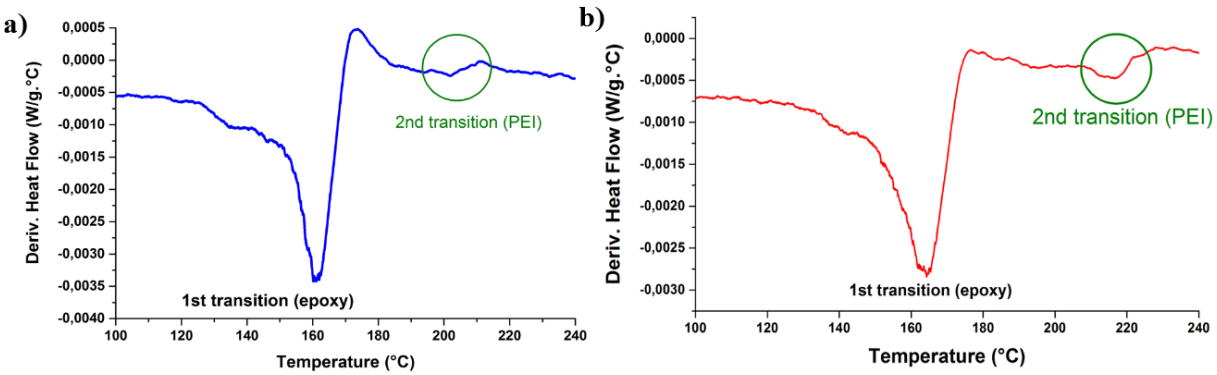

Figure 55: Derivative of heat flow with respect to temperature of (a) DM5PEI and (b) DM10PEI

3.3.2. Dynamic Mechanical Analysis: phase transitions

DMA is used to measure the storage modulus E', loss modulus E" and loss factor tan δ for DM, PEI, DM5PEI and DM10PEI and the exploited data are plotted in Figure 56. All the samples showed a stable value over wide range of temperature up till the glass transition of each material. Decay in the storage modulus takes place accompanied with peaks in the loss modulus and tan δ values indicating the presence of a transition in the system. T_α values corresponding to the glass transition temperature of each component are extracted from the loss modulus values. DM shows a constant stable value up till 176 °C identifying α-relaxation

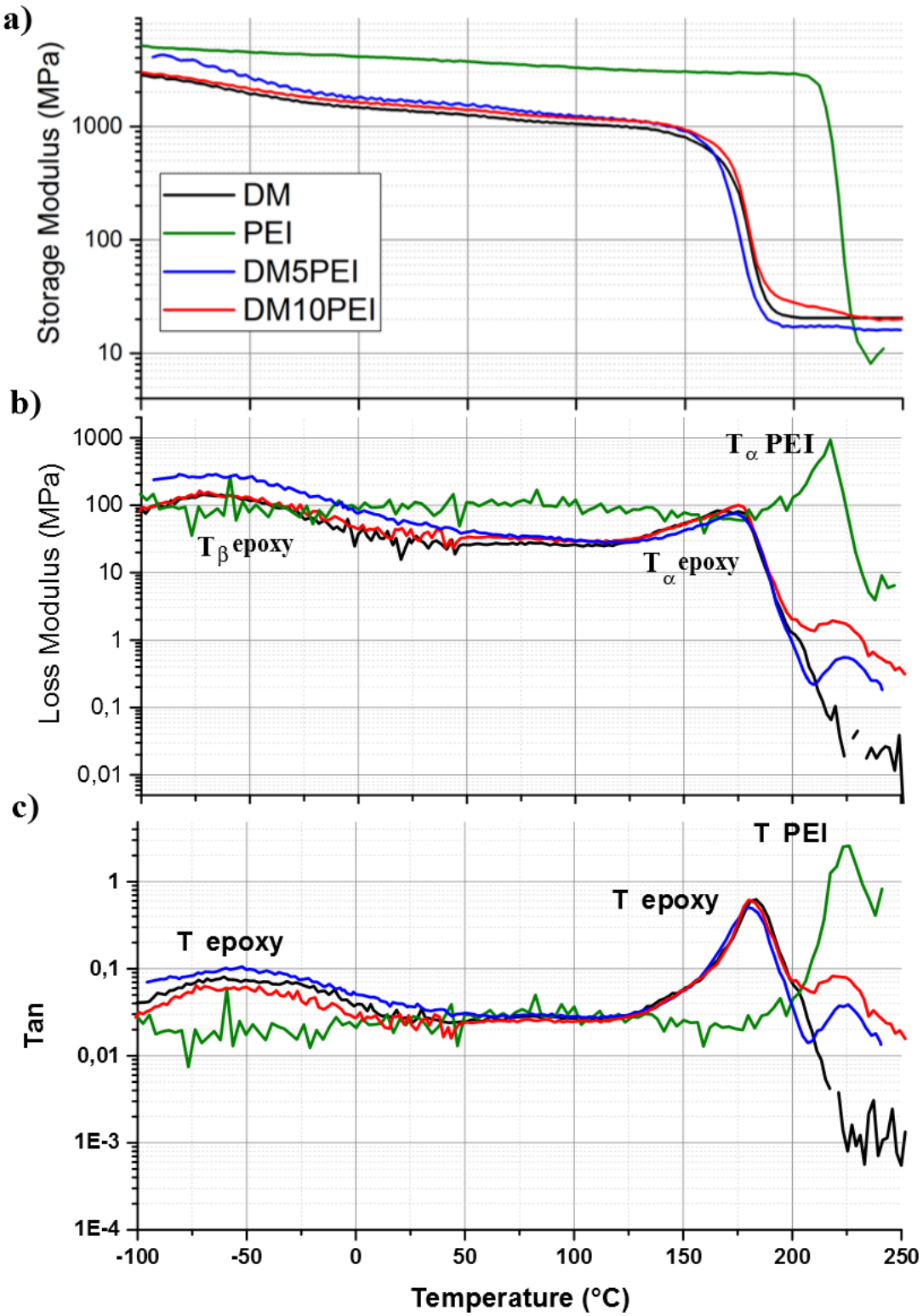

Figure 56: Storage Modulus E' (a) loss modulus (b) and loss factor Tan δ (c) as function of temperature of DM, PEI, DM5PEI and DM10PEI at 1 Hz.

temperature associated to the glass transition of the epoxy network and the system passes from the glassy state to the rubbery state. PEI has a higher storage modulus value than DM with a α-relaxation temperature at 218 °C corresponding to the glass transition temperature of the PEI system.

The blends with the addition of 5 and 10 wt. % of PEI to the epoxy network led to the same evolution of storage modulus as that of the neat system with the same decay phenomenon corresponding to T_α (epoxy). The addition of PEI into the epoxy network did not affect the storage modulus of the system neither in the glassy plateau nor the rubbery one. Epoxy/thermoplastic blends have shown similar behavior, where the thermoplastic does not affect the storage modulus below critical percentage, with PES:PEES and PS. Blending epoxy with 15 wt % of PES:PEES and 3 wt % of PS have shown particulate morphology and did not influence the storage modulus values [*Blanco'04*] [*Chau'15*].

Loss modulus curves in Figure 56 (b) underline that the neat epoxy network gives two loss peaks. One broad peak at low temperature with a maximum at -30 °C was assigned to the β relaxation (T_β) attributed to the movement of the hydroxyether units(-O-CH2-CH(OH)-CH2-) created by the crosslinking reaction and the initial epoxy prepolymer [Heux'97]. T_β was observed in the pure epoxy network as well as the blends showing no changing in this segmental motion in the presence of PEI. A second sharp peak corresponding to Tα associated to the glass transition temperature of epoxy network is observed at 176 °C. PEI pure sample also obtained one sharp peak with a maximum at 218 °C which is ascribed to T_α associated to the glass transition of PEI.

The phase separation phenomenon, suggested by SEM images, for the 5 and 10 wt. % blends is confirmed in the DMA measurements by the presence of two high-temperature relaxations associated to the epoxy network ($T_{\alpha1}$) and the PEI phase ($T_{\alpha2}$) respectively. DM and the two blends DM5PEI and DM10PEI exhibited the same temperature for α relaxation of the epoxy network proving that the epoxy network is totally separated from the thermoplastic phase. Alternatively, $T_{\alpha2}$ is slightly higher than pure PEI. This shift could be attributed to two different phenomena. First, a small amount of epoxy-amine is miscible in the PEI phase plasticizing it. Secondly, the presence of free volume, in which it has been shown that blending of polymers generates additional free volume, which can lower T_g by reducing the energy necessary for segmental motion [*Akay'94*] [*Gir'97*]. In the next part, these two possibilities will be discussed.

In addition to SEM images, more information about the morphology of the blends can be obtained by studying the amplitudes of loss factor peaks and, more specifically, the ratio of these amplitudes (a_2/a_1). This value appears to be very sensitive not only to the volume fraction but also to the shape of final morphology through the choice of the curing temperature. The characteristics of the two high temperature loss peaks, their maximum

temperature ($T_{\alpha 1}$, $T_{\alpha 2}$), their amplitudes (a_1, a_2) , the ratio of these amplitudes (a_2/a_1) as well as the values of the storage modulus before and after the α relaxation temperature are collected in Table 12. The amplitude of the peak corresponding to the epoxy network (a_1) remains constant with the addition of PEI. On the other hand, the amplitude of the peak corresponding to the PEI into the epoxy network is significantly reduced due to the low percentage of PEI present in the epoxy network comparing both blends [*Bonnet'01*].

Table 12: Temperatures (Tα1, Tα2), amplitudes (h1, h2) obtained from Tan δ curves Fig. 5(b), and storage modulus for DM, DM10PEI and PEI.

	T_α (°C)		Amplitude (a)		a_2/a_1	Morphology
	$T_{\alpha 1}$	$T_{\alpha 2}$	a_1	a_2		
DM	177		0.62		-	
PEI	217		2.58		-	
DM5PEI	177	224	0.48	0.04	0.083	Particulate
DM10PEI	177	221	0.57	0.08	0.14	Particulate

The ratio (a_2/ a_1) can be used to predict qualitatively the kind of morphology generated in thermoplastic/thermoset blends and to define if the structure of the network is inverted or not. In this studied case of DM5PEI and DM10PEI, its ratio is equal to 0.08 and 0.14 respectively. These values corresponds to the morphology of the separated nodules in the epoxy network as described by Girard-Reydet et al. [*Gir'97*] and confirms the particulate morphology observed by SEM.

The particulate morphology of PEI into the epoxy network did not affect the value of storage modulus of the epoxy network. Nevertheless it have been noted that the PEI nodules formed an obstacle to the propagation of mechanical crack and may participate to the crack blunting effect [*Gir'97*].

3.4. Electrical properties of epoxy blends

3.4.1. Experimental Dielectric response

Dielectric measurements were carried out on the studied systems to monitor the influence of the addition of the thermoplastic material into the epoxy network. The real (ε'_r) and the imaginary (ε''_r) parts of the relative permittivity were derived from measurements under a 5 V_{rms} sinusoidal applied voltage. Real part of relative permittivity is presented in **Figure 57**.

The neat epoxy network showed relative permittivity ε'_r values starting from 4.5 at low temperatures and increasing up to 6.5 at temperatures higher than ambient temperature. A small increase with a maximum value around 183 °C corresponds to the α relaxation of the epoxy system. PEI has relative permittivity ε'_r values lower by 30% than that of the neat epoxy network and constant on the whole range of temperatures. Choudhury et al. observed similar results for the relative permittivity ε'_r of PEI [*Chou'10*]. The introduction of PEI into the epoxy network decreased ε'_r in all the studied temperature range. The introduction of 5 wt. % and 10 wt. % of PEI led to a decrease of around 8 and 15 % respectively of the relative real permittivity. The shape of the curves was not influenced by the addition of PEI but it was only shifted to lower values with the increase of the PEI wt. %. The same influence of PEI is noticed under all the variation of temperature and frequency as seen in Figure 59 (a).

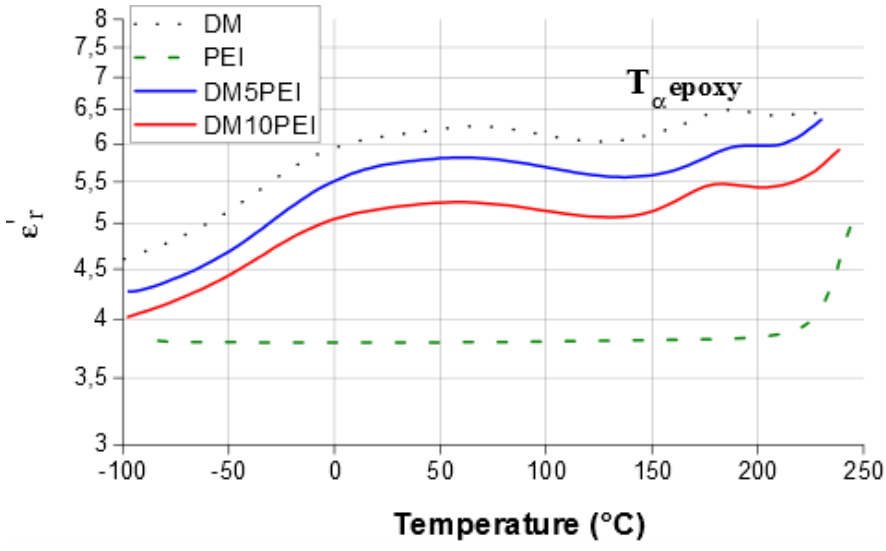

Figure 57: Relative real permittivity as function of temperature at 1 kHz

The imaginary part of relative permittivity values ε''_r of epoxy network shows two main identified transitions, Figure 58. The first broad transition that peaks at -30 °C corresponds to β transition associated to the movement of the hydroxyether units created by the crosslinking

reaction and the initial epoxy prepolymer. The second main transition starting at 170 °C corresponds to α transition of epoxy network that appears in the form of a shoulder superimposed on the conduction phenomenon; this transition was also observed in DMA measurements. PEI network exhibited one main α relaxation at 240 °C associated to the glass transition of PEI. The introduction of 5 and 10 %wt of PEI into the epoxy network lowered the relative imaginary permittivity by 6 and 15 % in the range of -100 °C to 200 °C. The mixture Epoxy / PEI showed also the presence of both α and β relaxations corresponding to epoxy network. α relaxation is shown in the blends as a shoulder superimposed on the conduction phenomenon as well. α transition corresponding to the PEI inclusion in the blends is not fully recognized due to the limitation of the experimental temperature at 250 °C.

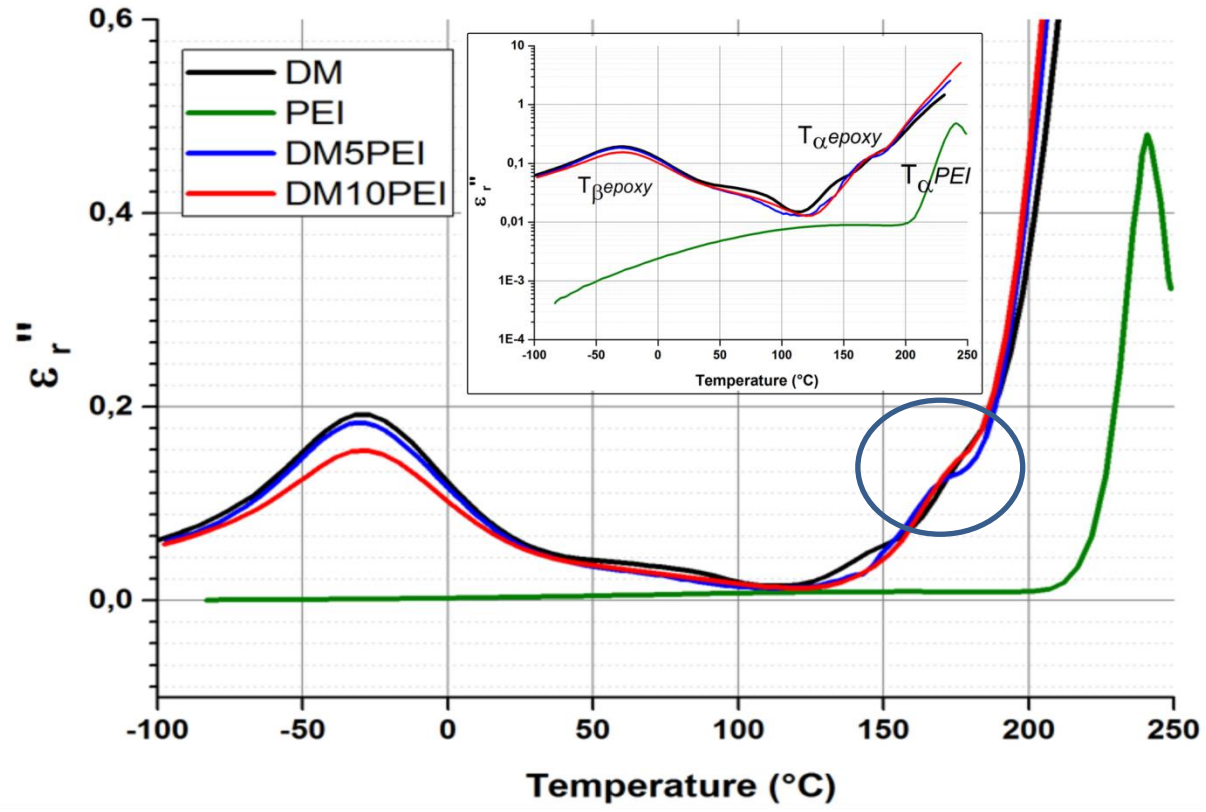

Figure 58: Dielectric loss and zoom on the dielectric loss; as function of temperature at 1 kHz for DM, PEI, DM5PEI and DM10PEI

Loss values tested for large ranges of frequency and temperature are represented in a 3D plot Figure 59 (b). The value of the losses ε''_r decreased slightly below Tα epoxy upon the addition of PEI in both weigh percentages 5 and 10 %. First relaxation, supposed to be the β relaxation of the epoxy network, is shifted from -80 °C up to 60 °C with the increase of frequency. When the temperature approaches the glass transition temperature of the epoxy system and at high frequencies, 10^2 – 10^6 Hz, α relaxation is recognized between 150 and 200 °C related to relaxation processes of the main chains of the cross-linked epoxy chains. Below these

frequencies, we can observe a huge increase in the loss values. This increase partially masks α relaxation of the epoxy network due to the augmentation of the concentration of charge carriers. This relaxation arises from the fact that free charges are immobilized in the material below T_α, and at sufficient high temperature, the charges can migrate in the presence of applied electric fields. As the temperature increases above the glass transition temperature, the conductivity of the system grows giving rise the increase of the concentration of charge carriers. This effect is seen in DM as well as the blends DM5PEI and DM10PEI. It is relatively higher in the blends where Maxwell-Wagner-Sillars (MWS) polarization can interfere, as this kind of polarization can exist in heterogeneous dielectrics. It's due to a delay in charge transfer at the interface between components with different dielectric permittivity [*Tsangris'96*].

Blending the epoxy with 5 and 10 wt% of PEI has decreased the value of the relative permittivity in its real and imaginary parts. If we compare it to similar studies discussed in the first chapter, such as the incorporation of inorganic 0.5 µm titania, it is noticed that the addition of 5 and 10 wt% have increased two times the values of relative real and imaginary parts of the permittivity [*Singha'08*]. It is noticed that the majority of the fillers have permittivity higher than that of the epoxy networks which is the inverse in our studied case as PEI has a permittivity value lower than that of pure epoxy. According to literature, when micro-fillers are added to the epoxy network, the permittivity of the final epoxy micro-composite is higher than that of the pure epoxy network [Nelson'14] [*Iyer'11*] [*Castellon'11*] [*Heid'15*]. Other mentioned examples have all shown an increase in the relative permittivity values using different sizes of particles in the micrometer range. Even though the particles have the same micrometer range size, they did not have the same influence on the final value of the permittivity value. It is true that the nature of the used micro-particles is different than the PEI thermoplastic used as they have higher permittivity values than the epoxy.

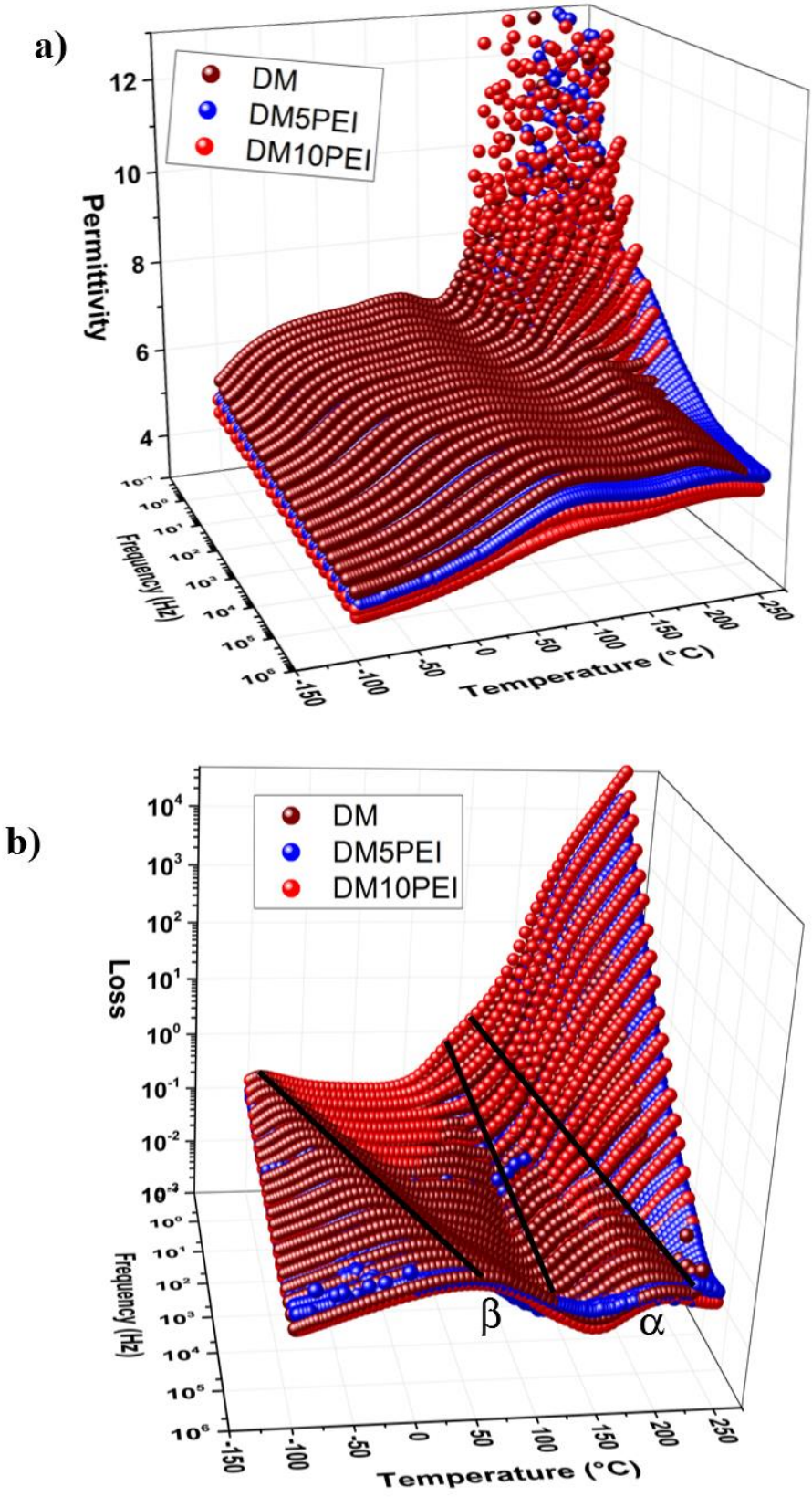

Figure 59: a) relative permittivity and b) dielectric loss; of DM DM5PEI and DM10PEI versus temperature and frequency

Thus, in general it can be concluded that the incorporation of inorganic micro-particles has increased the permittivity values which is in the contrary of what we have obtained in our work. Blending the epoxy with PEI thermoplastic has developed a homogenously distributed phase separated nodules in the epoxy system. PEI micro-nodules have a permittivity lower than that of epoxy decreasing the permittivity of the blend at 5 and 10 wt%.

The only way to decrease the permittivity value of the epoxy composite below the permittivity of the pure epoxy system using inorganic fillers was by adding nano-fillers with small critical values depending on their nature as discussed previously [*Iyer'11*] [*Katayama'13*] [*Heid'15*] [*Tuncer'07*] [*Singha'08*]. Tsekmes et al. reported a decrease in the permittivity value using low percentages of nanoparticles such as 0.2 vol % of surface treated boron nitride [*Tsekmes'14*]. The chemical bonding between the epoxy and the modified surface of the nanoparticles have caused the immobilization of the epoxy chain and thus caused the decrease in the relative real part of permittivity values. With increasing the percentage of the filler used the surface to volume ratio of the particles decreases with the presence of agglomerates that cause the increase in the permittivity values. The difference between our studied case and the reported studies using nano-particles is that the permittivity of the system is decreased without the use of nanoparticles but with the presence of micro-nodules of PEI.

Both the size and the percentage of the nano-particle used to be incorporated in the epoxy network have played a role in influencing the permittivity values [*Katayama'13*] [*Kochetov'12*]. The use of nano-particles is a delicate procedure to obtain the needed decrease in permittivity. All the presented critical values were much smaller than the 9.8 vol. % of organic PEI blended with the epoxy network used in our study. In comparison with the work of Fothergill et al. using 10 wt.% of TiO_2 with an average size of 23 nm, the relative permittivity response was highly elevated due to the percolation phenomenon [*Fothergill'04*]. The imaginary part of the permittivity values has always showed an increase comparing the epoxy nano-composites with the pure epoxy network.

The incorporation of micro and nano-particles to an epoxy network has led to a decrease in the permittivity value in comparison with the micro-composite but stayed with higher permittivity values than the pure epoxy network. So in all the discussed cases of epoxy composites with inorganic nano or micro-particles an increase in the permittivity values has been noticed with some exceptions using modified nano-particles at very low critical vol%. In the present study, the introduction of PEI into the epoxy network, forming a phase separated

system with particulate morphology, leads to a decrease of the relative permittivity ε'_r without increasing losses, behavior in total opposition to previous works on inorganic fillers. The presence of thermoplastic with a permittivity value lower than that of the pure epoxy system has decreased the permittivity of the blend by 15 %.

3.4.2. Modeling of dielectric response

Modeling of the relative permittivity of a complex material is concerned with the dielectric properties of the macroscopic heterogeneous system. The calculations that will be demonstrated concern the dielectric properties of a particle surrounded by the host material. Calculating the permittivity of a single particle in the host material give us the global idea of the macroscopic system. The model, derived and studied a lot in literature [Polder'46] [Fricke'53] [Altshuller'54] [Asami'02], is an analytical formula of the global dielectric response of composite material consisting of a host matrix filled with ellipsoidal particles as shown in Figure 60.

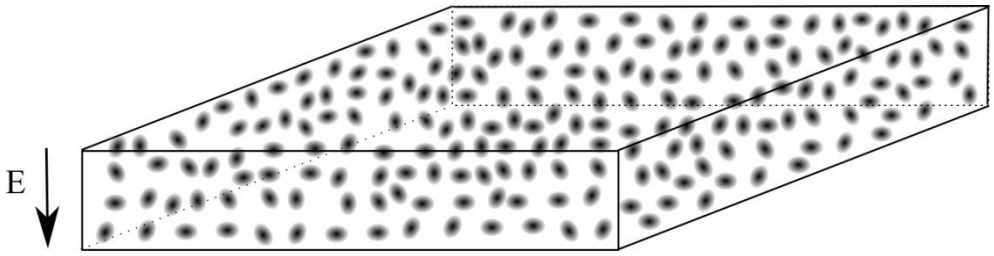

Figure 60: Epoxy host network with homogenously randomly oriented nodules

The effective permittivity ε_e^* of a medium having ellipsoidal inclusions can be expressed as:

$$\varepsilon_e^* = \varepsilon_2^* \left(1 + \frac{1}{3} \emptyset \sum_{k=x,y,z} \frac{\varepsilon_1^* - \varepsilon_2^*}{\varepsilon_2^* + (\varepsilon_1^* - \varepsilon_2^*) L_k} \right) \qquad \textbf{Eq. 48}$$

Where ε_2^* and ε_1^* are the measured complex permittivity of the epoxy network and the PEI network respectively, $\emptyset$ is the volume fraction equal to

$$\emptyset = \frac{4}{3} \frac{\pi abc}{lwh} \qquad \textbf{Eq. 49}$$

and L_k the depolarization factor in the direction characterized by index k (x, y, z). A standard result of electrostatics gives [*Asami'02*]:

$$L_x = \frac{abc}{2}\int_0^{+\infty} \frac{du}{(u+a^2)\sqrt{(u+a^2)(u+b^2)(u+c^2)}} \qquad \textbf{Eq. 50}$$

Where a, b and c denote the semiaxes of the ellipsoid, l, w and h are the dimension of the rectangular zone of epoxy network. The real and imaginary parts of the complex relative permittivity are separated using MATLAB software. In a particulate phase separated network, the nodules are homogenously dispersed in the epoxy network but they can have several orientations with respect to the applied electric field as shown in **Figure 60**. One simple nodule surrounded with the epoxy network is demonstrated in Figure 61.

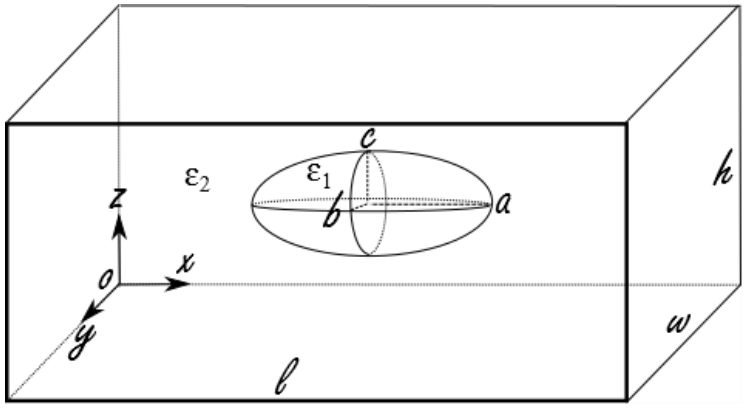

Figure 61: Scheme of the PEI nodule into the epoxy network

Modeling of the effective permittivity of DM5PEI and DM10PEI dielectric response was done from the experimental response of the pure systems of epoxy and PEI. The nodules in both blends are randomly oriented with respect to a given applied electric field as observed in the SEM image; Figure 46(a) and Figure 47 (a).

The volume fraction of PEI in the epoxy network is in our studied case, 5.05 vol.% and 9.8 vol.% for DM5PEI and DM10PEI respectively. L_k the depolarization factor was calculated using the dimensions of the nodules measured from the SEM images. As discussed earlier, the average diameter of the PEI nodules into the epoxy network is 1.5-2 µm in DM5PEI and 2-3 µm in DM10PEI and thus the average major radius (a) is taken as 0.75-1µm and 1-1.5 µm respectively. In both blends, the nodules are in an ellipse form having an average major radius (a), average minor radius (b) = 4a/5 and the second minor radius (c) considered to be in the same size as (b); taking into consideration that the size of the particles is measured in 2D plane. For the studied epoxy-PEI blend, L is calculated numerically using the value of (a) of an average of 1 leading to a value of 0.275 and 0.362 for L_x and L_y respectively with $Ly= L_z$.

SEM images showed that ellipsoidal nodules were regularly dispersed into the epoxy network. Furthermore, the system is considered to be randomly oriented with respect to the applied field. According to this fact, the summation of the three depolarization factors is applied in the proposed model. The modeled curves are calculated from the experimental permittivity of DM and PEI measured at 1 kHz and presented in Figure 62. In both blends the modeled curves are similar to the experimental one with a shift to higher values by an average of 5% for DM5PEI and 9 % for DM10PEI.

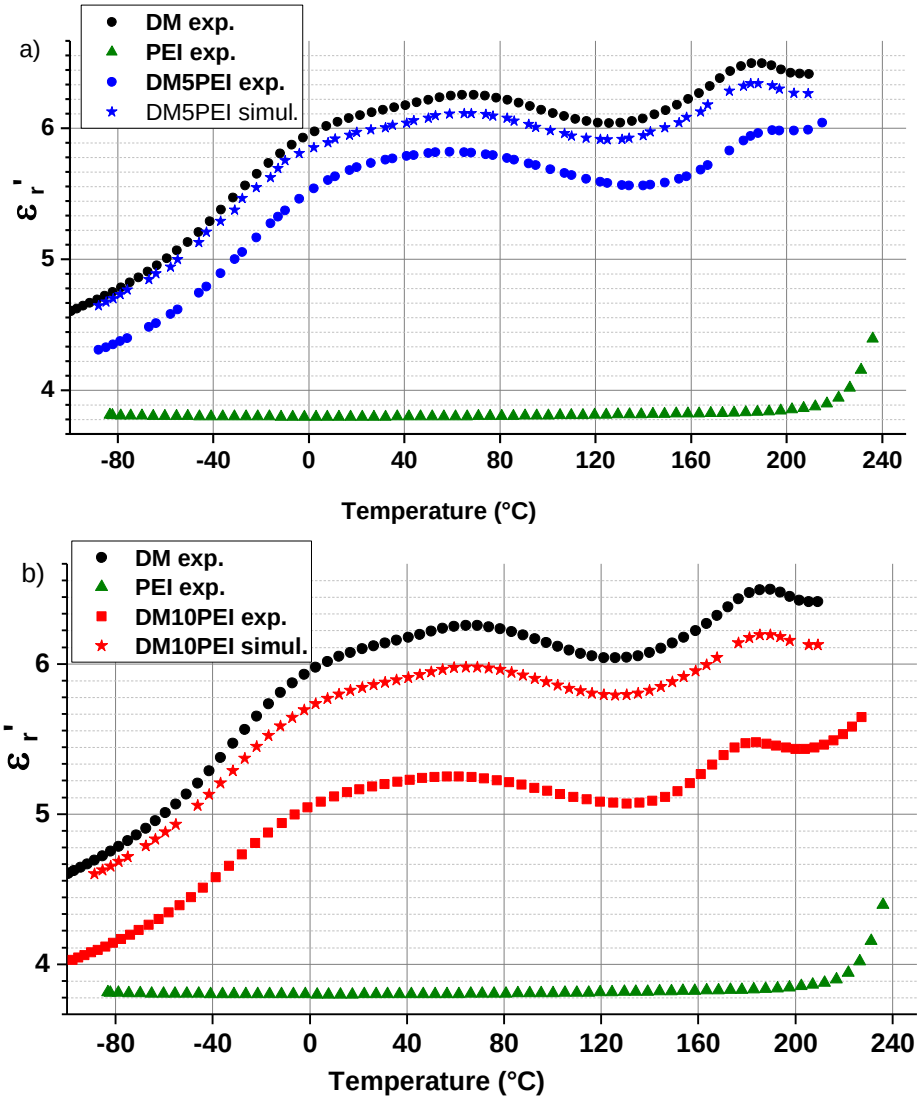

Figure 62: Experimental and effective modulated permittivity of (a) DM5PEI and (b) DM10PEI at 1 kHz

This shift can be explained by several assumptions. From the work of Balberg et al., it can be suggested that the excluded volume in PEI can be at the origin of this discrepancy, as the dimensions from a 2D plane have been taken into account, [*Balberg'84*]. We have seen that

blending of polymers might generate additional free volume which can affect the moduled value [*Akay'94*]. The increase in the free volume can decrease the density of the PEI nodules generating a decrease in the relative permittivity value of PEI and thus can affect the modulated value.

From the TEM images in Figure 48 (b) and 7 (b), an interphase seems to be present between some of the PEI nodule and the epoxy system. This interphase can be explained by low molar masses epoxy-amine dissolved in the PEI phase and can contain free volume as discussed previously. The presence of epoxy-diamine dissolved in a PEI phase can form a system that has different permittivity value; this interphase might affect the relative permittivity value of the blend. Noting that this interphase occupies 5% from the volume of the nodule and it is not present on all the nodules. It is present in around 20 % of the nodules which gives a total of 0.01 vol. % of the total volume of the blends. The presence of the interphase gives the shape of a core shell form with PEI being the core the interphase is the shell and they are embedded in the epoxy matrix. Modeling can be studied furtherly using core-shell model and not an ellipsoid or sphere as suggested by several theoretical work on such a model [*Lestriez'98*] [*Wang'08*] [Wong'00].

Moreover, and finally, as the effective permittivity is not only affected by the fraction volume and the permittivity of the different constituents, proper determination of the particle–particle and particle– network interaction potentials is necessary for further computing [*Brosseau'06*]. Additional studies can be further suggested in this domain.

3.5. Conclusion

In this chapter we have presented the experimental characterization results of the pure networks epoxy (DM) and PEI as well as two blends having 5 and 10 wt % of PEI (DM5PEI and DM10PEI).

The blends showed a phase separated PEI in the epoxy network with a homogenous distribution of nodules as seen by SEM and TEM images. The phase separation phenomenon was confirmed by obtaining two distinct glass transition temperatures related to the epoxy and PEI networks in both blends using DSC characterization. DMA and DEA have also pointed out the presence of the two transitions by the presence of α transition of PEI and DM correlated to the glass transition temperature of each network. DMA measurements have also confirmed the particulate morphology in the blends.

The addition of PEI to the epoxy blend did not have an influence on the thermal resistance of the pure epoxy network which has a good thermal stability up till 300 °C under air atmosphere. This thermal stability under a wide range of temperatures is an advantage for using the material within a power module as the future demands are to have a material that can handle high temperatures.

The relative permittivity of the blends has lower values than the pure epoxy network due to the low permittivity of the PEI nodules decreasing the permittivity of the blend. This decrease in the relative permittivity values is not seen in literature using inorganic micro-particles of the same size and was not performed previously in an organic-organic phase separated blend. This interesting decrease in the dielectric values was modulated as well to show a shift in the modulated curve towards higher value that can be considered due to the free volume existing in the blend during the preparation process. Low values of the permittivity values are an interesting value for the material subjected to be used under electric stress where the waveforms are high voltages.

In the following chapter, the conductivity as well as breakdown measurements are going to be discussed to show the influence of the addition of PEI in the epoxy matrix on these properties.

References

- **Akay'94:** Akay, M. & Cracknell, J. G. Epoxy resin–polyethersulphone blends. J. Appl. Polym. Sci. 52, 663–688 (1994).
- **Balberg'84:** Balberg, I., Anderson, C. H., Alexander, S. & Wagner, N. Excluded volume and its relation to the onset of percolation. Phys. Rev. B 30, 3933–3943 (1984).
- **Bishop'67:** Bishop, D. & Smith, D. THE THERMAL DEGRADATION OF EPOXIDE RESINS. Ind. Eng. Chem. 59, 32–39 (1967).
- **Blanco'04:** Blanco, I., Cicala, G., Motta, O. & Recca, A. Influence of a selected hardener on the phase separation in epoxy/thermoplastic polymer blends. J. Appl. Polym. Sci. 94, 361–371 (2004).
- **Bonnet'01:** Bonnet, A., Lestriez, B., Pascault, J. P. & Sautereau, H. Intractable high-Tg thermoplastics processed with epoxy resin: Interfacial adhesion and mechanical properties of the cured blends. J. Polym. Sci. B Polym. Phys. 39, 363–373 (2001).
- **Brosseau'06:** Brosseau, C. Modelling and simulation of dielectric heterostructures: a physical survey from an historical perspective. J. Phys. D: Appl. Phys. 39, 1277 (2006).
- **Bucknall'89:** Bucknall, C. B. & Gilbert, A. H. Toughening tetrafunctional epoxy resins using polyetherimide. Polymer 30, 213–217 (1989).
- **Castellon'11:** Castellon, J. et al. Electrical properties analysis of micro and nano composite epoxy resin materials. IEEE Transactions on Dielectrics and Electrical Insulation 18, 651–658 (2011).
- **Chau'15:** Chaudhary, S., Surekha, P., Kumar, D., Rajagopal, C. & Roy, P. K. Amine-functionalized poly(styrene) microspheres as thermoplastic toughener for epoxy resin. Polym. Compos. 36, 174–183 (2015).
- **Cho'93:** Cho, J. B., Hwang, J. W., Cho, K., An, J. H. & Park, C. E. Effects of morphology on toughening of tetrafunctional epoxy resins with poly(ether imide). Polymer 34, 4832–4836 (1993).
- **Chou'10:** Choudhury, A. Dielectric and piezoelectric properties of polyetherimide/BaTiO3 nanocomposites. Materials Chemistry and Physics 121, 280–285 (2010).
- **Fothergill'04:** Fothergill, J. C., Nelson, J. K. & Fu, M. Dielectric properties of epoxy nanocomposites containing TiO2, Al2O3 and ZnO fillers. in 2004 Annual Report Conference on Electrical Insulation and Dielectric Phenomena, 2004. CEIDP ’04 406–409 (2004).
- **Gir'96-2:** Girard-Reydet, E. et al. Reaction-induced phase separation mechanisms in modified thermosets. Polymer 39, 2269–2279 (1996).
- **Gir'97:** Girard-Reydet, E., Vicard, V., Pascault, J. P. & Sautereau, H. Polyetherimide-modified epoxy networks: Influence of cure conditions on morphology and mechanical properties. J. Appl. Polym. Sci. 65, 2433–2445 (1997).
- **Heid'15:** Heid, T., Fréchette, M. & David, E. Epoxy/BN micro- and submicro-composites: dielectric and thermal properties of enhanced materials for high voltage insulation systems. IEEE Transactions on Dielectrics and Electrical Insulation 22, 1176–1185 (2015).
- **Heux'97:** Heux, L., Halary, J. L., Lauprêtre, F. & Monnerie, L. Dynamic mechanical and 13C n.m.r. investigations of molecular motions involved in the β relaxation of epoxy networks based on DGEBA and aliphatic amines. Polymer 38, 1767–1778 (1997).

- **Hourston'92:** Hourston, D. J. & Lane, J. M. The toughening of epoxy resins with thermoplastics: 1. Trifunctional epoxy resin-polyetherimide blends. Polymer 33, 1379–1383 (1992).
- **Iyer'11:** Iyer, G., Gorur, R. S., Richert, R., Krivda, A. & Schmidt, L. E. Dielectric properties of epoxy based nanocomposites for high voltage insulation. IEEE Transactions on Dielectrics and Electrical Insulation 18, 659–666 (2011).
- **Katayama'13:** Katayama, J., Ohki, Y., Fuse, N., Kozako, M. & Tanaka, T. Effects of nanofiller materials on the dielectric properties of epoxy nanocomposites. IEEE Transactions on Dielectrics and Electrical Insulation 20, 157–165 (2013).
- **Katayama'13:** Katayama, J., Ohki, Y., Fuse, N., Kozako, M. & Tanaka, T. Effects of nanofiller materials on the dielectric properties of epoxy nanocomposites. IEEE Transactions on Dielectrics and Electrical Insulation 20, 157–165 (2013).
- **Kochetov'10:** Kochetov, R., Andritsch, T., Morshuis, P. H. F. & Smit, J. J. Thermal and electrical behaviour of epoxy-based microcomposites filled with Al2O3 and SiO2 particles. in Conference Record of the 2010 IEEE International Symposium on Electrical Insulation (ISEI) 1–5 (2010).
- **Kochetov'12:** Kochetov, R., Andritsch, T., Morshuis, P. H. F. & Smit, J. J. Anomalous behaviour of the dielectric spectroscopy response of nanocomposites. IEEE Transactions on Dielectrics and Electrical Insulation 19, 107–117 (2012).
- **Lestriez'98:** Lestriez, B. et al. Is the Maxwell–Sillars–Wagner model reliable for describing the dielectric properties of a core–shell particle–epoxy system? Polymer 39, 6733–6742 (1998).
- **Levchik'04:** Levchik, S. V. & Weil, E. D. Thermal decomposition, combustion and flame-retardancy of epoxy resins—a review of the recent literature. Polym. Int. 53, 1901–1929 (2004).
- **Nelson'04:** Nelson, J. K. & Fothergill, J. C. Internal charge behaviour of nanocomposites. Nanotechnology 15, 586–595 (2004).
- **Singha'08:** Singha, S. & Thomas, M. J. Dielectric properties of epoxy nanocomposites. IEEE Transactions on Dielectrics and Electrical Insulation 15, 12–23 (2008).
- **Singha'09:** Singha, S. & Thomas, M. J. Influence of filler loading on dielectric properties of epoxy-ZnO nanocomposites. IEEE Transactions on Dielectrics and Electrical Insulation 16, 531–542 (2009).
- **Tsangris'96:** Tsangaris, G. M., Kouloumbi, N. & Kyvelidis, S. Interfacial relaxation phenomena in particulate composites of epoxy resin with copper or iron particles. Materials Chemistry and Physics 44, 245–250 (1996).
- **Tsekmes'14:** Tsekmes, I. A., Kochetov, R., Morshuis, P. H. F. & Smit, J. J. The role of particle distribution in the dielectric response of epoxy–boron nitride nanocomposites. J Mater Sci 50, 1175–1186 (2014).
- **Wang'08:** Wang, M. & Pan, N. Predictions of effective physical properties of complex multiphase materials. Materials Science and Engineering: R: Reports 63, 1–30 (2008).
- **Wong'00:** Wong, C. P., Marinis, T., Jianmin Qu & Yang Rao. A precise numerical prediction of effective dielectric constant for polymer-ceramic composite based on effective-medium theory. IEEE Transactions on Components and Packaging Technologies 23, 680–683 (2000).

Chapter 4

Epoxy/Polyetherimide Blend Electrical Characterizations

We will present in this chapter the electrical characterization of the epoxy pure material as well as the blends. Conductivity measurements and breakdown voltage measurements are going to be discussed.

4.1. Conductivity measurements

Conductivity measurements were performed and recorded using two different techniques. The first one was done under high DC voltage from 1 kV to 15 kV at room temperature. The second one, at high temperatures the measurements are extrapolated from the dielectric characterization with variation of temperature between 120 °C and 250 °C under AC voltage.

4.1.1. Conductivity Measurements at room temperature

In this measurement the samples DM and DM10PEI have a thickness of 600 µm. DC electric field of 1.6, 5, 8.3, 11.6, 16.6 and 25 kV.mm-1 were applied for about one hour in the polarization stage and one hour in the depolarization stage at room temperature (21 °C). The electrodes, of 4 cm diameter, from both sides were accompanied with a thick layer of silicon to avoid partial discharges and the increased field at the edge of the metallized electrodes as well as increasing the by-pass path. Preliminary tests have pointed out that guard rings are not necessary for the applied field levels in our tests. The recorded current at each applied voltage with respect to time is presented in Figure 63.

The polarization current I_P followed a transient regime and then stabilized. The quasi-steady-state charging current is taken as the conduction current I_C. The current has increased with the increase of the applied field in both samples signifying the increase in the mobility of charge carriers in the material. Current values were influenced by the presence of PEI in the epoxy network showing higher values for DM10PEI than the pure DM sample, which is demonstrated in Table 13. As seen in Figure 63 the measurements performed for DM10PEI did not reach 3600 s therefore the noted values at 3000 are extrapolated but can have lower values.

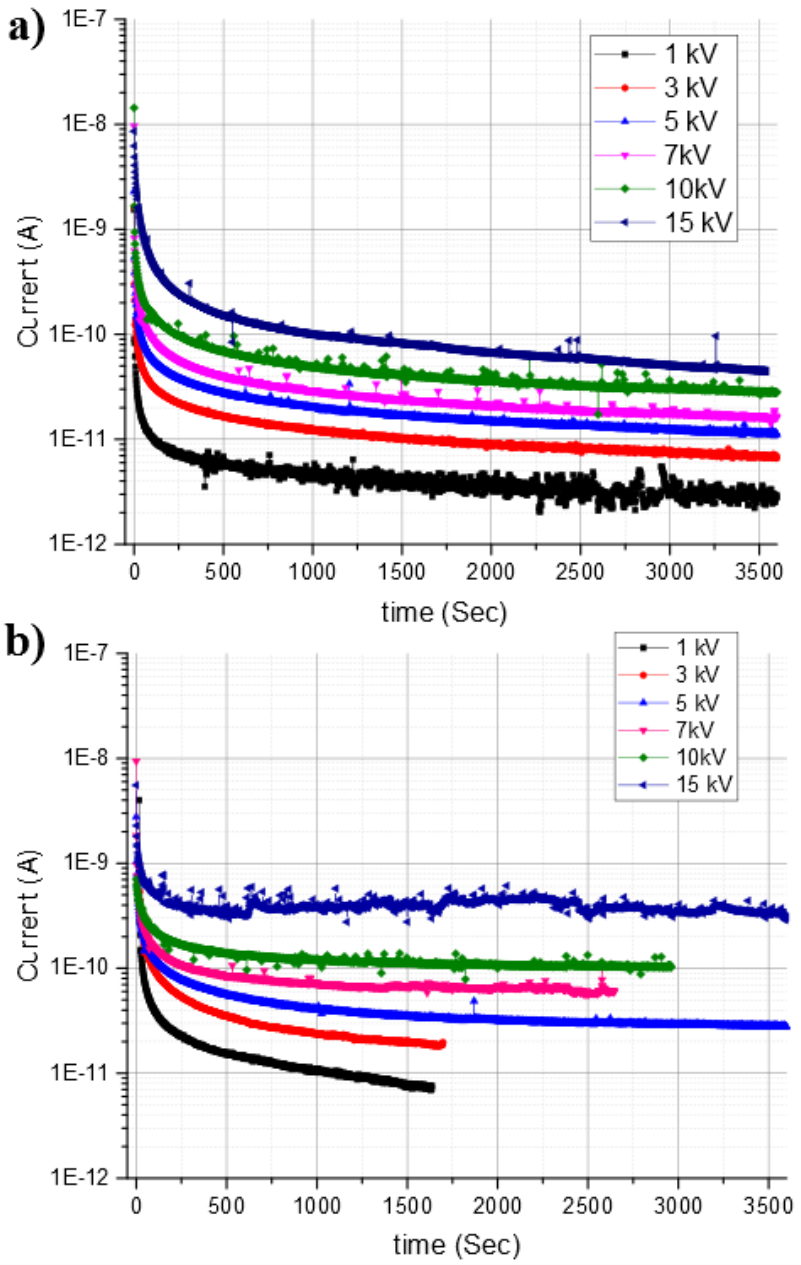

Figure 63: Current polarization curves with respect to different voltages for a) DM and b) DM10PEI

Table 13: Evolution of the measured current at different voltages and time in the polarization process

Voltage (kV)	Current (A)					
	DM			DM10PEI		
	500 sec	1500 sec	3000 sec	500 sec	1500 sec	3000 sec
1	5.4×10^{-11}	3.6×10^{-12}	3×10^{-12}	1.5×10^{-11}	$7{,}7 \times 10^{-12}$	$<6 \times 10^{-12}$
3	1.6×10^{-11}	10^{-11}	7.8×10^{-12}	3.5×10^{-11}	2×10^{-11}	$<2 \times 10^{-11}$
5	2.7×10^{-11}	1.6×10^{-11}	1.2×10^{-11}	5.5×10^{-11}	$3{,}5 \times 10^{-11}$	2.9×10^{-11}
7	4×10^{-11}	2.4×10^{-11}	1.7×10^{-11}	8.4×10^{-11}	$6{,}8 \times 10^{-11}$	5.9×10^{-11}
10	7.5×10^{-11}	4×10^{-11}	3.2×10^{-11}	1.4×10^{-10}	$1{,}3 \times 10^{-10}$	10^{-10}
15	1.4×10^{-10}	8×10^{-11}	5×10^{-11}	$3{,}7 \times 10^{-10}$	4×10^{-10}	3.5×10^{-10}

The currents show dependence with the time (t) and applied electric field (E), the transient current has been observed to decay following the power law [*Gupta'76*]:

$$I(t) = k.E.t^{-n} \qquad \textbf{Eq. 51}$$

where k is a constant that depends on the temperature used and n that is dependent of the material and can be obtained from the slope between I and E in isochrones demonstration. Different mechanisms can be proposed from the value of n such as [*Gupta'76*]:

- electrode polarization (n > 1)
- dipole orientation where dipoles are uniformly distributed in the material ($0 \leq n \leq 2$)
- charge injection leading to trapped space charge effects ($0 \leq n \leq 1$)
- tunneling of charge from the electrodes to empty traps ($0 \leq n \leq 2$)
- hopping of charge carriers from one localized state to another ($0 \leq n \leq 2$)

Current is presented with respect to applied electric field at different time in Figure 64 and the obtained slopes are extracted in Table 14.

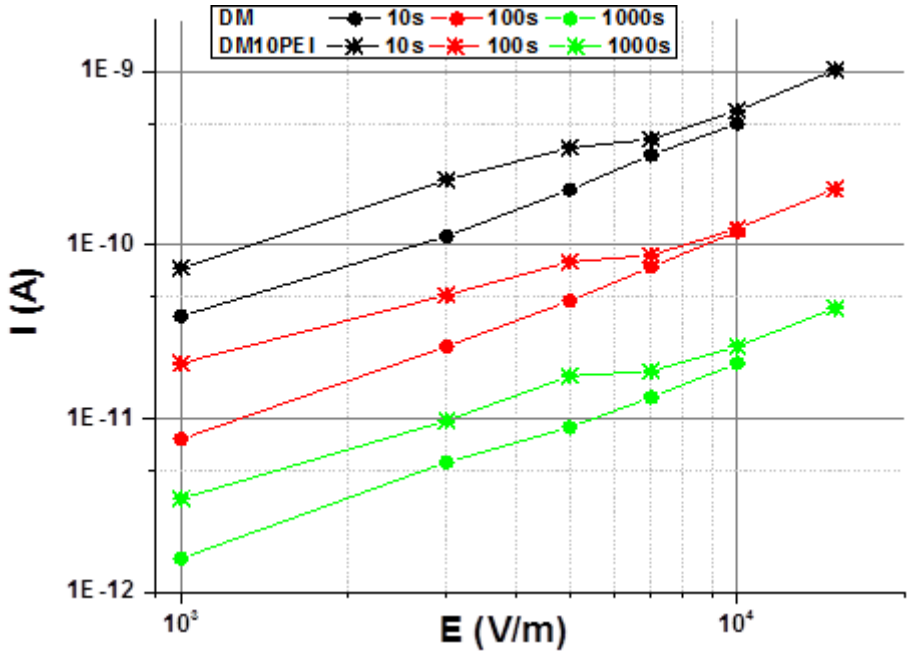

Figure 64: Isochrones currents obtained from depolarization current

Table 14: Obtained slopes from Isochrones presentation

Time (s)	10	100	1000
DM	1.1	1.19	1.1
DM10PEI	0.93	0.87	0.9

The slopes are in the same range, being slightly higher for the pure resin. The plots of the isochronal discharging currents at 10, 100 and 1000 attest the proportionality of the discharging currents to the applied field. The obtained slopes for DM can be referred to electrode polarization, dipolar orientation, tunneling and hopping effect. With the addition of PEI the slopes decrease below 1 suggesting charge injection leading to trapped space charge effects. The conduction phenomena are going to be more detailed in the following paragraphs.

Current reversibility between the polarization and the depolarization responses is studied for DM and DM10PEI and is presented in Figure 65. The presented response is at 5kV knowing that we obtained the same response with all the tested electric fields. It is seen from this presented graph that the response of the absorption and depolarization curves follow the same evolution with respect to time and under the same applied electric field. The slope for the two responses for DM is measured between 10 s and 1000 s and found to have the same value -0.68. The DM10PEI showed similar reversibility, with a slope of -0.65, between the two responses between 10 s and 600 s above which the absorption response starts to decay. This reversibility defines that the polarization phenomenon in this case depends on the dipolar movements and is not affected by space charge phenomenon [*Segui'00*].

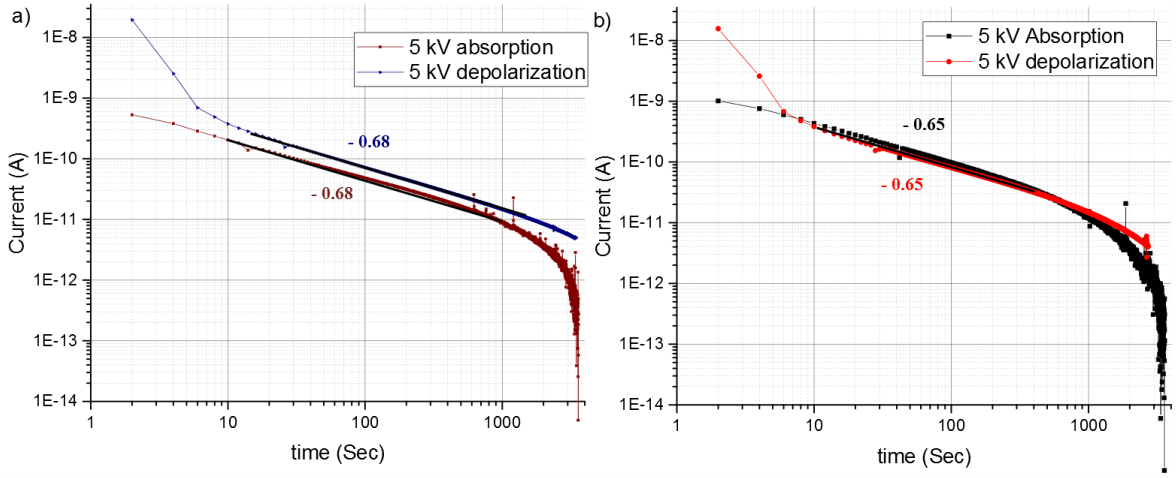

Figure 65: Absorption and depolarization at 5kV for a) DM and b) DM10PEI

The conduction current I_C is deduced from the average of the last 10 measurements for each applied electric field. Current densities were calculated from the measured I_C and the diameter of the electrodes used (4 cm).

Current densities at room temperature are plotted in log-log scale as function of the applied electric field (E) for DM and DM10PEI in Figure 66. The two curves present two different conduction modes separated by a threshold field Eth. Below threshold values, both

pure epoxy DM and DM10PEI have a linear relation between J and E with a slope of 1 corresponding to the Ohmic conduction phenomenon.

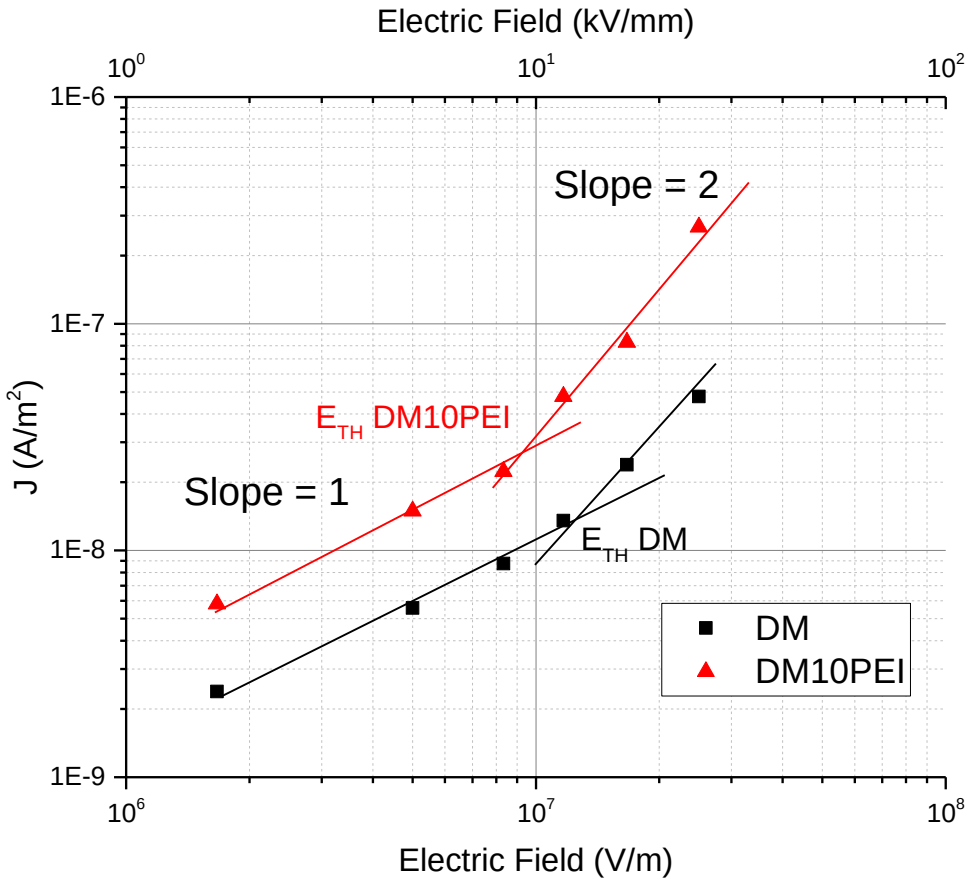

Figure 66: Conduction Current density versus applied electric field

Threshold field Eth for the blend was lower than that of DM having 9.2 kV.mm-1 and 12.5 $kV.mm^{-1}$ respectively. The difference between the two threshold fields is about 26%. A conclusion can be drawn that the PEI reduces the voltage range of the Ohmic regime, but this conclusion is deduced from the measurement done using 6 different electric fields. The slope above the threshold field can be modified when a bigger variation of electric field is applied. Changes in the slope result in the modification of the threshold field of both DM and DM10PEI.

Above the threshold field, a non-linearity in the conduction current appeared for both samples with a slope = 2. Similar phenomenon for pure epoxy network with anhydride hardener was obtained with higher threshold field of 17 $kV.mm^{-1}$ [Guill'06]. When the slope is equal to 2 the volume conduction phenomenon fits well with the space-charge-limited conduction model (SCLC). The current density (J) in this case is presented as following [Dissado'92]:

$$J = \frac{9\,\varepsilon_r \varepsilon_0\,\mu\,V^2}{8\,d^3} \qquad \textbf{Eq. 52}$$

where μ is the carrier mobility and d is the thickness of the sample.

Values of the relative permittivity are taken from the dielectric measurements at 25 °C and 0.1 Hz (ε_r DM = 6.4 and ε_r DM10PEI = 5.8). Carrier mobility μ at 10 kV is 8.06 x 10^{-10} and 2 x 10^{-9} cm^2 $V^{-1}s^{-1}$ for DM and DM10PEI respectively. These values are in the same range of what is found in literature for pure epoxy networks at 10 kV such as 2.3 x 10^{-10} cm^2 $V^{-1}s^{-1}$ [*Guill'06*] and 1.5 x 10^{-10} cm^2 $V^{-1}s^{-1}$ [*Castellon'11*].

To verify whether the conduction phenomenon obeys the Poole-Frenkel effect above the E_{th} value, conductivity values versus $\sqrt{E}$ were plotted in Figure 67. To fit this law the conductivity must have constant values with a negligible slope, which is not the presented case. Conductivity values are considered constant till 8.3 kV/mm after which the values begin to increase. From the obtained slopes (slope= β_{PF}/KT), β_{PF} is calculated to be 1.2 x 10^{-24} and 2.6 x 10^{-24} for DM and DM10PEI respectively. Calculating β_{PF} theoretically:

$$\beta_{PF} = \left(\frac{q^3}{\pi \varepsilon_0 \varepsilon_r}\right)^{1/2} \qquad \textbf{Eq. 53}$$

the obtained values are 4.7 x 10^{-24} and 5.03 x 10^{-24} concerning DM and DM10PEI respectively. β_{PF} calculated from the obtained slope or calculated theoretically vary by 50-70%. The conductivity does not fit the Poole-Frenkel law. Similar phenomenon was obtained when pure epoxy network was measured below its glass transition temperature. This law was confirmed when the temperature was only above the glass transition temperature of epoxy [*Guill'06*].

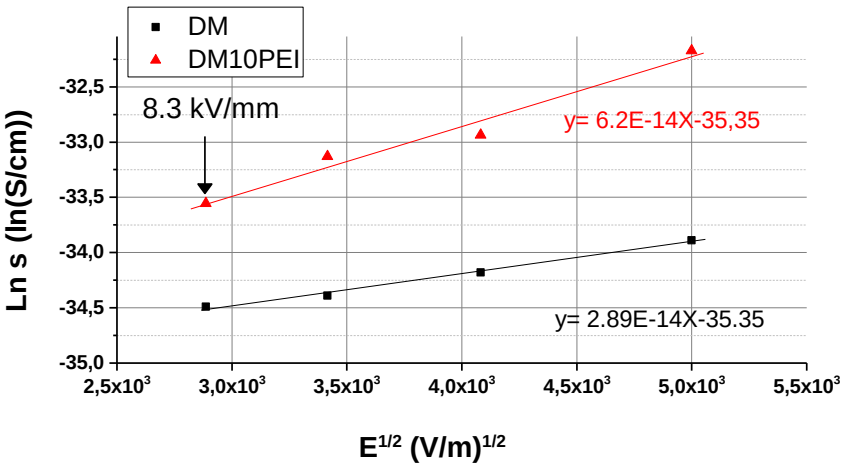

Figure 67: ln Conductivity versus $\sqrt{E}$ at room temperature.

The conduction currents could be controlled by the interface present between the electrode and the sample by the Schottky or the Fowler-Nordheim effect, the latter appears generally at high fields or very low temperatures. The current density emitted due to Schottky effect is presented as following:

$$J_s = A_s T^2 \exp\left(-\frac{\Phi_0 - \beta_s\sqrt{E_c}}{K_B T}\right) \qquad \textbf{Eq. 54}$$

where, A_s is the Richardson-Dushman constant for thermionic emission and E_c the field at the cathode. β_s is the Schottky constant:

$$\beta_s = \sqrt{\frac{q^3}{4\pi\varepsilon_0\varepsilon_r}} \qquad \textbf{Eq. 55}$$

where q is the elementary charge. Castellon et al. in their study showed that it is difficult to quantify the electric field at the cathode as it might be distorted by space charge [*Castellon'11*]. For that they proposed to add a dimensionless parameter γ as following:

$$E_C = \gamma \frac{V}{d} \qquad \textbf{Eq. 56}$$

with γ <1 for a contact dominant homocharges and γ >1 for a contact dominant heterocharges. The Schottky current becomes:

$$J_s = A_s T^2 \exp\left(-\frac{\Phi_0 - \beta_s\sqrt{\gamma\frac{V}{d}}}{K_B T}\right) \qquad \textbf{Eq. 57}$$

To verify this model, a plot of ln(J_s) versus $\sqrt{E}$ is presented in Figure 68. γ parameter can now be calculated from the slope obtained using the following equation:

$$\gamma = \frac{(slope)^2 (K_B T)^2 4\pi\varepsilon_0\varepsilon_r}{q^3}$$

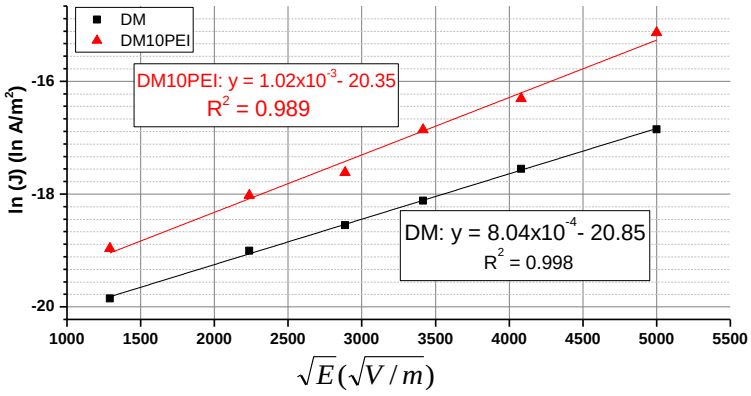

Figure 68: J versus $\sqrt{E}$ for Schottky model

Current densities of both DM and DM10PEI were proportional to $\sqrt{E}$ with slopes of the same range. The calculated γ are 1.79 and 2.45 for DM and DM10PEI respectively. As the values of γ are higher than 1 this implies that the heterocharges near the cathode increase the local field and tends to decrease the energy barrier at the interface. With the addition of PEI the injection field at the cathode is increased in comparison with the neat epoxy. Comparing with the work of Castellon et al. where for pure epoxy network the value of γ was 2.55. It has the same range as the blend of our work which is higher than our pure epoxy network. They have tested the influence of adding 60 wt% of silica micro-particles along with 2 to 5 wt% silica nanoparticles, in which the addition of either kinds of fillers have increased the current emission in the sample above the pure epoxy network values. The Schottky emission model can be validated by this approach where the value of γ showed the increase in the current emission with the addition of PEI to the pure epoxy network.

Fowler-Nordheim mechanism of charge injection is verified by the presenting ln $\frac{J}{E^2}$ in function of $\frac{1}{E}$ as shown in Figure 69. This representation did not show a straight line in both pure epoxy and the blend. Therefore the Fowler-Nordheim law is not applied in the studied case.

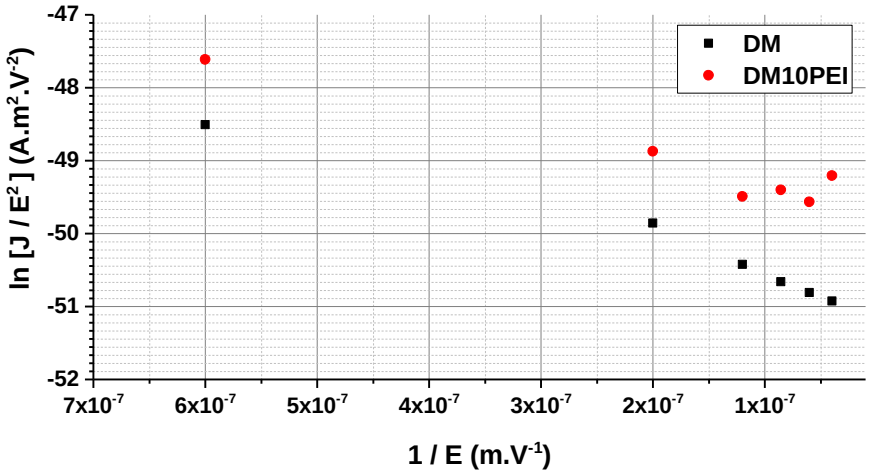

Figure 69: Representation of the Fowler-Nordheim injection mechanism

This characterization technique was done at room temperature. The current was seen to be ohmic below the threshold field for both samples. Above the threshold field two possible approaches were studied. First the results were shown to be not obeying the Poole-Frenkel law but it is suggested that they obey the volume phenomenon of SCLC approach. Contact emission phenomenon according to Fowler-Nordheim is not valid. Whereas, Schottky model was also investigated and shown to be probably valid. Further studies must be

considered for this kind of measurement and especially to monitor the distribution of the space charge inside the sample. Appropriate technique must be used to probe the charges carriers with better sensitivity and spatial resolution. For that the pulse electro-acoustic or the laser induced pressure pulse methods could give rise to interested data. The influence of the temperature must be also investigated

Comparing these values with the values obtained for silicone gels, it is given in the work of Do et al. that the conduction current obeys an ohmic law up till 2 kV/mm [Do'08]. The silicon tested was a commercial PDMS. The carrier mobility value was 0.86 x $10^{-7}$$cm^2V^{-1}s^{-1}$ which is three decades higher than that of pure tested epoxy network. Silicone gel obtained values that are similar to that of silicon oil and not solid materials. This fact gives an advantage of using the epoxy pure network or the epoxy and PEI blend as an encapsulating material in a power module.

4.1.2. Conductivity Measurements at high temperatures

In order to evaluate the DC conductivity (quasi-steady-state) at high temperatures, it is necessary to start by evaluating the changes taking place in the AC conductivity domain. Figure 70 presents the evolution of AC conductivity with respect to frequency for the pure epoxy and PEI materials as well as the two blends DM5PEI and DM10PEI. The temperature range evaluated is between 120 °C and 230 °C; knowing that the glass transition temperature of epoxy is T_g = 164 °C.

The conductivity σ_{AC} of the 4 studied samples showed a linear increase with the frequency having a slope equal to 1 at high frequencies. It is frequency dependent and follows the law $\sigma_{AC}(\omega) = \omega^s$ with $0 \leq s \leq 1$ characterizing hopping conduction [*Dyre'00*] [*Psarras'06*]. As the temperature increases the conductivity becomes more independent of the frequency. A horizontal plateau appears progressively expressing the thermal activation of the DC conductivity. The amplitude of this plateau corresponds to the DC conductivity at a given temperature. As the temperature increases, the mobility of the electrons increases shifting the plateau to higher frequencies. The plateaus appearing for DM, DM5PEI and DM10PEI seem to have the same influence with respect to frequency and temperature.

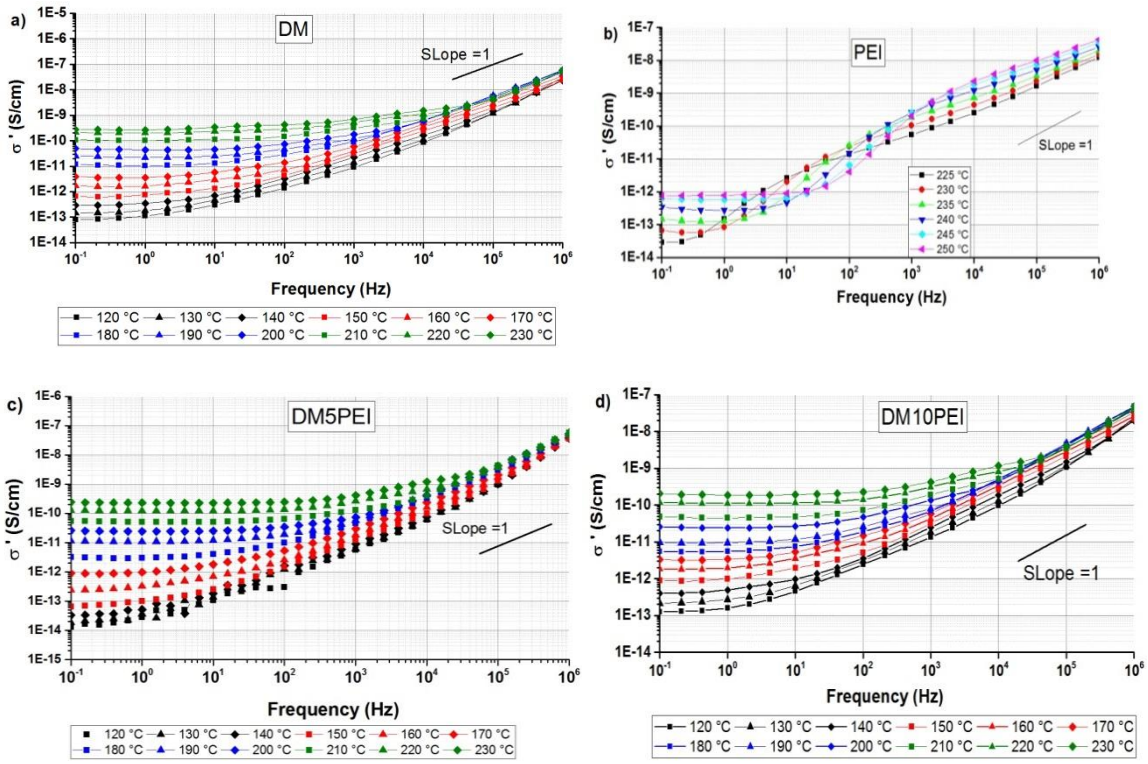

Figure 70: Evolution of AC conductivity in function of frequency for a) DM, b) PEI, c) DM5PEI and d) DM10PEI.

In comparison with similar works the values of the DC conductivity have lower values than what is obtained in literature. At 160 °C, in our studied for pure epoxy sample the DC conductivity σ_{DC} = 1.7 x 10^{-12} S.cm^{-1}. At the same temperature for epoxy cured with diamine (DDS) σ_{DC} = 1.3 x 10^{-10} S.cm^{-1}, epoxy cured with diamine (EDA) σ_{DC} = 1.5 x 10^{-9} S.cm^{-1} [*Jilani'15*] and epoxy cured with difunctional amine σ_{DC} = 6 x 10^{-8} S.cm^{-1} at 156 °C [*Smaoui'10*].

PEI sample has a T_g = 216 °C where above this temperature the appearance of the plateau starts at low frequencies. It is noticed that the values of σ_{DC} of PEI, at high temperatures, have lower values than the pure epoxy and the blends by three decades of difference. PEI sample is more resistive than the epoxy material.

Silicone gel material is considered a semi-conducting material above 60 °C, where its σ_{DC} values are higher than 10^{-12} S.cm^{-1} [*Locatelli'14*]. The epoxy on the other hand steps above 10^{-12} S.cm^{-1} starting from 150 °C. This gives a wider range of electrical insulation stability for epoxy under higher temperature range. In addition to that, blending epoxy with 5 and 10 wt% of PEI did not decrease this value.

Figure 71 presents the evolution of the DC conductivity of the pure material and the blends in function of temperature extrapolated from dielectric spectroscopy measurements at 0.1 Hz. The measured DC conductivity by dielectric spectroscopy has a linear slope above the glass transition temperature of epoxy for DM, DM5PEI and DM10PEI and above the glass transition of PEI for PEI film. All the slopes are well fitted with the Arrhenius law, where the obtained activation energies are presented in Table 15. The obtained activation energy above T_g of epoxy for DM, DM5PEI and DM10PEI are in the same range. This signifies that the blending PEI with the epoxy did neither affect the DC conductivity values nor the activation energy of the system. The value of the activation energy is in the same range of what is obtained in similar studies above the glass transition temperature of epoxy fitted with Arrhenius law. The activation energy of two kinds of epoxy with different diamine hardeners can be quite different as 0.45 eV for an epoxy/amine [*Smaoui'10*] and 0.85 eV for DGEBA/330DDS [Jilani'15].

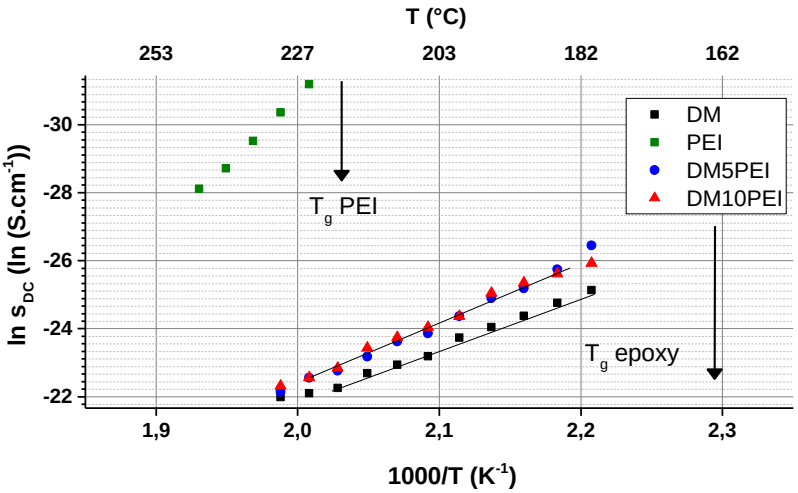

Figure 71: Evolution of the DC conductivity in function of temperature extrapolated from the AC conductivity values at 0.1 Hz

Table 15: Activation energy of DM, DM5PEI and DM10PEI, below and above the glass transition of epoxy; and the activation energy for PEI above the glass transition of PEI

Sample	Activation energy (eV)
DM	0.41
PEI	1.028
DM5PEI	0.46
DM10PEI	0.43

4.2. Breakdown voltage at room temperature

Breakdown voltage of the material is an important characterization of the material as it states the probable maximum voltage a material can resist before breaking down. Starting from the idea of having nodules of PEI in the matrix might ameliorate the breakdown property. These nodules have shown that they are stronger mechanically and can attenuate mechanical cracks. In addition to that, PEI has lower relative dielectric values as well as higher resistivity as seen from the conductivity measurements discussed above. To investigate their influence on the epoxy network, DC breakdown test was done on DM, PEI, DM5PEI and DM10PEI. For each kind of material more than 10 samples were tested and Weibull probability plots are extracted. It is shown that when the distribution is not scattered (with $\beta > 5$), the characteristic field is close to the center of the distribution; i.e. the value for which the probability density is maximum [*Chauvet'92*].

DM samples as presented by the Weibull distribution in Figure 72 (a) have shown a decrease in the breakdown value with respect to the thickness of the sample tested. The shape parameter $\beta = 7.6$ is greater than 5 giving the confidence to the presented results. The obtained scale parameter $\alpha = 195$ kV.mm^{-1}, the obtained breakdown voltage value for a DC test is higher than the majority of breakdown tests on different kinds of epoxy and hardeners. Nevertheless, we have to mention that the common used technique for such characterization is an AC breakdown test. The obtained values for pure epoxy networks vary from 40 to 100 kV.mm^{-1} [*Tuncer'07*] [Singha'08] [*Singha'09*] [*Preetha'10*] [*Iyer'11*] [*N*asciment'16].

Weibull distribution for DM10PEI samples is presented in Figure 72 (b). It is clear that depending on the thickness of the DM10PEI samples two different Weibull distributions can be extracted. Samples with thickness higher than 630 µm are categorized in the first distribution, while samples having a thickness less than 630 µm have another distribution. This phenomenon can be related to the presence of bubbles in the sample. As the sample is thicker, even though the mixing procedure is done under vacuum, the probability of having micro-voids is higher. By which the breakdown voltage decreases.

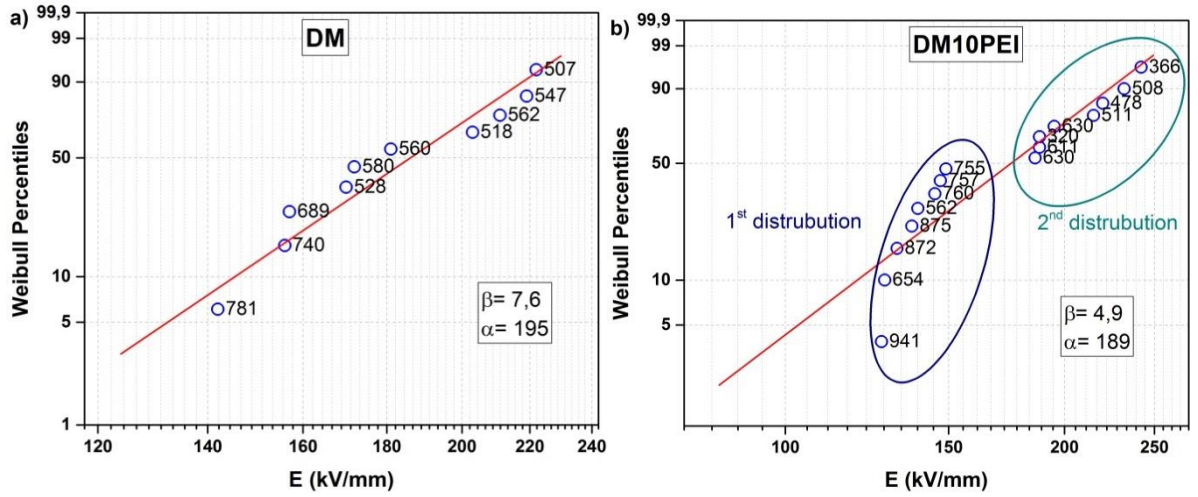

Figure 72: **Weibull distribution plot (95% confidence interval) for a) DM and b) DM10PEI; Thickness of the sample studied is presented on each point.**

Weibull distribution for the pure networks DM and PEI as well as the blends DM5PEI and the two parts of DM10PEI is presented in Figure 73. The scale parameter (α) and the shape parameter (β) are extracted into Table 16. It's clearly noticed that PEI have a greater breakdown voltage than the pure epoxy material or the blends. Blending epoxy with 5 wt% of PEI has increased the breakdown voltage of the epoxy system. Increasing PEI % to 10 wt% gave two different possibilities. The first one is when considering the 1st group of distribution of DM10PEI where the average thickness of the studied sample is 687 µm. Knowing that the average thickness of the studied DM and DM5PEI is 545 and 533 µm. The breakdown voltage of DM10PEI (1st) is 25 % lower than that of the pure epoxy network. This decrease is mainly attributed to the presence of voids into the samples that were not released during the preparation step. Considering the 2nd group of distribution of DM10PEI where their average thickness is 507 µm. This average thickness is in the same range of that studied for pure and DM5PEI sample. We can conclude here that the increase of the wt% of PEI into the epoxy network have increased the value of breakdown voltage. The particles confirmed the idea of resisting micro cracks that tend to propagate during a breakdown process. This gives the whole system the ability to withstand higher applied fields.

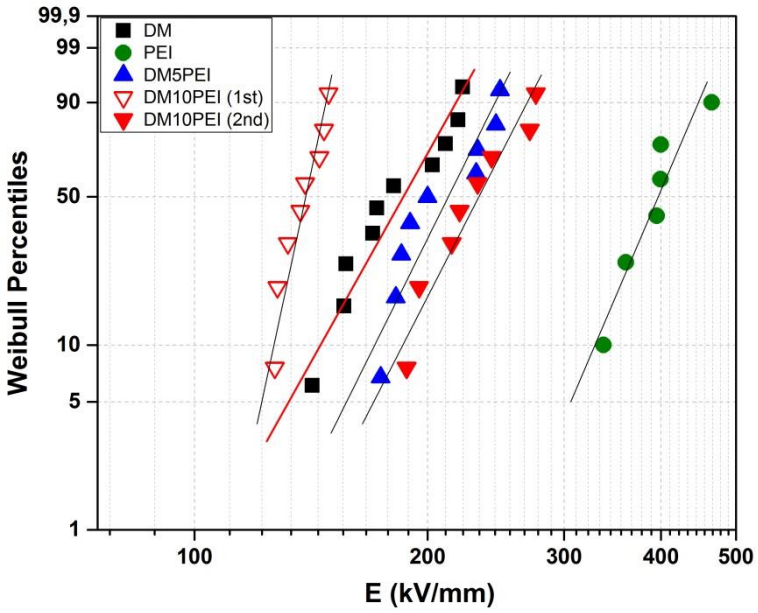

Figure 73: Weibull distribution plot (95% confidence interval) for DM, PEI, DM5PEI and DM10PEI

Table 16: Scale and shape parameter from Weibull distribution

Sample	Shape parameter: β	Scale parameter: α (kV/mm)	% with respect to DM
DM	7.6	195	-
PEI	10	412	-
DM5PEI	8.6	222	↗ 14%
DM10PEI (1st)	20	142	↘ 28.7%
DM10PEI (2nd)	8.3	244	↗ 25 %

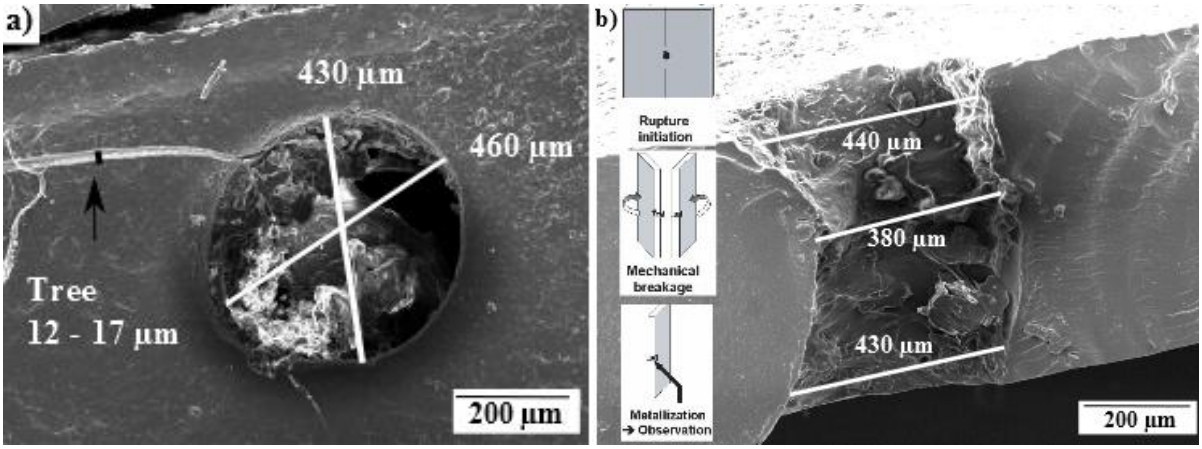

Figure 74: SEM images of the breakdown channel in DM10PEI sample a) face view and b) side view after breaking the sample as illustrated in the schemas

Figure 74 shows SEM images of the void tunnel formed in the bulk of the sample due to the electrical breakdown test. The samples are seen from the face and the side after breaking the sample in the middle of the hole present after the test. The hole has a circular shape with two diameters 430 and 460 µm with a narrower bulk as seen in Figure 74 (b). The size of the produced hole after the breakdown test is in similar value with what is obtained in other studies, such as the work of Iyer et al. on Epoxy/inorganic micro-composites [*Iyer'11*]. In the sphere–sphere configuration, a quasi-homogeneous field exists at the electrode-dielectric interfaces. The damage could thus equally initiate anywhere within the structure, and should hence first take place in the vicinity of the major flaws. As a result of this, it is not possible in this electrode configuration to identify a unique starting point and an end to the damage propagation.

Globally the addition of nano and micro inorganic-fillers to the epoxy network has shown a decrease in the breakdown voltage value. The used fillers have higher electrical conductivity and permittivity values with respect to the pure epoxy matrix and thus acted as defects in the material favoring the breakdown voltage at lower voltages [*Nelson'04*] [[*Iyer'11*] [*li'10*] [*Hu'06*]. In our studied blends the PEI nodules have lower electrical conductivity values as well as lower permittivity which enhance the breakdown voltage of the blend with respect to the pure epoxy network.

As discussed in chapter 2 the origin of the breakdown mechanism can be due to different aspects, the electrical, electromechanical and the thermal mechanism. It is rather difficult to determine the origin of the breakdown taking place due to the lack of temperature measurement at the surface and the difficulty to obtain the thickness variation of the sample during the experiment. Nevertheless the breakdown can be the result of the three mechanisms together with a variation in the percentage of contribution of each of the mechanism [*Dissado'92*]. This point must be studied in the future of this project.

4.3. Conclusion

In this chapter we have highlighted the influence of the PEI nodules on the electrical conductivity and the breakdown voltage measurements.

Conductivity measurements conducted at room temperature have shown similar conduction mechanisms before and after the threshold field E_{th}. Ohmic conduction contributed at low voltages and SCLC at high voltages with carrier motilities similar to what is found in literature. Poole-Frenkel law was not fitted to the presented results at room temperature. Whereas, Schottky injection was verified for both materials DM and DM10PEI having contact emission phenomenon at the interface between the electrodes and the sample.

DC conductivity measurements were extrapolated from the AC conductivity measured by the dielectric spectroscopy for high temperatures. The presence of PEI nodules into the epoxy matrix did not show an influence on the DC conductivity values nor on the activation energy deduced.

Finally, in breakdown voltage of epoxy network the measurements have shown an increase in their values with the increase of the wt% of PEI into the epoxy network. This enhancement is rarely seen in literature especially with the incorporation of micro-fillers as they act as defects. In the studied case the PEI nodules acted as obstacles for the breakdown voltage of the blends. In addition to that, the obtained breakdown voltage for pure epoxy and epoxy/PEI blend is higher than silicon gels.

Further investigations are needed to confirm the assumptions that have been made. For example, the analysis of the spatial space charges distributions in the material and the study of the partial discharge inception as a function of the rate of thermoplastic would make it possible to better evaluate this type of material.

References

- **Castellon'11:** Castellon, J. et al. Electrical properties analysis of micro and nano composite epoxy resin materials. IEEE Transactions on Dielectrics and Electrical Insulation 18, 651–658 (2011).
- **Chauvet'92:** Chauvet, C. Mise au point d'une méthodologie pour des essais de rupture a court terme en vue de la caractérisation des isolants synthétiques des cables haute-tension. (Toulouse 3, 1992).
- **Dissado'92:** Dissado, L. A. & Fothergill, J. C. Electrical Degradation and Breakdown in Polymers. (IET, 1992).
- **Do'08:** Do, M. T. Propriétés diélectriques des gels isolants : application aux composants d'électronique de puissance. (Université Joseph-Fourier - Grenoble I, 2008).
- **Dyre'00:** Dyre, J. C. & Schrøder, T. B. Universality of ac conduction in disordered solids. Rev. Mod. Phys. 72, 873–892 (2000).
- **Guill'06:** Guillermin, C., Rain, P. & Rowe, S. W. Transient and steady-state currents in epoxy resin. J. Phys. D: Appl. Phys. 39, 515 (2006).
- **Gupta'76:** Gupta, D. K. D. & Joyner, K. On the nature of absorption currents in polyethyleneterephthalate (PET). J. Phys. D: Appl. Phys. 9, 829 (1976).
- **Hu'06:** Hu, Y., Smith, R. C., Nelson, J. K. & Schadler, L. S. Some mechanistic understanding of the impulse strength of nanocomposites. in 2006 IEEE Conference on Electrical Insulation and Dielectric Phenomena 31–34 (2006).
- **Iyer'11:** Iyer, G., Gorur, R. S., Richert, R., Krivda, A. & Schmidt, L. E. Dielectric properties of epoxy based nanocomposites for high voltage insulation. IEEE Transactions on Dielectrics and Electrical Insulation 18, 659–666 (2011).
- **Jilani'15:** Jilani, W. et al. Effects of curing agent on conductivity, structural and dielectric properties of an epoxy polymer. Polymer 79, 73–81 (2015).
- **Li'10:** Li, Z., Okamoto, K., Ohki, Y. & Tanaka, T. Effects of nano-filler addition on partial discharge resistance and dielectric breakdown strength of Micro-Al2O3Epoxy composite. IEEE Transactions on Dielectrics and Electrical Insulation 17, 653–661 (2010).
- **Locatelli'14:** Locatelli, M. L. et al. Evaluation of Encapsulation Materials for High-Temperature Power Device Packaging. IEEE Transactions on Power Electronics 29, 2281–2288 (2014).
- **Nasciment'16:** Nascimento, E. do et al. Breakdown, free-volume and dielectric behavior of the nanodielectric coatings based on epoxy/metal oxides. J Mater Sci: Mater Electron 27, 9240–9254 (2016).
- **Nelson'04:** Nelson, J. K. & Fothergill, J. C. Internal charge behaviour of nanocomposites. Nanotechnology 15, 586–595 (2004).
- **Preetha'10:** Preetha, P. & Thomas, M. J. AC breakdown characteristics of epoxy alumina nanocomposites. in 2010 Annual Report Conference on Electrical Insulation and Dielectric Phenomena (CEIDP) 1–4 (2010).
- **Psarras'06:**Psarras, G. C. Hopping conductivity in polymer matrix–metal particles composites. Composites Part A: Applied Science and Manufacturing 37, 1545–1553 (2006).
- **Segui'00:** Segui, Y. Diélectriques - Courants de conduction. Techniques de l'Ingénieur. Ref: D2301(2000).
- **Singha'08:** Singha, S. & Thomas, M. J. Dielectric properties of epoxy nanocomposites. IEEE Transactions on Dielectrics and Electrical Insulation 15, 12–23 (2008).

- **Singha'09:** Singha, S. & Thomas, M. J. Influence of filler loading on dielectric properties of epoxy-ZnO nanocomposites. IEEE Transactions on Dielectrics and Electrical Insulation 16, 531–542 (2009).
- **Smaoui'10:** Smaoui, H., Arous, M., Guermazi, H., Agnel, S. & Toureille, A. Study of relaxations in epoxy polymer by thermally stimulated depolarization current (TSDC) and dielectric relaxation spectroscopy (DRS). Journal of Alloys and Compounds 489, 429–436 (2010).
- **Tuncer'07:** Tuncer, E. et al. Electrical properties of epoxy resin based nano-composites. Nanotechnology 18, 25703 (2007).

GENERAL CONCLUSION

The work presented in this thesis provides an evaluation of general properties of epoxy blends that are susceptible to be used as an encapsulating material for power modules working in wide range of temperatures and under high voltages.

The work is divided into two major parts, first the preparation of a phase separated epoxy/thermoplastic blend. Second, the characterization of the pure epoxy material as well as the blends was presented.

A principle condition in choosing the novel material is to respect the maximum temperature that the components of the module can resist without affecting their reliability, which is 200 – 300 °C. The chosen pure epoxy material is cured at 200 °C while the blends are cured at a maximum temperature of 185 °C.

The chosen epoxy/PEI blend is well studied in literature in terms of kinetics and final morphology of the mixture. Some mechanical tests were also performed showing an increase in the critical stress intensity values when blending the epoxy with 10 wt% of PEI. This is due to the presence of homogenously distributed phase separated particles of PEI in the epoxy network. The nodules acted as obstacles absorbing the propagation of the cracks and thus increasing the mechanical strength of the blend. From this particular point, an idea was built to study the influence of the phase separated nodules on the electrical breakdown characterizations, as the principle of propagation of cracks is the same in mechanical and electrical breakdown.

At the first stage, bibliographic work was done to understand the ability of having phase separated organic-organic blend which is different than mixing inorganic particles in an epoxy matrix and distributing them homogenously. The next step was to choose an epoxy and thermoplastic having high glass transition temperatures insuring the ability of the blend to sustain wide range of temperature without the presence of major relaxations. Knowing that, the chosen epoxy (DGEBA) has a T_g = 163 °C and the thermoplastic (PEI) has a T_g = 217 °C.

Different Characterization techniques were done to study the thermal, mechanical and electrical properties of the pure epoxy network as well as two blends with 5 wt% and 10 wt% of PEI.

Electronic Microscopy, SEM and TEM, showed the homogenous distribution of the phase separated PEI nodules in the epoxy network with an average diameter of 1.5 µm to 2 µm in DM5PEI samples and 2 µm to 3 µm in DM10PEI samples. An interphase layer was seen between PEI nodules and the epoxy network occupying 5% from the volume of the nodule. From the detected samples observed, the average percentage of the nodules having an interphase layer was 20 %, which can interfere in the mechanical and electrical responses.

The studied material is susceptible to replace silicone gel, nowadays used, acting as an encapsulating layer in a power module. The module placed in severe atmosphere such as the free zone near the engine of an airplane is subjected to different temperatures -50 °C to 300 °C. The chosen material must show thermal stability in such range of temperatures. TGA measurements showed good thermal stability of the pure epoxy network up to 350 °C under inert atmosphere and 300 °C under air atmosphere. This stability did not change in the presence of 5 and 10 wt% of PEI in the blend. This factor is an advantage to the chosen material as the nowadays used silicone gel can function well below 200 °C only.

Phase separation phenomenon was also detected by means of DSC and DMA. DSC measurements showed in the blends the presence of two different glass transitions corresponding to the epoxy and PEI materials. DMA measurements also showed the presence of the two transitions by the presence of α transition of epoxy and PEI corresponding to their glass transition temperatures. The presence of the PEI in the epoxy blend did not decrease the modulus of the epoxy network as well.

Electrical properties of the material is the most important factor to study, as the role of the encapsulating layer is to protect the power modules from the present high potential differences between the components of the module. For that, dielectric spectroscopy, DC conductivity measurements as well as breakdown voltage measurements were performed on the pure epoxy material and the epoxy/PEI blends.

The presence of the PEI nodule decreased the relative permittivity values by 8% and 15%, for DM5PEI and DM10PEI respectively, in the whole range of frequency and temperature studied. This decrease is in the contrary of the majority of studied epoxy composites with nano and micro inorganic fillers. Some exceptions were seen where the incorporation of nanofillers decreased relatively the permittivity values but by using very low critical percentages. In our work the present decrease of 15 % is when epoxy is blended with 10 wt% of PEI having micro-sized phase separated nodules. Along with that the relative loss did not

increase with the presence of the PEI nodule showing a relative decrease below the glass transition temperature and at high frequencies. Above the glass transition temperature and at low frequencies, high values of the loss correspond to the presence of α relaxation and to the increase of conductivity of the material as the temperature increases above T_g.

Theoretical modelling of the relative permittivity of the blends was calculated using the experimental results of the pure epoxy network and the PEI films. The model showed a close assumption of what is measured experimentally with a shift to higher values. This shift can be explained by different aspects: first the size of the nodules is taken from the 2D SEM images where the radius of the nodule in the third dimension used in the modelling is not the real one of the nodule. The second cause might correspond to the presence of free volumes that can be elaborated during the preparation process. Free volume cannot be quantified but can change the density of the present PEI nodules and thus change its relative permittivity which in its place affect the calculated model. Third, the interphase present between the two components epoxy and PEI can as well affect the calculated modelling as it can have different permittivity as well as it needs different models. In the chosen model, the interphase is neglected and the modelling is done considering a particle suspended in the middle of the epoxy matrix. Other researchers have elaborated a modelling process for core-shell particles in a matrix which can be furtherly studied.

In the conductivity measurements, it was shown that the pure epoxy network as well as the blends has conductivity values that are lower than 10^{-12} $S.cm^{-1}$ up till around the glass transition temperature. On the other hand, silicone gel becomes semi-conducting material above 60 °C. This is another advantage for replacing the nowadays used silicone gel with the novel proposed epoxy/PEI blend.

Finally the breakdown voltage measurements showed an increase in the breakdown voltage in the blends than the pure epoxy network. This increase is referred to the presence of the PEI nodules in the epoxy network. The PEI nodules can act as obstacles absorbing the beginning of the cracks that causes the breakdown of the sample. Our theory of enhancing the breakdown voltage in the presence of the PEI nodules such as the critical stress intensity was confirmed. This breakdown voltage values at room temperature is 10 times higher than what is found for silicone gel. This gives the chosen novel material a new factor to confirm its ability of replacing the silicone gel in the power module.

PERSPECTIVES

- *Perspectives on the epoxy/PEI blend:*

As it is presented the thermal, mechanical and electrical properties of the epoxy/PEI blends were studied in this thesis work. Nevertheless, more investigations can be done to develop a larger idea on the characteristics of this novel material.

Conductivity measurements at high voltages and different temperatures can be measured. Knowing that as the temperature increases the mobility of the electrons increases which can increase the values of the conductivity. Guillermin et al. showed that the phenomenon of current conduction have changed in an epoxy network below and above the glass transition temperature [*Guill'06*]. Concerning our studied material it might be hard to perform the conductivity measurements above the glass transition temperature as it is hard to find the adequate measurement tools than can function properly above 200 °C. But, measurements higher than room temperature can give wider idea as well.

As the power module is subjected to different range of temperatures for different variation of time, thermal aging can be performed on the pure epoxy material as well as the blends. The blends might have changes in the interphase between epoxy and PEI. The interphase can decrease, increase or even disappear which result in different characteristics of the material. Colombini et al. studied the influence of thermal aging of epoxy and 10 wt% of **PPE** (poly (phenylene ether)) [*COLO'99*]. They showed that after an aging at T_g – 20 °C for 45 h the volume of the interphase existing between the epoxy and the thermoplastic has decreased. All the characterization done can have different responses due to the aging process that can be furtherly studied.

In insulating materials, such as the epoxy/PEI blend, space charge can affects their performance dramatically. To study and control space charge effects it is necessary to determine and locate charges within the material. The evolution of the space charges under different external stresses and temperature can be performed. An example of such measurement is presented in the work of Smaoui et al. [*Smaoui'00*]. They have showed that space charge behavior was influenced by the temperature and the manufacturing process.

The studied epoxy/PEI blend can be deposited on a module to make a primary test of the performance of the blend with the module.

- *Perspectives on epoxy/thermoplastic blends:*

Higher weight percentages of PEI in the epoxy network shows the phenomenon of phase inverted matrix. 20 wt% of PEI for example shows the dispersion of epoxy in the PEI network. This blend has increased the critical stress intensity higher than that for epoxy and DM10PEI [*Gir'97*]. Electrical properties of this blend can be tested and evaluated. The comparison in this case cannot be correlated with epoxy/inorganic fillers or with the DM10PEI blend, as the matrix is PEI and not epoxy.

In this work we have presented the characteristics of an epoxy with PEI that has a high glass transition temperature. The phase separation phenomenon showed an influence on the electrical properties of the pure epoxy network. Another kind of thermoplastic that have high glass transition temperature and the ability to form along with the epoxy a phase separated matrix can be tested. This test can confirm the theory of having phase separated nodules in the epoxy network that enhance the electrical properties of the epoxy. Some thermoplastics with high glass transition temperatures and have shown phase separation phenomenon with epoxy network are: polysulphone (**PSF**) [Hedrick'91] [Hedrick'85] and Poly-ethersulfone (**PES**) [Blanco'03].

Thermoplastics having low glass transition temperature can be also blended with epoxy to form a phase separated system. Polystyrene is one example that was studied extensively with different percentages in the work of Rico et al. [*Rico'11*] [*Rico'11*]. The effect of the phase separation phenomenon on the electrical properties in this case can be also studied.

Epoxy with different glass transitions can also play a role in influencing the electrical properties of the module. The choice of hardener can change the glass transition temperature of the epoxy network as presented in **Table 17**.

Table 17: list of T_g corresponding to different kinds of epoxy

Epoxy	Hardener	Tg (°C)	ref
Bisphenol A	Tetramine	89	***Nelson'04***
Bisphenol-A	Amine	110	***Katayama'13***
DGEBA	diaminodiphenyl sulfone	99	***Lee'01***
DGEBA	anhydride MA	175	***Qipeng'92***
DGEBA	anhydride PA	133	***Qipeng'92***
DGEBA	anhydride HHPA	144	***Qipeng'92***

References

- **Blanco'03:** Blanco, I., Cicala, G., Faro, C. L. & Recca, A. Development of a toughened DGEBS/DDS system toward improved thermal and mechanical properties by the addition of a tetrafunctional epoxy resin and a novel thermoplastic. J. Appl. Polym. Sci. 89, 268–273 (2003).
- **Colo'99:** Colombini, D. et al. Effects of thermal treatments on the viscoelastic behavior of the interphase relaxation in a compatibilized thermoset/thermoplastic blend. Polymer 40, 935–943 (1999).
- **Gir'97:** Girard-Reydet, E., Vicard, V., Pascault, J. P. & Sautereau, H. Polyetherimide-modified epoxy networks: Influence of cure conditions on morphology and mechanical properties. J. Appl. Polym. Sci. 65, 2433–2445 (1997).
- **Guill'06:** Guillermin, C., Rain, P. & Rowe, S. W. Transient and steady-state currents in epoxy resin. J. Phys. D: Appl. Phys. 39, 515 (2006).
- **Hedrick'85:** Hedrick, J. L., Yilgör, I., Wilkes, G. L. & McGrath, J. E. Chemical modification of matrix Resin networks with engineering thermoplastics. Polymer Bulletin 13, 201–208 (1985)
- **Hedrick'91**: Hedrick, J. L. et al. Chemical modification of matrix resin networks with engineering thermoplastics: 1. Synthesis, morphology, physical behaviour and toughening mechanisms of poly(arylene ether sulphone) modified epoxy networks. Polymer 32, 2020–2032 (1991).
- **Katayama'13:** Katayama, J., Ohki, Y., Fuse, N., Kozako, M. & Tanaka, T. Effects of nanofiller materials on the dielectric properties of epoxy nanocomposites. IEEE Transactions on Dielectrics and Electrical Insulation 20, 157–165 (2013).
- **Lee'01:** Lee, J. & Yee, A. F. Inorganic particle toughening I: micro-mechanical deformations in the fracture of glass bead filled epoxies. Polymer 42, 577–588 (2001).
- **Nelson'04:** Nelson, J. K. & Fothergill, J. C. Internal charge behaviour of nanocomposites. Nanotechnology 15, 586–595 (2004).
- **Qipeng'92:** Qipeng G., Jinyu H., Liaohai G. and Zhuiliu F. phase separation in anhydride-cured epoxy resin containing phenolphthalein poly(ether ether keton). Eur. Polym. J. Vol. 28, No. 4, pp. 405-409, (1992).
- **Rico'11:** Rico, M., Lopez, J., Díez, F. J. & Bellas, R. Simulation of molecular fractionation and species distributions in phase separation of polystyrene-modified epoxy/monoamine–diamine blends. European Polymer Journal 47, 2432–2441 (2011).
- **Rico'12:** Rico, M., López, J., Montero, B. & Bellas, R. Phase separation and morphology development in a thermoplastic-modified toughened epoxy. European Polymer Journal 48, 1660–1673 (2012).
- **Smaoui'00:** Smaoui, H., Guermazi, H., Agnel, S., Mlik, Y. & Toureille, A. Space charge measurements by the thermal step method in epoxidic polymer materials. Polym. Int. 49, 1513–1518 (2000).

Abbreviations

Al	Aluminum
Al_2O_3	Alumina
AlN	Aluminum Nitride
AlSiC	Aluminum-(Silicon Carbide)
Au	Gold
BeO	Beryllium oxide
BPDA-PDA	(*BPDA: 3,4,3',4'-biphenyltetracarboxylic dianhydride – PDA: p-phenylenediamine*)
cBN	cubic boron nitride
CMC	Ceramic matrix composites
CTE	Coefficient of thermal expansion
CuMo	copper-molybdenum
CuW	copper – tungsten
DAB	Direct Aluminum Bonding
DC	Direct Current
DCB	Direct Copper Bonding
DDS	diaminodiphenyl sulfone
DEA	Dielectric Analysis
DGEBA	diglycidylether of bisphenol A
DMA	Dynamic mechanical analysis
DSC	Differential scanning calorimetry
EPPS	(3-glycidyloxypropyl)trimethoxysilane
Fe_2O_3	ferric oxide
GaAs	gallium arsenide
GaN	Gallium nitride
hBN	hexagonal boron nitride
HHPA	Hexahydrophthalic Anhydride
HVDC	high-voltage, direct current
IGBT	Insulated gate bipolar transistor
IMB	insulating metal baseplate
InP	indium phosphide

K_{IC}	critical stress-intensity
LCST	lower critical solution temperature
LED	Light-emitting diode
MA	Maleic anhydride
MCDEA	4,4-methylene bis(3-chloro-2,6-diethylaniline)
MCT	MOS-controlled thyristor
MDEA	4,4'-methylenebis-[2,6-diethylaniline]
MMC	Metal matrix composites
MOSFET	metal oxide semiconductor field effect transistor
NG	Nucleation growth
OTGB	o-tolyl biguanidine
PA	Polyamide
PDA	*1,4 phenylenediamine*
PDMS	polydimethylsiloxane
PEI	Polyetherimide
PES	Poly-ethersulfone
PI	Polyimide
PMPA-ODA PI	*poly (pyromellitic dianhydride-co-4,4'-oxydianiline)*
PPE	Polyphenyl ether
PSF	polysulphone
SCR	Silicon-Controlled-Rectifier
SD	Spinodal decomposition
SEM	Scanning electron microscopy
Si	Silicon
Si_3N_4	silicon nitride
SiC	Silicon carbide
SiO_2	Silica
TEM	Transmission electron microscopy
T_g	Glass transition temperature
TGA	Thermo-gravimetric analysis
TGMDA	tetraglycidyl methylenedianiline
TiO_2	Titania
TP	Thermoplastic
TS	Thermoset

UCST	upper critical solution temperature
VDP	vapor deposition polymerization
ZnO	Zinc Oxide
ZrO_2	Zirconia
ΔG_m	free energy of mixing
ΔH_m	Enthalpy
ΔS_m	Entropy
ε_r	Relative permittivity
Φ	Volume fraction
DM	Pure epoxy network
DM10PEI	Epoxy + 10 wt% PEI
ε'_r	Real part of the relative permittivity
ε''_r	Imaginary part of the relative permittivity
σ	Conductivity
ω	Angular frequency
τ	Relaxation time

Translation in French of the section “polymer composites and polymer blends”

I. Polymères composites et mélanges de polymères

Les composites, en général, sont des solides composés de différents matériaux qui diffèrent de par leurs propriétés, où les constituants individuels conservent leurs caractéristiques intrinsèques. Il existe plusieurs familles de matériaux composites. Les composites à matrice métallique (MMC) qui sont des matériaux utilisés largement dans l’industrie automobile, aéronautique et d’autres nombreuses applications en raison de leurs bonnes propriétés mécaniques et physiques [Ibrahim'91] [Lindroos'95]. Les composites à matrice céramique (CMC) sont utilisés dans de nombreuses applications haute température, en raison de leur très haute résistance au choc thermique ainsi que leur résistance au fluage ce qui permet la conception d’objets à fortes contraintes thermique et mécanique. Il existe un autre type de mélange à base de polymères, les composites constituées de mélange de polymères. Deux types de combinaison de matériaux existent, le premier constitué d’un mélange organique – inorganique (ou hybride) et le second un mélange organique – organique. Ces deux mélanges se distinguent de par leurs compositions ainsi que par leurs caractéristiques et applications.

Les composites et les mélanges à bases de résines époxy sont des matériaux qui présentent plusieurs avantages développés par la suite. Ils peuvent être utilisés comme matériaux composites en les combinant avec d’autres inorganiques ou d’autres matériaux organiques. Les études de composites époxy/charges se divisent en trois grands groupes qui diffèrent selon la quantité et la taille des charges introduites dans la matrice. Elles peuvent être de taille nanométrique, micrométrique, ou une combinaison des deux. Ils sont étudiés pour montrer l’influence des charges sur les différentes propriétés du réseau époxy et précisément les propriétés thermiques et électriques. La résine époxy est un polymère isolant électrique très utilisé en particulier en haute tension pour les transformateurs de puissance, les jonctions, les raccordements et les autres accessoires. D’un autre côté, les mélanges de polymères et surtout les mélanges époxy/thermoplastique sont également étudiés pour montrer l’effet résultant de l’incorporation d’un thermoplastique sur les propriétés mécaniques, thermiques et de résistance sur des solvants du réseau époxy.

Dans la partie suivante de ce chapitre, quelques exemples de l'influence de l'incorporation des charges inorganiques dans le réseau époxy sont présentés. L'influence de la taille, de la forme, de la nature des charges modifiées ou non modifiées ainsi que le pourcentage de charges sur les propriétés mécaniques et électriques de la matrice époxy sera discutée. En raison des critères recherchés pour un matériau d'encapsulation, les valeurs caractéristiques suivantes seront étudiées : les parties réelles et imaginaires de la permittivité, la résistivité, la conductivité DC, le claquage, et les propriétés mécanique et thermique. Rare sont les études analysant les propriétés électriques de mélanges époxy/thermoplastique polymère [Mac'92] [Lestriez'98]. Nous nous sommes donc intéressés à l'influence de tels mélanges sur la morphologie, ainsi que les propriétés thermiques et mécaniques du réseau époxy. Dans les chapitres suivants, les propriétés électriques d'un mélange époxy/thermoplastique vont être étudiées.

I.1. Composites polymères basé sur un mélange de polymères/charges.

Les composites polymères utilisés dans plusieurs applications technologiques sont utilisés comme isolants électriques dans l'industrie de l'énergie intégrant des charges inorganiques pour atteindre des propriétés électriques, mécaniques, thermiques spécifiques et, parfois afin de réduire le coût. Leurs propriétés dépendent donc de la nature de la charge minérale, de sa composition chimique, de sa taille, de sa forme, ainsi que du type de dispersion dans la matrice, et également des interactions matrice/charge gouvernées par les propriétés physiques.

Les composites époxy/inorganique avec des charges de tailles nanométrique et micrométriques, ont montré des améliorations mécaniques et thermiques par rapport aux composites classiques et ont donc donné lieu à plus d'attention dans de nombreuses applications. L'addition de ces matériaux dans la formulation réduit les coûts et améliore la résistance au feu par exemple. Khan et coll. ont montré que les propriétés mécaniques d'une matrice époxy ont été améliorées avec l'incorporation de nanoparticules de céramique [khan 15]. Ils ont rempli l'époxy avec quatre différents types de céramiques, dioxyde de zirconium ZrO_2, oxyde de zinc ZnO, oxyde ferrique Fe_2O_3 et de la silice SiO_2, de mêmes taille de 50 ± 5 nm. La bonne dispersion a été démontrée à l'aide de 2 % en poids des nanoparticules avec une augmentation de l'élasticité et de la dureté du matériau. L'addition de silice dans la matrice époxy a montré des valeurs plus élevées que celle de l'époxy pur et le reste des composites époxy (Fig. 1). En plus, la stabilité thermique a été améliorée avec l'addition de silice par

rapport à d'autres nanoparticules. Au cours de la dernière décennie, de nombreuses recherches ont été effectuées afin d'améliorer la ténacité des époxydes avec l'addition de charges inorganiques. Elles ont mis en évidence l'augmentation du module et de la température de transition vitreuse [Lee'01] [Kinloch'03] [Bala'05].

Le domaine des diélectriques et de l'isolation électrique a profité de cette évolution basée sur les composites époxy – inorganiques utilisant les nano ou micro charges. Plusieurs investigations ont été et sont toujours effectuées pour comparer les effets du micro, nano et micro/nano charges sur les caractéristiques électriques finales du réseau époxy.

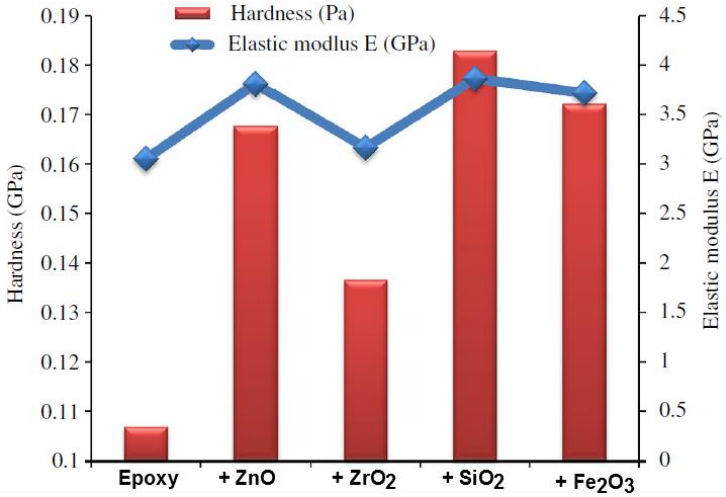

Fig. 1: Comparaison de la dureté et du module élastique pour des échantillons d'époxy pure et d'époxy renforcée [khan 15]

I.1.1. Micro-composites à base d'époxy.

Une étude sur l'influence de l'ajout de différents pourcentages massique de silice, de taille de 20 µm sur le réseau époxy a été étudiée expérimentalement par Kochetov et al. [Kochetov'10]. Comme la Fig. 2 (a) la montre, les valeurs de la permittivité électrique relative ont augmenté sous l'influence de l'augmentation de 20 à 40 % en poids des charges de silice. À 60 % en poids de silice, la valeur de la permittivité électrique relative a été réduite de 6 % par rapport à l'époxy pur. La raison de cette diminution est due à la grande quantité de matériau de remplissage, qui donne lieu à la limitation de la mobilité des chaînes, abaissant ainsi la permittivité relative apparente. La valeur de ε_r de la silice utilisée à 1 kHz est de 3.9, ce qui est légèrement supérieur à celui de l'époxy à 1 kHz qui est de l'ordre de 3.4. Les différentes charges montrent la même influence sur la matrice époxy lors de d'une variation de température jusqu'à 120 ° C comme illustré Fig. 2(b). En utilisant un pourcentage de silice élevé dans le réseau de l'époxy, le système peut être considéré comme un mélange de silice avec de l'époxy et non pas comme de l'époxy modifiée avec de la silice. Le réseau époxy

présent seulement 40 % en poids de l'ensemble du système et donc la valeur de permittivité finale ne peut être comparé au réseau époxy pur.

Avec l'addition de micro-charges dans le réseau époxy, la permittivité relative du micro-composite époxy est toujours supérieure à celle du réseau époxy pur comme on peut l'observer dans plusieurs études. Un exemple de cela a été reporté dans l'étude menée par Singha et al. sur des microparticules d'oxyde de Zinc de 0,5 µm [Singha'09] et des microparticules de titane 0,5 µm [Singha'08]. [Iyer 11] [Castellon'11] ont étudié l'influence des microparticules de silice de 16 µm pour des époxy silanisées. Ils ont montré qu'avec des surfaces modifiées par des micro-charges, l'introduction de micro-particules ne diminue pas la valeur de la constante diélectrique du composite mais au contraire l'augmente.,

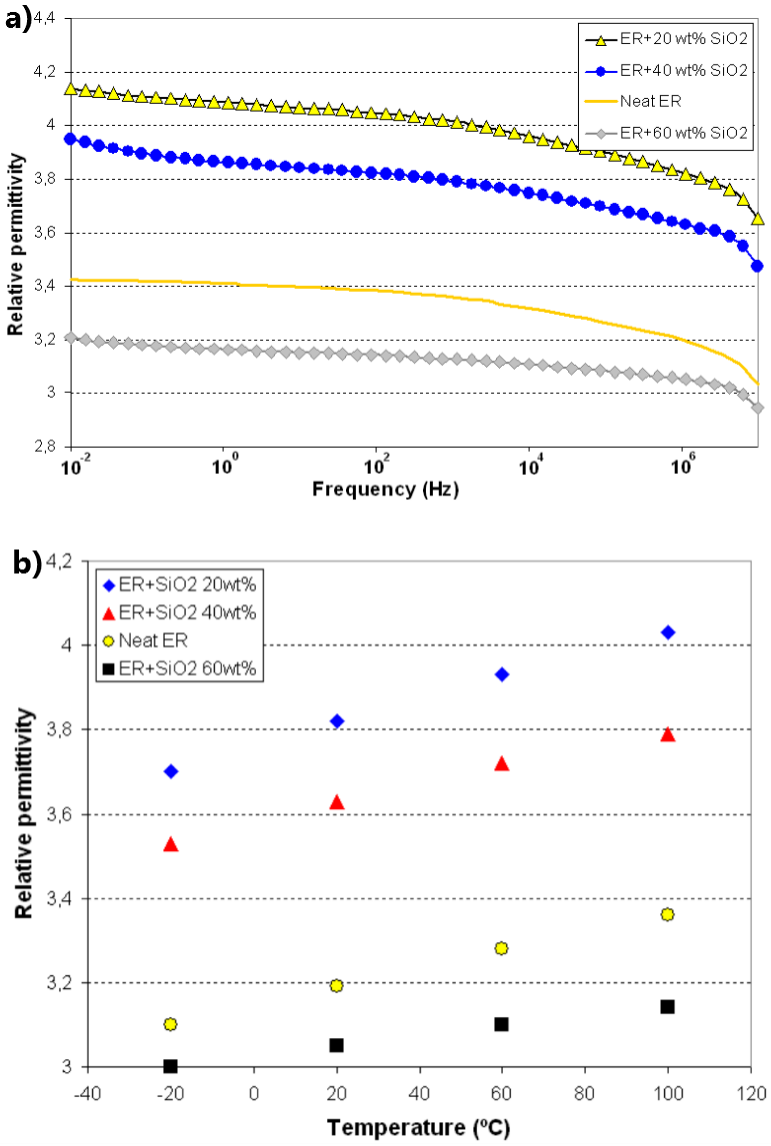

Fig. 2: Permittivité relative du composite époxy/silice (ER-SiO2) à 20 ° C en fonction de la fréquence (a) et à 1,15 MHz en fonction de la température [Kochetov 10].

Le Tableau 1 résume les valeurs des constantes diélectriques reportées dans la littérature. Un constant diélectrique élevé correspond à une grande capacité et donc à des courants réactifs plus élevés.

Tableau 1: Comparaison des différents types d'époxy et type de micro-charges sur les valeurs diélectriques

Réf	époxy + durcisseur	type de filler	taille	wt %	ε' @ 20 °C	ε''
Kochetov'10	Cycloaliphatic + anhydride	pure		0	3.2 @ 1MHz	-
		Alumina	4 µm	10-60	↗ 2.5 - 36 % avec la même influence jusqu'à 120 °C	-
		Silica	20 µm	20 -40	↗ 19 % - 13 %	-
				60	↘ 4.7%	
Singha'09	Cycloaliphatic + tetramine	pure		0	4.4 @ 1kHz	-
		ZnO	0.5 µm	5	↗ 4.5 %	-
Iyer'11	Cycloaliphatic + anhydride	pure		0	3.3 @ 1kHz	↗ (10^{-3} - 10^{3} Hz) ↘ (10^{3} - 10^{4} Hz)
		epoxy-silane modified Silica	16 µm	65	↗15 %	
Singha'08	Cycloaliphatic + tetramine	pure			4.5 @ 1kHz	tan δ 0.02 @ 1kHz
		Titania	0.5 µm	5	↗ 33 %	↗ 250 %
				10	↗ 100 %	↗ 900 %

Des tests de claquage ont également été effectués et montrent un comportement similaire à savoir une baisse de la tension de claquage avec l'augmentation du pourcentage de microparticules introduites, comme le montre le travail de Singha et al. sur des époxy chargées avec des particules de titane de 0,5 µm et des particules d'alumine de 50 à 60 µm [Singha'08]. Ils ont démontré que l'addition de microparticules, considérées comme naturellement isolantes dans l'époxy avec 10 % en poids de TiO_2 diminue la tension de claquage du réseau époxy de 52 kV/mm à 38 kV/mm sous tension alternative. Cette baisse de 26 % en raison de l'incorporation de TiO_2 particules est inférieure à l'effet de l'addition de 5 % en poids d'Al_2O_3 qui réduit la valeur de 37%. Li et al. ont effectué un test de claquage diélectrique AC similaire mais avec l'incorporation de 60% en poids de particules d'alumine ayant une taille de 10 µm [Li 10]. Dans ce cas apparaît une diminution de 54 % de la valeur de claquage. Un effet similaire a été démontré dans le travail de Hu et al., avec l'incorporation de 10 % en poids de particules de TiO2 ayant une taille de 1,5 µm [Hu'06]. La diminution présentée peut être due à l'introduction de défauts par ajout de micro-charges jouant un rôle important dans la réduction de la tension de rupture du composite. Le Tableau 2 présente une

brève comparaison de l'influence des différents types de charges utilisées sur le claquage et la résistivité du réseau époxy.

La plupart des micro-charges incorporées dans le réseau époxy ont diminué la valeur de tension de rupture par rapport à celle de l'époxy pure et augmente les valeurs de la constante diélectrique. Ce type de micro-composite apparaît intéressant pour des applications mécaniques mais pas pour les applications électriques.

Tableau 2: Comparaison de l'effet de micro-charges sur les valeurs de résistivité et de claquage sur des époxys chargés.

Ref	epoxy	Type de filler	taille	wt %	résistivité	E(kV/mm)
Singha'09	Cycloaliphatic + tetramine	pure		0	7 x 10^17	AC 56 kV/mm
		ZnO	0.5 µm	5	↘ 75 %	↘ 45 %
Iyer'11	Cycloaliphatic + anhydride	pure		0	-	AC 37 kV/mm
		Epoxy-silane modified Silica	16 µm	65	-	↘8 %
Singha'08	Cycloaliphatic + tetramine	pure			7.5 x 10 ^17	AC 52 kV/mm
		Titania	0.5 µm	10	↘ 20 %	↘ 27 %
		Alumina	50-60 µm	5	↘ 27 %	↘ 38 %
Li'10	Cycloaliphatic + amine	pure			-	AC 203 kV/mm
		Spherical Alumina	10 µm	60	-	↘ 56 %
Hu'06	Cycloaliphatic + amine	pure			-	DC 330 kV/mm AC 230 kV/mm
		Titania	1.5 µm	10%	-	DC ↘ 10 % AC ↘ 15 %

I.1.2. Epoxy Nano-composites

Durant la dernière décennie, l'intérêt de l'utilisation des charges de tailles nanométriques comme additifs aux matériaux polymères (nanocomposite) et plus précisément dans les matériaux à base d'époxy a augmenté. Un critère essentiel dans la préparation de ce type de matériel est l'uniformité dans la dispersion des nano charges dans le réseau époxy. Beaucoup de familles de nano charges ont été étudiés, tels que la silice, l'alumine, le titane, l'oxyde de zinc, le titanate de baryum. Ils sont utilisés avec ou sans modification de surface. Certaines des recherches ont montré une amélioration des propriétés électriques en dessous certains pourcentages critiques. Toutefois, il a été signalé que les nano-charges participaient à

la détérioration des caractéristiques électriques du réseau époxy. Un exemple est donné par Katayama et al., où ils ont étudié l'influence de trois nanoparticules différentes traités en surfaces sur les propriétés électriques du réseau époxy [Katayama 13]. Les charges sont traitées afin de rendre leurs surfaces hydrophobes et compatibles avec la matrice époxy. Ils ont incorporé 5 % en poids de nanoparticules au réseau époxy. Les trois nanoparticules sont le dioxyde de titane, de la silice et de la boehmite d'alumine {hydroxyde d'oxyde d'aluminium (AlO)}. Les dioxydes de titane et de silice ont une forme sphérique avec une taille de 50 nm et 14 nm respectivement, tandis que la boehmite d'alumine avait une forme d'assiette de taille de 10 x 45 x 45 nm. Il ressort clairement de la Fig. 3 que la permittivité relative (ε'_r) et les pertes (ε''_r) sont significativement plus élevées avec l'incorporation de boehmite d'alumine et de titane que dans l'époxy pure et l'époxy avec des nanoparticules de silice. L'addition de nanoparticules de silice ne diminue pas les valeurs de la constante diélectrique mais réduit relativement la valeur des pertes à des concentrations de 5 % en poids. Les charges de silice ont des tailles plus petites que les nano-charges utilisées dans cette étude. Ils ont la plus grande surface spécifique par rapport au dioxyde de titane et à la boehmite d'alumine et semble avoir la plus forte interaction avec la matrice époxy qui restreindrait le mouvement moléculaire de la résine époxyde.

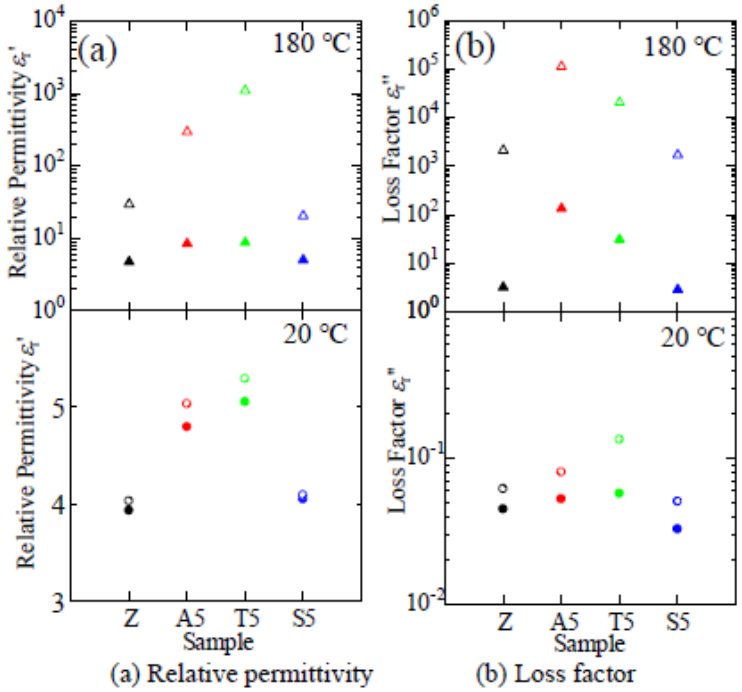

Fig. 3: E 'r (a) et ε''r (b) mesurée à 0,1 (ouvert) et 63 Hz (solide). (Z) époxy soignée, alumine de boehmite (A5), Titania (T5) et de la silice (S5) [Katayama 13].

Cette diminution du facteur de perte dans les basses fréquences par rapport au réseau époxy pur a été rarement reportée dans la littérature pour d'autres matériaux du même type à cette valeur de concentration. La compatibilité entre les charges et le réseau de l'époxy est un facteur clé agissant sur l'influence des propriétés électriques. Si l'interaction entre la matrice epoxy et les nano charges est faible, l'effet inverse se produirait. La faible interaction peut conduire à la présence de vides qui ont une influence négative sur les propriétés électriques du réseau époxy et peut améliorer les tensions de claquage.

Plus de recherches sont à faire pour expliquer ce phénomène unique, la diminution de la permittivité ainsi que la façon dont les particules interagissent avec le polymère n'est pas bien définie. La plupart des études portant sur l'incorporation des nanoparticules dans le réseau époxy montre que la diminution de la valeur du constant diélectrique a lieu en dessous d'un pourcentage critique de nano-charges. Néanmoins, la valeur du facteur de perte reste supérieure à celle du réseau époxy pur. Seules quelques rares études ont indiqué que la permittivité reste dans la même gamme de valeurs ou relativement plus basses. Tsekmes et al. ont étudié l'effet des nanoparticules de nitrure de bore (BN) comme charges dans un réseau d'époxy [Tsekmes'14]. Les particules de BN, d'un diamètre de 70 nm, ont été modifiées avec de l'EPPS ((3-Glycidyloxypropyl) trimethoxysilane) pour améliorer l'adhésion entre matrice époxy et les charges.

Les concentrations utilisées étaient de 0,2, 0,5, 0,6, 1 et 5 % de nano-charges dans le réseau époxy. Le mélange des nanoparticules dans la matrice époxy à l'aide de différentes techniques, nano mélangeur, speedmixer, solvant ne conduit pas à un effet significatif du processus de dispersion vers la morphologie du composite. De légères différences peuvent être observés sur les réponses diélectriques et s'expliquent par la quantité d'eau absorbée dans le composite, plutôt que de la distribution des particules. La permittivité complexe est indiquée sur la Fig. 4. Les nanocomposite avec de faibles concentrations de charges ($\leq$ 1 vol %) présentent une plus faible permittivité relative (ε'_r) par rapport à l'époxy pure. La permittivité relative du composite époxy a diminué avec l'augmentation du pourcentage de charges quand la concentration de charge est inférieure ou égale à 0,6 % en volume. Cependant, au-delà de cette concentration critique de charges, la permittivité relative commence à augmenter pour atteindre des valeurs supérieures à l'époxy pure. La diminution des valeurs de ε'_r est attribuée à la modification de la surface des particules.

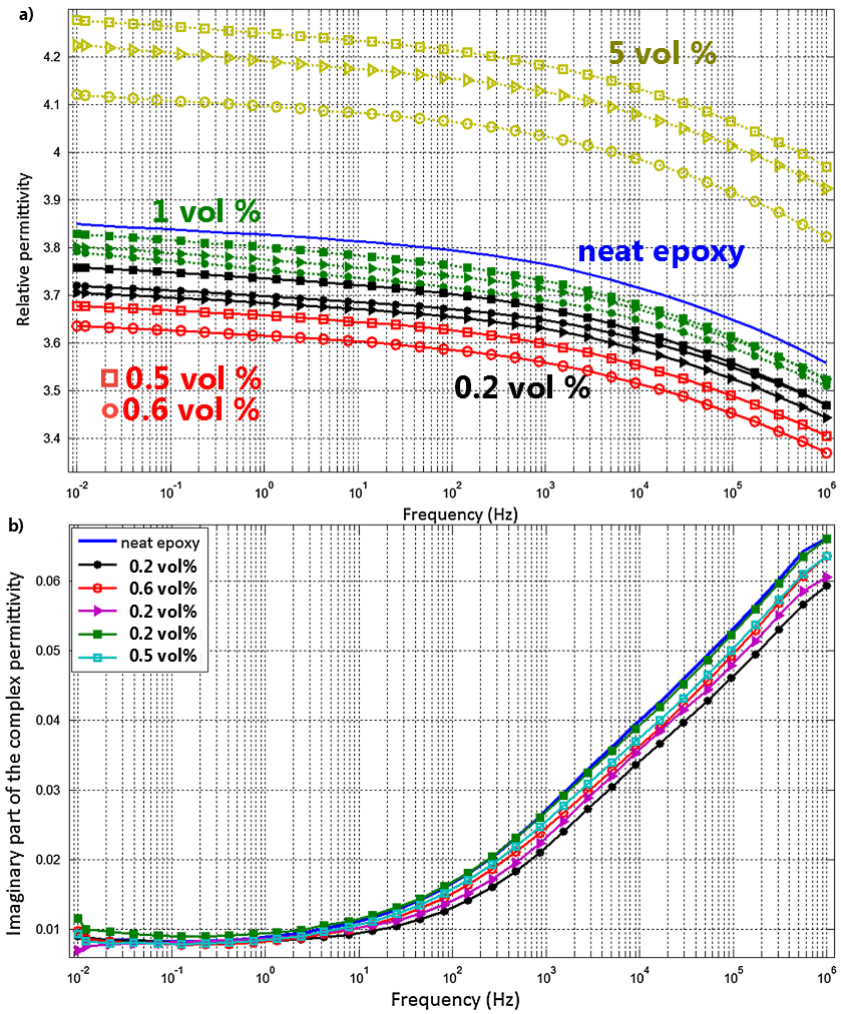

Fig. 4: a) ε'r de l'époxy pure et de tous les nanocomposites produits et b) ε ''r de l'époxy pure et des nanocomposites avec un taux de charges < 1 vol % (en appliquant différentes techniques) à 20 ° C [Tsekmes 14]

La liaison chimique entre les charges et les chaînes d'époxy aboutit à l'immobilisation des chaînes d'époxy et donc diminue la permittivité relative. La surface spécifique des nanoparticules augmente entre 0,2 et 0,6 % en volume et ainsi donne la possibilité d'immobiliser une plus grande quantité de chaînes d'époxy et diminue la valeur de la permittivité relative. Au-dessus de ce pourcentage critique (0,6 % en volume), des nanoparticules commencent à s'approcher les unes des autres et peuvent former des agglomérats qui diminue par la suite la surface spécifique et augmentant ainsi les valeurs de la constante diélectrique relative. En outre, la partie imaginaire a été étudiée et divisée en deux cas de part et d'autres de la concentration critique. Ci-dessus, la partie imaginaire avait des valeurs plus élevées que l'époxy pure et en dessous de cette valeur critique les nanocomposite montrent des valeurs de ε'_r inférieures seulement à des fréquences élevées. Cette diminution des valeurs imaginaires à haute fréquence est aussi due à l'immobilisation des chaînes

latérales d'époxy à proximité de particules. Ceci donne lieu à la suppression du processus de relaxation β et en conséquence diminue la valeur des pertes.

Le but de cet exemple était de montrer que l'incorporation des nanoparticules avec un réseau d'époxy pourrait diminuer les valeurs de permittivités en dessous d'une concentration critique. Néanmoins, leur effet sur la permittivité imaginaire est instable et dépend de la surface d'interaction entre les charges et le réseau de l'époxy, de la taille des charges, de la fréquence et de la température utilisées. D'autres recherches ont permis d'évaluer l'influence des nano-charges sur la permittivité des composites époxys où plusieurs explications de résultats ont été proposées, comme le travail de Kochetov et al. sur des nanoparticules modifiées en surface d'alumine, de nitrure d'aluminium et d'oxyde de magnésium [Kochetov'12]. Le Tableau 3 présente une comparaison de l'influence des différents types de nano-charges modifiés sur les valeurs de la permittivité relative du composite époxy.

Tableau 3: Influence de différentes sortes d'époxy et de nano-charges modifiées sur les valeurs diélectriques

Ref	epoxy	Type de filler	taille	wt %	ε' @ 20 °C	ε'' @ 20 °C
Katatayama'13	Cycloaliphatic + amine	pure			3.9 @ 63 Hz	4.5×10^{-2} @ 63 Hz
		plate like shape **Bohemite alumina**	10 x 45 x 45 nm	3 - 5 %	↗ 23 %	↗ 11 %
		spherical titania	50 nm	3 - 5 %	↗ 31 %	↗ 50 %
		spherical fumed **silica**	14 nm	3 - 5 %	↗ 2.5 %	↘ 22 %
Tsekmes'14	Cycloaliphatic + anhydride	pure		vol%	3,75 @ 1kHz	0,026 @ 1kHz
		hBN	av. 70 nm 30 - 300 nm	0.2	↘ 1 %	↘1 4 %
				0.5	↘ 4 %	↘ 7 %
				0.6	↘ 5.5 %	↘ 11 %
				1	=	↘ 3 %
				5	↗ 11 %	↗ 4 %
kochetov'12	Cycloaliphatic + anhydride	pure		wt%	3,55 @ 1kHz	
		spherical **Alumina**	30 nm	0.5	↘ 2 %	les pertes diélectriques du composite contenant jusqu'à 5 % en poids ne diffèrent pas beaucoup par rapport aux époxy purs
				2	↘ 7 %	
				5	↘ 1.5 %	
				10	↘ 1.5 %	
		spherical, cubic, hexagonal **AlN**	60 nm	0.5	↘ 2 %	
				2	↘ 3 %	
				5	↗ 3 %	
				10	↗ 9 %	
		spherical and cubic **MgO**	22 nm	0.5	↘ 13 %	
				2	↘10 %	
				5	↘ 9 %	
				10	↘ 7 %	
		spherical **Silica**	20 nm	0.5	↗ 3 %	
				2	↗ 4 %	
				5	↗ 6 %	
		spherical **BN**	70 nm	10	↘ 1.5 %	

La tension de claquage est également un facteur important dans l'étude des nanocomposites parce que les concentrations de charges jouent également un rôle important sur le claquage. Nascimento et al. Ont étudié l'effet de l'intégration de nanoparticules ayant différents diamètres, oxyde de zinc de 100 nm et nanoparticules d'alumine de 10 nm [Nascimento'16]. Les concentrations utilisées étaient de 0,4, 1,2, 2,4 et 6 vol% pour les composites d'alumine et 0,2, 0,6, 1,2 et 3 vol% pour les composites de ZnO. La tension de claquage de l'époxy pure, composée de DGEBA comme notre époxy et de o-tolyl biguanidine, OTGB ($C_9H_{13}N_5$), comme durcisseur, était de 47 kV/mm. L'utilisation de 0,4 % en volume d'alumine a augmenté cette valeur de 45 %. Au-dessus de 0,4 % en volume, cette valeur a diminué et ils ont obtenu une valeur similaire à celle trouvée pour 6 % en volume par rapport à l'époxy pure. L'incorporation de ZnO a montré une augmentation de 25 % à l'aide de seulement 0,2 % en volume. De la même façon, au-dessus de cette concentration le claquage avec 3 % en volume est devenu inférieure à celui de l'époxy pure. Les résultats montrent clairement que l'incorporation des nanoparticules ne doit pas dépasser des concentrations critiques très faibles pour augmenter le niveau de tension de claquage. En outre, le pourcentage critique en dessous duquel le claquage est amélioré dépend strictement de la taille des nanoparticules. Le nombre absolu de particules augmenteraient rapidement d'un facteur de 1000 en changeant la taille des particules d'un facteur 10 seulement, par exemple de 100 nm à 10 nm. L'utilisation de ≈ 3 vol % de 10 nm alumine a augmentait la tension de claquage de 20 %, tandis que l'utilisation du même pourcentage de 100 nm ZnO a diminuait la valeur de 20 %. En raison de sa petite taille, 10 nm d'alumine n'atteignent pas ce pourcentage de percolation à 3 % en volume et influence la tension de claquage en la diminuant. Lorsque le diamètre des particules est petit, e.g. moins que 50 nm, l'influence est meilleure en raison de grandes régions d'interfaces avec des charges de petites particules, alors qu'avec de plus grandes tailles de nanoparticules (> 50 nm) de très petits pourcentages critiques suffisent pour augmenter le claquage du réseau époxy [Tsekmes'15-1]. Plus les particules sont petites, plus la couche inter-faciale relative est grande et plus le volume d'interface total est grand. Avec une bonne compatibilité entre l'époxy et la charge, en dessous des valeurs de seuil de percolation critiques, les charges immobilisent le mouvement des chaînes polymères et contribuent ainsi à augmenter les valeurs de claquage. Mais au-dessus du seuil de percolation, les interfaces peuvent agir comme un pont et donc des chemins de conductivité sont créés conduisant à la diminution de rupture diélectrique.

Le phénomène de dispersion des charges est un autre facteur essentiel à considérer pour l'étude de l'influence des charges sur les propriétés électriques du réseau époxy. Hu et

al. ont montré qu'en intégrant 10 % en poids de TiO2 de 23 nm dans un réseau d'époxy augmente la tension de claquage de 18 % [Hu'06] alors que Nelson et al. ont montré que l'utilisation des mêmes nanoparticules avec la même concentration aboutit à une diminution de la tension de claquage de 12 % [Nelson'04]. La seule différence entre ces deux études est la procédure de mélange. Hu et al. ont obtenu une meilleure dispersion et ainsi augmente la valeur de la tension de claquage. D'autres recherches ont mis en évidence une augmentation de la tension de claquage de nanocomposite par rapport à la matrice époxy pure. Imai et al ont étudié l'influence de plusieurs types de charges (ZnO, TiO2 et de silicate multicouches) de taille inférieure à 20 nm et ont montré une augmentation de la tension de claquage par 12 à 57 % en utilisant 5 et 7,5 % en poids de nanoparticules respectivement [Imai'08]. Même si la taille des nanoparticules (20 nm) est petite, cette augmentation de la valeur de claquage peut s'expliquer par le fait que le pourcentage critique au-delà duquel les agrégats sont créés n'est pas atteint. D'autres études ont également signalé une augmentation des valeurs de claquage [Ding'04] [Singha'09] [Iyer'11], [Tsekmes'15-1]. Différentes études utilisant des nanoparticules de différentes tailles et de différents pourcentages montrent une diminution dans la rupture diélectrique des nano-composites en comparaison avec le réseau époxy pur même à des pourcentages de faible poids. Dans ce cas, l'explication proposée est la présence d'incompatibilité à l'interface entre le réseau de l'époxy et les charges [Singha'08] [Preetha'10] [Tuncer'07] [Tsekmes'15-1].

Des résultats contradictoires sur la performance des nanocomposite chargés ont été signalés et les mécanismes sous-jacents ne sont pas bien compris. Tel que discuté, plusieurs facteurs peuvent interférer avec l'influence de l'incorporation des nanoparticules sur les propriétés électriques du réseau époxy. Afin d'augmenter la valeur de tension de rupture ou diminuer les valeurs de la constante diélectrique, les nanoparticules doivent être relativement petites (< 50 nm) et devraient avoir une compatibilité de surface sinon elles agiront comme des défauts. En outre, une modification de surface adéquate pour les charges peut être ajoutée ainsi que la maîtrise de la dispersion pour éviter des agrégats permettent d'améliorer les performances en terme de claquage.

I.1.3. Epoxy Micro/Nano-composites

Des discussions précédentes sur les micro et nano composites époxy, on remarquera que les époxy chargés par des microparticules souffrent d'une tension de claquage faible ainsi que d'une augmentation des valeurs de constante diélectrique. En revanche, une incorporation de nano charges a montré quelques améliorations essentielles. C'est pourquoi durant ces

dernières années, certains chercheurs ont suggéré que l'ajout de nano-charges à un mélange de micro-composite époxy peut être utile pour augmenter la tension de rupture et diminuer la permittivité. Il a été constaté que la modification de nano-charges dans un micro-composite époxy augmente les valeurs de rupture diélectrique, mais en général des valeurs plus basses que le réseau époxy pur sont mesurées. L'avantage de ce genre de mélange a été l'augmentation des valeurs de conductivité thermique et pas l'amélioration des propriétés électriques du composite époxy. Guo et al. ont démontré l'influence de l'ajout de 5 et 2 % en poids d'alumine de 30 nm et de titane de 10 nm dans une époxy modifiée avec 63 et 65 % en poids de micro-alumine allant de 12 à 21 µm [Guo 14]. Le champ de claquage de l'époxy pure (69 kV/mm) a diminué de 17 % lors de l'utilisation de l'alumine. Avec l'ajout de nano-alumine cette valeur a augmenté de 8 % et a diminué de 4 % avec l'ajout de nano-titane, en comparaison avec des micro-composite époxy. En comparaison avec la présence de nano-charges seulement, les nano-alumine ont diminué le champ de claquage de l'époxy pure de 25 % et les nano-titane de 12 % comme indiqué sur la Fig. 5. Plus la permittivité du nanofiller minéral est grande, plus le champ de claquage est élevé, sachant que la constante diélectrique de l'alumine est de 10 [Thorp'90] et la permittivité du titane est de 100 [Wypych'14].

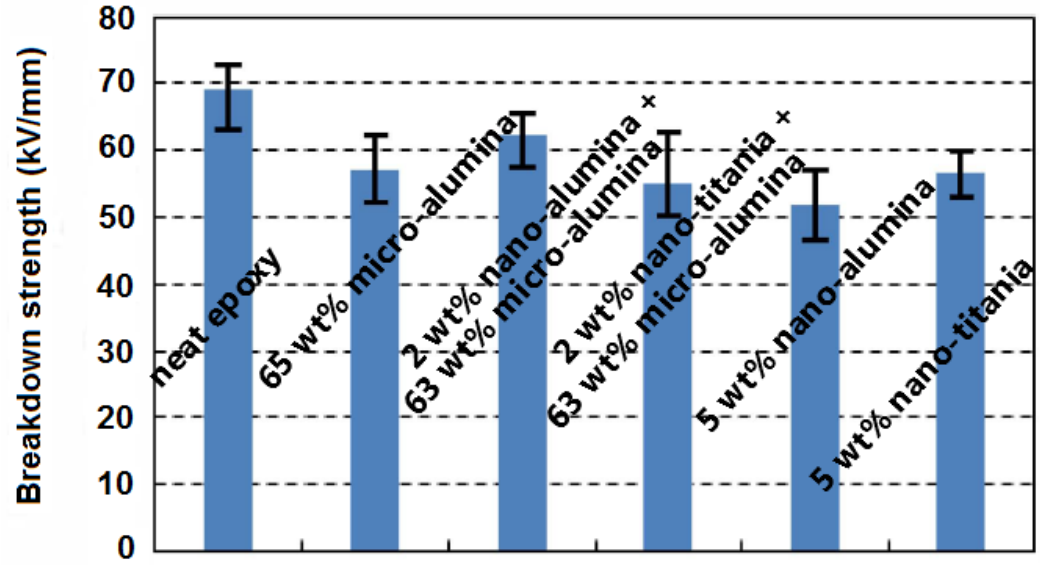

Fig. 5: Résistance de rupture des composites époxy [Guo 14]

Un effet similaire a été observé sur la rupture diélectrique avec l'incorporation de nano charges dans un micro-composite époxy, tel que décrit par Li et al. sur des nano-micro composites alumine/époxy [Li 10] et par Tsekmes et al. [Tsekmes 15-2]. Ce dernier a montré l'influence de l'ajout de particules de tailles nanométriques hexagonales de nitrure de bore (hBN) et de charges de nitrure de bore cubique (cBN) sur des composites époxy de type

micro-alumine et micro-silice. Les particules de hBN tant cBN ont été modifiés avec duEPPS ((3-glycidyloxypropyl) trimethoxysilane) pour améliorer l'adhésion entre le réseau de l'époxy et les nano-charges. Ils ont observé que l'addition de petites quantités de charges nanométriques (moins de 1 % en volume) améliore aussi bien le comportement thermique qu'électrique des micro-composites à base d'époxy. Néanmoins, les valeurs de claquage sont restées inférieurs à celui d'un époxy pur. Les valeurs diélectriques des matériaux composites nano-micro a montré un comportement similaire, où l'incorporation de nano charges à un micro-composite époxy a diminué la valeur de la constante diélectrique en comparaison à celle obtenu pour un micro-composite mais est resté supérieure à celle d'une matrice époxy pure, comme le montre Castellon et al. [Castellon 11]. Ils ont étudié l'influence de l'ajout de 5 % en poids de charges de tailles nanométriques de silice sphériques de 20 nm à une époxy micro-composite contenant 60, 62,5 et 65 % en poids de silice ayant une taille de 16 µm traités avec époxy-silane pour modifier la surface. Comme illustré à la Fig. 6, l'addition de 5 % en poids de nanoparticules a augmenté la valeur de la constante diélectrique de 2 % pour les 65 % wt micro-composite et a diminué de 2 % pour les 60 % en poids. Les valeurs sont plus élevées en moyenne de 17% que les valeurs du constant diélectrique relatif. Cette diminution des valeurs de constante diélectrique peut être liée à la diminution des microparticules dans le réseau de l'époxy. Il semble pour le moment difficile de comprendre la véritable cause de cette diminution de la valeur de la constante diélectrique relative du micro-composite.

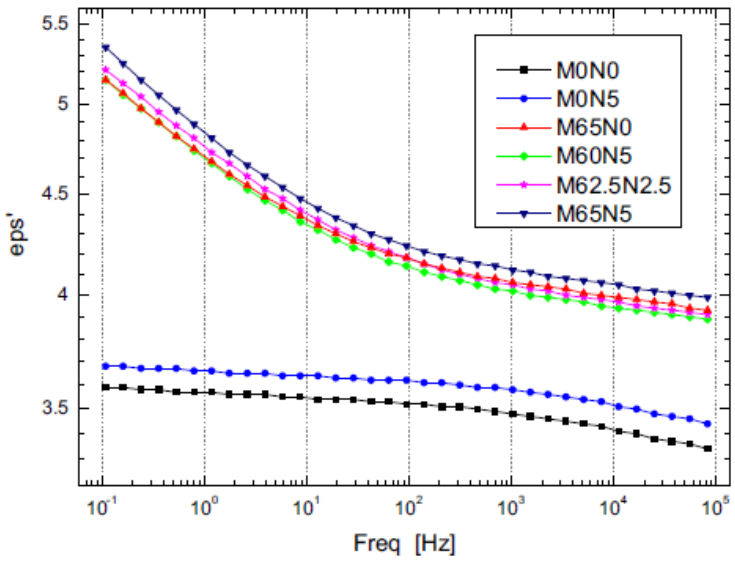

Fig. 6: Permittivité réelle en fonction de la fréquence à 40 ° C. M0NO époxy pure, époxy M0N5 époxy+ 5 wt % nano-particules, M65N0 époxy + wt 65 % micro-particules, M60N5 époxy + 60 wt % micro + 5 wt % nano, M62.5N2.5 époxy + 62,5 wt % micro + 2,5 wt % nano, M65N5 epoxy + 65 wt % micro + 5 wt % nano [Castellon 11].

1.2.1.4. Conclusion sur le composite polymère

Le choix d'un réseau époxy est dû à ses caractéristiques isolantes et l'opportunité de d'avoir des nouvelles propriétés lors de l'addition de micro ou nano charges. La discussion précédente a montré qu'en règle générale, l'ajout de micro-particules à un réseau époxy ne permettait pas d'obtenir une amélioration significative des propriétés électriques du réseau époxy tels que la permittivité relative et la tension de claquage. Quelques améliorations électriques dans les valeurs de la permittivité relative et la tension de claquage sont possibles pour des conditions particulières prenant en compte l'incorporation de nanoparticules avec une taille critique, le mélange, la modification de la surface des charges et le pourcentage critique de charges introduites. Enfin, l'intégration de nanoparticules dans un micro-composite époxy n'a ni diminué la permittivité ni augmenté la tension de claquage par rapport à un réseau époxy pur. Dans le paragraphe suivant, on décrira un nouveau matériau constitué d'un mélange de polymères organiques (époxy thermodurcissable et thermoplastique). Les propriétés thermiques, mécaniques et électriques du mélange époxy/thermoplastique proposées seront discutées.

I.2. Mélanges de polymères

Les mélanges de polymères sont obtenus en mélangeant deux ou plusieurs polymères afin de fusionner les caractéristiques de chacun d'eux. Le mélange de polymère existant est une approche pratique et efficace pour créer de nouveaux matériaux. Ils sont conçus et fabriqués pour modifier certaines propriétés afin de répondre aux exigences des applications ciblées. Quelques travaux ont été réalisés pour des applications mécaniques où une des propriétés, le plus souvent la ténacité est amélioré. En fait, lors du mélange de deux polymères trois différents types de mélanges se distinguent ; mélanges complètement miscibles, non miscibles et compatibles. Le mélange de polymère miscible a une structure monophasée qui agit comme si c'est un polymère individuel. Une seule température de transition vitreuse peut être observée. Les mélanges non miscibles sont constitués de deux polymères avec deux transitions vitreuses observées. Enfin des mélanges de polymères compatibles qui sont appelés des semi-mélanges non miscibles, puisqu'ils sont considérés comme des mélanges non miscibles qui présentent des propriétés physiques macroscopiquement homogènes. Les principales interactions dans un mélange de polymères sont des liaisons d'hydrogène, des interactions de Van der Waals et des interactions dipôle-dipôle. La deuxième loi de la thermodynamique permet d'établir la miscibilité dans un mélange de polymères par l'énergie libre de mélange ΔG_m montré Eq. 1:

$$\Delta G_m = \Delta H_m - T\,\Delta S_m \qquad \text{Eq. 58}$$

où ΔH_m et ΔS_m sont l'enthalpie et l'entropie de mélange à une température T. La miscibilité est satisfaite lorsque $\Delta G_m < 0$, mais les principaux facteurs qui peuvent influencer la miscibilité de polymère sont l'entropie, l'énergie d'interaction, le volume libre et les interactions spécifiques tels que les liaisons hydrogènes [Chen 99]. La miscibilité des polymères non polaires peut être estimée par l'équation de Flory-Huggins (Eq. 2) [Flory 53]:

$$\frac{\Delta G_m}{RT} = \left(\frac{\varphi_1}{N_1} ln\, \varphi_1 + \frac{\varphi_2}{N_2} ln\, \varphi_2 + \varphi_1 \varphi_2 . \chi_{12}\right) \qquad \text{Eq. 59}$$

où ΔG_m est la variation d'énergie libre due à l'interaction non polaire, R est la constante des gaz, T est la température absolue, φ représente la fraction volumique, N est le nombre de segments de la chaîne, χ, le paramètre d'interaction de Flory-Huggins et les indices 1 et 2 font référencent aux polymères mélangés. Les deux premiers termes du côté droit de l'équation 2 sont associés à l'entropie du mélange alors que le troisième terme est lié à l'enthalpie du mélange. De cette équation et connaissant les valeurs des masses moléculaires des polymères et leurs fractions volumiques, on peuvent estimer les résultats expérimentaux en connaissant χ, le paramètre d'interaction. Un diagramme de phase peut être ainsi créé, qui est présenté à la Fig. 7.

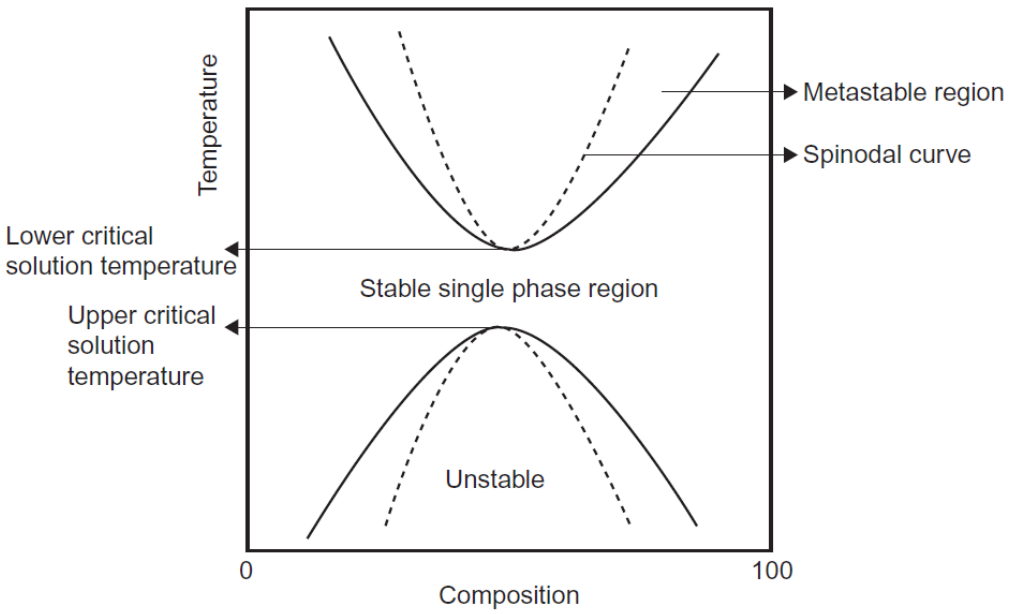

Fig. 7: température - diagramme de phase de composition d'un mélange binaire de polymère

Après avoir trouvé la bonne température de miscibilité à l'aide d'une concentration spécifiée, le mélange miscible peut subir deux phénomènes différents. Tout d'abord, le mélange peut rester miscible au cours de la réaction de polymérisation formant une structure unifiée ayant des caractéristiques singulières. Dans le cas contraire, le mélange peut subir un phénomène de séparation de phases entre les deux polymères donnant deux caractéristiques distinctes qui représentent chaque polymère mélangé. Lorsque deux polymères se mélangent à basse température et que les phases se séparent en chauffant, ils sont qualifiés de "lower critical solution temperature" (LCST) tandis que si les deux polymères restent séparés à la température ordinaire et forme une seule phase à haute température, ils sont dits "upper critical solution temperature" (UCST). Dans n'importe quel mélange la limite entre les compositions stables et métastables est appelée la binodale et la limite entre les compositions métastables et instables est appelée le spinodale. Dans la région métastable, la séparation de phase s'effectue par une nucléation croissance " nucleation-growth " (NG). Ce processus peut conduire à la formation de petits domaines riches en polymère (gouttelettes) dans une matrice polymère-pauvre. Si le mélange a atteint la région instable la séparation de phase se produit par "spinodale démixing" (SD). Ce processus conduit à la formation d'une structure bi-continue dans laquelle les phases polymères riches et les phases pauvres en polymère sont les deux phases continues. Cette phase est transformée en nodules homogènes séparés de la phase pauvre en polymère dans un domaine riche en polymère lorsque le temps au bout duquel la composition est à l'équilibre est atteint [Gir'96]. Ainsi, la miscibilité dans les mélanges de polymères est fonction de la température et chaque mélange binaire de polymères peut être caractérisé par un paramètre d'interaction [Chen'99].

La majorité des polymères sont incompatibles les uns avec les autres (mais ce n'est pas une règle générale), et les mélanger par plusieurs types de méthodes aboutit habituellement à deux phases. Cependant, et comme discuté, à partir de calculs et la connaissance de leurs caractéristiques, même les mélanges binaires les plus incompatibles doivent présenter un certain degré de mélange moléculaire. En choisissant la température adéquate des conditions de mélange, la miscibilité des polymères pourrait être obtenue. Par le mélange de différents types de structures polymères peuvent être obtenus comme : mélange de polymères phase séparée, copolymère greffé et copolymères séquencés. Le régime a démontré en Fig. 8 que les structures possibles où solide et pointillés indiquent respectivement le polymère 2 et le polymère 1 et les points indiquent les liens croisés ou des liaisons covalentes. Le phénomène de séparation de phase dans un mélange de polymères va être abordé dans le mélange époxy.

Le copolymère greffé (b) est représenté par un polymère collé sur le côté de l'autre, auquel cas copolymère à blocs (c) est démontré en chaînes collés sur la fin.

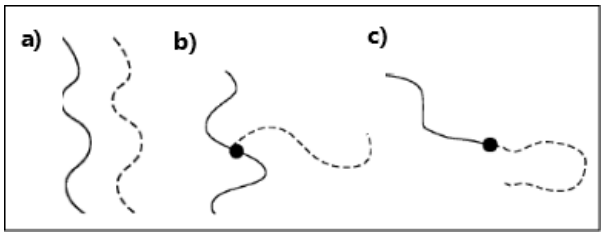

Fig. 8: Combinaisons de deux polymères. (a) mélanges de polymères ; (b) copolymère de greffon ; (c) un copolymère à blocs [Jacq'03].

I.3. Mélanges époxy

Un époxy est un polymère thermodurcissable, obtenu par la mise en réseau du prepolymer époxy avec un genre choisi de durcisseur. Un prepolymer époxy typique utilisé pour générer un réseau polymère à deux ou plus de groupes d'époxy par molécule. Sachant que les fonctionnalités d'un prepolymer époxy sont définies par le nombre de groupes époxy qui jouent un rôle majeur dans la formation du réseau polymère. Par exemple, diglycidylether de bisphénol A (DGEBA) a deux groupes époxyde dans sa structure tandis que tetraglycidyl methylenedianiline (TGMDA) possède quatre groupes époxy par molécule, comme indiqué dans la Fig. 9.

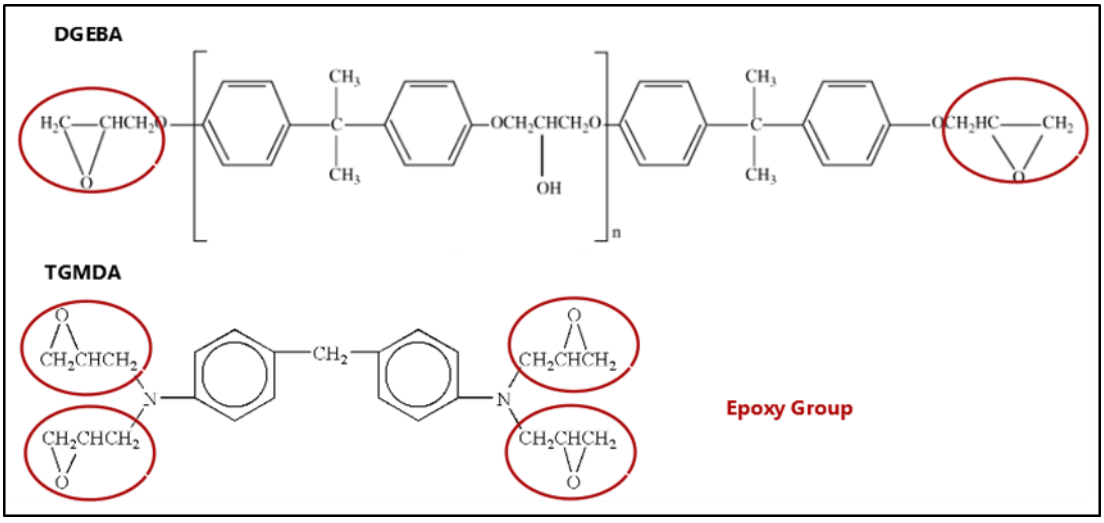

Fig. 9: Structures différentes d'époxy

Quelques exemples de durcisseurs utilisés sont des amines, les anhydrides, les phénols et les thiols. Les amines et les anhydrides sont les durcisseurs les plus utilisés et évalués. En général, les aliphatiques, cyclo aliphatiques ou diamines aromatiques sont utilisés pour générer un polymère réticulé par réaction avec le DGEBA. La combinaison la plus courante

est l'époxy cyclo aliphatique accompagné avec un durcisseur anhydride comme on le voit dans la majorité des études électriques fait le micro et nano composites de l'époxy évoqué précédemment. Le réseau époxy réticulé est bien connu dans plusieurs domaines industriels tels que dans l'industrie électronique, tel que discuté dans la section composite polymère, l'aéronautique et l'industrie automobile pour les applications d'adhésifs et revêtements. Parmi les raisons de ce choix sont :

- Propriétés isolantes élevées ayant des tensions de claquage élevées 100-200 kV/mm [Li 10] [Hu'06] [tuncer'07].
- Aucuns produits volatils émis au cours de la réaction de polymérisation, ce qui est intéressant pour le processus de production.
- Le grand nombre de monomères époxyde et durcisseurs, qui permettent de moduler les caractéristiques (température de transition vitreuse, propriétés mécaniques, propriétés thermiques, etc.). Grande adhérence à une variété de surfaces en raison de groupes polaires présents dans la structure.
- Initiateurs peuvent interférer dans l'étape de polymérisation et donner de nouvelles propriétés.

Pour obtenir un réseau époxy la réaction se passe par deux principales transformations structurelles, de gélification et de vitrification. En passant de la région de liquide dans la région caoutchouteuse, avec une molécule tridimensionnelle occupant tout le volume réactionnel est appelée la transformation de la gélification. La vitrification se déroule lors du passage de la région caoutchouteuse à la région de verre solide. Lorsque la région de verre solide est atteinte, l'évolution de réaction s'arrête et la température de transition vitreuse (Tg) est définie comme étant dans le même ordre de la température de réaction. Ce phénomène s'explique par Enns et al. où ils résument ce phénomène par un diagramme T-T-T de temps-température-transformation comme illustré à la Fig. 10 [Enns 83]. Le temps nécessaire pour atteindre la gélification ou la transformation de vitrification dépend de la température.

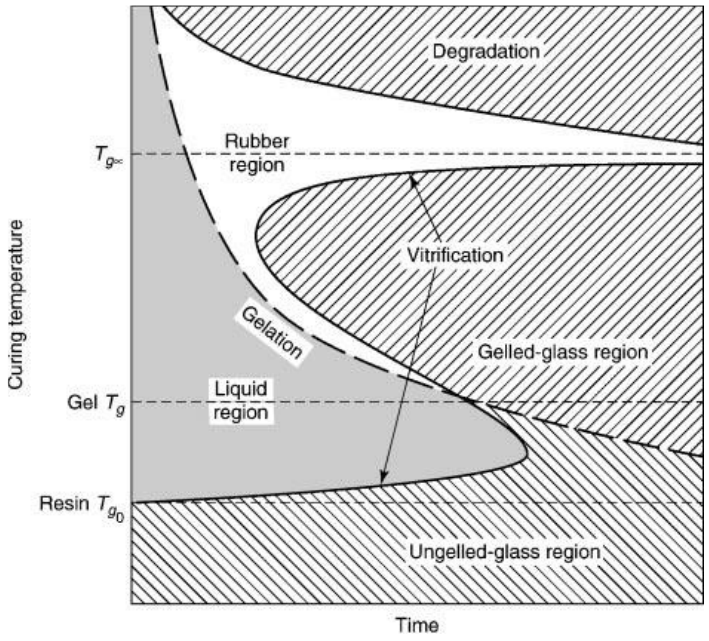

Fig. 10: Diagramme temps-température-transformation [Enns 83].

Dans ce travail, nous sommes intéressés par les mélanges époxy et plus précisément l'époxy/thermoplastique mélanges ayant phénomène de séparation de phase. La réaction des thermodurcissables (époxy) en présence de matières thermoplastiques peut produire la plupart du temps un système phase séparé avec différentes morphologies. L'époxy, selon la résine et le durcisseur choisi, peut avoir des températures de transitions vitreuses différentes. Une liste de différents de transition vitreuse (Tg) est présentée dans le Tableau 4. Dans l'industrie électronique, tel que discuté dans les critères requis pour le remplacement de la couche d'encapsulation, les matériaux choisis doivent avoir une bonne stabilité thermique dans une large gamme de températures allant de -50 ° C jusqu'à 300 ° C. Pour cette raison les thermoplastiques qui vont être discutés sont classés ayant la température de transition vitreuse élevée.

Tableau 4: liste des Tg correspondant à différents types d'époxy

Epoxy	Durcisseur	Tg (°C)	ref
Bisphenol A	Tetramine	89	***Nelson'04***
Bisphenol-A	Amine	110	***Katayama'13***
DGEBA	DDS aromatic diaminodiphenyl sulfone	99	***Lee'01***
DGEBA	anhydride MA	175	***Qipeng'92***
DGEBA	anhydride PA	133	***Qipeng'92***
DGEBA	anhydride HHPA	144	***Qipeng'92***

Beaucoup d'exemples de mélange à l'aide de thermoplastiques Tg hautes ont été étudiées et élaborées dans la littérature comme le polysulfone (PSF) {Tg = 187 ° C} [Hedrick 91] [Hedrick 85], Polyethersulfone (PES) {Tg = 190 ° C} [Blanco'03] et poly-etherimides (PEI) {Tg = 217 ° C} [RIF 97], [Bucknall 89] [Bonnet 99]. Par exemple, Blanco et al. ont démontré une époxy phase séparée et un copolymère, de 40 : 60 mélange de Polyethersulfone: polyetherethersulfone (40PES:60PEES). Ils ont utilisé un époxy de type DGEBA guéri par une diamine. L'image de SEM de 15 % en poids de thermoplastique PES : PEES dans le réseau de l'époxy est montré Fig. 11 où l'on a observé des particules morphologie associée à séparation de phase dans le cadre d'un mécanisme spinodal.

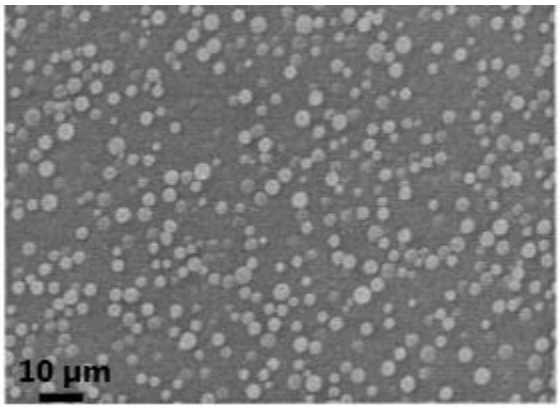

Fig. 11: Microscopie SEM époxy/15 wt % PES [Blanco'03]

La réaction de polymérisation dans un mélange de thermo-dur/thermoplastique s'appelle la séparation des phases induite par réaction, par lequel plus de thermodurcissable/thermoplastique mélanges sont préparés [Williams 97] [Pascault'00]. Le mélange initial de thermodurcissable/thermoplastique est miscible sous température et homogène ; le phénomène de séparation de phase se déroule dans la guérison de la thermodurcissable menant à plusieurs types de morphologie. La morphologie définitive d'un thermodurcissable (TS) / thermoplastique (TP) mélange phase séparée peut être estimée en utilisant un schéma de conversion – composition à température constante, comme illustré à la Fig. 12.

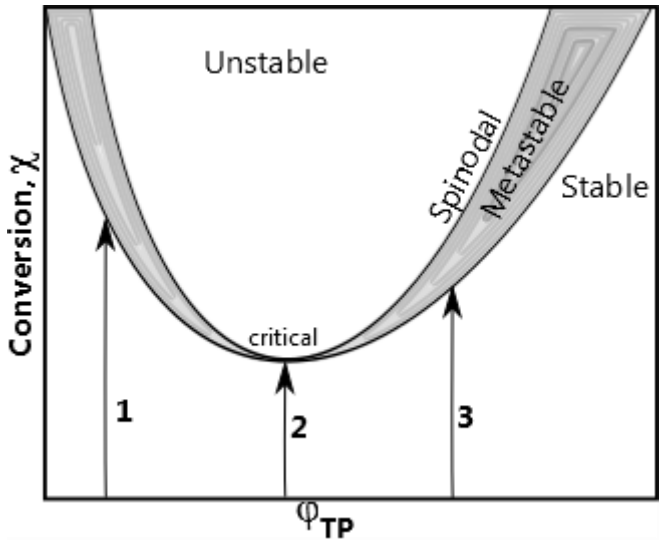

Fig. 12: Conversion – diagramme de transformation de Composition à température constante ; 1, 2 et 3 sont des trajectoires différentes, à partir de différentes concentrations initiales de TP/TS et menant à différentes morphologies [Pascault'00]

La morphologie finale obtenue à une température choisie dépend de la fraction de volume choisie comme on le voit dans le diagramme. Si φ TP (fraction volumique de thermoplastique) est situé dans la partie gauche du pourcentage critique, la morphologie finale comprendra une dispersion de particules riches en thermoplastique dans une matrice riche en thermodurcissable, nommé la morphologie particulate, comme illustré dans le schéma 1 de la Fig. 13. En revanche, lorsque la fraction de volume se trouve sur le côté droit du pourcentage critique, la morphologie définitive sera présentée dans le schéma 3. Il représente, ainsi, une dispersion de particules riches en thermodurcissable à matrice thermoplastique riche qui est souvent appelé morphologie de phase inversé. Enfin, à proximité du pourcentage critique, une variété de morphologies peuvent être développée, tels que les structures bicontinuous, double de morphologies de phase et de ruban comme structures [Pascault'00].

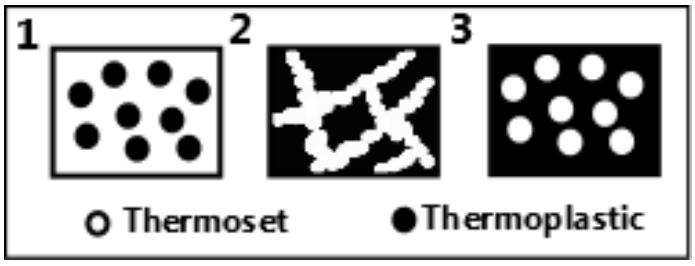

Fig. 13: Morphologie des particulate (1), bicontinuous (2) structure et morphologie (3) Phase inversé

Le mélange de thermodurcissable/thermoplastique est utilisé pour améliorer les propriétés de l'initiale thermodurcissable, telles que les propriétés mécanique, thermique et résistance au solvant. Un nouveau matériau est toujours généré avec de nouvelles propriétés

distinctes diffèrent de celles de la pure thermodurcissable. Un exemple typique de la ténacité à augmenter en thermodurcissable-thermoplastique mélanges est préparé par la réaction induite de la phase de séparation est illustré à la Fig. 14. DGEBA-MDEA était le système époxy-amine mélangé avec PPE, Polyphenyl éther [Pascault'00].

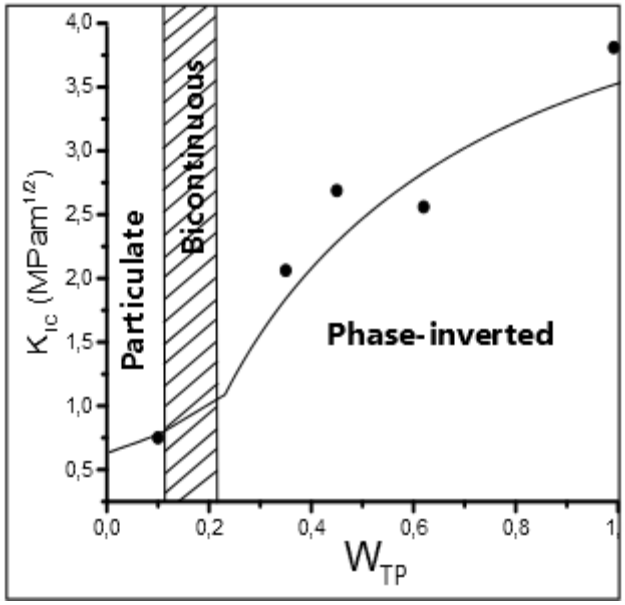

Fig. 14: K_{IC} en fonction de la fraction massique thermoplastique pour EPI / mélange DGEBA-MCDEA, préparé par la réaction induite par la phase de séparation [Pascault'00].

La ténacité des mélanges thermodurcissable-thermoplastique est habituellement exprimée en termes d'intensité de contrainte critique K_{IC} (MPa.m$^{1/2}$). En phase particulate morphologie à 10 % en poids de thermoplastique K_{IC} présentait une augmentation de 20 % en comparaison avec le réseau époxy pur. Cette fonction décrit la capacité d'un matériau à résister à des fissures et arrêter la fracture. La présence des particules thermoplastiques souples dans un réseau rigide époxy a agi comme une barrière contre la propagation de la fissure et ainsi permis d'augmenter la valeur de K_{IC}. La propagation de fissure est atténuée par des particules thermoplastiques distribuées de façon homogène. La valeur de K_{IC} éprouve une plus grande augmentation dans la région quand le thermoplastique devient la phase continue qui est décrite comme la phase inversé structure. Le thermoplastique pure a une valeur de K_{IC} supérieure que d'époxy pure qui joue un rôle dans l'augmentation de la valeur du mélange lors de réalisation de la morphologie phase inversé.

Peu d'études analysent les propriétés électriques d'un réseau de mélange polymère thermodurcissable/thermoplastique. Jilani et al. ont présenté les propriétés diélectriques d'un réseau d'époxy [Jilani'15]. Les durcisseurs utilisés dans la polymérisation de la résine époxyde ont un effet significatif sur la structure de l'époxy qui à son tour influe sur les

propriétés diélectriques. Ils ont suggéré que le polymère époxy avec un durcisseur aromatique, DDS (diaminodiphenyl sulfone), est plus adapté aux applications comme isolateurs, que le polymère issu de l'aliphatique durcisseur, c'est-à-dire l'ethylenediamine. En effet la conductivité du durcisseur aliphatique est plus élevée que les aromatiques. Il n'y a aucune étude présentée sur les propriétés électriques des mélanges époxy avec séparation de phase, donc notre comparaison va être faite avec le composite époxy déjà présenté.

Quand le mélange thermodurcissable-thermoplastique a la morphologie particulate, comme nous l'avons dit les particules thermoplastiques agissent comme une barrière contre toute propagation de fissure en passant par le matériel. Cette caractéristique intéressante donne naissance à l'idée d'avoir la même influence dans la création de fissures lors d'un essai de tension de rupture. Notre hypothèse est que la morphologie particulaire du mélange s'arrêterait les arborescences qui se déroule sur des tensions élevées s'appliquant au réseau époxy, augmentant la capacité de la résine en tension résister et lui donnant une tension de valeur de claquage supérieure. Cette hypothèse va être discutée avec un nouveau matériau proposé dans le chapitre précédent.

I.3. Conclusion générale

Dans ce chapitre, le module de puissance et plus précisément un module IGBT est présenté en définissant tous ses composants internes et leurs caractéristiques. Le point faible de ces modules est aujourd'hui la couche d'encapsulation utilisée (gel silicone) qui ne permet pas d'augmenter la tension et la température dans un module de puissance. Le gel silicone doit être remplacé pour permettre l'amélioration des tenues en températures et en tensions. Certains matériaux proposés pour remplacer les matériaux présents ont été répertoriés. Dans ce chapitre, nous suggérons l'utilisation de mélanges de polymères pour remplacer l'encapsulation et/ou la couche de passivation actuelle. Les mélanges de polymères peuvent être divisés en deux groupes principaux : composites organiques/inorganiques et organiques/organiques mélanges.

Un état de l'art des composites organiques/inorganiques tels que époxy/nano et micro-composites a été fait; montrant que l'utilisation de micro-charges incorporées dans un réseau époxy diminue la valeur de rupture diélectrique et augmente les valeurs de la constante diélectrique relative. Dans certains cas particuliers comme avec des microparticules d'alumine la conductivité thermique du composite est améliorée. Cet effet est considéré comme un inconvénient étant donné les propriétés isolantes nécessaires dans un module de puissance, comme l'utilisation de modules exige une amélioration dans les propriétés électriques des matériaux proposés. L'incorporation de nano-charges nécessite de suivre plusieurs conditions critiques afin d'améliorer les valeurs de rupture diélectrique ou diminuer les valeurs de la constante diélectrique relative. Ainsi la taille des nanoparticules doit être petite et leurs surfaces doivent être compatibles avec le réseau époxy. Elles doivent être dispersées d'une façon homogène sinon les nanoparticules forment des agrégats agissant comme des défauts dans la matrice. En outre, une méthode appropriée de dispersion doit être utilisée pour éviter l'insertion d'espaces vides et pour permettent une distribution homogène des nanoparticules. Des pourcentages critiques très faibles selon la taille de la nanoparticule ne doivent pas être dépassées afin d'augmenter la surface spécifique sans pour autant atteindre le niveau de percolation. L'incorporation des nanoparticules dans des micro-composites ne montrent aucune influence intéressante par rapport à un réseau d'époxy pure.

Le mélange organique/organique est le matériau que nous proposons basé sur un mélange de thermodurcissable/thermoplastique, à savoir un mélange d'époxy. Les processus de préparation et de transformation ont été expliqués en donnant la procédure de préparation

d’un mélange d’époxy/thermoplastique à phases séparées. Dans les chapitres suivants les caractéristiques du mélange époxy/thermoplastique à phase séparé vont être discutées.

I.4. Dans ce travail de doctorat

Dans ce travail de doctorat, le matériel étudié choisi est un mélange de thermodurcissable/thermoplastique admettant une séparation de phases. Ce genre de matériel est habituellement utilisé pour améliorer les propriétés mécaniques du réseau thermodurcissable dans la littérature. Le thermodurcissable est une résine époxy DGEBA avec un durcisseur de type amine aromatique, choisi en raison de sa température de transition vitreuse élevée (T_g époxy + amine = 164 ° C). Cette température de transition vitreuse élevée confirmera la stabilité du système dans une large gamme de températures. Le thermoplastique mélangé avec de l'époxy est du polyetherimide (PEI) ayant une température de transition vitreuse supérieure à celle du réseau époxy. Le mécanisme de séparation de phases de ce mélange a été étudié dans le travail de thèse d'Anthony Bonnet et Emmanuel Girard-Reydet. Ils ont décrit comment trouver le point critique de conversion et obtenir un matériau homogène à phase séparée. L'intensité de contrainte critique a également été étudiée montrant une augmentation de ses valeurs avec l'ajout de 10 % en poids de PEI. Les propriétés mécaniques s'étant améliorées avec ces types de mélanges, nous espérons obtenir également un gain sur les propriétés électriques.

Nous allons présenter différents pourcentages de PEI à une température permettant le processus de séparation de phase, qui va être caractérisé au moyen de la microscopie électronique (TEM et SEM).

L'influence du thermoplastique utilisé dans ce mélange va être analysée thermiquement et mécaniquement par analyse calorimétrique différentielle (DSC), par analyse thermogravimétrique (TGA) et par analyse mécanique dynamique (DMA).

On étudiera les caractéristiques électriques à l'aide de l'analyse diélectrique (DEA), des mesures de conductivité DC extrapolées de l'analyse diélectrique ainsi que d'une mesure de courant de conduction. Les performances en termes de claquage en DC à la température ambiante seront évaluées dans les chapitres suivants.

FOLIO ADMINISTRATIF

THESE DE L'UNIVERSITE DE LYON OPEREE AU SEIN DE L'INSA LYON

NOM : HALAWANI DATE de SOUTENANCE : 14 Février 2017

Prénoms : Nour

TITRE : Matériaux innovants pour le packaging

NATURE : Doctorat Numéro d'ordre : 2017LYSEI010

Ecole doctorale : EEA

Spécialité : Energie & Sciences de la matière et des matériaux

RESUME :

This work deals with the study of thermoset-thermoplastic blend (epoxy-amine/poly-etherimide phase separated) to assess the electrical and thermal performances. These materials would be new candidates to replace the encapsulation layer in semiconductors, for example ones used as switches in power electronic applications. Polymers blends would be a novel candidate as an insulator for the system. Pure epoxy system as well as Epoxy/Polyetherimide blends where characterized by transmission electron microscopy, scanning electron microscopy, differential scanning calorimetry, thermogravimetric analysis, dynamic mechanical analysis, dielectric analysis with analytical modelling, electrical conductivity and breakdown voltage measurements.
These complementary techniques were used first to investigate the presence of the phase separation phenomenon and secondly to quantify the separated nodules size. The effect of this phase separation was examined and showed a decrease in the dielectric values of 15 % and an increase in the breakdown voltage compared to the pure epoxy system. It was finally modelled to show a close assumption of what is found experimentally.

MOTS-CLÉS: Material engineering, Organic-Organic Blend, Epoxy, PEI, Electrical properties

Laboratoire (s) de recherche : AMPERE & IMP

Directeur de thèse: Hervé Morel

Président de jury : Stéphane HOLE

Composition du jury :

NASSIET, Valérie	Professeur des Universités, ENI de Tarbes	Rapporteuse
HOLE, Stéphane	Professeur des Universités, UPMC- Sorbonne Universités	Rapporteur
MIJANGOS-UGARTE, Carmen	Professeur, ICTP-Madrid	Examinatrice
GRISERI, Virginie	Maître de Conférences, LAPLACE-Toulouse	Examinatrice
MOREL, Hervé	Directeur de Recherche, INSA-LYON	Directeur de thèse
PRUVOST, Sébastien	Maître de Conférences HDR, INSA-LYON	Co-directeur de thèse
AUGE, Jean-Louis	Maître de Conférences, UCBL-Lyon1	Encadrant
GAIN, Olivier	Ingénieur de Recherche, UCBL-Lyon1	Co-encadrant